Standoff Sensing Technology Based on Laser-Induced Breakdown Spectroscopy: Advanced Targeting, Surveillance and Reconnaissance in Security and Architectural Heritage Applications

M. Inmaculada Gaona Fernández

DOCTORAL THESIS

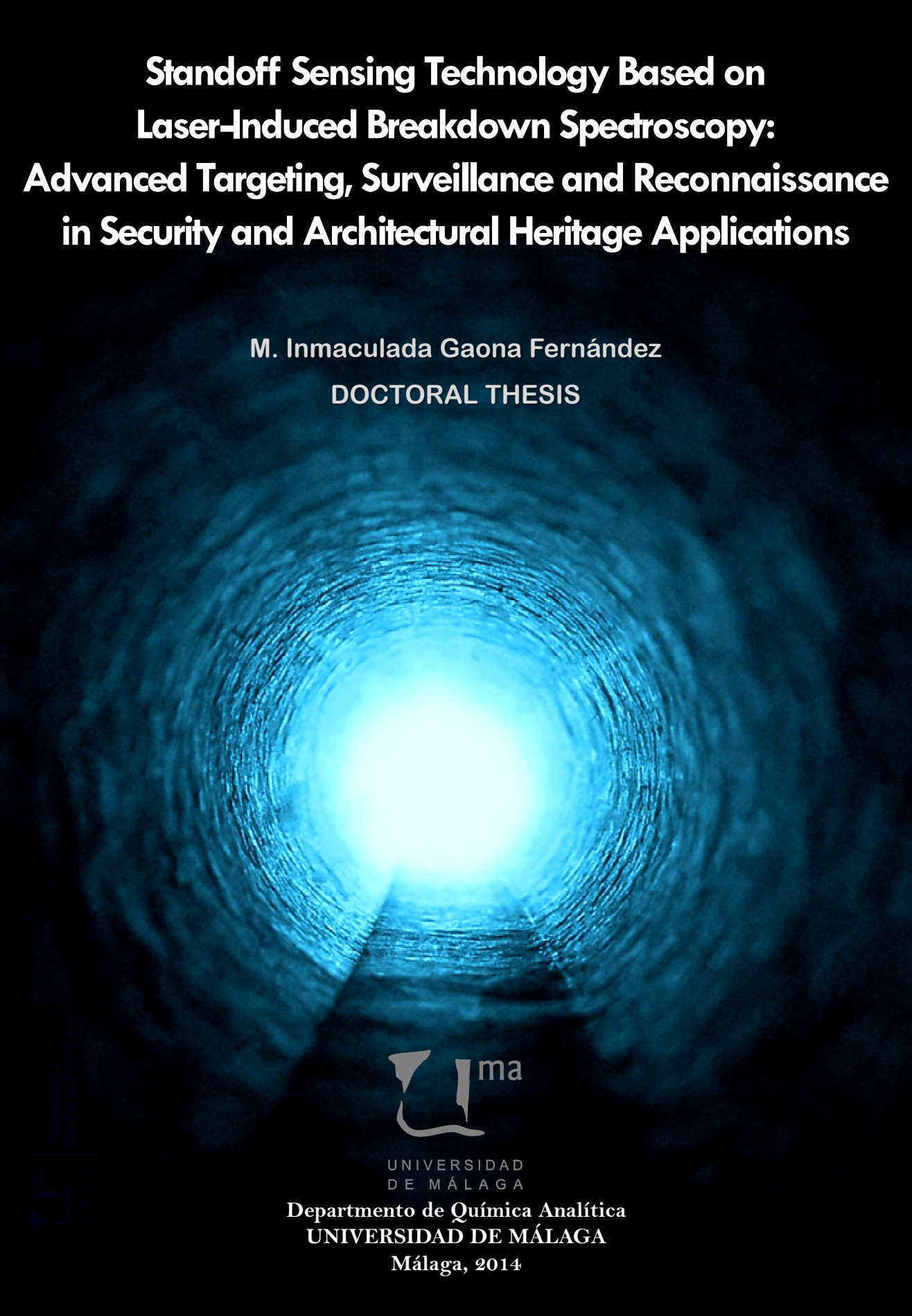

UNIVERSIDAD
DE MÁLAGA

Departmento de Química Analítica
UNIVERSIDAD DE MÁLAGA

Málaga, 2014

UNIVERSIDAD
DE MÁLAGA

Facultad de Química
Departamento de Química Analítica

Standoff Sensing Technology Based on Laser-Induced Breakdown Spectroscopy: Advanced Targeting, Surveillance and Reconnaissance in Security and Architectural Heritage Applications

Tesis Doctoral

M. Inmaculada Gaona Fernández

Málaga
2014

UNIVERSIDAD
DE MÁLAGA

Standoff Sensing Technology Based on Laser-Induced Breakdown Spectroscopy: Advanced Targeting, Surveillance and Reconnaissance in Security and Architectural Heritage Applications

by

M. INMACULADA GAONA FERNÁNDEZ

THESIS SUBMITTED IN PARTIAL FULFILMENT
OF THE REQUIREMENTS TO APPLY
FOR THE DEGREE OF DOCTOR IN CHEMISTRY

Department of Analytical Chemistry
University of Málaga
Málaga, Spain

2014

Standoff Sensing Technology
Based on Laser-Induced Breakdown Spectroscopy:
Advanced Targeting, Surveillance and Reconnaissance
in Security and Architectural Heritage Applications

por

M. INMACULADA GAONA FERNÁNDEZ

José Javier Laserna Vázquez
Catedrático de Universidad
Departamento de Química Analítica
Universidad de Málaga

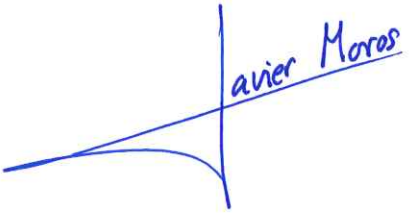

Javier Moros Portolés
Doctor en Química
Departamento de Química Analítica
Universidad de Málaga

Memoria de Tesis presentada para optar al Título de Doctor en Química

M. Inmaculada Gaona Fernández
Málaga, Mayo de 2014

JOSÉ JAVIER LASERNA VÁZQUEZ, Catedrático de Química Analítica de la Universidad de Málaga y **JAVIER MOROS PORTOLÉS**, Investigador Postdoctoral del Departamento de Química Analítica de la Universidad de Málaga,

CERTIFICAN

Que **Dña. MARÍA INMACULADA GAONA FERNÁNDEZ** ha realizado la presente Tesis Doctoral titulada "***Standoff Sensing Technology Based on Laser-Induced Breakdown Spectroscopy: Advanced Targeting, Surveillance and Reconnaissance in Security and Architectural Heritage Applications***" bajo su dirección en el Laboratorio Láser del Departamento de Química Analítica de la Universidad de Málaga y autorizan su presentación para optar al grado de Doctor en Química.

Y para que así conste a los efectos oportunos, firman la presente en Málaga, Mayo de 2014.

Prof. José Javier Laserna Vázquez

Dr. Javier Moros Portolés

DECLARATION

To certify that the work involved in this Doctoral Dissertation is based on original work done by me under the guidance of Prof. José Javier Laserna Vázquez and Dr. Javier Moros Portolés in the Laser Laboratory of the Department of Analytical Chemistry at the University of Málaga, and has not been included in any other Doctoral Thesis submitted previously for the award of any degree.

Málaga
May 2014

M. Inmaculada Gaona Fernández

CERTIFICATE

We certify that the research work presented herein is based on an original work conducted by Miss M. Inmaculada Gaona Fernández under our guidance in the Laser Laboratory of the Department of Analytical Chemistry at the University of Málaga, and it is not neither partial nor total part of any other Doctoral Dissertation previously submitted for the award of any doctorate degree.

Prof. José Javier Laserna Vázquez

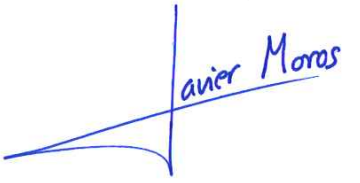

Dr. Javier Moros Portolés

AKNOWLEDGEMENTS

Como estudiante de doctorado el sacrificio y la constancia hasta concluir mis estudios no solo se deben a mi único esfuerzo, sino también a esas personas que con su apoyo me motivaron hasta lograr dicho objetivo con su ánimo y su paciencia. Mi más sincero agradecimiento a todos aquellos que siempre estuvieron ahí brindándome su ayuda.

En primer lugar, agradecer a Javier Laserna no solo el haberme permitido formar parte de este grupo de investigación y darme la oportunidad de descubrir todo este mundo, sino también la confianza que ha depositado en mí para la realización de este trabajo.

Un agradecimiento muy especial, ya que sin su colaboración quizás la realización de esta Tesis no habría sido posible, a Javier Moros, por haberme apoyado y orientado con tanto interés y entrega durante toda esta labor científica.

A Patricia Lucena agradecerle el que me haya ayudado y guiado durante mis primeros pasos dentro del laboratorio y gran parte de este trabajo.

A mis compañeros, a los cuales siempre recordaré con un especial cariño: Fran, Ángel, Tomás, Salva, Irene, Marina, Luisa, Diana, José Miguel, Carmen, Javier, Luciano, Juan Antonio, Alicia y Gabriel. Gracias por permitirme formar parte de vuestras vidas y por todos esos buenos momentos que hemos compartido durante estos años. Muy especialmente agradecerle a Jorge y Xavi todos esos buenos ratos que hemos pasado juntos, por estar siempre ahí con palabras de ánimo y sobre todo por su amistad.

También con todo el cariño, agradecer a toda mi familia, mis padres y mi hermana María Jesús, el apoyo y ayuda incondicional que siempre me han

ofrecido para que pudiera alcanzar mis metas. Gracias por toda la dedicación y el esfuerzo siempre mostrado para que yo pudiese salir adelante.

Al instituto de investigación *ENEA* en Frascati (Italia), por brindarme la oportunidad de trabajar con ellos durante mi estancia de investigación, especialmente a Violeta Lazic por su amabilidad y cortesía.

Al Ministerio de Economía y Competitividad, Secretaría de Estado de Investigación, Desarrollo e Innovación, por la concesión de la ayuda de formación para la investigación (FPI) a través del proyecto CTQ2007-60348 y con la cual ha sido posible realizar esta Tesis doctoral.

"*Si yo pudiera enumerar cuánto debo a mis grandes antecesores y contemporáneos, no me quedaría mucho en propiedad.*"

Johann W. Goethe

¡MUCHAS GRACIAS A TODOS!

This page is left blank intentionally

Table of Contents

Publicaciones y
Divulgación Científica

UNIVERSIDAD
DE MÁLAGA

Table of contents

Security & Forensics

This page is left blank intentionally

RESUMEN
(Spanish Summary)

Cumpliendo con el REGLAMENTO DE LOS ESTUDIOS DE DOCTORADO DE LA UNIVERSIDAD DE MÁLAGA, aprobado en el Consejo de Gobierno de la Universidad de Málaga de 9 de Octubre de 2012, y por el hecho de que la presente Memoria de Tesis Doctoral está íntegramente redactada en inglés, la siguiente sección incluye un resumen de la misma en español.

RESUMEN de la TESIS DOCTORAL

Dada la alta versatilidad que ofrece la espectroscopia de emisión asistida por láser (LIBS) en modo s*tandoff* para el análisis de objetivos distantes, el interés en el diseño y el uso de este tipo de sensores ha ido en aumento en los últimos años. Sus capacidades para realizar un análisis simultáneo, multielemental y en tiempo real de todo tipo de muestras sin ningún tratamiento previo, todo ello desde distancias de decenas de metros, hacen que *standoff* LIBS sea considerada hoy en día una tecnología analítica de vanguardia. Todos estos atributos han permitido su uso en una gran diversidad de campos de aplicación como la seguridad, el medio ambiente, la protección del patrimonio cultural y la exploración espacial, entre los más destacados. No obstante, la operatividad de esta técnica analítica a distancia entraña una mayor complejidad que su aplicación a escala de laboratorio.

Bajo estas premisas, en la presente Memoria de Tesis se han abordado desde los aspectos más fundamentales de la aplicación de *standoff* LIBS hasta su potencial para ser utilizada en situaciones en las que, por unos motivos u otros, el acceso del operador a la muestra es limitado o nulo, poniendo así de manifiesto su valía en la resolución de problemas reales.

- ***Aspectos fundamentales***

Principales causas que afectan a la incertidumbre de la señal analítica en la operación con LIBS en modo *standoff*.

A pesar del enorme potencial que muestra la técnica LIBS, existen aspectos de rendimiento que restringen su operación a distancia con respecto a su uso en contacto directo. En la presente memoria de Tesis, se aborda quizás uno de los temas más sensibles en este tipo de operaciones: la elevada variabilidad en la respuesta analítica registrada desde objetivos lejanos. Una circunstancia que, sin duda, puede deteriorar la selectividad y la sensibilidad de la respuesta analítica.

Para dilucidar las causas responsables de dicha variabilidad, se ha llevado a cabo una exhaustiva evaluación de las alteraciones sufridas por los pulsos láser tras su propagación a través de la atmósfera al llegar al objetivo, así como por las imágenes de los correspondientes plasmas inducidos. De este modo se analizan de forma aislada las variaciones en cada uno de los caminos ópticos.

En una escala microscópica, los pequeños gradientes de temperatura sobre la superficie terrestre causan movimientos atmosféricos aleatorios y cambios en su índice de refracción, por medio de pequeñas turbulencias instantáneas. Estas turbulencias inducen una serie de fenómenos en el haz láser durante su propagación, tales como *beam wander* (variaciones aleatorias en la posición del centroide del haz), *beam spreading* (dispersión del haz) y *scintillation* (centelleo causado por las fluctuaciones de intensidad en el frente de onda). Aunque estas alteraciones vacilantes que afectan al azar a la transmisión del pulso láser pueden surgir simultáneamente, no están necesariamente relacionadas.

En una primera investigación, se han evaluado las alteraciones sufridas por sucesivos pulsos láser tras propagarse una distancia de 30 metros en el interior de un túnel parcialmente cerrado. Para ello, ayudados con un analizador de haz (*beam profiler*) situado en el objetivo, se monitorizaron diversas propiedades de un total

de 500 pulsos láser, tales como su posición –respecto a un punto de referencia marcado por el primer pulso–, su energía y su tamaño.

Los resultados de esta prueba han mostrado que, aunque los movimientos turbulentos a pequeña escala son estadísticamente isotrópicos (sin una dirección espacial preferente), los sucesivos pulsos láser exhiben un desplazamiento continuo y aleatorio en ambas direcciones sobre la superficie impactada. No obstante, se ha observado que las perturbaciones a lo largo del eje horizontal (12%) son mayores que las que se producen en la dirección vertical (5%). Este comportamiento se justifica por la geometría del experimento, en el que el haz se transmite en paralelo a la superficie del suelo, y por lo tanto experimenta un mayor desplazamiento en la dirección horizontal a causa de la trayectoria preferencial de las corrientes de convección en el interior del túnel de experimentación. Pese a estos cambios en el posicionamiento de los pulsos láser, su energía al alcanzar el objetivo se mantiene prácticamente inalterable (una variabilidad de apenas un 5%). No obstante, los sucesivos pulsos láser sufren cambios más significativos en su correspondiente diámetro efectivo (variabilidad de un 10%), un efecto que está estrechamente relacionado con el fenómeno de la dispersión del haz. Esta circunstancia conduce a variaciones (15%) en la energía por unidad de área (*irradiancia*) de los pulsos láser y, como consecuencia, en las propiedades de los sucesivos plasmas inducidos. Unas variaciones, que es de esperar, sean propagadas hasta la emisión óptica final.

Paralelamente, se ha evaluado la luz emitida por 500 plasmas inducidos consecutivamente sobre aluminio al ser colectada desde la distancia por el sensor utilizando el analizador de haz como dispositivo receptor. En esta ocasión se monitorizaron también propiedades de dichas imágenes tales como, su posición, su luminosidad (flujo radiante) y sus dimensiones. Los resultados de esta investigación han revelado que, aún recorriendo un camino óptico idéntico, el posicionamiento de las imágenes colectadas se mantiene prácticamente uniforme en ambos ejes (variabilidades de apenas un 0,2%). A pesar del desplazamiento posicional para la

incidencia de los pulsos láser en el objetivo, este hecho no parece tener repercusiones en el posicionamiento de la imagen del plasma en el dispositivo receptor. Esta circunstancia se justifica por las características particulares de la unidad utilizada para la captación de la luz (telescopio *Cassegrain*). De forma similar, tampoco se ha detectado una variación significativa (4%) en las dimensiones de las imágenes de los plasmas.

Por el contrario, en cuanto a los parámetros radiométricos de las imágenes del plasma se refiere, se han observado fluctuaciones significativas (variabilidad de un 10%) y aleatorias para el flujo radiante de las imágenes de plasma. Dichas variaciones se derivan del carácter fluctuante de los plasmas formados, como consecuencia de las oscilaciones en el nivel de *irradiancia* que alcanza el objetivo descritas anteriormente. Esta circunstancia se traduce en una fluctuación de orden similar –17%– de la *irradiancia* de los plasmas (utilizada como un indicador del nivel de luz emitida). Por ello, se puede establecer que son las propias alteraciones en la densidad de energía por unidad de área que ocurren en el objetivo, las que se reflejan en la imagen recogida. En definitiva, que la imagen del plasma no sufre ningún tipo de alteración al ser colectada.

Finalmente, con el fin de confirmar cualquier influencia de factores atmosféricos sobre la señal luminosa en su retorno, se han tomado mediciones sincronizadas de la emisión óptica de sucesivos plasmas desde unos centímetros de los mismos junto con las intensidades de sus correspondientes imágenes desde el sensor emplazado a 30 m del objetivo. De esta forma, mientras que las alteraciones observadas cerca del objetivo se asocian con distorsiones sufridas por los pulsos láser en su transmisión, las perturbaciones percibidas desde el sensor se corresponden con fluctuaciones sufridas por las imágenes de los plasmas durante su colección. Si bien ambas señales no pueden compararse rigurosamente por las diferencias en los sistemas de colección utilizados, los resultados han revelado una

correlación directa entre la variabilidad de las intensidades de emisión de los plasmas inducidos y sus correspondientes imágenes colectadas por el sensor.

Con ánimo de ampliar las evaluaciones sobre la distorsión de los pulsos láser, se han llevado a cabo estudios similares en campo abierto y a distintas distancias entre el sensor y el objetivo. Los resultados de esta experimentación han revelado que, independientemente de la distancia a la que este emplazada la muestra (en un rango entre 30 m y 90 m), la cantidad de energía para los pulsos láser se mantiene prácticamente constante; con una variabilidad inter-rango de no más de un 2%. Paralelamente, las medidas del tamaño de las huellas dejadas por los pulsos láser a estas distancias han mostrado un aumento lineal con el incremento del rango de trabajo. Además, con el aumento de la distancia de operación, se ha observado una creciente dispersión en la distribución de la energía de los pulsos láser como consecuencia del mayor recorrido para la propagación del haz. Por ello, en ausencia de efectos atmosféricos severos que puedan atenuar el haz láser, es ésta creciente y aleatoria variabilidad en la distribución de energía la causa responsable de las fluctuaciones de la *irradiancia* que actúa en el objetivo. Unas fluctuaciones que son mayores a medida que aumenta la distancia sensor-muestra, y que revierten directamente en una baja repetitividad de las emisiones ópticas registradas.

La contribución de todos estos efectos ha revelado una disminución de la señal LIBS con el inverso de la cuarta potencia de la distancia a la par que un aumento progresivo en la variabilidad de dicha señal con el incremento de la distancia, causada principalmente por la disminución, y por la alteración aleatoria cada vez mayor, de la irradiancia sobre los objetivos cada vez más distantes.

- ***Aplicaciones standoff LIBS***

Tras analizar detalladamente el coste, desde un punto de vista analítico, que implica la operatividad con la técnica LIBS a distancia, se ha evaluado su potencial para ser utilizada en distintas aplicaciones del mundo real.

1. Evaluación del patrimonio histórico

I. Sondeo multielemental en la Catedral de Málaga

El patrimonio cultural es un valioso recurso y un legado único de nuestro pasado. Ya se trate de objetos, monumentos o lugares arqueológicos, todos ellos informan y ayudan a conectarnos con nuestros orígenes culturales. Es por tanto, un insustituible tesoro digno de ser conservado. Por desgracia, la rápida y continua evolución de la sociedad ha provocado un gran deterioro en ellos. Tanto los efectos antropogénicos como los derivados de causas naturales, pueden ocasionar deterioro en el patrimonio cultural. Esto ha provocado un creciente interés científico por su conservación y protección frente a posibles daños causados por la contaminación.

La disponibilidad de información analítica sobre dicho patrimonio resulta fundamental para acometer cualquier tipo de prevención previa que evite su deterioro así como para diseñar planes posteriores para su limpieza. Sin embargo, la evaluación científica de este tipo de materiales demanda requisitos analíticos muy particulares. Uno de ellos es que ninguna modificación significativa o alteración se produzca sobre el objeto, evitando así comprometer su valor. Además, si bien en ocasiones las obras de arte pueden trasladarse al laboratorio para su análisis, en otros casos esta opción resulta inviable. Por ello, la capacidad de trabajar *in situ* y en tiempo real es a menudo necesaria. Finalmente, la compleja o limitada accesibilidad del operador hasta el objeto de análisis hace inservibles prácticamente la inmensa mayoría de técnicas de análisis convencionales. Estas circunstancias requieren de tecnologías analíticas capaces de operar a distancia, de forma rápida, con sensibilidad adecuada, y todo ello sin causar daños al material. En definitiva, un escenario propicio para *standoff* LIBS.

Así pues, por primera vez se ha utilizado un sistema *standoff* LIBS para caracterizar la composición de los materiales de construcción, así como su

contaminación, en uno de los monumentos arquitectónicos más emblemáticos del renacimiento en Andalucía como es la Catedral de Málaga. En concreto, se ha realizado un análisis multielemental sobre los diferentes materiales que componen la fachada principal: arenisca (que integra prácticamente la totalidad el cuerpo principal de la fachada), diferentes tipos de mármoles (empleados para las esculturas y numerosos detalles arquitectónicos), así como ornamentos metálicos.

Caracterización multielemental de la composición de los materiales

Con el objetivo de evaluar la composición química de la arenisca, se ha realizado un barrido superficial, con una resolución lateral de 2 cm, de una sección de 40 cm × 40 cm sobre de una de las cornisas, situada a 35 m del sensor LIBS. Los mapas químicos derivados de dicho análisis han revelado emisiones atómicas intensas de Si, Al, Ca y Mg junto con otras más débiles de Mn, Sr y Fe. Unos resultados que encajan perfectamente con la descripción mineralógica del material, identificado como una arenisca intermedia constituida por *protocuarcitas* y *subarcosas*, que están compuestas de cuarzo (70–90% SiO_2), feldespatos [$M(Al_xSi_yO_8)$] y dolomita (5–25% [$CaMg(CO_3)_2$]).

También se ha caracterizado la composición de las secciones de mármol más significativas dentro de la escena escultórica central que adorna la fachada. Esta sección está compuesta por tres tipos de mármoles, fácilmente distinguibles por sus colores blanco, rojo y negro relacionados con su distinta procedencia.

Si bien todas las respuestas de emisión de los mármoles están dominadas por emisiones de Ca junto con pequeñas contribuciones de Al y Ti, se han detectado distintos aportes de Mg y Sr en cada uno de ellos. Estas características distintivas permiten no sólo distinguir composicionalmente los mármoles, sino también aventurar su posible origen desde las distintas canteras de Málaga de acuerdo con su geología. Así pues, es posible sugerir que el mármol blanco procede de alguna cantera dolomítica cercana (Monda, Coín, Mijas o Alhaurín de la Torre), mientras

que los mármoles negros y rojos pueden provenir ambos de Alhaurín el Grande, dónde se ubica la cantera más cerca que únicamente proporciona materiales calcíticos. Finalmente, las reducidas diferencias en el análisis de otros mármoles emplazados en diferentes secciones han permitido establecer que los mármoles del mismo color aparentan tener un mismo origen.

Finalmente, se ha interrogado la composición de un par de detalles metálicos. Como se ha observado, mientras uno de ellos está constituido exclusivamente por Pb, el otro se corresponde con una aleación de Cu-Pb comúnmente llamada *molybdochalkos* (95% Cu/5% Pb) o viejo metal griego, muy utilizada durante la época renacentista. El empleo de un material más maleable, como el Pb puro, o un material más rígido, como la citada aleación, se justifica en base a los requerimientos de cada ornamento.

Caracterización multielemental de la contaminación de los materiales

El impacto de la contaminación del aire durante el transcurso de los años daña severamente los materiales de construcción. En ambientes urbanos, los contaminantes atmosféricos más preocupantes como, SO_2, SO_4^{2-}, NO_x, NO_3^-, Cl^-, CO_2, O_3.... provienen en gran parte de las emisiones de los vehículos. Además, las piedras calizas y los metales son unos materiales altamente sensibles a este tipo de contaminantes. Así pues, se han abordado distintas evaluaciones en aras de obtener una rápida información *in situ* sobre el perfil de la contaminación, tanto a corto como a largo plazo, de los materiales caracterizados anteriormente.

En primer lugar, para caracterizar la contaminación a corto plazo se ha ejecutado la valoración de la polución discreta sobre los ornamentos metálicos. La evaluación espectroscópica ha revelado la presencia de elementos contaminantes, a saber, Mg, Fe, Si, Ca, Al, Ti, Mn y Sr. Estos resultados sugieren que, además de los elementos omnipresentes principalmente debido al material particulado que arrastra viento que sopla desde la costa cercana (Mg, Si, Ca, Al, y Sr), también están

involucradas en la contaminación fuentes antropogénicas (Fe, Ti, y Mn) derivadas de la emisión de los motores del tráfico rodado de las zonas urbanas.

En segundo lugar, para evaluar la contaminación a largo plazo se han analizado los depósitos de polvo acumulados en diferentes detalles decorativos con relieves pronunciados y geometría compleja. La información espectroscópica del depósito acumulado sobre una de las columnas de mármol de la fachada ha revelado la presencia de Fe, Si, Mn, Pb y Ba, junto con un aporte adicional de Al, Ti, Mg y Sr (elementos que constituyen su composición original). En definitiva, un depósito formado por la acumulación de elementos derivados de las mismas fuentes citadas anteriormente. Además, esta información espectroscópica obtenida desde la distancia encaja perfectamente con la obtenida por otra técnica analítica (espectroscopia de emisión óptica de plasma acoplado inductivamente –*ICP-OES*–) utilizada para evaluar dicho depósito en el laboratorio.

Finalmente se ha valorado el patrón de comportamiento de estos contaminantes a través un perfil en profundidad por la actuación de 500 pulsos láser sucesivos sobre dos secciones de dicha columna de mármol. La información espectroscópica obtenida para las secciones "*sin*" y "*con*" depósito visible de polvo se ha evaluado en base a la relación de intensidad de cada elemento contaminante con respecto al elemento mayoritario en el mármol, el Ca.

De este modo, en el caso de la sección "sin" depósito aparente de polvo las relaciones de Al/Ca (0,43) y Ti/Ca (0,52) han mostrado valores promedio en torno a 0,5, mientras que las proporciones para los restantes contaminantes se han establecido próximas a 0, debido a su ausencia en la mencionada sección. Hay que mencionar que cualquier destaque hacia mayores valores de estas relaciones está atribuido al efecto conjunto de contaminación discreta depositada sobre la superficie del mármol y la incidencia de los pulso láser en posiciones nuevas como consecuencia del fenómeno de *beam wander* anteriormente comentado. Por el contrario, en el caso de la sección "con" depósito los valores de las relaciones Al/Ca

y Ti/Ca han mostrado cambios sustanciales, incrementándose su valor promedio hasta 0,63 y 0,72, respectivamente.

Estas mismas proporciones han sido cuantificadas a partir de la información espectroscópica obtenida de un adorno formado por los tres tipos de mármol (blanco, rojo y negro) y emplazado en una zona más protegida de la fachada. Se ha encontrado pues, que las relaciones de intensidad Al/Ca y Ti/Ca, aún siendo similares para estos tres mármoles, difieren con respecto a las anteriores. Esta circunstancia evidencia como el nivel de contaminación cambia de una zona a otra en función de la mayor o menor exposición a las inclemencias meteorológicas. Además, en el caso del mármol blanco se ha evidenciado una caída sustancial en los valores de ambas relaciones a medida que los pulsos láser profundizan más en la muestra. Esta circunstancia indica una disminución de los contenidos de Al y Ti con respecto al Ca, lo que sugiere que estos dos elementos pueden ser contaminantes relevantes incrustados en la superficie. Al mismo tiempo, este comportamiento dispar entre el mármol blanco y los mármoles rojo y alude a una mayor estabilidad de las incrustaciones en las superficies de estos últimos. Este hecho encaja perfectamente con el mayor efecto que causa la sulfatación en mármoles calcíticos que en dolomíticos.

En resumen, todas estas investigaciones reflejan claramente el enorme potencial de la técnica *standoff* LIBS para la caracterización multielemental completa del patrimonio histórico, ya sea de su composición o de su contaminación, tan sólo disponiendo de una clara línea de visión hasta el objetivo.

2. Anticipación de amenazas y evaluación de evidencias forenses

I. Localización y detección distante de huellas dactilares de explosivos

En los últimos tiempos, numerosos ataques terroristas lanzados indiscriminadamente hacia objetivos militares y la población civil han dejado claro que la detección de explosivos requiere una especial atención. A pesar de las numerosas estrategias desplegadas en estos últimos años para hacer frente a este asunto, la tecnología LIBS, por sus atributos operacionales, ha llegado a ser una herramienta atractiva para anticipar este tipo de amenazas.

Tras la manipulación de una sustancia, las manos de un operador pueden quedar contaminadas con residuos de dicha sustancia, que posteriormente pueden ser transferidos en forma de impresión sobre aquellas superficies con las que el operador tenga contacto directo. Las características de este residuo dependen de un gran número de factores como, su naturaleza, la presión ejercida para su deposición, el sustrato donde se deposite, las condiciones ambientales, etc. Todo ello conduce a variaciones en un amplio rango en las propiedades del residuo, tales como sus dimensiones superficiales, su espesor, así como su masa y homogeneidad en su distribución.

Así pues, se ha llevado a cabo una estimación de la concentración superficial de algunos materiales energéticos a partir de sus correspondientes deposiciones dactilares sobre superficies de vidrio. Independientemente del explosivo considerado, para todas las impresiones dactilares se han encontrado pesos inferiores a 1 mg, aunque con una variabilidad de hasta el 50%. Esta circunstancia evidencia la elevada heterogeneidad de este tipo de huellas. Como consecuencia de todo esto, la detección de residuos dejados por huellas dactilares humanas contaminadas de explosivo se convierte en todo un desafío analítico para LIBS, ya que en ocasiones ni siquiera es posible adquirir información espectral relacionada, máxime cuando se pretende hacerlo desde la distancia.

En este sentido, se ha evaluado la capacidad de *standoff* LIBS para localizar y detectar residuos de huellas dactilares de explosivos desde una distancia de unos 30 m a partir de la exploración láser de superficies.

Para ello, se han depositado varias huellas dactilares de residuos explosivos, tanto orgánicos (*DNT, TNT*, *RDX* y *PETN*) como inorgánicos (*cloratita*), sobre superficies de aluminio y vidrio situadas a unos 30 m de distancia del sensor. A partir de la información espectral derivada de la interrogación láser, se han construido mapas químicos de distribución de tales residuos. Estos mapas de distribución se basan en emisiones de Na y CN que caracterizan al explosivo *cloratita* y los residuos orgánicos, respectivamente. Así pues, sólo aquellos pulsos láser que impactan sobre la huella revierten en dicha señal de emisión característica, de mayor o menor intensidad según la cantidad de analito presente. La especificidad de estas señales a la presencia del residuo se ha corroborado a partir de la interrogación de superficies simplemente contaminadas por mera manipulación sin haber tenido contacto previo con los explosivos. Los resultados han demostrado que mientras la manifestación de la emisión de CN si atiende exclusivamente a la presencia de una traza orgánica, la presencia de la señal de Na puede deberse a un solo contacto del operador con la superficie, o bien a una contaminación ambiental. Sin embargo, estas emisiones de Na se han observado bastante inferiores con respecto a las vinculadas a la presencia de una huella de *cloratita*.

Junto con la cantidad de residuo depositada a partir de una huella dactilar, la homogeneidad en su distribución también resulta un factor crítico para su localización y detección. En este sentido, la probabilidad de localizar una huella sobre una superficie queda estrechamente ligada a la resolución con la que se interroga la superficie. La definición del contorno de la huella y la distribución del residuo dentro de ella resultan mucho mejores cuando se aumenta la resolución del interrogatorio, es decir, el área se examina con una mayor densidad de pulsos láser.

No obstante, una resolución excesivamente grande puede encaminar a resultados erróneos cuando se existe una proximidad innecesaria o un solapamiento entre los eventos láser, por la información espectral alterada que puede derivarse de estas situaciones.

Por tanto, se ha tratado de valorar el impacto que tiene este parámetro operacional en la localización y detección de huellas dactilares. Para tal fin, sobre la base de plantillas idénticas de huellas dactilares en una superficie de Al (9 huellas en una área de 81 cm^2) y vidrio (3 huellas en un área de 30 cm^2) se han realizado exploraciones bidimensionales con diferentes resoluciones de pulsos láser. Sobre la base de estos escaneos, se han computado una serie de estadísticas de detección para cada resolución en términos del número de pulsos láser que han impactado en las distintas huellas y que proporcionan, a partir de su información espectral, una lectura positiva sobre la presencia de la misma, así como el porcentaje de huellas localizadas. Los resultados han puesto de manifiesto que, independientemente del residuo y de la superficie que se traten, una resolución lateral de 10 mm permite detectar con una fiabilidad del 100% todas las huellas dactilares que se encuentran en el área interrogada. Es necesario indicar en este punto que la resolución lateral del sensor *standoff* LIBS utilizado para estas pruebas está limitada a un valor mínimo de 1,5 mm, que se corresponde con el diámetro del pulso láser cuando se enfoca a una distancia de 30 m.

Finalmente, se ha evaluado otro factor importante en la detección de residuos explosivos en situaciones reales, como es la sensibilidad de la respuesta de emisión de huellas dactilares depositadas que han ido envejeciendo y han estado expuestas al efecto de la contaminación ambiental, circunstancias que pueden provocar la desaparición de la huella o un enmascaramiento de la misma. Para este ensayo, se han preparado una serie de placas de aluminio (4 × 4 cm^2) sobre las que se ha depositado una huella dactilar del explosivo *cloratita*. Las muestras se han almacenado en una instalación parcialmente cerrada, de fácil acceso para la

contaminación del medio ambiente pero fuera del alcance de la acción del viento o la lluvia, por un periodo máximo de 30 días. Durante estos días, la temperatura ha fluctuado entre los 18 y 24 grados centígrados, mientras que la humedad relativa ha oscilado entre 45% y 60%. Paralelamente, dado que el experimento se ha realizado en un área cerca de la costa marina, pudiéndose depositar sobre las muestras sales mediante aerosoles procedentes del agua del mar, dos placas-control de aluminio, exentas de residuo forzado, han sido sometidas al mismo ambiente. Estas muestras de control nos han permitido establecer el valor umbral de Na procedente partículas atmosféricas. Valores por encima de este umbral deben ser necesariamente debidos a la huella dactilar explosiva.

Posteriormente, se ha realizado una prueba de detección ciega utilizando 36 pulsos láser sobre las huellas explosivas sometidas a distintos días de exposición ambiental. Para una mejor evaluación de la respuesta LIBS de las huellas de cloratita depositadas sobre las placas de aluminio expuestas a la contaminación, se ha considerado la relación de intensidades de emisión Na/Al, vinculadas a las respuestas respectivas de las partículas de residuos (huella dactilar cloratita y/o partículas atmosféricas) y la superficie donde se depositan.

Los resultados muestran como, para muestras sometidas a un mayor número de días de exposición, el contenido de Na total en la muestra aumenta por la mayor acumulación de partículas ambientales sobre la huella explosiva. No obstante, en ellas es cada vez más complejo encontrar un valor de relación Na/Al a lo largo de los 36 posiciones interrogadas que difiera significativamente del valor umbral definido por las muestras-control. Por tanto, siendo siempre conscientes de la influencia de las condiciones atmosféricas que acontecen y a tenor de lo expuesto, se puede concluir que, la sensibilidad de la técnica LIBS para la localización y detección de huellas explosivas distantes prevalece durante un cierto período de tiempo.

II. Identificación de residuos explosivos

Para estos escenarios extremos, aunque la operación en *standoff* ofrece ventajas de seguridad, la complejidad en su uso es más que evidente. Pese a la eficacia de la técnica LIBS en la localización y detección de trazas explosivas localizadas a una determinada distancia, una de las principales complicaciones radica en la capacidad de identificación cuando se trata de trazas orgánicas debido a la similitud de sus respuestas analíticas, como consecuencia de su composición elemental similar. Así pues, para hacer frente a esta reducida selectividad, son necesarias herramientas matemáticas (algoritmos quimiométricos) que ayuden a extraer la máxima información posible de los datos analíticos disponibles y permitan distinguir entre residuos explosivos y trazas innocuas.

Aunque diferentes enfoques quimiométricos aplicados a las emisiones ópticas han permitido abordar con eficacia la clasificación de datos tomados a distancia, su operatividad es limitada. Dado el carácter multifactorial de la respuesta *standoff* LIBS, puesto que la intensidad de emisión se ve afectada principalmente por la distancia sensor-muestra y el nivel de *irradiancia* en el objetivo, la efectividad de los modelos diseñados a partir de estos enfoques sólo puede garantizarse para aquella información que ha sido adquirida en condiciones operativas totalmente coincidentes con las utilizadas para obtener la información empleada en el modelado. De lo contrario, el etiquetado incorrecto de la muestra está más que garantizado.

Por este motivo, se ha afrontado el diseño de un modelo de clasificación que, más allá de resultar útil únicamente a unas condiciones (distancia e *irradiancia*) operativas concretas, pueda flexibilizarse para operar sobre información adquirida en otras circunstancias.

Para ello, haciendo uso de las técnicas de aprendizaje máquina (utilizadas por primera vez para información tomada con una configuración *standoff* LIBS), se ha tratado de diseñar e implementar un algoritmo quimiométrico capaz de distinguir,

para distintas situaciones operativas, residuos orgánicos de explosivos (*DNT*, *TNT*, *RDX* y *PETN*) de trazas de productos de uso diario (potenciales confusantes) como aceite de oliva, aceite de motor, crema de manos, gasolina y cera de coche.

Previamente se ha caracterizado la información espectral (obtenida desde una distancia de 30 m y con una *irradiancia* de 8,2 GW cm^{-2}) de todas estas trazas orgánicas, cuando se localizan sobre una superficie de aluminio en aras de identificar cuáles son las emisiones ópticas disponibles para afrontar la identificación de las mismas. Más allá de las señales relacionadas con el soporte, se ha observado que, mientras la banda de emisión asociada al fragmento CN se pone de manifiesto, la señal atribuida al grupo C_2 queda enmascarada por señales vinculadas al óxido de aluminio (Al_mO_n). Junto con estas señales, también se han reconocido emisiones atómicas asociadas a H_α, N y O. Sin embargo, estas emisiones no pueden considerarse ni distintivas ni exclusivas de la presencia de trazas de orgánicos; su aparición en la respuesta espectral del sustrato de aluminio sin residuo indica que su procedencia está relacionada con la atmósfera circundante. No obstante, como los efectos en el ambiente envolvente están estrechamente relacionados con las trazas que se están interrogando, estas emisiones atómicas pueden resultar provechosas de forma indirecta en la identificación de las mismas.

Una vez establecidas las señales de emisión útiles –CN, H_α, N, y O– para afrontar la identificación, se ha procedido a dilucidar cuales de ellas resultan más funcionales para categorizar los residuos orgánicos. Para ello, las citadas emisiones (intensidad original de las líneas, sin ningún tipo de pre-procesado matemático) procedentes de todos y cada uno de los residuos sobre aluminio, se han representado gráficamente de forma combinada en diagramas de dispersión n-dimensionales. A partir de los gráficos construidos, se ha computado un estimador denominado región discriminatoria residual (*RDR*) basado en las respectivas dimensiones de las nubes de datos asociadas a cada tipo de residuo, de acuerdo con su peligrosidad, y su grado de solapamiento. Este parámetro permite identificar

de una forma rápida, que tipo de gráfico (o en definitiva que combinación de variables espectrales) ofrece las máximas diferencias entre los dos tipos de residuos, explosivos e innocuos. Este estimador abarca un rango de valores entre 0 (cuando las nubes de datos son totalmente diferenciables) y 2 (cuando las nubes de datos están completamente solapadas y resultan indistinguibles).

De entre todos los gráficos construidos, se ha encontrado que el más útil para diferenciar los residuos de acuerdo con su peligrosidad corresponde con el diagrama tridimensional que implica las emisiones de CN, H_α y O. Este diagrama ofrece una descripción muy completa del comportamiento del residuo frente a la radiación. Por un lado, la señal de CN informa sobre su patrón de fragmentación durante la ablación, mientras que las emisiones de H_α y O advierten del efecto del plasma de dicha traza sobre el aire que lo rodea.

A continuación, sobre este subespacio de dispersión, se han diseñado y evaluado varios clasificadores (funciones matemáticas que actúan como frontera de separación) que permiten etiquetar una nueva traza como peligrosa o innocua en base a la ubicación espacial de la coordenada generada a partir de sus emisiones implicadas. Aunque la exactitud y la precisión de todos los clasificadores diseñados se han encontrado en torno al 90% y al 80%, respectivamente, los resultados han puesto de manifiesto que el mejor modelo para evaluar la naturaleza de las trazas orgánicas consideradas es un clasificador basado en mezclas Gaussianas (*mogc*), que ofrece tasas de falsos positivos y falsos negativos de 8% y 3%, respectivamente. Esto implica que solo algunos de los residuos inofensivos son identificados como casos de riesgo, mientras que son muy pocas las trazas explosivas que pasan desapercibidas.

Una vez materializado este modelo supervisado para etiquetar la naturaleza peligrosa de los residuos a unas condiciones de operatividad, se ha considerado la posibilidad de transferir su utilidad a nuevas circunstancias de análisis.

Para ello, tomando como punto de partida el clasificador original (r_0= 30 m, I_0= 8,2 GW cm^{-2}), se pretende abordar la identificación de un objetivo bajo nuevas condiciones ($r_0+\Delta r$, $I_0-\Delta I$) mediante una auto-adaptación. Este proceso consiste en transferir el modelo de clasificación a las nuevas condiciones mediante la corrección de los coeficientes de su hiperplano a la nueva situación, como indican las siguientes expresiones matemáticas:

$$f(x,y,z) = \left(x^a + y^b + z^c + D\right)_{r_0,\, I_0} \qquad \text{(hiperplano original)}$$

$$\left(x^a + y^b + z^c + D\right)_{(r_0+\Delta r,\, I_0-\Delta I)} = \frac{\left(x^a + y^b + z^c + D\right)_{r_0, I_0}}{\left(\frac{r_0 + \Delta r}{r_0}\right)^n} \qquad \text{(hiperplano adaptado)}$$

Es necesario resaltar que la adaptación del hiperplano es cambiable de acuerdo con las características del sensor *standoff* LIBS utilizado. Como ya se ha comentado anteriormente, para el caso particular de nuestro sensor, un incremento del rango de trabajo lleva implícita una disminución de la *irradiancia* que alcanza el objetivo, debido a una mengua en la capacidad de enfoque. No obstante, pueden encontrase situaciones en las que la operatividad del sensor a diferentes distancias no distorsione dicha capacidad de enfoque. De acuerdo con ello, el rango de valores que *n* puede adoptar abarca desde 2 hasta 4. En este sentido, un valor de 2 implica una preservación del nivel de irradiancia al cambiar la distancia (corrige la atenuación en la luz emitida sólo debido al incremento en el rango de operación). Por el contrario, un valor de 4 modifica los coeficientes del hiperplano cuando acontecen simultáneamente los dos pretextos. En la presente investigación, se ha abarcado un rango de distancia desde 30 m hasta 50 m. Dicho aumento en la distancia sensor-muestra conlleva un incremento en el diámetro del haz láser desde 1,5 mm hasta 3,8 mm y su correspondiente disminución implícita

en el nivel de irradiancia desde 8,2 GW cm^{-2} hasta 1,3 GW cm^{-2}. Por tanto, *n* adopta el valor de 4.

En base a todas estas consideraciones, se ha adaptado el modelo supervisado (hiperplano original diseñado para 30 m) para interrogar residuos sobre superficies de aluminio situadas a 40 m y 50 m, mediante sendos modelos semi-supervisados de clasificación. En estas condiciones, si bien las emisiones ópticas de las trazas son mucho menos intensas, su comportamiento relativo mantiene un patrón bastante similar.

A través de parámetros de rendimiento, tales como exactitud, precisión y tasas de error, los resultados han mostrado cómo la eficacia en la categorización de los residuos se degrada considerablemente cuando el modelo supervisado se utiliza para evaluar información adquirida bajo otras condiciones. Por el contrario, si se hace uso de un modelo adecuadamente adaptado (semi-supervisado) a las nuevas circunstancias, el rendimiento de la identificación en términos de exactitud y precisión se preserva, sin aumentar significativamente las tasas de falsos negativos y falsos positivos. Pese a que las diferencias dentro de las respuestas de emisión de los residuos son mucho menores cuanto más alejado está el escenario de análisis, los modelos adaptados sustentan una fiabilidad en la identificación de cerca del 95%.

Estos hallazgos reflejan, no solo el enorme potencial de esta nueva estrategia para identificar desde la distancia residuos orgánicos sobre superficies de aluminio de acuerdo con su peligrosidad, sino también su versatilidad para afrontar dicha operación en base a la respuesta de emisión transitoria asociada a *standoff* LIBS.

III. Detección de amenazas radiológicas

Si bien los materiales radiactivos son hoy en día una herramienta valiosa en casi todos los campos de la ciencia y la tecnología moderna, es más que evidente la peligrosidad que entraña su dispersión, ya sea por causas naturales o de forma

malintencionada ("*bombas sucias"*). Por ello, al igual que la detección e identificación de explosivos, su monitorización, categorización y cuantificación desde una situación segura, es también una aplicación demandada en lo que atañe a la seguridad. El desarrollo de tecnologías rápidas y eficientes para controlar y hacer frente a los riesgos que implica una contaminación de este tipo, es de crucial interés, y en este sentido, *standoff* LIBS presenta las virtudes necesarias para hacer frente a estas demandas.

Así pues, se han evaluado las capacidades que ofrece *standoff* LIBS para detectar, caracterizar y cuantificar elementos radioactivos a partir de la interrogación láser desde la distancia (30 m) de diversos objetos vinculados con el mobiliario urbano.

La capacidad para detectar y caracterizar cualquier tipo de residuo está vinculada a la composición de la superficie sobre la que se encuentra, ya que ambos son ablacionados por el pulso láser y participan de la composición global del plasma producido. Por ello, la primera investigación ha ido dirigida a establecer la selectividad de la técnica para este cometido. Para ello, se han evaluado las respuestas de emisión óptica de una variedad de sustitutos radiactivos, como ^{59}Co, ^{88}Sr, ^{130}Ba, ^{133}Cs, ^{193}Ir y ^{238}U, cuando se encuentran depositados en forma de residuo sobre superficies de aluminio, arcilla, hormigón y vidrio, ubicadas a 30 m de distancia. Los resultados han evidenciado que, si bien algunas de las señales espectrales asociadas a los sustitos radioactivos pueden estar enmascaradas, en mayor o menor medida, por las correspondientes características espectrales de la superficie dónde se encuentran, al menos es posible en todas las situaciones evaluadas disponer de una señal distintiva libre de interferencias que permite la detección y caracterización del analito de interés.

Debe mencionarse que, las señales espectrales de algunos de los analitos evaluados, como el ^{88}Sr y ^{130}Ba cuando se encuentran en una superficie de aluminio, han puesto de manifiesto la formación de óxidos, (Sr_mO_n y Ba_mO_n) por medio de

bandas de emisión relacionadas. Por el contrario, analitos como el ^{59}Co e ^{193}Ir en esta misma superficie no manifiestan emisiones de sus correspondientes óxidos, aunque también pueden formarlos, pero si revelan bandas de emisión asociadas al óxido de aluminio (Al_mO_n). Finalmente, en el caso del ^{133}Cs y el ^{238}U, las bandas de emisión de sus respectivos óxidos, Cs_mO_n y U_mO_n, están acompañadas por emisiones de Al_mO_n.

Estas situaciones se justifican por la menor o mayor afinidad de los analitos por el oxigeno atmosférico y su consiguiente reacción menos o más favorecida termodinámicamente para formar los óxidos. Es necesario comentar que, si bien las manifestaciones de las emisiones asociadas a estos óxidos conducen a una alteración general de los espectros de los elementos, su aparición puede resultar en un indicador exclusivo de la presencia de un elemento en particular.

Una vez establecida la capacidad de detección, se ha examinado la sensibilidad de *standoff* LIBS para establecer la mínima cantidad de analito presente en el escenario que puede ser advertida. Para ello se han establecido los límites de detección (*LODs*) de los elementos considerados sobre las distintas superficies. Con este propósito, micro volúmenes de disoluciones acuosas de las pertinentes sales se han dispersado homogéneamente sobre áreas acotadas en cada soporte. Con fines comparativos, también se han determinado los *LODs* para la operación en contacto directo, trabajando a idénticas condiciones de irradiación.

Los resultados han puesto de manifiesto que los *LODs standoff* varían desde unos pocos hasta varios cientos de microgramos por centímetro cuadrado. Algunas diferencias en los *LODs* de los distintos residuos localizados en un mismo soporte se han detectado, además de por las propiedades espectrales intrínsecas de los elementos, en relación con sus capacidades para la formación de óxido. El *LOD* de un analito puede cambiar dado que la formación de óxidos altera la población de sus estados atómicos e iónicos. Claros ejemplos de esto son los casos de ^{88}Sr y ^{130}Ba en aluminio. A pesar de los bajos *LODs* reportados para estos elementos, la

capacidad para su detección se subestima. Su tendencia a formar óxidos conduce a emisiones menos intensas de sus correspondientes líneas de emisión atómicas e iónicas. Por ello, es de esperar que los *LODs* sean sustancialmente menores (mejor) que los estimados –17 μg cm^{-2} y 2 μg cm^{-2} para ^{88}Sr y ^{130}Ba, respectivamente.

También se han detectado diferencias en los *LODs* de un particular analito cuando se localiza sobre diferentes superficies. Estas diferencias significativas en su sensibilidad resultan de las propiedades químicas y físicas de la matriz. Por ejemplo, a pesar de la baja tasa de ablación alcanzada en el vidrio puro, la sensibilidad para la detección de los residuos es elevada. Esta circunstancia se debe a la presencia del residuo en sí, que induce una absorción óptica mayor. Además, la escasa contribución de la superficie de vidrio a la señal de emisión final conduce a una mayor relación señal-ruido (*SNR*). Por otro lado, aunque los plasmas producidos en superficies de aluminio, de arcilla y de hormigón son más intensos, se ponen de manifiesto diferencias significativas en la sensibilidad de detección. Las variaciones en los *LODs* para un mismo analito en estas diferentes superficies se aclaran a través de las propiedades de los plasmas formados. Para verificar esto, se han computado la temperatura electrónica (T_e) y la densidad del número de electrones (N_e) de los plasmas procedentes de residuos de Ba en estas superficies. Los resultados han corroborado que la sensibilidad a la detección mejora (*LODs* menores) cuanto mayores son los valores de T_e y N_e.

En cuanto a la sensibilidad de *standoff* LIBS, al compararla con la obtenida para la configuración de contacto directo, se han observado diferencias pronunciadas entre los *LODs* de ambos enfoques al computar la detección en términos de cantidad absoluta. Este hecho es una consecuencia directa de sus diferencias en el área de muestreo, 1500 μm de diámetro en el caso de *standoff* por los 450 μm en el caso del contacto directo; una circunstancia que también acentúa cualquier falta de uniformidad en la distribución de los residuos.

Finalmente, se ha abordado la aplicabilidad de *standoff* LIBS en dos potenciales escenarios reales: la monitorización de una fuga radiológica accidental y la recopilación de evidencias forenses tras una dispersión radiológica premeditada.

Para el estudio de la liberación accidental de materiales radiactivos al medio ambiente, se ha contaminado un pedazo de azulejo de suelo de terracota rústica (30 × 30 cm^2) con residuos de ^{193}Ir, ^{88}Sr, ^{59}Co, y ^{133}Cs, repartidos en cuatro cuadrantes (12 × 12 cm^2 cada uno) , uno para cada elemento. Esta superficie situada a 30 m de distancia del sensor se ha examinado mediante LIBS, a lo largo de la dirección normal a la superficie interrogada, con una resolución lateral de 1 cm. A partir de las emisiones particulares de cada analito ha sido posible construir unos mapas químicos que definen perfectamente el contorno y el perfil de distribución espacial de las deposiciones originales para los elementos en cuestión. Esto demuestra que la identidad particular de cada analito puede vigilarse con precisión y sin interferencias de otras emisiones más destacadas dentro de la señal espectral.

En el caso de la dispersión premeditada de material radioactivo, *standoff* LIBS se ha destinado a la captación de evidencias forenses en materiales "testigo" de un escenario simulado de *post-detonación*, a partir de la detección paralela de la fuente de radioactividad y el correspondiente propulsor explosivo responsable de su dispersión. Hay que mencionar aquí que las evidencias químicas identificables en este tipo de desechos son muy limitadas, principalmente para el explosivo propulsor. Como los productos de postcombustión que resultan de la detonación de un explosivo orgánico principalmente son vapor de agua y gases como el CO, H_2 y N_2, los residuos post-voladura esperados se limitan a carbono sólido y trazas procedentes de la no-reacción explosiva, acompañadas de impurezas interferentes.

En este contexto, se han realizado dos ensayos de detección *standoff* LIBS sobre posibles escombros resultantes de las detonaciones de "bombas sucias" basadas en combinaciones a distintos niveles del explosivo *TNT*, junto con ^{133}Cs y

^{59}Co, dispersado en áreas bien definidas (2 × 10 cm^2 cada uno) a lo largo de una superficie de aluminio (15 × 15 cm^2), emulando los fragmentos de contenedores metálicos sellados que almacenan la fuente radiactiva. A partir de las emisiones atómicas particulares de ^{133}Cs y ^{59}Co, y de la señal molecular de CN como marcadores del material explosivo, ha sido posible construir unos mapas químicos que definen perfectamente presencia o ausencia, así como la distribución espacial de la evidencia. No obstante, hay que hacer notar que para la mezcla de *TNT* con ^{59}Co algunas evidencias pasan desapercibidas, ya que prácticamente el componente explosivo no se detecta a menos que esté en una proporción del 75%. Por el contrario, en el caso hipotético de una bomba sucia basada en ^{133}Cs, tanto el simulante radioactivo como el explosivo se detectan cualquiera que sea su concentración en la mezcla. Por lo tanto, el interrogatorio de este escenario revela evidencias de una detonación. Además, hay que destacar que la detección simultánea de *TNT* y ^{133}Cs en una proporción de 25:75 encaja con una pequeña cantidad de explosivo que ha sobrevivido a la explosión.

En resumen, todas estas investigaciones acreditan el notable potencial de *standoff* LIBS para la anticipación, monitorización o ciencia forense de cualquier tipo de amenaza.

This page is left blank intentionally

Objectives

In recent times, the emergence of new requirements and the growing of analytical demands have forced to both the generation of new practices and the innovative development of the conventional techniques in the field of analytical chemistry. Every day more and more, instances requiring analytical techniques operating *in situ* are more frequent due to the difficulty to carry away the sample towards the lab facilities or the need of its assessment there where it is located. This circumstance has been possibly the responsible cause of the aggressive expansion on the development of field-deployable laser-based sensors.

Among the different laser analytical techniques, founded each on the particular physical process caused by the interaction of laser radiation with matter, emission spectroscopy assisted by laser ablation (also called laser-induced breakdown spectroscopy, –LIBS–) occupies an outstanding competitive position. Its numerous advantages like the versatility for sampling of solid, gaseous or liquid targets with little or no preparation and the simultaneous multielemental response in real-time, have made it an increasingly important analytical tool. Furthermore, its ability to deal with the analysis of samples at distances of several meters from a portable platform has placed this technique in the forefront of the analytical technologies.

Indeed, all these attractive features have led LIBS to be used on a wide range of real-world applications as materials analysis, environmental monitoring, art restoration/conservation, military and safety needs, forensics and biomedical studies, and even more recently space exploration. Notwithstanding all the gains made, there is yet a range of challenges ahead to deal with, in order to place LIBS at its *standoff* scheme to the highest technology readiness level.

Therefore, the main objective of the present Doctoral Thesis is the assessment of the feasibility to use LIBS at *standoff* configuration in the inspection and the surveillance of "*extreme*" scenarios. Thus, towards this general goal, several particular objectives must be pursued.

While it is true that the *standoff* scheme for LIBS offers numerous advantages to the analysis, the most critical issue for its performance is the large variability observed in the emission responses of distant targets. For that reason, the main causes behind this instability within the spectral responses should be identified with the aim of improving the main analytical figures of merit of any developed application. This particular investigation will involve an assessment of how the optical path affects to the laser pulses delivered to the distant target as well as to the light emitted by produced plasmas when are gathered by the sensor.

As regards the applicability of the technique is concerned, its strengths and weaknesses should be addressed in those instances in which the distant analysis is a real need. Thus, the "*extreme*" term herein refers to those sampling scenarios that involve a limiting physical access, either due to the nature of the site or to ensure good operator safety. In this connection, the architectural heritage and the security applications will be considered.

- Architectural heritage is a valuable source of history and a unique and irreplaceable legacy of our past. However, the vast majority of this architectural heritage is immovable, therefore demanding the use of a technique operating *in situ*. Furthermore, in some cases by virtue of dimensions and structure, the physical access of the operator to the analysis area is limited. Thus, the usefulness of a *standoff* approach is more than evident. In this sense, a case study of an architectural heritage will be selected to perform a qualitative elemental analysis on the materials involved in its construction. A chemical characterization, from their original composition up to any cause responsible of their deterioration, should be executed. This surveillance will facilitate an ongoing control of their conservation status as well as the design of any future conservation plan.

- In last times, numerous terrorist attacks on military targets and civilians, indiscriminately, have made clear that the detection of threats requires a latent attention. This is the reason why any technique able to anticipate these threats would be welcome. Again, the need of an analytical tool operating at a distance, against the possible risk to human life, is mandatory. In this context, an evaluation of the LIBS analysis potential for the advanced recognition of any danger evidence from a safety distance will be addressed. Through the laser interrogation of distant objects, the detection and location of inconspicuous residues from a minimal contamination should be attained by exploiting optical emissions. Additionally, the design and implementation of any data treatment tool that allows the labeling of these residues, either the particular identity or the hazardousness, should be also welcome.

- Regrettably, in some cases it is inevitable that the incident occurs. At these circumstances, the analytical techniques to the identification of forensic evidences would come into play. Although some of these evidences can be transferred to the lab facilities, other must be investigated at the own place where the incident happens. Thus, the suitability of a LIBS-based fieldwork sensor for fingerprinting any identifiable evidence on witness debris should be evaluated. Likewise, the analytical potential of LIBS to detect, identify, and even quantify, expected post-disaster chemical residues on a variety of substrates and in the presence of interferents should be explored.

Introduction

1 Laser-Induced Breakdown Spectroscopy (LIBS)

1.1 The origins

It was back in the year 1917 when Albert Einstein suggested the process of stimulated emission that would lead to the ensuing development of the laser. From his conjectures, electrons, besides absorbing and emitting light spontaneously, could be stimulated to emit light of a particular wavelength [1]. However, it took nearly 40 years to scientists until achieving the amplification of such emissions, thereby validating the Einstein's predictions and, at once, marking the beginning on the evolution of lasers towards the powerful tools that are today. Thus, in 1953, James P. Gordon and Herbert J. Zeiger, together with Charles H. Townes, conceived the first amplification of microwaves by stimulated emission (maser) [2]. But it was not until 1960 when Theodore H. Maiman constructed the first device to amplify light by stimulated emission (laser) using photographic flashlamps as pump source and a cylinder of ruby, whose ends were coated with silver to turn them into reflective surfaces, acting therefore as a resonator [3]. In a parallel effort, Sorokin and Stevenson published their achievement of lasing in a four-level system, using, at low temperature, calcium fluoride crystals doped with uranium [4]. However, it was in 1961 when the laser that would evolve into the most often used today to initiate the plasma was introduced; a solid state laser using neodymium doped into various hosts like yttrium, aluminum, and garnet; although its operation was not published until 1964 by Geusic, Marcos, and Van Uitert [5].

Early on, lasers were primarily used as an ablation source with excitation. Thus, the laser-induced plasma virtually advanced in parallel with these early days of the laser, as reflected in an abstract presented by Brech and Cross mentioning the plasma as a spectral source [6, 7]. This first publication was followed by a series of different developments and applications of the laser spark, from the first

analytical use for spectrochemical analysis of surfaces [8] up to the appearance of the first commercially available laser micro-spectrum analyzer. Thus, in 1970, Scott and Strasheim published the first study of laser plumes useful for spectrochemical analysis [9]. Following this, Schroeder et al. described circuits for time-resolution and to record the temporal profile of plasma emissions from single pulses [10]; the direct laser spectrochemistry (LIBS –laser-induced breakdown spectroscopy–) was starting out.

From then up until the present day, due to the ongoing need for analytical methods increasingly more demanding, LIBS has been advancing significantly not only in the knowledge of its fundamental aspects but also in developments in its instrumental components; advances that are reflected on its usage for a wide range of new and interesting applications [11].

Along the following sections, although briefly, a detailed description on the most basic aspects of LIBS will be provided.

1.2 Laser-matter interaction & plasma formation

Lasers provide the ability to accurately deliver different amounts of energy into confined regions of matter in order to achieve distinct responses. These responses of matter to incident laser can be categorized into two groups: thermal and mechanical effects. Thermal effects refer to heating, melting, vaporization (sublimation), boiling, and phase explosion, whereas mechanical response involves deformation and resultant stress in materials [12].

The details of the matter response depend on the particular material system and the laser conditions. Just for instance, if laser-induced excitation rates are slow compared to the thermalization time, then the process is denoted as photothermal, and the absorbed laser energy can be considered as being directly transformed into heat. In this case, the matter response is a function of the local matter heating and cooling rates, maximum temperatures reached, and temperature gradients. A laser

heating with energy dosages below the threshold of melting can activate a variety of temperature dependent processes within the matter but does not necessarily involve melting of material. In contrast, energy doses above that threshold can lead to the formation of transient deposits of molten material on the surface [13, 14].

The particular process of laser ablation lies in the removal of material from a target by direct absorption of laser energy. Although laser ablation is possible with intense continuous-wave (*CW*) radiation, it is usually discussed in the context of pulsed lasers. The onset of ablation occurs above a threshold fluence, which will depend on the absorption mechanism, particular material properties, microstructure, morphology, the presence of defects, and on laser parameters. Furthermore, a variety of mechanisms for material removal may be active during laser ablation also depending on the particular material system and laser processing parameters such as wavelength, fluence, and pulse length [15]. *Fig. 1* depicts a brief survey of some of the numerous phenomena and complicated processes involved during laser-matter interaction and the ensuing target ablation.

Laser energy absorption

When a large amount of laser energy is tightly focused on the matter, the absorbed photons lead to the production of electrons with a certain amount of kinetic energy. At very high electron densities ($N > 10^{17}$ cm^{-3}), electron-electron collisions dominate over electron-matter collisions and electrons begin to behave collectively and thermalize each other. Once common temperature −thermal equilibrium among electrons− is reached, they transfer their kine. c energy to the matter via recombination and phonon generation. Consequently, a wide variety of thermal phenomena such as a rapid local heating, melting and intense evaporation are caused. Therefore, a sequence of phase transitions occur: from solid to liquid, and from liquid to vapor [13].

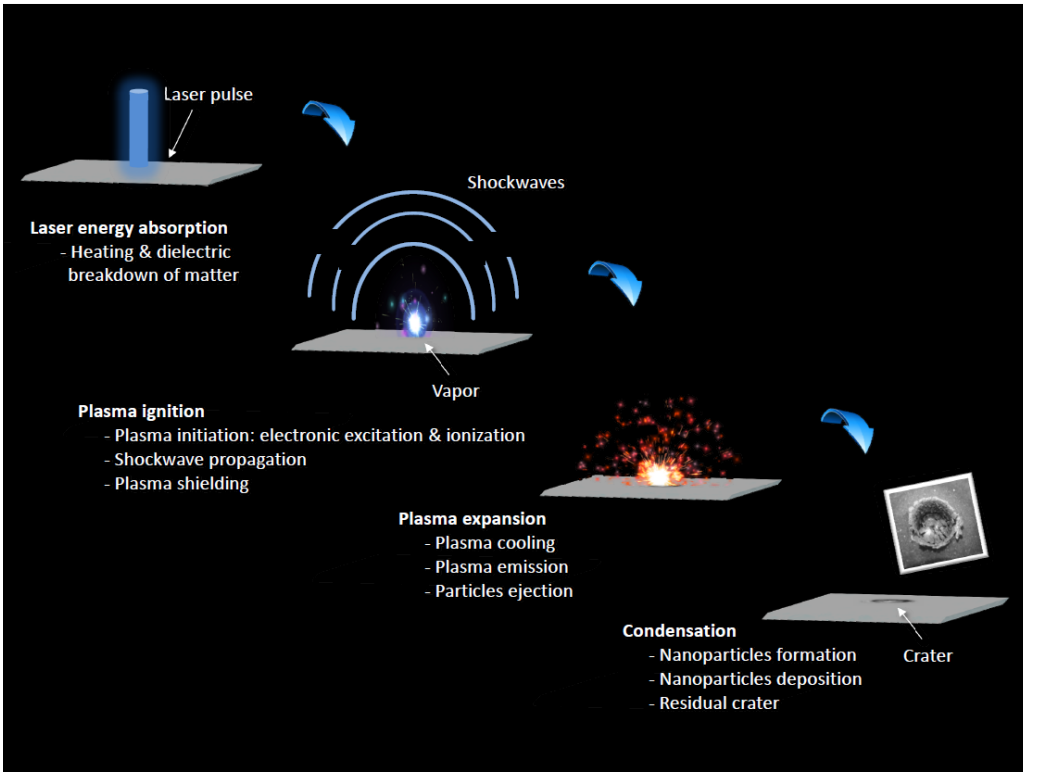

Fig. 1. *Chronological sequence of the main phenomena that occur during laser-assisted ablation process.*

Plasma Ignition

As the temperature continues to increase to the vaporization point, the sputtered target material is gasified and ionized, thus leading to the formation of plasma containing electrons, ions, and neutral as well as excited species of the ablated matter. A highly directed plume ejected from the irradiated zone accompanies the material removal. As this plasma plume with high pressure expands immediately and rapidly outward, shock wave is formed. Shock wave front expands and propagates in the surrounding atmosphere. In this meantime, shock wave front continues to absorb the energy of the laser that keeps expediting it. Thereby, although the radius of shock wave front increases, its velocity of propagation slows down and its intensity is decreasing. Shock waves decay into acoustic pulses to propagate in sonic speed in the surrounding atmosphere [16].

Like the shock wave, the ejected plasma plume propagates against the incident beam, *shielding* the material completely through the absorption of the later part of a laser pulse. Consequently, this "*shielding effect*" not only changes the actual energy flux received by the matter but also causes a reheating of the plasma itself. This effect is commonly produced in the case of nanosecond laser pulses, whereas is not evidenced for ultrafast (*pico-* and *femtosecond*) laser pulses, because the total temporal length of the pulse impacts the target before plasma formation [17-19].

The dense plasma plume not only can absorb and scatter light but also may exchanging energy with the targeted material. Undoubtedly, the distance of the plasma from the surface is the critical factor. Absorption by the solid through the plasma is much more efficient than by laser irradiation when plasma stays close to the surface. In this case, the blackbody radiation emitted by the vapor plasma is absorbed very strongly [20].

Plasma Expansion

During the propagation, plasma is directly ejected outward in all directions. Notwithstanding this, the vaporized material expands in a non-isotropic manner, that is, with a higher amount of dense and partially ionized gas spreading out preferentially normal to the surface along the laser pulse direction.

At a very early stage, due to the high level of ionization, plasma radiation with a very wide spectrum from ultraviolet to infrared is composed of background continuous spectrum and linear spectrum due to elements including in the plasma. The continuous spectrum of radiation is mainly attributed to *Bremsstrahlung* and recombination radiation processes [21]. During the *Bremsstrahlung* process, photons are emitted due to the transition of free-state to free-state contributed by free electrons and ions accelerated or decelerated through collisions. However, during the recombination event free electrons are captured to be bound-state by

ions in electron-ion collision and neutral atoms and molecules are created; meanwhile excessive energy is emitted in the form of electromagnetic radiation. As the temperature of free electrons of plasma descends quickly during these processes, background continuous intensity decays more rapidly than the spectral lines. It is for this reason that the plasma spectral irradiance is usually gathered after a reduced period of time –a few nanoseconds– from the laser pulse incidence. The spectroscopic analysis of the optical emissions from spectral lines provides qualitative and quantitative information on the elemental composition of the sample as well as on the temperature and particle density of the plasma itself [22].

Condensation

Although the dominating species leaving the target surface are principally atoms and ions, besides these species the material plume also consists of particles, with dimensions ranging from nm till μm. The smallest particles (nm size) are generally formed upon expansion of the plasma into the ambient. When the vapor plume expands, plasma gradually cools down, thus leading to the nucleation and condensation of the vapor atoms, which results on the formation of nanoparticles and growth toward clusters. Nevertheless, the origin of these particles might come along a different route since in the case of ultrashort laser pulses this cloud of nanoparticles is a direct consequence of its interaction with the target material. In the same vein, during its expansion into the ambient the produced plasma also causes larger particles (μm size). These particles are expected to be created by direct mass ejection as a consequence of different mechanisms (photomechanical fracture, liquid splashing …) depending on the material nature.

As a result, whatever the way, the complete removal of the material leads to a negligible residual microcrater on the target as the most evident physical sequel of the whole ablation process [23].

1.3 The plasma plume

As commented, laser ablation event produces a transient, highly luminous plasma plume that expands rapidly away from the irradiated target. This tiny plume of light, in addition to be by itself a direct indicator of how the ablation occurs, contains valuable qualitative and quantitative information about the composition of the target. However, the properties of this plasma plume (morphology, dynamics, temperature, density ...) as well as the information that it contains and reveals depend on several factors. The following describes the most relevant information on what variables influence the produced plasma and what are the main parameters characterizing the plume.

1.3.1 Factors affecting the plasma plume

As exemplified in *Fig. 2*, the properties of laser-produced plasmas are strongly influenced by the irradiation conditions like the laser pulse duration (τ), the laser wavelength (λ), and the laser pulse energy (E). Undoubtedly, also the type of material to be ablated is a key asset to the induced plasma due to the specific mechanisms governing laser energy absorption within it. Finally, the ambient surrounding, not only in composition but also in pressure, plays a critical role since it is the medium where the plasma evolves. Next, through some brief information, the main impacts of these parameters will be detailed.

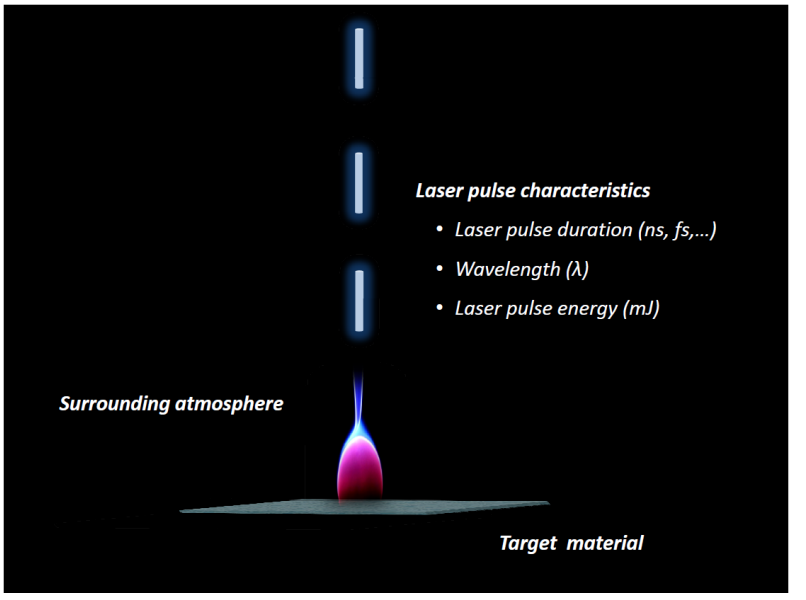

Fig. 2. *Pictorial summary of the variables affecting the laser-induced plasma plume.*

Laser Pulse Characteristics

Irradiation conditions are likely to be by far the most important factors influencing the plasma plume properties since they participate doubly; first, during its interaction with the material and, then, with the induced plasma itself. To facilitate understanding, effects of laser parameters on the plasma have been disaggregated as follows [24].

- ***Influence of laser pulse duration (τ)***

Differences in laser pulse length result in essential changes in the produced plasma due to the different rate of energy deposition and the variable mechanisms of energy redistribution and dissipation within the material. In the case of nanosecond (*ns*) pulses the laser−plasma interac on during the plasma evolution plays an important role. As discussed above, while the leading edge of the laser pulse produces the plasma, the remaining part of the pulse overheats the ejecting plume instead of interacting with the target. Consequently, plasma plume exhibits two distinguishable regions, a

bright spot located just above the sample surface and other high radiation-intensity region behind the expanding plasma front [25, 26]. In contrast, this phenomenon is not observed during ablation using ultrafast (*pico*- and *femtosecond*) laser pulses. However, depending on the irradiated material and at the very beginning of ablation, a non uniform distribution of intensity regions at the plume may be also evidenced. Under these circumstances, such uniformity obeys to a different reason; the size of the ablated material. The high intensity region that evolves close to the material surface moves slower and undergoes low constraint, is associated to larger clusters. In the other edge, a less intense plasma front that propagates rapidly and experiences a strong constraint from the surrounding involves atoms and smaller particles [27, 28].

- ***Influence of laser wavelength (λ)***

A large variety of laser wavelengths ranging from ultra-violet through visible to near infrared can be used for laser ablation. However, laser wavelength marks the mechanism of interaction of the laser pulse with the material, the onset of ablation (either thermal or photochemical), and the resulting plasma plume.

Differences in absorption rate between radiations lead to different propagation behavior of the produced plasma. While a large λ (IR - 1064 nm) produces larger axially extended plasmas, a short λ (UV - 266 nm) generates plasmas much more confined. Thus, for IR ablation, the surrounding atmosphere is effectively mixed with the ejected vapor, whereas, for UV ablation, the surrounding ambient is principally evacuated by the expansion of the vapor plume. The usage of the different λs has also revealed changes in the ablated matter. Thereby, beyond those variations, 266 nm have shown to generate a much larger amount of atomic particles than 1064 nm.

Consequently, UV ablation leads to hotter and much denser plasmas than IR ablation [29-32].

- ***Influence of laser pulse energy (E)***

Last but not less important, the laser pulse energy (*E*) is also an influential parameter that alters the induced plasma plume. Indeed, rather than the absolute energy, it is the density of energy –termed either as ***fluence*** (energy expended per unit area, $J \cdot cm^{-2}$) or as ***irradiance*** (the rate at which energy is deposited on the target per unit area, $W \cdot cm^{-2}$)– the key factor influencing ablation [33]. Due to the dependence on the spot size over which the laser beam is focused and to the flexibility in the laser energy frame for values of these variables, identical irradiance/fluence levels might be reached by fitting focusing distance and energy delivered. Nonetheless, any modification on these parameters influences on the amount of ablated mass and, consequently, on the produced plasma plume. The raise of these variables influences on plasma morphology and dynamics. At high irradiance, plasmas, containing a large amount of ablated matter, have higher internal energy and expand into hemispherical shapes and push the surrounding ambient far enough in front of them. In contrast, at low irradiance, the lower ablation rates lead to plasmas with less energy that expand in the radial direction rather than in the longitudinal direction [34]. Additionally, with the increase of these variables, hotter and denser plasmas will be obtained [35].

Interrogated Material

Like the irradiation conditions, the type and nature of the analyzed material also plays a crucial role to the ablation process. Undoubtedly, variation of plasma parameters for samples at different states of matter –solid, liquid and gas– is more than obvious because of the different energy thresholds required to its particular

ablation. However, for materials at the same state also a change on plasma parameters may occur. Due to the differences on physical and chemical properties of materials, a *matrix effect* on the laser-induced plasma plume parameters is evidenced. As expected, the larger the differences on materials properties, the higher the variation of their respective plasma parameters [36]. Furthermore, even the processes occurring at the surface of the same target may be altered when it is featured at different morphologies. The degree of compaction clearly affects plume dynamics as well as particles ejected [37]. Also, in this direction of influence of sample structure, the ablated mass is in inverse proportion with hardness [38].

Surrounding atmosphere

As mentioned before, due to the sample evaporation, the plasma expands at supersonic velocity toward the ambience in front of the target. Consequently, atmosphere surrounding is also of major relevance for plasma properties (size, shape, temperature, density ...) and the dynamics (spatial and temporal evolution) either of the plasma in itself or of its intrinsic features, since it is the medium where the plume progresses. In short, the nature and pressure of ambient environment influence not only the morphology profiles of plasmas but also the physical parameters defining their states.

The ablation process is strongly affected due to differences in density, mass, ionization potential, and thermal characteristics of different background atmospheres. In this sense, the composition of the surrounding atmosphere alters the dynamic interaction of the plasma with the ambient gas, because of distinct physical processes like the interpenetration of gas components into the plasma and the radiative recombination occur [39].

The expansion of the laser-induced plasma is related to the mass density of the gas. Hence, at the same pressure, the confining effect on the plasma is stronger in the case of atmospheres with larger density. Consequently, plasmas with high

temperature and electron density, which slowly decay, are obtained for such high-density surrounding atmospheres. Additionally, although more easily ionized due to a less breakdown threshold, gas with a large mass density favors the production of a beneficial environment where plasma *shielding* occurs. Confined laser plasmas with a sufficient amount of electrons can absorb a significant portion of the laser pulse through inverse *Bremsstrahlung*. This circumstance causes a decrease in the vaporization rate of the material, thereby reducing the mass removal during LIBS but leading to stronger LIBS signals due to the plasma re-excitation. Furthermore, the possibility of far more complex variations for the properties of the ejected plasmas as a function of the reactive nature of the atmosphere is not in any way ruled out [40-43].

In the same direction, the pressure under which plasmas are evolving also influences the characteristics of induced plumes through several effects like deceleration, shock waves formation, thermalization of ablated species and clustering processes. In general, density and temperature of plasmas decreases in parallel with the ambient pressure. These parameters vary critically with plasma morphology, which in turn strongly depends on ambient pressure. A larger confinement of the plume near the target surface, with a decreasing of the plume front dispersion, is noticed as the pressure increases. Subsequently highly distinguishable plumes in terms of size and luminosity are obtained. The slower expansion of the plasma leads to a slower cooling, thereby deriving on emission intensities that remain longer, since the recombination processes occur more rapidly because energy exchange between particles inside the plume is more efficient [44, 45].

Although particular influences of all these variables involving the ablation scenario have been addressed in isolation, it should be highlighted that all of them act together, thereby affecting the whole chain of possible events occurring during plasma formation and hinders the interpretation of all the episodes.

1.3.2 Physical parameters of the plasma plume

Once produced the plume, there are some physical parameters such as the temperature (T_e), the electron number density *(*N_e) and the atom and ion number densities that allow its characterization. Their determination is important to improve understanding the dissociation, atomization, ionization, and excitation processes occurring in the plasma. Since these parameters are directly associated to the radiation emitted by plasmas, their computation is usually based on the spectroscopy of such radiation (spectral line and continuum emission). However, the description of plasmas states and the evaluation of these essential parameters using optical emission spectroscopy are strictly connected to the concept of thermodynamic equilibrium [46].

For plasma to be in this complete state, all processes are balanced and characterized by a single temperature. Therefore, radiation emitted is equal to the radiation absorbed [22, 47].

As far as plasma temperature is concerned, the vast majority of measurements are based on the optically thin emission lines of neutral atoms and ions. The most common approach to determine the plasma temperature is the so-called *Saha–Boltzmann* plot method by the following expression:

$$\ln\left(\frac{\lambda_{mn} I_{mn}}{A_{mn} g_m}\right) = -\frac{E_m}{KT_e} + \ln(hcN) \qquad \text{(Equation 1)}$$

where λ_{mn} is the wavelength of the transition lines, I_{mn} is the integrated line intensity of the transition involving an upper level (m) and a lower level (n), A_{mn} (s^{-1}) is the transition probability, g_m (s^{-1}) is the statistical weight, and E_m (eV) is the excited upper level energy. T_e (K) and *K (*$eV \cdot K^{-1}$*)* are the electron temperature and the

Boltzmann's constant, respectively; h (J·s) is the Plank's constant, c (m·s^{-1}) is the speed of light and N (*f-T-*) (m^{-3}) is the total number density.

If a graph is constructed for various lines of successive ionization stages of the same element with the left side of Equation 1 as the ordinate and the energy of the excited upper level as the abscissa, a straight line, whose slope yields the temperature, is expected [48].

On the other hand, diagnosis of electron density within LIBS plasmas may also be based on the emission spectrum of the plume, more specifically, from the prof le of the spectral lines [49]. Among the optical emission spectroscopic methods proposed, the broadening of emission lines due to the *Stark* effect has been the most widely used. This effect (briefly discussed in *section 1.4*) is due to the collisional processes between the emitting atoms and electrons and ions, resulting in a broadening of the line and a shift of the peak wavelength. This effect is considered the dominant broadening when compared with other mechanisms due to collisions with neutral atoms (*i.e.*, resonance and Van der Waals broadenings) [22].

In this method absolute intensities of spectral lines are not required, and merely the *full-width-at-half-maximum* (*FWHM* –$\Delta\lambda_{1/2}$–) or the total *Stark* shift d_{total} of the broadened line, expressed by Equations 2 and 3, respectively, are sufficient.

$$\Delta\lambda_{\frac{1}{2}} = 2w\left(\frac{N_e}{10^{16}}\right) \qquad \text{(Equation 2)}$$

$$d_{total} \approx \left[\frac{d}{w} \pm 2.00A(1-0.75R)\right] w \frac{N_e}{N_e^{ref}} \qquad \text{(Equation 3)}$$

In these equations, w is the electron-impact (half) width, A is the ion broadening parameter, R is the ratio of the mean distance between ions and the *Debye* radius and N_e^{ref} is a reference electron density, usually of the order of 10^{16} or

10^{17} cm^{-3}, at which the parameters *w* and *A* are measured. Thus, the electron density *(N_e)* is extracted by matching the line width with the calculated one or by comparing the measured shift with the value predicted by the approximated formula in Griem's book [50].

As pointed out earlier, laser-induced plasmas are transient in their nature and have a very short temporal existence. Thus, we finally want to emphasize that these commented parameters suffer, like the plasma in itself, both a temporal and a spatial evolution. Consequently, values of these parameters may vary from an earlier to a later stage of the plasma lifetime as well as from the inner to the outer positions within the plume during its expansion.

1.4 Plasma emission

The radiation emitted from laser-induced plasmas consists of a broadband light emission together with species-specific spectral lines. Although these last signals are the relevant signature used for LIBS, there are also additional dominant processes of radiation from plasmas such as *Bremsstrahlung* and recombination radiation.

Fig. 3 depicts a schematic illustration of the emission spectra of LIBS plasma for different time delays with respect to the irradiation of the laser pulse. As observed, the optical emission spectrum of the plasma changes during its lifetime in a temporal window spanning from several tens of nanoseconds up to several microseconds. An specific optical emission from the plasma can be observed depending on the temporal settings for signal gathering, that is, the time between plasma formation and the start of its observation (delay time, t_d) and the time period over which the plasma light is registered (gate width time, t_b).

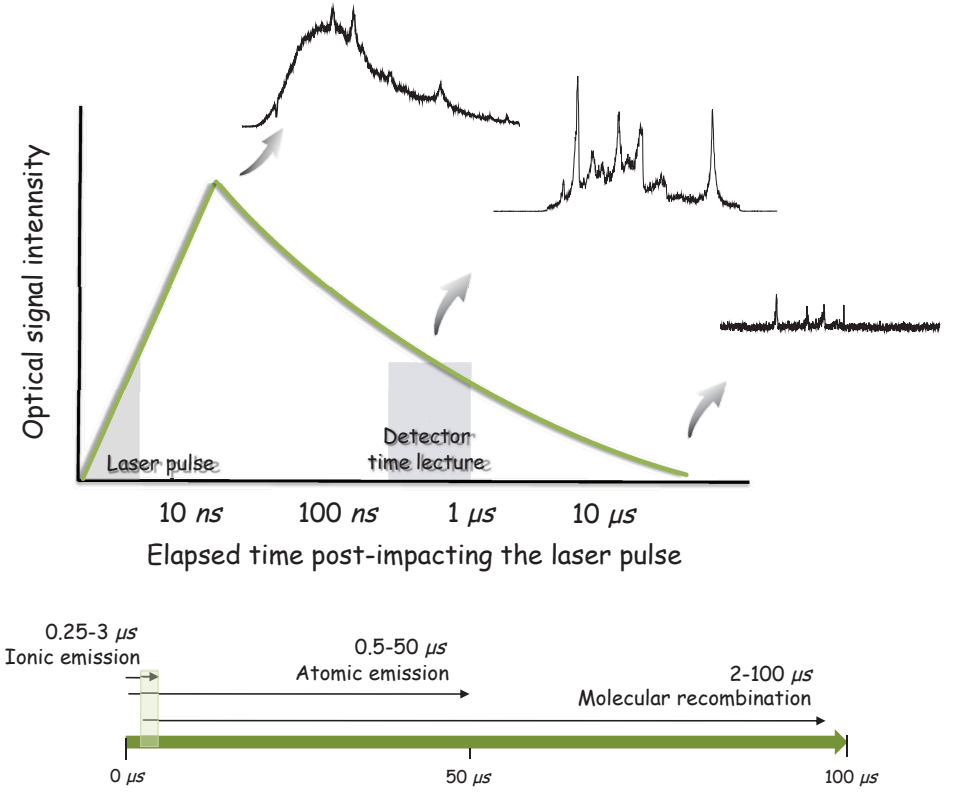

Fig. 3. Temporal evolution of the optical intensity according to the transient nature of the plasma plume.

At earliest time, the plasma emits predominantly a "white light", thereby leading to a continuous spectrum of radiation, mainly attributed to *Bremsstrahlung* and recombination radiation processes (see *section 1.2*). As a result, only some faint peaks of the line intensities of atoms and ions are evidenced together the continuum emission. At this instance, the ratio of the peak intensity of an emission line to the neighboring intensity of the spectral continuum emission is low.

Next, when the plasma cools down, the strong white light emitted as a continuum signif cantly subsides in intensity. In contrast, emissions from atomic and ionic species in various states of excitations as well as from parent molecules directly fragmented can be clearly observed. Additionally, emissions from small

molecular fragments coming from atomic recombination can also emerge. At this point, the ratio peak intensity to continuous background increases notably.

Finally, as the elapsed time enlarges, the plasma temperature decreases further and the emission peaks are dying out towards their total extinction.

Beyond this temporal effect over the emission signals various absorption processes and line broadening mechanisms causing distortions in the spectral line profiles exist. In the case of very dense plasmas, an effect known as *self-absorption* occurs, that is, the plasma itself absorbs its own emission. Because of the characteristic temperature and electron density gradients of the plasma, while its outer layer is populated by "cool" atoms, residing mostly in the ground state, the central core of the plasma contains a high density of excited atoms. As these atoms decay to the ground state, transitions are element specific and quantized, the emitted photons corresponding to resonance transitions have a high probability of being reabsorbed by those atoms of the same species in the outer layers [12, 16].

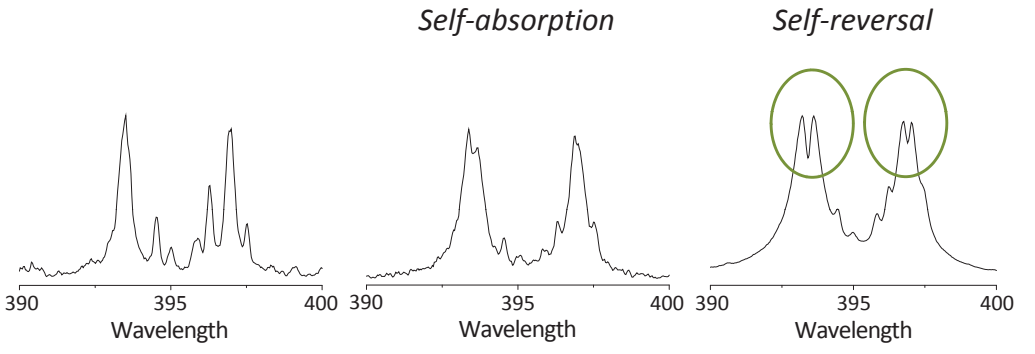

Fig. 4. Line distortion effects on Ca (II) at 394 and 396 nm from a marble sample**.**

As an example, *Fig. 4* shows how the shape of single lines of Ca(II) at 394 and 396 nm are affected due to a large spatial heterogeneity in the plasma observed during the selected time window. When the concentration of Ca atoms in the sample increases, the number of "cooler" Ca atoms in the outer layer of the plasma also increases. Consequently, the spatial heterogeneity in density of atoms in the

microplasma raises, and *self-absorption* effect becomes evident. As observed, the onset of *self-absorption* leads not only to a reduction of observed intensity of the emission line but also to a slight broadening. Then, if this distortion continues successively an extreme effect known as *self-reversal* is evidenced. In such a case the single emission lines reflect a prominent cleft at the center as well as an additional broadening.

Both effects are usually observed for emission lines in which the lower level of the transition is the ground state or close to the ground state and are associated to an optical thickness condition of the plasma with respect to the concerned element [16, 51-53].

Beyond the effects of absorption on the LIBS signal width, there are also additional mechanisms causing emission line broadening. Leaving aside factors associated to the instrumentation, e.g. those related to the overall spectrometer resolution, several effects inherent to the plasma plume exist: *Doppler* due to the temperature, *Stark* due to the electrical field and collisional due to the surrounding gas pressure.

The *Doppler* broadening only depends on the absolute temperature and the atomic mass of the emitting species. The *Doppler* width arises due to random thermal motions of the emitting atoms and dominates the line shape near its center. The resulting line profile has a *Gaussian* profile. The *Stark* line broadening is subject to the presence of a great density of electrons and ions, and it results from atom interactions with the charged particles through the electric fields induced by themselves. This effect is the primary mechanism influencing the emission spectra, and the resulting broadened profile is usually fitted to a *Lorentz* profile [52-56].

For the sake of the relationship of these effects with the use of emission lines for analysis, let's conclude this section with an important consideration. Either qualitative or a quantitative analysis, the basic assets of any LIBS measurement are

the emission signals recorded from single plasma. As commented, both intensity and profile of a spectral line play a crucial in the study of spectroscopic information related to the concerned emitter. Consequently, the presence of such broadening effects may significantly alter LIBS analysis. Fortunately, the broadening occurs in the analyte itself and varies with the decaying of plasma. Thus, since emission from plasma can be temporarily resolved, such broadening may become less important if emission from plasma is gathered when it is coming down after its formation.

2 Operating with LIBS

2.1 LIBS instrumental components

As commented, in its basic form, a LIBS measurement is carried out from the matter ablation, forming laser microplasma on or in the sample containing atoms excited, and then collecting and spectrally analyzing the light emitted by these atoms. So, LIBS is a method that uses instrumentation similar to that used by other atomic emission spectroscopy (*AES*) methods. However, LIBS reveals a larger simplicity because it uses the laser pulse as a sole source, not only to "prepare" the sample in plasma form but also to "excite" the atoms for emitting the light, without any adjacent device.

In order to provide a better understanding on the operation using a LIBS based device, the fundamental instrumentation employed together with its functionality will be clearly, although briefly, here described.

Fundamentally, the main constituents in a LIBS experimental set-up may be summarized as follows: a pulsed laser source used to form the microplasma, an optical system (lens, mirrors or fiber optic) that enables the focusing of laser pulses and the collecting of the plasma light, a detection system (spectrometer) to resolve

spectrally light into its particular emissions, and a computer for data acquisition and treatment. Triggering and synchronization of the system is, in general, electronically controlled.

As an example, *Fig. 5* depicts typical LIBS experimental together with its basic performance. As shown, the delivered laser pulse is guided by a mirror towards a focusing lens that forms microplasma on or in the sample in the focal volume of the laser pulse. Then, the light emitted by the plasma is collected up to the tip of an optical fiber, which guides the light towards the entrance of a spectrometer. Once there, light is analyzed spectrally and the photoelectrical signal gathered is converted into a digital signal (LIBS spectrum) interpretable by the operator.

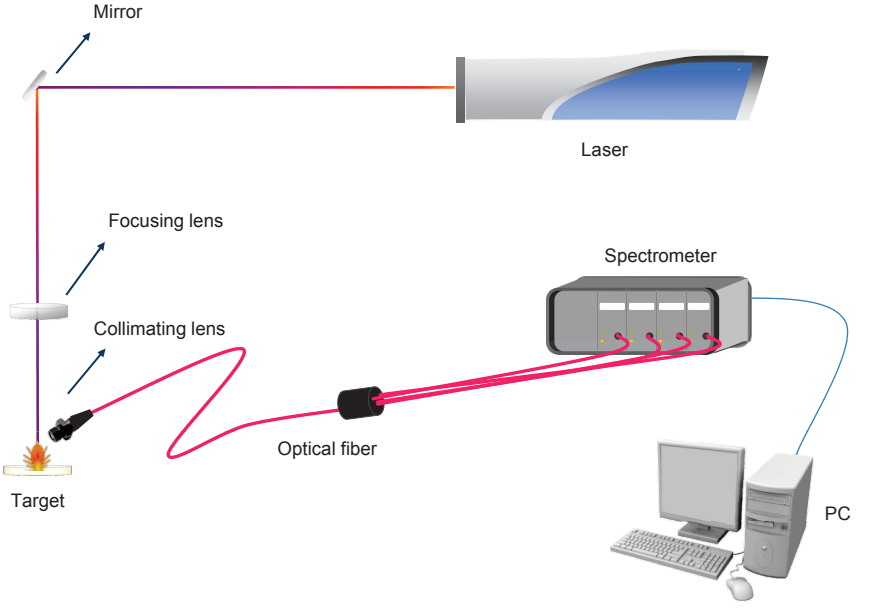

Fig. 5. Typical LIBS experimental set-up.

The push from analytical companies since the invention of the laser in 1960 started a deep development of instrumental components for LIBS that still is in place fifty years later. Notwithstanding this, through this section only the most common components being used nowadays further than an historical overview are summarized [57].

- **High-power pulsed laser**

The laser is, by far, the most important component of LIBS. This radiation source, that is responsible to form the plasma plume and induce the excitation of the atoms, is an amplified light of high intensity whose intrinsic properties are coherence, monochromaticity and directionality [58].

A great variety of lasers operating under different parameters (wavelength, pulse length ...) exist, and the choice of the type of laser to a LIBS experiment depends on both the requirements and the demands of the analysis. In any case, solid-state lasers, mainly Q-switched flashlamp pumped Nd:YAG with pulse lengths in the order of nanoseconds, are the most commonly used. *Fig. 6* depicts an schematic diagram of a pulsed Nd:YAG laser system.

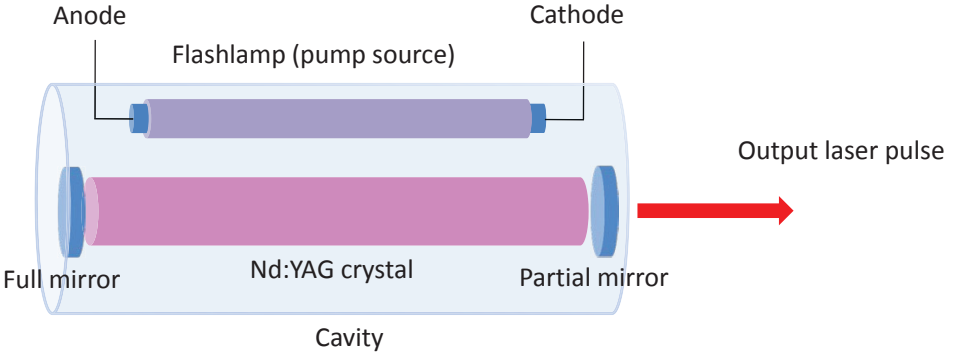

Fig. 6. Schematic diagram of a pulsed Nd:YAG laser system.

As shown, this excitation source consists in a crystalline solid of neodymium-doped yttrium aluminum garnet (Nd:$Y_3Al_5O_{12}$) as amplifier or active medium. This laser crystal, located inside of an optical cavity, receives energy from flashlamps which act as pumping mechanism for stimulating emission of radiation. Two mirrors fitted at the ends of the optical cavity are used to provide feedback the light emitted by the amplifier, thus providing to the laser pulse all its inherent qualities.

For obtaining brief, high-energy pulses, this laser operates under the so called Q-switching mode. The basic idea is that, whereas the pumping action is

continuous, thereby storing a large population inversion (many atoms in an upper level) until the lasing condition is satisfied, the light is allowed to travel back and forth between the mirrors only for a brief time to achieve the laser action. Those brief periodic intervals are controlled by an acousto-optic coupler, which scatters the incoming light from acoustic waves in a crystal. Thus, optical amplification is possible when there is no density change along the light path through the crystal. In contrast, when the light scattering occurs, laser action is prevented.

Nd:YAG lasers are preferred for the vast majority of LIBS applications due to they provide an easy to use, compact and reliable source of laser pulses of high focused power density. Furthermore, the fundamental wavelength (1064 nm) can be easily shifted to provide harmonic wavelengths, thereby covering from the near IR, through the visible (532 nm), to the UV (355 nm and 266 nm) spectral regions [16].

- **Optical system**

The set of optical components within a LIBS experimental set-up is intended to assist in the two core processes for emission spectroscopy assisted by laser ablation: First, the guiding and focusing of the laser pulses onto the target, to generate plasma, and then the collecting of the light emitted from such plasma.

- *The focusing system*. In its most basic scheme, the focusing system consists of a guiding mirror (with high reflectivity to the laser wavelength) that orientates the laser pulses towards the sample. Then, a focusing lens (in general, a plane-convex lens) tightly condenses the laser beam diameter to the minimum at its focal point. The distance between this lens and the sample establishes the spot diameter of the laser beam onto the sample surface. Thus, any variation of the lens-to-sample distance affects the laser-induced damage, the created plasma, and everything it stands for [59].

- *The collection system.* The gathering of light emitted from plasma can be performed through different configurations. Although the plasma light can be directly focused onto the entrance slit of a spectrograph, it is much more beneficial collecting the light using an optical fiber. In order to reinforce this, let's consider the exemplary *Fig. 7*, where these two options are exemplified. As seen, when light is directly focused onto a slit, only a minute portion of the plasma volume is gathered. Consequently, slight changes in plasma position can lead to significant variations on the appearance of the acquired spectrum in terms of absolute and relative emission intensities due to any spatial gradient for the excited atoms. On the contrary, gathering light with a bare fiber optic pointed at the sample allows collection of light from all parts of the plasma since it reduces sensitivity to alignment because of a wide acceptance angle for light. Furthermore, the amount of light into the fiber can be raised by using a collimating lens to focus as many as possible plasma light onto the tip of the optical fiber [16].

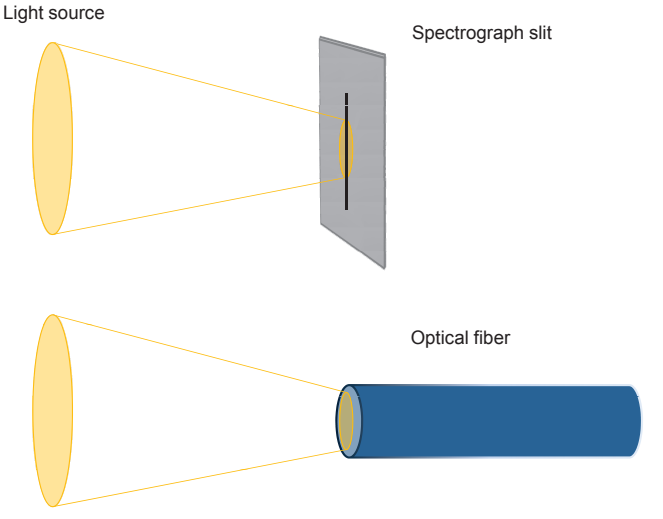

Fig. 7. Example on options for plasma light collection: directly onto both the slit of a spectrograph (on the top) and the tip of an optical fiber (on the bottom).

- **Spectrometer**

Once gathered, light is transported towards an analyzing system to convert it into a spectral pattern. This system is typically referred to as the spectrometer, an imaging system that draws a plurality of monochromatic images of the entrance slit onto a detector plane. The two key configurable components of this system are the spectrograph, or optical bench, and the detector. Although numerous devices suitable for a wide range of spectroscopy applications exist [52, 60, 61], the most widely spectrometer used for LIBS results from the combination of a *Czerny–Turner* spectrograph and a *charge-coupled device* (CCD). In this section, we will briefly report on their main optical components and how these different components work together to form the complete system.

The *Czerny-Turner* spectrograph consists of two concave mirrors and one diffraction grating. Light entering through the slit is collimated by the first mirror towards the diffraction grating. Once there, light is dispersed into its component wavelengths. Finally, the dispersed radiation is imaged by the second mirror onto the focal plane of the iCCD camera to be recorded and analyzed [52].

The *charge-coupled device* (CCD) is a common mechanism with an array of cells to capture the light image by the photo-electric effect for converting such optical image to an electrical signal. The packets of charge are first shifted, simultaneously, down the row of cells, in discrete time. Next, at the end of the cells line, the quantity of electrical charge from each different picture element (*pixel*) is used to represent its analog quantity, such as the emission intensity at each particular wavelength; LIBS spectrum is built.

LIBS systems based on CCDs are preferable in many applications, since they are more robust and more affordable in comparison with iCCDs. Furthermore, CCDs principally provide a better signal-to-noise ratio (*SNR*) because of its higher quantum efficiency and its lower overall noise. However, when very weak signals in

the presence of an intense background are involved, the use of an iCCD may be more advantageous to detection, due to their gating capability [62, 63].

Despite this basic configuration described, it must be highlighted that any LIBS experiment may be customized by more additional components depending on the analytical needs.

2.2 LIBS configurations

Due to the relative experimental simplicity, the most basic and typical configuration of LIBS to obtain the immediate emission response of the analytes is the *single-pulse* laser ablation [64]. At this configuration, *single-pulses* at one spot on a sample, *i.e.* one laser pulse per pump pulse, are used to induce the plasma. This configuration is suitable for spatial resolution or depth profile analysis, such as analysis of inclusions and thin films, since it avoids fractionation (alterations of the aspect ratio of the crater depth and diameter) related to crater formation.

However, when it seeks to use LIBS for some analytical solutions, there are several concerns with *single-pulse* ablation, including small quantity of ablated mass that consequently induces weak emission intensity, poor measurement reproducibility, and the aforementioned fractionation.

This is the reason why the use of further configurations based on several controlled laser pulses (*double-pulse* and *multi-pulse*) but without losing the flexibility of one-step LIBS, have been also explored.

As far as *double-pulse* configuration is concerned, a pair of laser pulses temporarily separated, from tens of nanoseconds to a few microseconds, is used. Furthermore, whatever the delay time between pulses, *double-pulse* configuration can operate under different geometries. *Fig. 8* exemplifies four possible arrangements of how the two delivered pulses can be combined [65].

As seen, in the collinear geometry (A), the *double-pulse* burst lies on a single line of delivering. In contrast, in the cross-beam scheme (B), both lasers pulses coincide at the target surface making certain angle with each other. Finally, the orthogonal geometries (C and D) involve two synchronized laser pulses aligned perpendicularly to each other. However, at these instances, the order in which the two laser pulses are arranged in time leads to different effects on laser ablation. Thus, for re-heating (C), while the first pulse is used to ablate mass from the sample surface, the second pulse is applied to re-heat such ablated mass. for pre-ablation (D), the first pulse, delivered parallel to the target surface, is focused above the target to generate the air plasma, while the second pulse focuses perpendicularly to the target surface for ablation [66].

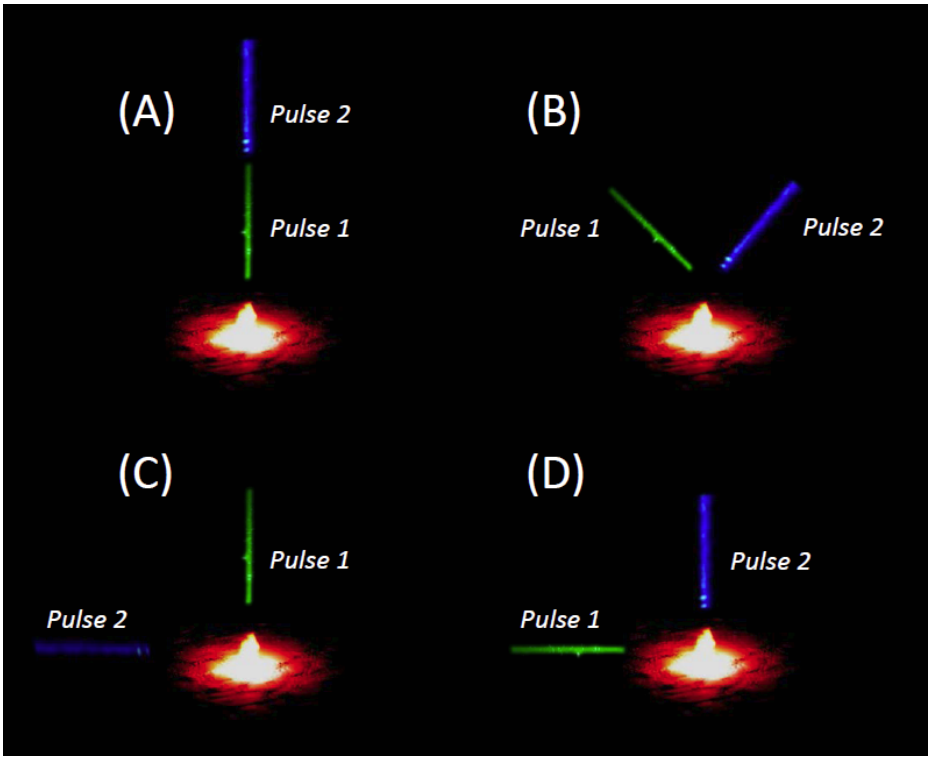

Fig. 8. Schematic diagrams of double-pulse LIBS geometries: (*A*) Collinear, (*B*) Cross-beam, (*C*) Orthogonal re-heating, (*D*) Orthogonal pre-ablation.

Whatever the geometry, the use of *double-pulse* LIBS leads to a more efficient ablation, keeping the energy of plasma for longer times, which turns in a higher ionization degree, better fulfillment of the local thermodynamic equilibrium condition and in a more stable signal. In addition, emission signals are significantly enhanced, thereby leading to a higher analytical sensitivity [67].

Beyond these numerous benefits that provide the use of *double-pulse* configuration as compared to a *single-pulse*, it has a much larger versatility, since dual-wavelength *double-pulse*, as well as dual-pulse length *double-pulse*, configurations may be implemented [68-70].

The possibility of improving the analytical performance by using multiple pulses from a single laser source, have been also investigated. Laser bursts, containing a variable number of pulses with different duration and separated by distinct inter-pulse gaps, can be used [71]. Using the *multi-pulse* configuration, analytical figures of merit significantly improve with respect to those of *single-* or *double-pulse* LIBS. For *multi-pulse* laser ablation at the same spatial location, the ablation rate increases as the pulse number increases and the pulse-to-pulse temporal distance within the pulse train decreases. In addition, pulse trains enhance the plasma intensity as well as its electron temperature, its density and the ensuing emission signal [72, 73].

2.3 LIBS operational approaches: *field-deployable* sensors

During the last years, LIBS has become a very attractive *field-portable* technology because of its operational simplicity as well as its attributes, like relatively small size and weight, its capability to *in situ* analysis with no sample preparation, its technologically mature, rugged, and affordable components, a real-time response and an inherent high sensitivity [74, 75]. Thus, whatever its configuration, the integration of small high-power laser transmitters with miniature

fiber optic spectrometers and laptop computers, has led to a rapid evolution of LIBS analytical equipment, from benchtop instruments towards compact portable and *field-deployable* units, generally assembled with commercial "*off-the-shelf*" components.

In this vein, the flexibility of these systems has allowed them to adapt to changing operational scenarios, thereby enabling the use of *hand-held* portable as well as distant analyzers. *Fig. 9* exemplifies the different operational LIBS approaches of these *field-portable* sensing systems. The most relevant design features and particular qualities relating to each system will be briefly described below.

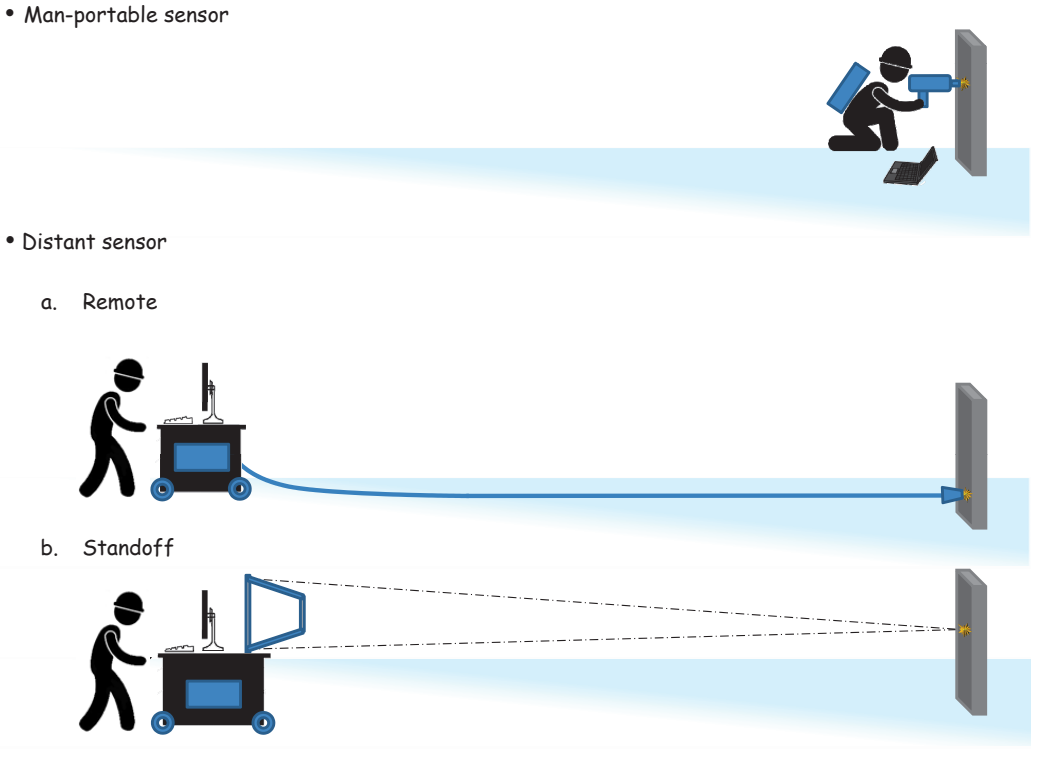

Fig. 9. Operational approaches of the *field-portable* sensing LIBS systems.

2.3.1 Man-portable sensors

Miniaturization (size and weight reduction) of LIBS components has been extended to such physical boundaries that have allowed the design and development of *man-portable* LIBS analyzers for *in situ* chemical screening. Despite that designs can be varied, in general, the overall system involves the laser power supply, a main unit that consists of a specially adapted backpack and encloses the spectrometer and the computer components, and a *hand-held* probe that houses in the laser head together with the focusing and collection optics arrangements [76].

Basically, the *hand-held* probe has an automatic focusing system to generate a series of laser plasmas on surfaces over a range of short distances. Then, a fiber-optic cable guides the plasma emission from the probe to the spectrograph.

An external power supply may provide autonomy of several hours to the sensor, thereby permitting its transportation to anywhere. User may have also an unfettered control of operational variables via wireless by means of a personal digital assistant (*PDA*) device, which, in parallel, permits data visualization [77-79].

2.3.2 Distant sensors

Despite the huge usefulness of these *man-portable* instruments on numerous screening applications, there are particular scenarios where its use is limited, e.g. when there is a hostile environment (potential risk in handling the sample to be analyzed) and/or there is a restricted physical access up to the target. At these circumstances, LIBS is usually performed remotely (via a controlled displacement of the sensing platform), or at *standoff* distance (where the sensing platform and the target are physically separated by distances up to several tens of meters) [80].

There is much controversy surrounding the terminology, distinction between *remote* and *standoff* approaches. The *ChemCam* –the first spectroscopic-based sensing instrument for Mars– on the NASA's Curiosity rover is the most striking example [81]. The sensor is located at ca. 55 millions of kilometers from the end-

users, but close to the envisaged target, that would be considered as a *remote* approach. However, LIBS data are collected by the Rover at a distance of up to 7 meters from the Martian sample, that is, a *standoff* approach.

For this reason, the following distinction between approaches has been considered herein: while *remote* analysis focuses on delivery of the laser energy to the sample by fiber optic, *standoff* refers to the distant focusing of laser pulses on a far away object.

A. Remote LIBS

At this operational approach, part of the instrumentation involving the sensor is displaced up to the sample. In general, *remote* LIBS (*R-LIBS*) utilizes an optical fiber system to conduct the active sensing. Furthermore, within this approach, two working methods can be considered: first, the use of a unique fiber optic cable capable of transmitting the laser energy through the fiber to the sample specimen and collect the optical emission from the luminous plasma plume and to conduct it to the spectrometer for analysis; second, the employment of an individual fiber optic cable for each specific process, the launch and the collection.

The earliest investigation related to the use of a unique optical fiber to deliver the laser radiation to the target and to collect the light emission from plasma, for distances of up to 100 m between the *remote* location and the analyzer, was proposed by Davies et al [82]. Only one year later, *R-LIBS* was extended to the use of a dual-optical fiber probe, but only at 4 m away [83]. Nonetheless, these operating distances have been adapted in parallel with the increasing day-to-day analytical demands [84, 85].

B. Standoff LIBS

Despite all the profits provided by *R-LIBS*, the requirement of a physical access for its potential use is more than an issue. This is the reason why, *standoff*

LIBS (*ST-LIBS*) was suggested for elemental analysis of distant targets located in scenarios where any physical access was not possible, but an immediate optical access was available. At this approach, both the laser radiation delivered up to a target located at several meters distance and the returning light from the induced plasma are transmitted through a "transparent" atmosphere in an *open-path* configuration [86].

It was *Cremers* who first demonstrated the feasibility of LIBS for ranged purposes, in 1987, [87] through the use of optical components for beam conditioning, guiding and focusing, as well as optics for light collection. Analysis at distances spanning from 0.5 to 2.4 m between the system and the target was possible at that time.

Since then, the solutions of *ST-LIBS* to a large field of applications [88, 89], as analytical demands and technology evolves, have promoted this approach as the cutting-edge sensing scheme that it is today.

Despite that *standoff* approach can be categorized as the most appealing scheme of LIBS, it implies greater complexity as compared to *hand-held* and *remote* operations. Beyond the series of constraints on the specifications of the instrumental components entailed, the circumstances associated to the "transparent" atmosphere through which the light propagates contribute to raise difficulties [90].

For such reasons, and for being the matter that is dealt in the present Memory of Thesis, more detailed comments on *ST-LIBS* will be provided in the next sections.

3 Fundamentals of standoff LIBS

ST-LIBS uses an *open-path* configuration in which both the laser beam and the returning plasma light are transmitted through the atmosphere. Analysis using this approach requires the production of analytically useful plasma at distance and the gathering of a sufficient amount of emitted light, thereby imposing requirements on the specifications of the components of the LIBS set-up: the laser, the optical system used for laser focusing and plasma light collection as well as on the spectrograph and detector [91].

The first limitation of *ST-LIBS* lies in the difficulties of obtaining enough energy density at long distance to generate such efficient plasmas. Up to date, two different schemes have been proposed to produce power densities sufficiently high to result in excitation of the distant samples; either using nanosecond laser pulses [92] or by employing femtosecond laser pulses, not only in conventional LIBS [93] but also through self-guided filaments induced in air [94, 95]. However, although the use of femtosecond pulses allows extending the analysis at longer distances, with kilometer range predicted [96] as compared to the distance range of tens of meters of nanoseconds pulses, the vast majority of *open-path* LIBS measurements have been conducted using this latter strategy. For this reason, in addition to be the same approach used in the works comprising the core of this Doctoral Thesis, we will put increased emphasis on the nanosecond scheme.

At this particular case, beyond the operational parameters of the laser (energy and wavelength), the density of energy (typically ≥ 1 $GW \cdot cm^{-2}$) at the target is a function of the distance (inversely proportional) and of the optical system –focusing mirror (or lens) diameter– (directly proportional). Hence, for a given laser pulse energy, the energy density produced on the distant target mainly depends on

the minimum radius achievable for the beam spot (ω) expressed for a Gaussian laser beam by:

$$\omega\ (\mathrm{m}) = \frac{2\pi r\lambda}{D} M^2 \qquad \text{(Equation 4)}$$

where, *r* refers to the sensor-to-target distance, λ indicates the laser wavelength, *D* designates the laser beam diameter at the focusing optics and M^2 denotes the beam quality parameter.

The imperfections on the spot size are caused by spherical aberrations and by the diffraction limit dictated entirely by the diameter of the focusing optics, generally a reflecting mirrors system. Obeying the laws of classical optics, spherical aberrations prohibit alter the focusing of the entire incident light from the same source to a precise point, whereas due to the diffraction, the diameter of focus linearly increases with focusing distance [97]. These circumstances aggravate difficulty to tightly focus the laser pulses at long distances.

In the same connection, laser pulses' focusing is also affected by the depth of focus (*DOF*) of the beam or confocal parameter. This factor is a measure of how much the focus must be accurately adjusted to dispose of the greatest energy density on the distant target. For the focal length of the optical component, the beam has its minimum width, that is, it achieves its best focus. Hence, in any location earlier or afterwards from this point, the beam gradually grows "out of focus". Thus, *DOF* is the axial distance within which the beam radius lies within a factor $\sqrt{2}$ of its minimum value, and is defined by the following expression:

$$DOF = \frac{8\lambda}{\pi}\left(\frac{r}{D}\right)^2 M^2 \qquad \text{(Equation 5)}$$

As shown, this factor also varies as the square of the sensor-to-target distance and as the reciprocal of the square of the input laser beam diameter at the focusing optics. As a consequence, the larger the distance of analysis, the wider the depth of focus, and hence precision on focusing becomes less critical. Nonetheless, this alleviated strictness for focusing the laser pulses is accompanied by a higher uncertainty on the disposed energy density on the distant target [91, 97].

For all these reasons, the components for guiding laser beam fulfill a critical role in producing the required irradiance to induce plasma at the envisaged location. Thus, the laser beam is preferable to be expanded prior its focusing. This stage allows focusing laser energy on the sample surface to a sufficient small spot size at far distance. Indeed, the larger the beam expansion the tighter the focusing. Furthermore, undesired dielectric breakdown of the air, along the laser path on the vicinity of the target, is no induced. More detailed information on the laser focusing systems with both refracting and reflecting optics for *standoff* LIBS analysis with nanosecond pulses can be found on [91] and the references therein.

A second limitation for *ST-LIBS* occurs once the plasma plume has been produced. Beyond the factors affecting plasma intensity, as the laser wavelength, laser power density, surrounding air, and nature of the sample, how many photons received from range *R* can be collected by the detector depends on several additional factors as identified by the LIDAR (light detection and ranging) equation [98]:

$$N_r(R) = \left(\frac{\varepsilon_t \lambda}{hc}\right)(\Delta R) T_a^2(R) \beta_{\varpi}(R) \left(\frac{A_r}{R^2}\right) \xi(R) T_0 + N_{bg} \qquad \text{(Equation 6)}$$

where ε_t is the transmitted pulse energy (J), $\frac{hc}{\lambda}$ is the transmitted photon energy (J·ph^{-1}), ΔR is the range bin (m), T_a is the atmospheric one-way path transmittance, β_{ϖ} is the angular scattering coefficient (m^{-1}·sr^{-1}), $\frac{A_r}{R^2}$ is the projected

solid angle of receiver as seen from scatterer at range *R* (sr), ξ is the overlap function (which depends only on the overlap of the area of laser radiation with the field of view of the receiver optics) based on geometric considerations, T_0 is the optics transmittance, and finally, N_{bg} are received background photons. Hence, diffuse light from plasma, as occurs for the laser beam delivered, is also altered by the distance. Attenuation via a loss of intensity evolves with the inverse of the range squared.

In this same context, the medium through which the light propagates is inherently connected with the analysis distance. Thus, atmosphere imposes additional restrictions to the use and measurement of optical radiation at long-range distances [99].

Effects of the atmosphere on light propagation

The atmosphere is a dynamic system of considerable complexity composed of gases, particulates, and aerosols whose physical and chemical properties vary as a function of time, altitude, and geographical location. The propagation of optical radiation through the atmosphere (just a few meters over land surface) depends upon the physical composition of the atmosphere, such as particulate matter suspended in the air such as soil particles, dust, and organic particles from vegetation, fog, haze, water droplets, and several optical interaction phenomena. Hence, in the following paragraphs, we consider some of the basic interactions involved in the transmission, absorption, emission, and scattering of light as it passes through the atmosphere.

While all of these interactions may be encapsulated as part of an overall radiative transfer process, some distinct optical phenomena such as molecular absorption, *Rayleigh* scattering, *Mie* or aerosol scattering, and molecular emission will be separately addressed. To do that, these basic phenomena will be discussed following a brief outline of the fundamental equations for the transmission of light

in the atmosphere centered around the *Beer-Lambert*'s law, which expresses the linear transmission (or absorption) of monochromatic light by species in the atmosphere.

$$I(\lambda, t', r) = I(\lambda, t', 0)e^{-\int_0^r \kappa(\lambda)N(r',t)dr'} \quad \text{(Equation 7)}$$

where $I(\lambda, t', r)$ indicates the intensity of the optical beam after passing through a path length of r, λ is the wavelength of the monochromatic light, t' reflects the potential propagation delay, $\kappa(\lambda)$ is the extinction coefficient and denotes the optical attenuation from the species per unit of species density and length, and $N(r', t)$ is the temporal and spatial variability for the concentration of the attenuating species. It must be also emphasized that, the extinction coefficient encompasses here all the phenomena contributing to the attenuation, that is, linear absorption, *Rayleigh* scattering, and *Mie* scattering.

The molecular absorption of light is one of the most basic optical phenomena of the atmosphere that can cause the extinction of the optical beam [100]. Molecular absorption is a selective attenuation of radiation that propagates at specific optical wavelength in the atmosphere caused from the interaction between photons and atoms or molecules (N_2, O_2, H_2, H_2O, CO_2, O_3, CH_4, NO_2, etc.). This selective phenomenon leads to the disappearing of the incident photon and an elevation of the temperature. The absorption coefficient depends on the type of gas molecules and on their concentration because photon absorption is primarily associated with individual optical absorption transitions between the allowed quantized energy levels of the molecule. As a result, the spectral transmission of the atmosphere presents from opaque zones, called atmospheric blocking windows, up to transparent zones, called atmospheric transmission window.

Together with molecular absorption, other phenomenon involved in extinction of radiation as it propagates is *Rayleigh* (or molecular) scattering. This

phenomenon is associated with optical scattering where the physical size of the scatterers is much lower than the wavelength of light (*i.e.*, atmospheric molecules). The incoming electro-magnetic (optical) field perturbs and displaces the weakly bound electronic cloud surrounding the gaseous molecule, thereby causing an elastic scattering of the optical radiation [101, 102].

In the same connection, *Mie* scattering is similar to *Rayleigh* scattering, except the size of the scattering sites is on a similar order of magnitude as the wavelength of the incident light, and is, thus, due to aerosols and fine particulates in the atmosphere [103]. Finally, an additional different regime for light dispersion is the geometric scattering, caused by those particles that have a larger diameter as compared to the wavelength of the incident radiation.

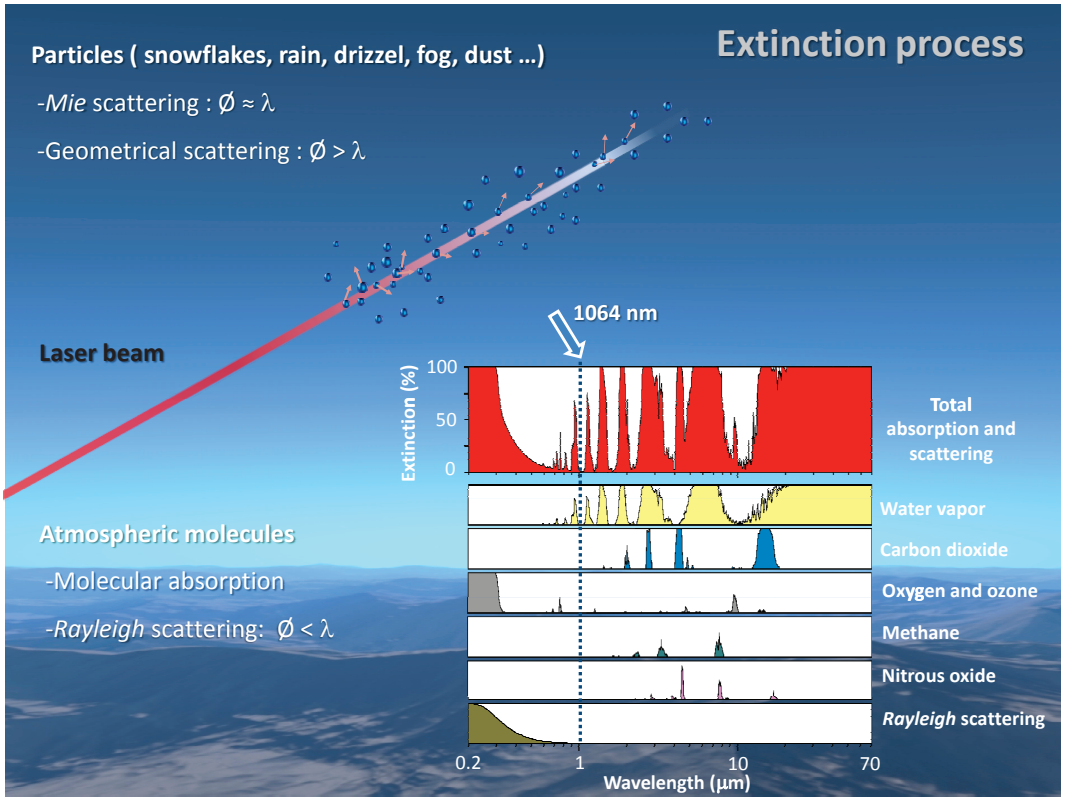

Fig. 10. Schematic diagram of those physical phenomena affecting the energy of a laser beam when propagates through the atmosphere. Inset shows in detail both, blocking and transmission windows of the atmosphere.

As exemplified in *Fig. 10*, a beam of light may be attenuated by these above commented phenomena when propagating along a distance *r* through a lossy medium. However, selection of a specific laser wavelength can alleviate the interferences caused by the atmosphere. In the particular case of a wavelength of 1064 nm, a high spectral transmission of the atmosphere is evidenced. In this case, molecular absorption and *Rayleigh* scattering can be neglected. Hence, only those aerosols that behave as "*Mie* and geometrical scatterers", like snowflakes, rain and drizzle drops, fog, windblown sand and dust, might cause a significant lose of energy to the laser beam.

Hence, the difficulty to state any "typical" optical property for aerosols since they widely vary, depending on their particle size and their chemistry, the moisture content of their surrounding air, etc., runs in parallel with the complexity to operate with *ST-LIBS*.

Atmospheric turbulences also contribute to distort light. Turbulences are characterized by both chaotic and random changes of atmosphere properties, and occur with low momentum diffusion (spreading of atmospheric properties), high momentum convection (vertical transference of atmospheric properties), and rapid variation of pressure and temperature of air in both space and time [103-105]. Such turbulences cause currents of air, dust, or fluids that run counter to the main current, that is, the so-called eddies. Under the influence of inertial forces, the larger eddies break up into smaller eddies to form a continuing trend of eddies. Thus, the energy from a macroscale, or *outer scale of turbulence* (large masses), is transferred into a microscale, or *inner scale of turbulence* (ever smaller masses), to such an extent that energy dissipates through molecular diffusion. This transference of energy is known as the length scale of *Kolmogorov*, who first proposed the theory of turbulence and the notion of cascading energy. In essence,

this dynamic mixing of the turbulent eddies is the responsible cause for which atmosphere loses its uniform characteristics [107].

This turbulent mixing combined with both temperature and pressure fluctuations induce a random behavior in one of the most significant parameters of the atmosphere for optical wave propagation, the index of refraction *n*. Such small-scale inhomogeneities into atmospheric quantities manifest themselves as refraction index fluctuations, which cause the most serious optical effects on a propagating electromagnetic wave. The scattering by refractive-index inhomogeneities can lead to a variety of deleterious effects on a laser beam that has traversed a relatively long distance in the atmosphere. These undesired consequences can be briefly summarized as follows:

- ✓ *Beam wander* effect describes a random pointing –"*dancing*"– of the instantaneous centroid ("*hot spot*") of the beam on distinct positions at the receiver plane [107, 108]. Related to this effect, a *jitter* of the beam, that suggests the whole beam moving around its unperturbed position at the receiver plane, caused by distortions in its wavefront phase, can also occurs.

- ✓ *Beam spreading* effect refers to a beam divergence from phase variations, beyond the dimensions attributed to the usual diffraction spreading [109, 110].

- ✓ *Scintillation* effect indicates random temporal and spatial variations in received energy from the transmitted light [111, 112].

- ✓ *Loss* of *spatial coherence* that reduces the ability to focus the light beam to a small spot, thereby limiting the maximum intensity that is produced at the focal point [113].

Fig. 11 seeks to graphically exemplify some of these effects on the laser beam when traverses a distance across the atmosphere. As shown, the disparity on laser beam pointing over target surface with respect to the theoretical focusing position reflects the *wandering* of the beam (on the left). In addition, these random variations on directionality and positioning of the transmitted beam may be accompanied by distortions on spatial and temporal distributions of the beam laser with its propagation through the atmosphere; the mentioned *scintillation* phenomenon (on the right). In any case, although these faltering alterations may arise simultaneously, they do not always correlate with each other.

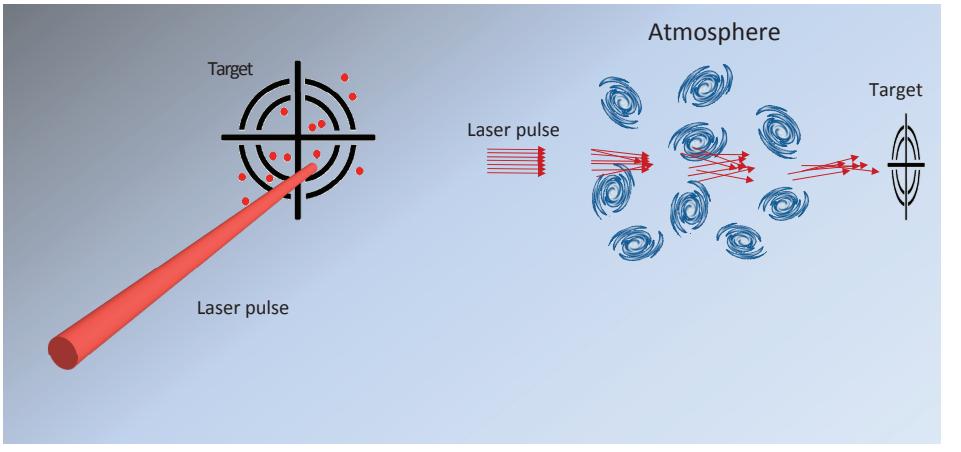

Fig. 11. Illustrative examples on the most relevant disturbances exerting influences on the behavior of the light when propagating along its optical path: *beam wandering* (on the left) and *scintillation* (on the right).

In summary, all variations along the propagation path may affect not only the ability to direct a laser beam up to a distant target from the LIBS sensor but also the gathering of the light from the induced plasma plume. Factors such as the pointing stability of the laser beam, the energy density incident on the distant target,

determined by the energy emitted by the laser, its divergence, its attenuation and its modification, have an impact on the quality and the reproducibility of produced distant plasmas. All this, added to the pointing stability of the plasma image at the receiver optics, turns any operation with LIBS at *standoff* configuration into a complex task. Without any doubt, effects on the qualitative and quantitative analytical information are more than an issue.

4 LIBS applications

4.1 General overview

Since laser radiation is a high-quality form of electromagnetic energy, the laser measuring methods as well as its applications evidenced a very dynamical development as soon as the laser was invented. Furthermore, due to the close tie between the special properties of laser radiation and the spectroscopic methods, the laser-based spectroscopic methods soon became powerful tools for fundamental investigations. Amongst all of them, LIBS could be considered as the most appealing method, since, when their features are compared, LIBS is the only method that allows for a simultaneous multispecies analysis of a substance in all its states of aggregation. This distinguishing feature, together with many other (listed in *Table 1*), has pushed forward LIBS as a very attractive and popular technique in the field of chemical analysis. Hence, although sometimes LIBS seems not to offer decisive advantages over already established methods, to numerous applications LIBS takes a step forward either in terms of throughput, simplicity, or sensitivity [56].

Although LIBS is not without some disadvantages (matrix effects, spectral interferences and µdevastating consequences), its several advantages over conventional elemental analysis methods have led LIBS to be one of the few

analytical techniques that blends the vast majority of features required to address the analytical demands of nowadays [64].

Table 1. Salient characteristics of LIBS

Distinguishing feature	Observations
✓ No sample preparation	Laser plasmas can be induced on all samples without any prior neither physical nor chemical treatment.
✓ All states of aggregation	Laser plasmas can be induced on all samples whatever their forms, their conditions, or their states. While we must recognize additional difficulties to produce plasmas on liquids and gases.
✓ Real time analysis	Information about multielemental composition of the analyzed sample can be displayed in a matter of seconds.
✓ Useful in many and simultaneous spectral regions	Simultaneous collection of a broad spectral range, from UV to near IR regions, is allowed.
✓ Plentiful information	Provides such huge volume of information, that is, on numerous occasions, requires its combination with well-suited chemometric tools.
✓ *Standoff* analysis	Either in an *open-path* or through a fiber probe, whatever the number of laser pulses delivered (one, two or multiple), plasmas can be induced on distant targets and spectral information contained in its light can be gathered.
✓ Simple, compact, portable, inexpensive,	Despite complexity of phenomena involving laser ablation of matter, LIBS is easily implemented. Furthermore, improvement on their components has allowed it to be compacted in robust and movable instruments, beyond to be also amenable of a relatively low-cost.
✓ Compatible with other methods	The high degree of matching to other laser-based core techniques (e.g. Raman, IR and LIF) leads to broaden the versatility of LIBS through its participation within an spectroscopic framework of detection.
✓ *3D* resolution	Together with the capability to directly address a bidimensional analysis of a sample surface, the sequential delivering of successive laser pulses to the same point confers a unique *3D* capability (depth profiling analysis).
✓ Absolute (standardless)	Although calibration-free LIBS (*CF-LIBS*) technique is gaining acceptance and success in certain experimental situations, LIBS cannot yet to be considered a technique that does not require standards to address quantification purposes.

In this vein, LIBS has been used for countless purposes. Applications of LIBS include all industrial fields, involving from analysis of food up to nuclear materials. So, the potential of LIBS in food industry has been demonstrated, just for instance, for the rapid identification of bacterial pathogens, like E. coli O157:H7 and S. enteric, on various foods (eggshell, milk, bologna, ground beef, chicken, and lettuce) and surfaces (metal drain strainer and cutting board) [114], to the identification, quality control, traceability, and adulteration detection of extra virgin olive oils [115] and for *in situ* or online detection of trace elements on the surface of fresh potatoes [116, 117].

The ability of LIBS to the steel making and processing industry is also broad, through the analysis of substances ranging from top gas of the blast furnace, via liquid steel up to finished products [118]. Laser plasmas have been also used for identifying and quantifying the major metals present in the most used alloys in the jewellery industry, namely binary or ternary Au–Ag–Cu combinations [119, 120], as well as to the analysis of some minor components (Ni, Pb, Sn and Zn) on bronzes (copper-based-alloys) [121, 122].

Other useful LIBS applications lie in the analysis of cultural heritage objects [123]. The analysis of selected paint materials such as lithopone, a white inorganic pigment, and two synthetic organic paint formulations, lemon yellow and phthalocyanine blue [124], the characterization of a ceramic vase originally attributed to the I century CE [125], and the categorization of surface degradation pathologies, chromophores, and opacifying elements through stratigraphic analysis of ancient Roman glass samples [126], are only some examples of that.

LIBS has also demonstrated versatility in the widespread scenarios of geochemical and environmental analysis, through the identification and characterization of geological materials, like soils, rocks and sediments [127], as well as in the agricultural sciences to the direct interrogation of plant materials [128].

The beneficial use of LIBS when apply in biomedical field has been also outlined [129, 130]. Just to cite some examples, LIBS has been used to diagnose the state of human teeth through the characterization of the elemental composition of their healthy and infected parts [131]. The information contained in LIBS spectra has been also able to differentiate between different types of tissue samples from chicken brain, lung, spleen, liver, kidney and skeletal muscle [132]. Its *in vitro* possibilities and its effectiveness for the identification of both breast and colorectal cancer from frozen human tissues as well as determining the disease grade and severity have been also outlined [133]. Even the application of LIBS for *in situ* quantitative estimation of elemental constituents distributed in different parts of renal- and urinary-calculus obtained directly from patients by surgery [134, 135] as well as to differentiate live pathogens (*B. anthracis Sterne*) strains, live vaccines (*F. tularensis*) strains, and UV-killed hantavirus strains on substrates has been also evaluated [136].

Last but not least, LIBS has been also applied to forensic science research interests. The discrimination of float glasses from automobiles [137, 138] and the determination of uranium-235/uranium-238 isotope ratios in air at atmospheric pressure with the aim to design of a *field-portable* unit for nuclear safeguard inspection [139], to mention just a few.

4.2 Specific applications of *standoff* LIBS

Within the broad range of LIBS applications, there are some purposes that, due to their particular aspects, require implementation of *standoff* approach to operate. Whatever the reason, either a physical inability to have access up to the concerned target or the potentially hazardous nature of the scenario involved, distance is the key factor. In a graphical manner, a summary of instances for which *ST-LIBS* has been susceptible of being considered is projected in *Fig. 12*.

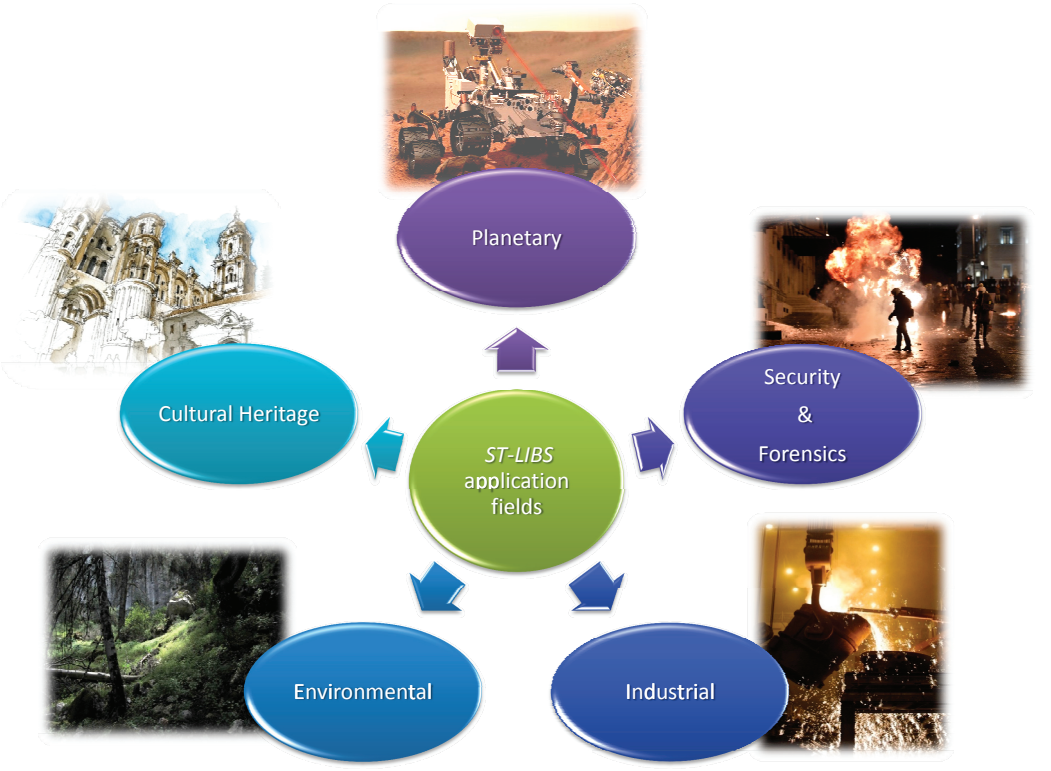

Fig. 12. Main application fields of *ST-LIBS*.

In this vein, a short outline of such particular application fields is presented below.

- ***Planetary sciences***

Perhaps, the use of *ST-LIBS* for space exploration can be considered one of the most exotic applications of the technique. The *ChemCam* instrument package on the *Mars Science Laboratory* (*MSL*) rover, *Curiosity*, is the first planetary science instrument to employ LIBS for determining elemental compositions of geological samples (rocks and soils) on another planet within 7 m of the instrument. [140-142] *ChemCam* supports *MSL* with

5 capabilities: I) *remote* active removal of surface dust and coatings or weathering rinds from rocks to determine their underlying composition through depth profiling; II) passive spectroscopy over the 240–905 nm range; III) image of the targeted area to place the LIBS analysis in a geological context; IV) quantitative elemental compositions including light elements like hydrogen and some elements to which LIBS is uniquely sensitive (e.g., Li, Be, Rb, Sr, Ba, B, C, N, and O); and V) a *remote* classification of rock and soil characteristics. Arguably it is the biggest challenge to demonstrate the versatility of LIBS in the geochemical field. After the publication of the first LIBS spectrum*, whose preliminary analysis indicates that it is consistent with basalt, which is known from previous missions to be abundant on Mars, one of the findings of the *ChemCam* instrument along the Curiosity rover traverse on the Martian soil chemistry at the submillimeter scale has been the identification of two principal soil types: a *fine-grained mafic* type and a locally derived, *coarse-grained felsic* type [143].

*The first LIBS spectrum can be seen on this website: (http://www.nasa.gov/mission_pages/msl/multimedia/pia16089.html)

- ***Security & Forensics***

Another important scope of application for which *ST-LIBS* is deemed mandatory is the security field. In response to the increasing threat to homeland security, the need for versatile, rapid, and robust *standoff* sensing systems has emerged in order to prevent, control and mitigate chemical, biological, radiological and nuclear (*CBRN*) threats.

Although explosive residues have been the most assayed targets [144, 145], the detection and discrimination of biological warfare agent surrogates have been also addressed [146].

ST-LIBS, either in an isolated form or combined with other laser-assisted spectroscopic techniques like Raman [147-149], operated at *single-shot* or dual pulse configurations and combined with adapted chemometric algorithms [150, 151], has revealed its capabilities to sensitively and accurately detect explosives.

All these successful findings open up opportunities for *ST-LIBS* to be used in forensic purposes at the scene of the attack, thereby avoiding the manipulation of the proofs and evidences up to the lab facilities.

- ***Industrial***

As commented before, it was *Cremers* who predicted a successful implementation of *ST-LIBS* in the industrial field. When he demonstrated the identification of the main elemental components of eight metals at distances between 0.5 and 2.4 m from the focusing lens and light-collection optics by using a single laser pulse to record each spectrum, the bases were in place [87].

Although numerous applications such as steel characterization, in-process monitoring for control of metallic samples with scale layers, on-site analysis of slag samples in secondary metallurgy and field characterization of raw materials, among others, demonstrated the technology, it was later when the steel industry took advantage of these advances.

ST-LIBS was implemented to direct tracking of some metallurgical industry situations related to measurements of steel composition under both harsh and high-temperature environment of a steel plant. Important examples are the analytical control of the continuous casting of molten steel [152], or the hot coils of intermediate materials in a rolling mill [153].

The feasibility of *ST-LIBS* was demonstrated for small stainless steel samples at temperatures up to 1200 °C with a system separated 0.5 m from

the sample placed inside a laboratory furnace [154]. A transportable *ST-LIBS* instrument was tested in a quality control laboratory-scale induction furnace of 1 kg capacity, before to be assessed at the stainless steel factory of Acerinox, S.A., located in Los Barrios (Cádiz, Spain) for the *on-line* elemental analysis of its molten steel. The overall beam path measured between the instrument and the crucible was approximately 7.5 m [155].

While, sometimes, the complexity of the plant forces the laser beam and the measuring radiation to be guided close to the liquid steel or immersed in it using a moveable lance to gain access to the melt surface from the top, the actual dimensions of production furnaces in a steel plant entail a high risk for the instrumentation in terms of exposure to such a vast radiation source. Hence, it seems reasonable that any attempt to perform an on-site analysis of hot steel should be preferably directed under a *standoff* approach. Use of *ST-LIBS* in this anticipated routine analysis of compositions from smelters during their manufacturing minimizes or eliminates risky and lengthy hotsampling operations in steel production as well as reduces any delay the production cycles.

- ***Environment***

The instrumentation portability and the versatility for *in situ* measurements of raw samples have rendered *ST-LIBS* also suitable for analytical applications in the in the broad field of environmental science. Since soil is the most affected environmental compartment through heavy metal contamination, with important implications on the equilibrium of ecosystems, the detection and measurement of levels of toxic metals in soils are among the most important issues of *ST-LIBS*. Rocks, soils, leaves and barks from trees, as well as stones and wall fragments from a factory or its surrounding buildings from a coastal site subjected to a high industrial

activity, have been qualitatively and quantitatively analyzed at a distance of 12 m (although in laboratory, rather than *in situ*) [156]. A large suite of similar geological materials (natural carbonate, fluorite and silicate) has been studied, using both *single-* and *double-pulse* LIBS, at distances of 25 m to identify their distinguishing characteristics in terms of minor impurities for their further sorting. [157]. *ST-LIBS* detection and analysis of Hg, As, Pb, Zn, Cd and Cr on environmental land samples like soils and vegetation powder have been also demonstrated [158].

More investigations into the applicability frontiers of *ST-LIBS* have been considered to the detection of unidentified pollutants into the air and water. Thus, in the interest of establish the potential of LIBS to fulfill the detection of air pollutants originated from sources such as vehicle emissions, power plants, refineries, and industrial processes, the technique has been intended to the detection of aerosols by producing optical breakdown at 10 meters of distance, and detecting the analytical signal resulting from the optical discharge [159]. In addition, due to the need of *in situ* chemical sensors in this field, the metal pollution analysis of aqueous samples from industrial plants and wastewater must be mentioned [160, 161].

Finally, although it has not been yet applied in a real scenario, a highly appealing of *ST-LIBS* is the detection of elements found in one extreme and hostile ocean environment [162, 163]. *ST-LIBS* measurement on deep-ocean is perhaps the next most ambitious and exciting challenge.

- ***Cultural Heritage***

While the most appealing features of LIBS have lead to its applicability to numerous tasks in the field of cultural heritage analysis [164], the vast majority of matters are focused on the close-contact analysis

of pieces of arts, such as sculptures [165], ceramics [166], metallic objects and paintings [167, 168]. Although some of them are tested without leaving their original locations, like museums, historical buildings and excavation sites, the exploitation of *ST-LIBS* is taking a long time to attain its huge potential.

There are only a few contributions that demonstrate the capability of *ST-LIBS* as a valuable tool is this field. First, a mobile LIDAR sensor intended to distant cleaning of cultural heritage items using LIBS imaging combined with laser-induced fluorescence (LIF). The experiments on ablative cleaning of stone surfaces were performed with a system–target distance of 60 m [169, 170]. Second, rather than an *open-path* sensor, a *remote* LIBS instrument based on a fiber optic cable to deliver the laser beam energy for the recognition and identification of archeological bronzes containing a high oxidation degree submerged in the Mediterranean Sea at depths up to 30 m [171]. This study directly verifies the feasibility of LIBS analysis for drowned assets, such as sunken ships and their content. The information obtained from findings is of primary importance prior to planning recovery activities and taking decisions about whether the object must be moved or not.

All these examples above show evidences on the complicated goals that *ST-LIBS* has met but, at the same time, they reflect no more than first steps on the long road that LIBS researchers have to travel. Hence, the work presented in this Thesis seeks to contribute our grain of sand for making progress towards the maturity and the exploitation of *ST-LIBS* as a leading-edge analytical tool.

5 References

[1] A. Einstein, Zur quantentheorie der strahlung (on the quantum theory of radiation) *Physikalische Zeitschrift* 18 (1917) 121–128.

[2] A.L. Shawlow, C.H. Townes, Infrared and optical masers, *Phys. Rev.* 112 (1958) 1940–1949.

[3] T.H. Maiman, Stimulated optical radiation in ruby, *Nature* 187 (1960) 493–494.

[4] P.P. Sorokin, M.J. Stevenson, Stimulated infrared emission from trivalent uranium, *Phys. Rev. Lett.* 5 (1960) 557–559.

[5] J.E. Geusic, H.M. Marcos, L.G. Van Uitert, Laser oscillations in Nd-doped yttrium aluminum, yttrium gallium and gadolinium garnets, *Appl. Phys. Lett*. 4 (1964) 182–184.

[6] J. Hecht, Laser pioneers, *Academic Press*, New York (1992).

[7] F. Brech, L. Cross, Optical microemission stimulated by a ruby laser, *Appl. Spectrosc.* 16 (1962) 59.

[8] J. Debras-Guédon, N. Liodec, De l'utilisation du faisceau d'un amplificateur a ondes lumineuses par émission induite de rayonnement (laser á rubis), comme source énergetique pour l'excitation des spectres d'émission des elements, *C.R. Acad. Sci.* 257 (1963) 3336–3339.

[9] R.H. Scott, A. Strasheim, Laser induced plasmas for analytical spectroscopy, *Spectrochim. Acta Part B* 25 (1970) 311–332.

[10] W.W. Schroeder, J.J. van Niekirk, L. Dicks, A. Strasheim, H.v.d. Piepen, A new electronic time resolution system for direct reading spectrometers and some applications in the diagnosis of spark and laser radiations, *Spectrochim. Acta Part B* 26 (1971) 331–340.

[11] L. Radziemski, D. Cremers, A brief history of laser-induced breakdown spectroscopy: from the concept of atoms to LIBS 2012, *Spectrochim. Acta Part B* 87 (2013) 3–10.

[12] J.P. Singh, S.N. Thakur, Laser-induced breakdown spectroscopy, *Elsevier*, Amsterdam (2007).

[13] A.W. Miziolek, V. Palleschi, I. Schechter, Laser-induced breakdown spectroscopy (LIBS), fundamentals and applications, *Cambridge University Press*, New York (2006).

[14] Y.I. Lee, K. Song, J. Sneddon, Laser-induced breakdown spectroscopy, *Nova Science Publishers*, Huntington (2000).

[15] D.B. Chrisey, G.K. Hubler, Pulsed laser deposition of thin films, *Wiley-Interscience*, New York (1994).

[16] D.A. Cremers, L.J. Ramdziemski, Handbook of laser-induced breakdown spectroscopy, *Wiley*, Chichester (2006).

[17] X. Mao, W. Chan, M. Caetano, M.A. Shannon, R.E. Russo, Preferential vaporization and plasma shielding during nano-second laser ablation, *Appl. Surf. Sci.* 96–98 (1996) 126–130.

[18] J.A. Aguilera, C. Aragón, F. Peñalba, Plasma shielding effect in laser ablation of metallic samples and its influence on LIBS analysis, *Appl. Surf. Sci.* 127–129 (1998) 309–314.

[19] X.L. Mao, A.C. Ciocan, R.E. Russo, Preferential vaporization during laser ablation inductively coupled plasma atomic emission spectroscopy, *Appl. Spectrosc.* 52 (1998) 913–918.

[20] J.R. Ho, C.P Grigoropoulos, J.A.C. Humphrey, Gas dynamics and radiation heat transfer in the vapor plume produced by pulsed laser irradiation of aluminum, *J Appl. Phys.* 79 (1996) 7205–7215.

[21] G. Bekefi, Radiation processes in plasmas, *John Wiley & Sons*, New Jersey (1966).

[22] C. Aragón, J.A. Aguilera, Characterization of laser induced plasmas by optical emission spectroscopy: a review of experiments and methods, *Spectrochim. Acta Part B* 63 (2008) 893–916.

[23] Y. Zhou, B. Wu, S. Tao, A. Forsman, Y. Gao, Physical mechanism of silicon ablation with long nanosecond laser pulses at 1064 nm through time-resolved observation, *Appl. Surf. Sci.* 257 (2011) 2886–2890.

[24] F.J. Fortes, J. Moros, P. Lucena, L.M. Cabalín, J.J Laserna, Laser-induced breakdown spectroscopy, *Anal. Chem.* 85 (2013) 640–669.

[25] Y. Zhou, B. Wu, A. Forsman, Time-resolved observation of the plasma induced by laser metal ablation in air at atmospheric pressure, *J. Appl. Phys.* 108 (2010) 093504-1–093504-7.

[26] Y. Zhou, S. Tao, B. Wu, Backward growth of plasma induced by long nanosecond laser pulse ablation, *Appl. Phys. Lett.* 99 (2011) 051106-1–051106-3.

[27] E. Axente, S. Noël, J. Hermann, M. Sentis, I.N. Mihailescu, Subpicosecond laser ablation of copper and fused silica: initiation threshold and plasma expansion, *Appl. Surf. Sci.* 255 (2009) 9734–9737.

[28] R.E. Russo, X.L. Mao, C. Liu, J. González, Laser assisted plasma spectrochemistry: laser ablation, *J. Anal. At. Spectrom.* 19 (2004) 1084–1089.

[29] M. Hanif, M. Salik, M.A. Baig, Quantitative studies of copper plasma using laser induced breakdown spectroscopy, *Opt. Laser Eng.* 49 (2011) 1456–1461.

[30] N.M. Shaikh, S. Hafeez, B. Rashid, M.A. Baig, Spectroscopic studies of laser induced aluminum plasma using fundamental, second and third harmonics of a Nd:YAG laser, *Eur. Phys. J.* 44 (2007) 371–379.

[31] J.R. Freeman, S.S. Harilal, B. Verhoff, A. Hassanein, B. Rice, Laser wavelength dependence on angular emission dynamics of Nd:YAG laser-produced Sn plasmas, *Plasma Sources Sci. Technol.* 21 (2012) 055003-1–1055003-7.

[32] Q. Ma, V. Motto-Ros, F. Laye, J. Yu, W. Lei, X. Bai, L. Zheng, H. Zeng, Ultraviolet versus infrared: effects of ablation laser wavelength on the expansion of laser-induced plasma into one-atmosphere argon gas, *J. Appl. Phys.* 111 (2012) 053301-1–053301-11.

[33] J.D. Ingle, S.R. Crouch, Spectrochemical analysis, *Prentice Hall*, Englewood Cliffs (1988).

[34] M. Cirisan, J.M. Jouvard, L. Lavisse, L. Hallo, R. Oltra, Laser plasma plume structure and dynamics in the ambient air: the early stage of expansion, *J. Appl. Phys.* 109 (2011) 103301-1–03301-17.

[35] W.F. Luo, X.X. Zhao, Q.B. Sun, C.X. Gao, J. Tang, H.J. Wang, W. Zhao, Characteristics of the aluminum alloy plasma produced by a 1064 nm Nd:YAG laser with different irradiances, *Pramana-J. Phys.* 74 (2010) 945–959.

[36] J.A. Aguilera, C. Aragón, C. Madurga, V. Manrique, Study of matrix effects in laser induced breakdown spectroscopy on metallic samples using plasma characterization by emission spectroscopy, *Spectrochim. Acta Part B* 64 (2009) 993–998.

[37] R. Viskup, B. Praher, T. Stehrer, J. Jasik, H. Wolfmeir, E. Arenholz, J.D. Pedarnig, J. Heitz, Plasma plume photography and spectroscopy of Fe–Oxide materials*, J. Appl. Surf. Sci.* 255 (2009) 5215–5219.

[38] T.A. Labutin, A.M. Popov, V.N. Lednev, N.B. Zorov, Correlation between properties of a solid sample and laser-induced plasma parameters, *Spectrochim. Acta Part B* 64 (2009) 938–949.

[39] A. De Giacomo, M. Dell'Aglio, R. Gaudiuso, S. Amoruso, O. De Pascale, Effects of the background environment on formation, evolution and emission spectra of laser-induced plasmas, *Spectrochim. Acta Part B* 78 (2012) 1–19.

[40] M. Young, M. Hercher, Dynamics of laser-induced breakdown in gases, *J. Appl. Phys.* 38 (1967) 4393–4400.

[41] Y. Iida, Effects of atmosphere on laser vaporization and excitation processes of solid samples, *Spectrochim. Acta Part B* 45 (1990) 1353–1367.

[42] M. Kuzuya, H. Matsumoto, H. Takechi, O. Mikami, Effect of laser energy and atmosphere on the emission characteristics of laser-induced plasmas, *Appl. Spectrosc.* 47 (1993) 1659–1664.

[43] J.A. Aguilera, C.A. Aragón, Comparison of the temperatures and electron densities of laser-produced plasmas obtained in air, argon and helium at atmospheric pressure, *Appl. Phys. A Mater.* 69 (1999) S475–S478.

[44] J.S. Cowpe, R.D. Pilkington, J.S. Astin, A.E Hill, The effect of ambient pressure on laser-induced silicon plasma temperature, density and morphology, *J. Phys. D Appl. Phys.* 42 (2009) 165202-1–165202-8.

[45] A.K. Shuaibov, L.V. Mesarosh, M.P. Chuchman, Features of the formation of a laser flare from aluminum in the presence of a background gas, *J. Opt. Technol.* 78 (2011) 358–361.

[46] G. Cristoforetti, E. Tognoni, L.A. Gizzi, Thermodynamic equilibrium states in laser-induced plasmas: from the general case to laser-induced breakdown spectroscopy plasmas, *Spectrochim. Acta Part B* 90 (2013) 1–22.

[47] D.W. Hahn, N. Omenetto, Laser-induced breakdown spectroscopy (LIBS), part I: review of basic diagnostics and plasma–particle interactions: still-challenging issues within the analytical plasma community, *Appl. Spectrosc.* 64 (2010) 335A–366A.

[48] J.A. Aguilera, C. Aragón, Multi-element Saha–Boltzmann and Boltzmann plots in laser-induced plasmas, *Spectrochim. Acta Part B* 62 (2007) 378–385.

[49] N. Konjević, M. Ivković, S Jovićević, Spectroscopic diagnostics of laser-induced plasmas, *Spectrochim. Acta Part B* 65 (2010) 593–602.

[50] H.R. Griem, Plasma spectroscopy, *McGraw-Hill*, New York (1974).

[51] I.B. Gornushkin, C.L. Stevenson, B.W. Smith, N. Omenetto, J.D. Winefordner, Modeling an inhomogeneous optically thick laser induced plasma: a simplified theoretical approach*, Spectrochim. Acta Part B* 56 (2001) 1769–1785.

[52] R. Noll, Laser-induced breakdown spectroscopy: fundamentals and applications, *Springer-Verlag*, Berlin (2012).

[53] H.R. Griem, Spectral line broadening by plasmas, *Academic Press*, New York (1974).

[54] H.R. Griem, Principles of plasma spectroscopy, *Cambridge University Press*, New York (1984).

[55] I.B. Gornushkin, L.A. King, B.W. Smith, N. Omenetto, J.D. Winefordner, Line broadening mechanisms in the low pressure laser-induced plasma, *Spectrochim. Acta Part B* 54 (1999) 1207–1217.

[56] D.W. Hahn, N. Omenetto, Laser-induced breakdown spectroscopy (LIBS), part II: review of instrumental and methodological approaches to material analysis and applications to different fields, *Appl. Spectrosc.* 66 (2012) 347–419.

[57] M. Baudelet, B.W. Smith, The f rst years of laser-induced breakdown spectroscopy, *J. Anal. At. Spectrom.* 28 (2013) 624–629.

[58] A.E. Siegman, Lasers, *University Science Books*, Sausalito (1986).

[59] M. Chen, Y.H. Liu, X.D. Liu, M.W. Zhao, Role of lens to sample distance during laser-induced damage in zinc targets, *Laser Phys. Lett.* 9 (2012) 730–733.

[60] R. Noll, V. Sturm, Ü. Aydin, D. Eilers, C. Gehlen, M. Höhne, A. Lamott, J. Makowe, J. Vrenegor, Laser-induced breakdown spectroscopy–from research to industry, new frontiers for process control, *Spectrochim. Acta Part B* 63 (2008) 1159–1166.

[61] C. Haisch, U. Panne, R. Niessner, Combination of an iCCD with an Echelle spectrograph for analysis of colloidal material by LIPS, *Spectrochim. Acta Part B* 53 (1998) 1657–1667.

[62] M. Mueller, I.B. Gornushkin, S. Florek, D. Mory, U. Panne, Approach to detection in laser-induced breakdown spectroscopy, *Anal. Chem.* 79 (2007) 4419–4426.

[63] M.T. Taschuk, Y. Godwal, Y.Y. Tsui, R. Fedosejevs, M. Tripathi, B. Kearton, Absolute characterization of laser-induced breakdown spectroscopy detection systems, *Spectrochim. Acta Part B* 63 (2008) 525–535.

[64] A.P.M. Michel, Review: applications of single-shot laser-induced breakdown spectroscopy, *Spectrochim. Acta Part B* 65 (2010) 185–191.

[65] V.I. Babushok, F.C. De Lucia, Jr., J.L. Gottfried, C.A. Munson, A.W. Miziolek, Double pulse laser ablation and plasma: laser induced breakdown spectroscopy signal enhancement, *Spectrochim. Acta Part B* 61 (2006) 999–1014.

[66] D.N. Stratis, K.L. Eland, S.M. Angel, Effect of pulse delay time on a pre-ablation dual-pulse LIBS plasma, *Appl. Spectrosc.* 55 (2001) 1297–1303.

[67] A. De Giacomo, M. Dell'Aglio, D. Bruno, R. Gaudiuso, O. De Pascale, Experimental and theoretical comparison of single-pulse and double-pulse laser induced breakdown spectroscopy on metallic samples, *Spectrochim. Acta Part B* 63 (2008) 805–816.

[68] V. Piscitelli, M.A. Martínez L., A.J. Fernández C., J.J. González, X.L. Mao, R.E. Russo, Double pulse laser induced breakdown spectroscopy: experimental study of lead emission intensity dependence on the wavelengths and sample matrix, *Spectrochim. Acta Part B* 64 (2009) 147–154.

[69] Y. Lu, V. Zorba, X. Mao, R. Zheng, R.E. Russo, UV fs–ns double-pulse laser induced breakdown spectroscopy for high spatial resolution chemical analysis, *J. Anal. At. Spectrom.* 28 (2013) 743–748.

[70] P.K. Diwakar, S.S Harilal, J.R Freeman, A. Hassanein, Role of laser pre-pulse wavelength and inter-pulse delay on signal enhancement in collinear double-pulse laser-induced breakdown spectroscopy, *Spectrochim. Acta Part B* 87 (2013) 65–73.

[71] N. Jedlinszki, G. Galbács, An evaluation of the analytical performance of collinear multi-pulse laser induced breakdown spectroscopy, *Microchem. J.* 97 (2011) 255–263.

[72] R. Sattmann, V. Sturm, R. Noll, Laser-induced breakdown spectroscopy of steel samples using multiple Q-switch Nd:YAG laser pulses, *J. Phys. D Appl. Phys.* 28 (1995) 2181–2187.

[73] Z. Fu, B. Wu, Y. Gao, Y. Zhou, C. Yu, Experimental study of infrared nanosecond laser ablation of silicon: the multi-pulse enhancement effect, *Appl. Surf. Sci.* 256 (2010) 2092–2096.

[74] R.S. Harmon, F.C. De Lucia, A.W. Miziolek, K.L. McNesby, R.A. Walters, P.D. French, Laser-induced breakdown spectroscopy (LIBS) – an emerging field-portable sensor technology for real-time, in-situ geochemical and environmental analysis, *Geochem. Explor. Environ. Anal.* 5 (2005) 21–28.

[75] F.J. Fortes, J.J. Laserna, The development of fieldable laser-induced breakdown spectrometer: no limits on the horizon, *Spectrochim. Acta Part B* 65 (2010) 975–990.

[76] J. Cuñat, F.J. Fortes, L.M. Cabalín, F. Carrasco, M.D. Simón, J.J. Laserna, Man-portable laser-induced breakdown spectroscopy system for in situ characterization of karstic formations, *Appl. Spectrosc.* 62 (2008) 1250–1255.

[77] K.Y. Yamamoto, D.A. Cremers, M.J. Ferris, L.E. Foster, Detection of metals in the environment using a portable laser-induced breakdown spectroscopy instrument, *Appl. Spectrosc.* 50 (1996) 222–233.

[78] J. Cuñat, F.J. Fortes, J.J. Laserna, Real time and in situ determination of lead in road sediments using a man-portable laser-induced breakdown spectroscopy analyzer, *Anal. Chim. Acta* 633 (2009) 38–42.

[79] F.C. De Lucia, Jr, A.C. Samuels, R.S. Harmon, R.A. Walters, K.L. McNesby, A. LaPointe, R.J. Winkel, Jr., A.W. Miziolek, Laser-induced breakdown spectroscopy (LIBS): a promising versatile chemical sensor technology for hazardous material detection, *IEES Sensors J.* 5 (2005) 681–689.

[80] U. Panne, Laser remote sensing, *Trends Anal. Chem.* 17 (1998) 492–500.

[81] C. Fabre, S. Maurice, A. Cousin, R.C. Wiens, O. Forni, V. Sautter, D. Guillaume Onboard calibration igneous targets for the Mars Science Laboratory Curiosity rover and the Chemistry Camera laser induced breakdown spectroscopy instrument, *Spectrochim. Acta Part B* 66 (2011) 280–289.

[82] C.M. Davies, H.H. Telle, D.J. Montgomery, R.E. Corbett, Quantitative analysis using remote laser-induced breakdown spectroscopy (LIBS), *Spectrochim. Acta Part B* 50 (1995) 1059–1075.

[83] B.J. Marquardt, S.R. Goode, S.M. Angel, In situ determination of lead in paint by laser-induced breakdown spectroscopy using a f ber-optic probe, *Anal. Chem.* 68 (1996) 977–981.

[84] A.I. Whitehouse, J. Young, I.M. Botheroy, S. Lawson, C.P. Evans, J. Wright, Remote material analysis of nuclear power station steam generator tubes by laser-induced breakdown spectroscopy, *Spectrochim. Acta Part B* 56 (2001) 821–830.

[85] B. Bousquet, G. Travaillé, A. Ismaël, L. Canioni, K. Michel-Le Pierrès, E. Brasseur, S. Roy, I. le Hecho, M. Larregieu, S. Tellier, M. Potin-Gautier, T. Boriachon, P. Wazen, A. Diard, S. Belbèze, Development of a mobile system based on laser-induced breakdown spectroscopy and dedicated to in situ analysis of polluted soils, *Spectrochim. Acta Part B* 63 (2008) 1085–1090.

[86] B. Sallé, P. Mauchien, S. Maurice, Laser-induced breakdown spectroscopy in open-path conf guration for the analysis of distant objects, *Spectrochim. Acta Part B* 62 (2007) 739–768.

[87] D.A. Cremers, The analysis of metals at a distance using laser-induced breakdown spectroscopy, *Appl. Spectrosc.* 41 (1987) 572–579.

[88] J.L. Gottfried, F.C. De Lucia, Jr., C.A. Munson, A.W. Miziolek, Laser-induced breakdown spectroscopy for detection of explosives residues: a review of recent advances, challenges and future prospects, *Anal. Bioanal. Chem.* 395 (2009) 283–300.

[89] J.L. Gottfried, F.C. De Lucia, Jr., C.A. Munson, A.W. Miziolek, Double-pulse standoff laser-induced breakdown spectroscopy for versatile hazardous materials detection, *Spectrochim. Acta Part B* 62 (2007) 1405–1411.

[90] J. Laserna, R. Fernández Reyes, R. González, L. Tobaria, P. Lucena, Study on the effect of beam propagation through atmospheric turbulence on standoff nanosecond laser induced breakdown spectroscopy measurements, *Opt. Express* 17 (2009) 10265–10276.

[91] B. Sallé, P. Mauchien, S. Maurice, Laser-induced breakdown spectroscopy in open-path configuration for the analysis of distant objects, *Spectrochim. Acta Part B* 62 (2007) 739–768.

[92] F.C. De Lucia, Jr., J.L. Gottfried, C.A. Munson, A.W. Miziolek, Multivariate analysis of standoff laser-induced breakdown spectroscopy spectra for classification of explosive-containing residues *Appl. Optic.* 47 (2008) G112–G121.

[93] Ph. Rohwetter, J. Yu, G. Mejean, K. Stelmaszczyk, E. Salmon, J. Kasparian, J. Wolf, L. Woste, Remote LIBS with ultrashort pulses: characteristics in picosecond and femtosecond regimes, *J. Anal. At. Spectrom.* 19 (2004) 437–444.

[94] K. Stelmaszczyk, P. Rohwetter, Long distance remote laser-induced breakdown spectroscopy using filamentation in air, *Appl. Phys. Lett.* 85 (2004) 3977–3979.

[95] Ph. Rohwetter, K. Stelmaszczyk, I. Woste, R. Ackermann, G. Mejean, E. Salmon, J. Kasparian, J. Yu, J. Wolf, Fillament-induced remote surface ablation for long range

laser-induced breakdown spectroscopy operation, *Spectrochim. Acta Part B* 60 (2005) 1025–1033.

[96] M. Durand, A. Houard, B. Prade, A. Mysyrowicz, A. Durécu, B. Moreau, D. Fleury, O. Vasseur, H. Borchert, K. Diener, R. Schmitt, F. Théberge, M. Chateauneuf, J.F. Daigle, J. Dubois, Kilometer range filamentation, *Optic. Express* 21 (2013) 26836–26845.

[97] M. Born, E. Wolf, Principles of optics: electromagnetic theory of propagation, interference and diffraction of light, *Cambrige University Press*, Cambrige (1999).

[98] R.M. Measures, Laser remote chemical analysis, *John Wiley & Sons*, New York (1988).

[99] A. Ferrero, J.J. Laserna, A theoretical study of atmospheric propagation of laser and return light for stand-off laser induced breakdown spectroscopy purposes, *Spectrochim. Acta Part B* 63 (2008) 305–311.

[100] H. Horvath, Atmospheric light absorption—A review, *Atmos. Environ.* 27A (1993) 293–317.

[101] B. Edlén, The dispersion of standard air, *J.O.S.A. A* 43 (1953) 339–344.

[102] A.T. Young, Rayleigh scattering, *Appl. Optic.* 20 (1981) 533–535.

[103] T. Wriedt, Mie theory: a review in the Mie theory, 169 *Springer Series in Optical Sciences, Springer-Verlag*, Berlin (2012).

[104] J. Vitásek, J. Látal, S. Hejduk, J. Bocheza, P. Koudelka, J. Skapa, P. Šiška, V. Vašinek, Atmospheric turbulences in free space optics channel, *IEEE* (2011) 104–107.

[105] D.K. Borah, D.G. Voelz, Estimation of laser beam pointing parameters in the presence of atmospheric turbulence*, Appl. Optic.* 46 (2007) 6010–6018.

[106] F. Dvořák, J. Diblík, Study of the temperature turbulences effect upon the optical beam in atmospheric optical communications, *Radioengineering* 20 (2011) 575–580.

[107] L.C. Andrews, R.L. Phillips, Laser beam propagation through random media, *SPIE PRESS*, Washington (2005).

[108] M.M. Malley, G.W. Sutton, N. Kincheloe, Beam-jitter measurements of turbulent aero-optical path differences, *Appl. Optic.* 31 (1992) 4440–4443.

[109] R.L. Fante, Electromagnetic beam propagation in turbulent media, *IEEE Proceedings* 63 (1975) 1669–1692.

[110] G. Gbur, E. Wolf, Spreading of partially coherent beams in random media, *J.O.S.A. A* 19 (2002) 1592–1598.

[111] L.C. Andrews, R.L. Phillips, C.Y. Hopen, Laser beam scintillation with applications*, SPIE Press*, Washington (2001).

[112] L.C. Andrews, R.L. Phillips, Laser beam propagation in the turbulent atmosphere, *SPIE Press*, Bellington (2005).

[113] A. Schweinsberg, J. Kuper, R.W. Boyd, Loss of spatial coherence and limiting of focal plane intensity by small-scale laser-beam f lamentation, *Phys. Rev.* 84 (2011) 053837-1–053837-4.

[114] R.A. Multari, D.A. Cremers, J.A. Dupre, J.E. Gustafson, Detection of biological contaminants on foods and food surfaces using laser-induced breakdown spectroscopy (LIBS), *J. Agric. Food Chem.* 61 (2013) 8687–8694.

[115] J.O. Cáceres, S. Moncayo, J.D. Rosales, F.J. Manuel de Villena, F.C. Alvira, G.M. Bilmes, Application of laser-induced breakdown spectroscopy (LIBS) and neural networks to olive oils analysis, *Appl. Spectrosc*. 67 (2013) 1064–1072.

[116] V. Juvé, R. Portelli, M. Boueri, M. Baudelet, J. Yu, Space-resolved analysis of trace elements in fresh vegetables using ultraviolet nanosecond laser-induced breakdown spectroscopy, *Spectrochim. Acta Part B* 63 (2008) 1047–1053.

[117] W. Lei, V. Motto-Ros, M. Boueri, Q. Ma, D. Zhang, L. Zheng, H. Zeng, J. Yu, Time-resolved characterization of laser-induced plasma from fresh potatoes, *Spectrochim. Acta Part B* 64 (2009) 891–898.

[118] R. Noll, H. Bette, A. Brysch, M. Kraushaar, I. Mönch, L. Peter, V. Sturm, Laser-induced breakdown spectrometry—applications for production control and quality assurance in the steel industry, *Spectrochim. Acta Part B* 56 (2001) 637–649.

[119] L.E. García-Ayuso, J. Amador-Hernández, J.M. Fernández-Romero, M.D. Luque de Castro, Characterization of jewellery products by laser-induced breakdown spectroscopy, *Anal. Chim. Acta* 457 (2002) 247–256.

[120] A. Jurado-López, M.D. Luque de Castro, Rank correlation of laser-induced breakdown spectroscopic data for the identification of alloys used in jewelry manufacture, *Spectrochim. Acta Part B* 58 (2003) 1291–1299.

[121] A. De Giacomo, M. Dell'Aglio, O. De Pascale, R. Gaudiuso, R. Teghil, A. Santagata, G.P. Parisi, ns- and fs-libs of copper-based-alloys: a different approach, *Appl. Surf. Sci.* 253 (2007) 7677–7681.

[122] A. Elhassan, A. Giakoumaki, D. Anglos, G.M. Ingo, L. Robbiola, M.A. Harith, Nanosecond and femtosecond laser induced breakdown spectroscopic analysis of bronze alloys, *Spectrochim. Acta Part B* 63 (2008) 504–511.

[123] F. Fotakis, D. Anglos, V. Zafiropulos, S. Georgiou, V. Tornari, Lasers in the preservation of cultural heritage: principles and applications, *CRC Press, Taylor & Francis*, Boca Raton (2007).

[124] O. Kokkinaki, C. Mihesan, M. Velegrakis, D. Anglos, Comparative study of laser induced breakdown spectroscopy and mass spectrometry for the analysis of cultural heritage materials, *J. Mol. Struct.* 1044 (2013) 160–166.

[125] S. Legnaioli, F. Anabitarte García, A. Andreotti, E. Bramanti, D. Díaz Pace, S. Formol, G. Lorenzetti, M. Martini, L. Pardini, E. Ribechini, E. Sibilia, R. Spiniello, V. Palleschi, Multi-technique study of a ceramic archaeological artifact and its content, *Spectrochim. Acta Part A* 100 (2013) 144–148.

[126] T. Palomar, M. Oujja, M. García-Heras, M.A. Villegas, M. Castillejo, Laser induced breakdown spectroscopy for analysis and characterization of degradation pathologies of Roman glasses, *Spectrochim. Acta Part B* 87 (2013) 114–120.

[127] R.S. Harmon, R.E. Russo, R.R. Hark, Applications of laser-induced breakdown spectroscopy for geochemical and environmental analysis: a comprehensive review, *Spectrochim. Acta Part B* 87 (2013) 11–26.

[128] D. Santos, Jr., L.C. Nunes, G.G. Arantes de Carvalho, M. da Silva Gomes, P.F. de Souza, F. de Oliveira Leme, L.G. Cofani dos Santos, F.J. Krug, Laser-induced breakdown spectroscopy for analysis of plant materials: a review, *Spectrochim. Acta Part B* 71–72 (2012) 3–13.

[129] S.J. Rehse, H. Salimnia, A.W. Miziolek, Laser-induced breakdown spectroscopy (LIBS): an overview of recent progress and future potential for biomedical applications, *J. Med. Eng. Technol.* 36 (2012) 77–89.

[130] V.K Singh, A.K Rai, Prospects for laser-induced breakdown spectroscopy for biomedical applications: a review, *Lasers Med. Sci.* 26 (2011) 307–315.

[131] R.K. Thareja, A.K Sharma, S. Shukla, Spectroscopic investigations of carious tooth decay, *Med. Eng. Phys.* 30 (2008) 1143–1148.

[132] F.Y. Yueh, H. Zheng, J.P. Singh, S. Burgess, Preliminary evaluation of laser-induced breakdown spectroscopy for tissue classification, *Spectrochim. Acta Part B* 64 (2009) 1059–1067.

[133] A. El-Hussein, A.K. Kassem, H. Ismail, M.A. Harith, Exploiting LIBS as a spectrochemical analytical technique in diagnosis of some types of human malignancies, *Talanta* 82 (2010) 495–501.

[134] V.K. Singh, A.K. Rai, P.K. Rai, P.K. Jindal, Cross-sectional study of kidney stones by laser-induced breakdown spectroscopy, *Lasers Med. Sci.* 24 (2009) 749–759.

[135] J. Anzano, R.J. Lasheras, Strategies for the identification of urinary calculus by laser induced breakdown spectroscopy, *Talanta* 79 (2009) 352–360.

[136] R.A. Multari, D.A. Cremers, M.L. Bostian, Use of laser-induced breakdown spectroscopy for the differentiation of pathogens and viruses on substrates, *Appl. Optic.* 51 (2012) B57−B64.

[137] C.M. Bridge, J. Powell, K.L. Steele, M. Williams, J.M. MacInnis, M.E. Sigman, Characterization of automobile float glass with laser-induced breakdown spectroscopy and laser ablation inductively coupled plasma mass spectrometry, *Appl. Spectrosc.* 60 (2006) 1181–1187.

[138] C.M. Bridge, J. Powell, K.L. Steele, M.E. Sigman, Forensic comparative glass analysis by laser-induced breakdown spectroscopy, *Spectrochim. Acta Part B* 62 (2007) 1419–1425.

[139] F.R Doucet, G. Lithgow, R. Kosierb, P. Bouchard, M. Sabsabi, Determination of isotope ratios using laser-induced breakdown spectroscopy in ambient air at atmospheric pressure for nuclear forensics, *J. Anal. At. Spectrom.* 26 (2011) 536–541.

[140] R.C. Wiens, S. Maurice, The ChemCam Team, The ChemCam instruments on the Mars Science Laboratory (MSL) rover: body unit and combined system performance, *Space Sci. Rev.* 170 (2012) 167–227.

[141] S. Maurice, R.C. Wiens, The ChemCam Team, The ChemCam instrument suite on the Mars Science Laboratory (MSL) rover: science objectives and mast unit description, *Space Sci. Rev.* 170 (2012) 95–166.

[142] R.C. Wiens, S. Maurice, The ChemCam Team, The ChemCam instrument suite on the Mars Science Laboratory rover curiosity: remote sensing by laser-induced plasmas, *Space Sci. Rev.* 170 (2012) 166–223.

[143] P.Y. Meslin, O. Gasnault, O. Forni, S. Schröder, A. Cousin, G. Berger, S. M. Clegg, J. Lasue, S. Maurice, V. Sautter, S. Le Mouélic, R. C. Wiens, C. Fabre, W. Goetz, D. Bish, N. Mangold, B. Ehlmann, N. Lanza, A.M. Harri, R. Anderson, E. Rampe, T.H. McConnochie, P. Pinet, D. Blaney, R. Léveillé, D. Archer, B. Barraclough, S. Bender, D. Blake, J.G. Blank, N. Bridges, B.C. Clark, L. DeFlores, D. Delapp, G. Dromart, M.D.

Dyar, M. Fisk, B. Gondet, J. Grotzinger, K. Herkenhoff, J. Johnson, J.L. Lacour, Y. Langevin, L. Leshin, E. Lewin, M.B. Madsen, N. Melikechi, A. Mezzacappa, M.A. Mischna, J.E. Moores, H. Newsom, A. Ollila, R. Perez, N. Renno, J.B. Sirven, R. Tokar, M. de la Torre, L. d'Uston, D. Vaniman, A. Yingst, MSL Science Team, Soil diversity and hydration as observed by ChemCam at Gale Crater, Mars, *Science* 341 (2013) 1238670-1–1238670-10.

[144] C. López-Moreno, S. Palanco, J.J. Laserna, F. De Lucia, Jr., A.W. Miziolek, J. Rose, R.A. Walters, A.I. Whitehouse, Test of a stand-off laser-induced breakdown spectroscopy sensor for the detection of explosive residues on solid surfaces, *J. Anal. At. Spectrom.* 21 (2006) 55–60.

[145] J.L. Gottfried, F.C. De Lucia, Jr., C.A. Munson, A.W. Miziolek, Laser-induced breakdown spectroscopy for detection of explosives residues: a review of recent advances, challenges and future prospects, *Anal. Bioanal. Chem.* 395 (2009) 283–300.

[146] J.L. Gottfried, F.C. De Lucia, Jr., C.A. Munson, A.W. Miziolek, Standoff detection of chemical and biological threats using laser-induced breakdown spectroscopy, *Appl. Spectrosc.* 62 (2008) 353–363.

[147] J. Moros, J.A. Lorenzo, P. Lucena, L.M Tobaria, J.J. Laserna, Simultaneous Raman spectroscopy-laser-induced breakdown spectroscopy for instant standoff analysis of explosives using a mobile integrated sensor platform*, Anal. Chem.* 82 (2010) 1389–1400.

[148] J. Moros, J.A. Lorenzo, J.J. Laserna, Standoff detection of explosives: critical comparison for ensuing options on Raman spectroscopy–LIBS sensor fusion, *Anal. Bioanal. Chem.* 400 (2011) 3353–3365.

[149] J. Moros, J.J. Laserna, New Raman-laser-induced breakdown spectroscopy identity of explosives using parametric data fusion on an integrated sensing platform, *Anal. Chem.* 83 (2011) 6275–6285.

[150] J.L. Gottfried, F.C. De Lucia, Jr., C.A. Munson, A.W. Miziolek, Strategies for residue explosives detection using laser-induced breakdown spectroscopy, *J. Anal. At. Spectrom.* 23 (2008) 205–216.

[151] J.L. Gottfried, F.C. De Lucia, Jr., A.W. Miziolek, Discrimination of explosive residues on organic and inorganic substrates using laser-induced breakdown spectroscopy, *J. Anal. At. Spectrom.* 24 (2009) 288–296.

[152] L. Sun, Y. Xin, Z. Cong, Y. Li , L. Qi, Online compositional analysis of molten steel by laser-induced breakdown spectroscopy, *Adv. Mater. Res.* 694–697 (2013) 1260–1266.

[153] R. Noll, V. Sturm, Ü. Aydin, D. Eilers, C. Gehlen, M. Höhne, A. Lamott, J. Makowe, J. Vrenegor, Laser-induced breakdown spectroscopy–From research to industry, new frontiers for process control, *Spectrochim. Acta Part B* 63 (2008) 1159–1166.

[154] S. Palanco, L.M. Cabalín, D. Romero, J.J. Laserna, Infrared laser ablation and atomic emission spectrometry of stainless steel at high temperatures, *J. Anal. At. Spectrom.* 14 (1999) 1883–1887.

[155] S. Palanco, S. Conesa, J.J. Laserna, Analytical control of liquid steel in an induction melting furnace using a remote laser induced plasma spectrometer, *J. Anal. At. Spectrom.* 19 (2004) 462–467.

[156] C. López-Moreno, S. Palanco, J.J. Laserna, Remote laser-induced plasma spectrometry for elemental analysis of samples of environmental interest, *J. Anal. At. Spectrom.* 19 (2004) 1479–1484.

[157] J.L. Gottfried, R.S. Harmon, F.C. De Lucia, Jr., A.W. Miziolek, Multivariate analysis of laser-induced breakdown spectroscopy chemical signatures for geomaterial classification, *Spectrochim. Acta Part B* 64 (2009) 1009–1019.

[158] X. Fang, S.R. Ahmad, Elemental analysis in environmental land samples by stand-off laser-induced breakdown spectroscopy, *Appl. Phys. B* 115 (2014) 497–503.

[159] L.A. Álvarez-Trujillo, A. Ferrero, J.J. Laserna, Preliminary studies on stand-off laser induced breakdown spectroscopy detection of aerosols, *J. Anal. At. Spectrom.* 23 (2008) 885–888.

[160] J.R. Watcher, D.A. Cremers, Determination of uranium in solution using laser-induced breakdown spectroscopy, *Appl. Spectrosc.* 41 (1987) 1042–1048.

[161] J.P. Singh, F.Y. Yueh, H. Zhang, K.P. Karney, A preliminary study of the determination of uranium, plutonium and neptunium by laser induced breakdown spectroscopy, *Rec. Res. Dev. Appl. Spectrosc.* 2 (1999) 59–67.

[162] A.P.M. Michel, M. Lawrence-Snyder, S.M. Angel, A.D. Chave, Laser-induced breakdown spectroscopy of bulk aqueous solutions at oceanic pressures: evaluation of key measurement parameters, *Appl. Optic* 46 (2007) 2507–2515.

[163] A.P.M. Michel, M.J. Lawrence-Snyder, S.M. Angel, A.D. Chave, Oceanic applications of laser induced breakdown spectroscopy: laboratory validation, *Proceedings of MTS/IEEE* 1 (2005) 741–747.

[164] S. Georgiou, D. Anglos, C. Fotakis, Photons in the service of our past: lasers in the preservation of cultural heritage*, Contemp. Phys*. 49 (2008) 1–27.

[165] I. Osticioli, J. Agresti, C. Fornacelli, I. Turbanti Memmi, S. Siano, Potential role of LIPS elemental depth profiling in authentication studies of unglazed earthenware artifacts, *J. Anal. At. Spectrom.* 27 (2012) 827–833.

[166] A. Erdem, A. Cilingiroglu, A. Giakoumaki, M. Castanys, E. Kartsonaki, C. Fotakis, D. Anglos, Characterization of Iron age pottery from eastern Turkey by laser-induced breakdown spectroscopy (LIBS), *J. Archaeol. Sci.* 35 (2008) 2486–2494.

[167] L. Caneve, A. Diamanti, F. Grimaldi, G. Palleschi, V. Spizzichino, F. Valentini, Analysis of fresco by laser induced breakdown spectroscopy, *Spectrochim. Acta Part B* 65 (2010) 702–706.

[168] A. Staicu, I. Apostol, A. Pascu, I. Iordache, V. Damian, M.L. Pascu, Laser induced breakdown spectroscopy stratigraphic characterization of multilayered painted surfaces, *Spectrochim. Acta Part B* 74−75 (2012) 151–155.

[169] R. Grönlund, M. Lundqvist, S. Svanberg, Remote imaging laser-induced breakdown spectroscopy and remote cultural heritage ablative cleaning, *Opt. Lett.* 30 (2005) 2882–2884.

[170] R. Grönlund, M. Lundqvist, S. Svanberg, Remote imaging laser-induced breakdown spectroscopy and laser-induced fluorescence spectroscopy using nanosecond pulses from a mobile lidar system*, Appl. Spectrosc.* 60 (2006) 853–859.

[171] S. Guirado, F.J. Fortes, V. Lazic, J.J. Laserna, Chemical analysis of archeological materials in submarine environments using laser-induced breakdown spectroscopy. On-site trials in the Mediterranean Sea*, Spectrochim. Acta Part B* 74–75 (2012) 137–143.

Experimental

Publicaciones y
Divulgación Científica

UNIVERSIDAD
DE MÁLAGA

Standoff LIBS sensor

The present section encloses a deep description on the LIBS based sensor that has been used to perform the research works involving the present Doctoral Thesis. The system has been entirely designed, engineered and operatively adapted at the University of Málaga during the last 6 years. A graphical scheme of this LIBS sensor, coined as ***Demostrador#2***, for a distant performance of both laser ablation and optical emission measurements is displayed in *Fig. 1*.

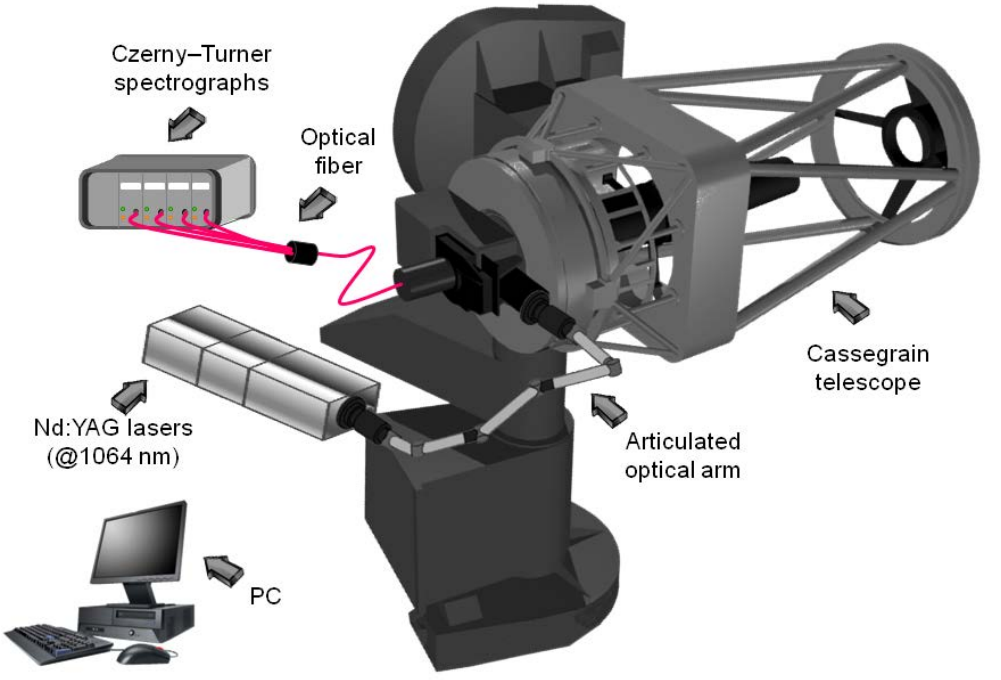

Fig. 1. Schematic representation of the *standoff* LIBS sensor set-up

As shown, the main components within the LIBS experimental set-up are summarized as follows: the pulsed laser source used to induce the plasma plume, the optical system (lens, mirrors and optical fiber) that permits the delivering and

focusing of laser pulses on the surface of the distant target as well as the collection of the emitted light from the plasma plume, a detection system (spectrometer) to resolve spectrally such a light into its particular emissions, and a computer for data acquisition and treatment.

Next, a complete description of each one of the subsystems integrating it will be provided.

Pulsed laser source

Standoff LIBS sensor uses a Twins B system (Quantel, France) as excitation source. The Twins B system is integrated by two independent high-power compact Q-Switched Nd:YAG oscillators (with super Gaussian resonators) jointly mounted on an 'U' shaped optical bench. Together with the two laser heads, a complementary frontal unit houses a module of optics to spatially combine the two infrared (@1064nm) laser beams in a polarizer. The two collinear output pulses have the same plane of polarization. For the fundamental wavelength, each laser delivers output energy of 850±2 mJ per pulse (at a repetition rate of 10 Hz). The length of each laser pulse is of 5.5 ns. Both lasers are synchronized by coaxial cables fitted with miniature connectors (BNCs, for *Bayonet Neill–Concelman*), which quick connect-disconnect radio frequencies in the multi-megahertz range. The entire Twins B system is controlled via a built-in RS-232 interface. Despite of this, a temporal gap of 600 ns between both laser pulses and inherent to such electronics has been measured for our system.

Optical system

The optics of the sensor can be grouped into three major blocs: an articulated optical arm, an *In/Out compartment* that houses a suite of lenses and

mirrors and, finally, a telescope.

The **articulated optical arm** (*Applied Photonics Ltd., UK*) guides the laser pulses from the irradiation source up to the In/Out box by consecutive reflections. The arm (*Fig. 2A*) is composed by two flanges (input and output at either end), two tubes (50 mm OD) and five rotating "knuckle joints", each of which contains a high-energy mirror to reflect the fundamental laser line. The two tubes are of a length of ≈550 mm, thereby giving to the arm length a little bit more than a meter. Each mirror is mounted in aluminum alloy housing precision-engineered with three micro-positioner screws for angular fine adjustments of the mirror. The articulated arm is fully engaged to a launch module (*Fig. 2B*), which contains the optics required to launch the laser pulses, as well as an alignment device. This last consists of a diode laser emitting Class 3B radiation (@635 nm, 5 mW). This device allows not only the alignment of the laser beam within the articulated arm but also can be used as a reference for the pointing of the laser beam at a distance.

A) B)

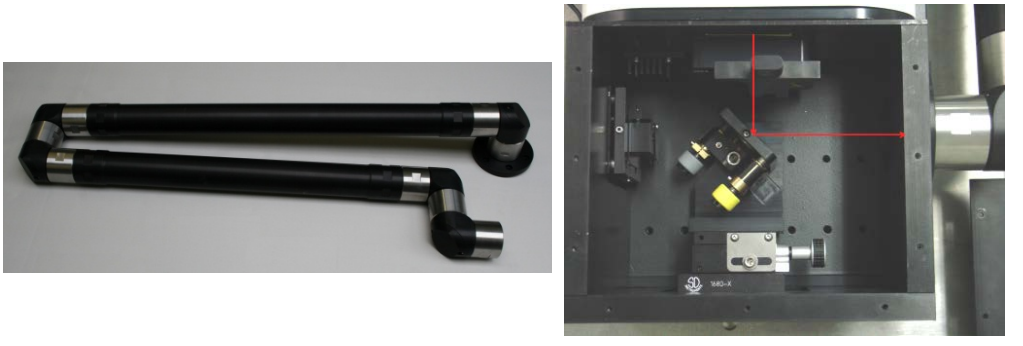

Fig. 2. Pictures in detail of the articulated optical arm (A) and the launch module (B) –seen from above–. Note: Red arrows indicate the path of the laser beam.

The ***In/Out compartment*** confers a coaxial arrangement to the sensor, that is, the processes of delivering of laser pulses and the plasma light collection

partially share the same optical path. *Fig. 3* graphically shows in plan and a perspective view of the compartment. As seen, within the cubicle, the optical components that integrate the emission arrangement are an expander system, involving two lenses, and a dichroic mirror.

During the emission process, the incoming collimated laser beam is tightly focused when passes through the pair of lenses (anti-reflecting coated for @1064 nm) placed just at the exit of the articulated arm. Hence, first, a diverging lens (focal length -63 mm) expands the laser beam. Then the converging lens (focal length 250 mm) focuses the beam on the dichroic mirror made of BK7 glass (2", transmission range from 330 nm up to ~ 1000 nm). This mirror is placed at 45° angle and reflects the laser pulses through a 400 mm aperture towards the telescope. All these components are mounted on micrometric translational stages for a fine tune on laser beam alignment.

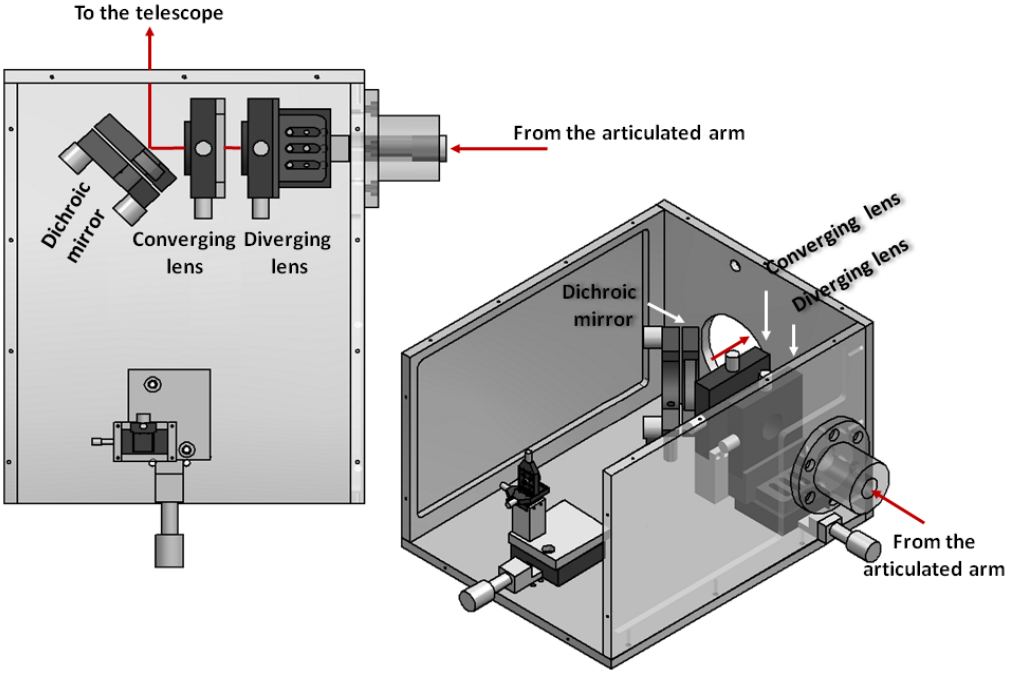

Fig. 3. Graphical schemes in plan and perspective of the *In/Out compartment*.

The final component of the optical system is a classical Cassegrain *open truss* **telescope** (Optical Guidance Systems). This classical Cassegrain design uses two reflecting mirrors. The primary mirror is a parabolic mirror (40 cm in diameter, radius of curvature of 80 cm, focal ratio of ca. f/4). The secondary mirror is a convex mirror with a hyperbolic shape (10 cm in diameter, radius of curvature of -260 cm). The magnification factor of the secondary mirror is in the range of 3× to 5×, giving the overall optical system a focal ratio of f/14.25. The telescope is assembled in a fork mount with features appropriate to a pointing and scanning sensor. The fork allows telescope movement between some boundaries: azimuthal tilt angle (side-to-side), <120°; polar tilt angle (up-and-down), <240°.

The role of the telescope within the sensor is twofold: first, during the light delivering process, it is designated to focus the laser pulses on the distant targets; second, during the light collecting process, it gathers the light emitted from faraway plasmas induced. A basic outline of these two processes is graphically depicted in *Fig. 4*.

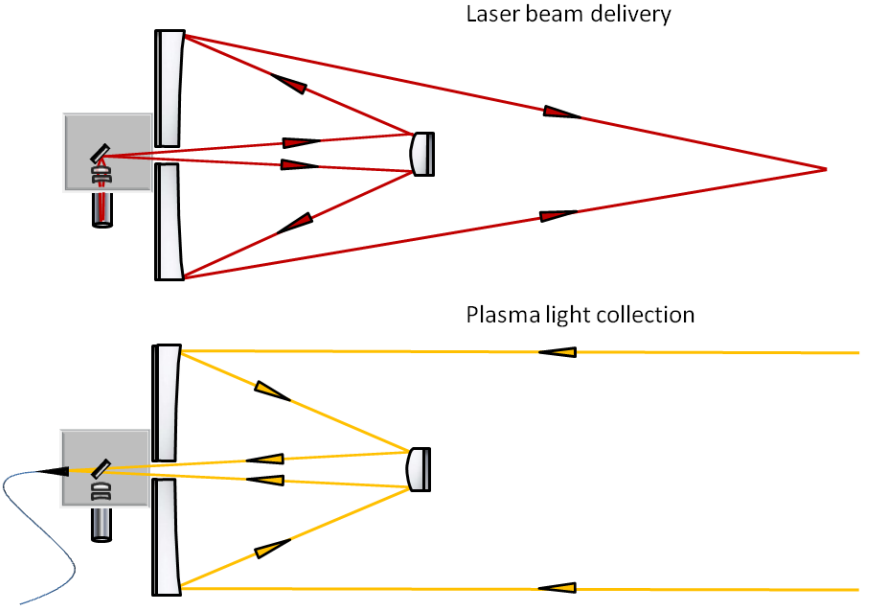

Fig. 4. Basic outline of the dual role of the telescope for laser pulses delivering (upper) and plasma light collection (lower).

Hence, during the light delivering process, the laser beam coming from the *In/Out compartment* enters the telescope through an aperture in the primary mirror towards the secondary mirror. Once reflected here, the beam is directed to the primary mirror that, finally, reflects the laser beam towards the distant target. The operational range, i.e. beam focusing distance, is easily adjusted by changing the distance between the reflecting mirrors. While the primary mirror remains fixed, the secondary mirror is driven through a servo-motor. A rangefinder is in tune with this autofocus system to change the gap between mirrors, thereby allowing the laser beam focusing at the envisaged distance.

Fig. 5 graphically exemplifies the switching of the focusing position as a function of the gap between the reflecting mirrors.

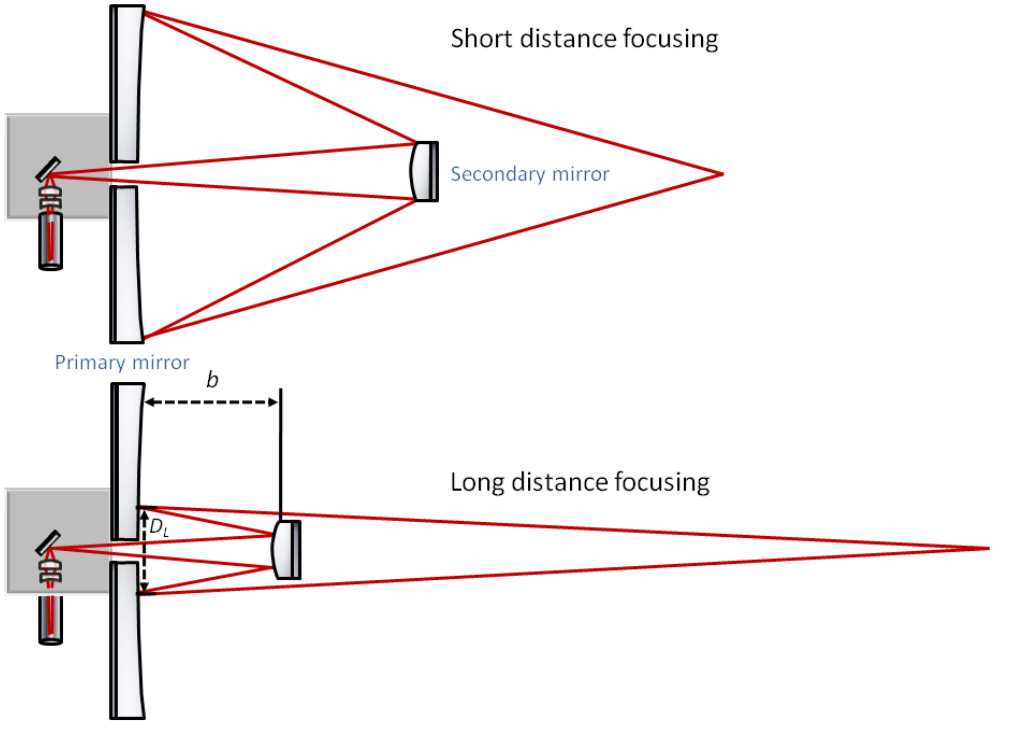

Fig. 5. Basic outline on the dependence of the gap between telescope reflectors and the focusing position.

As shown, the focusing distance is in inverse proportion to the gap between the mirrors (*b*). The larger the space between the mirrors the shorter the distance at which the laser beam can be focused. Narrowing the gap between mirrors reduces the illuminated area (D_L) within the primary mirror, thereby displacing the focus point to greater distances. It should be also noted that, in order to reduce any obstruction of the light at the reflecting mirrors, the laser beam is delivered slightly *off-axis* with respect to the normal angle of such optical elements. However, despite this performance, the focusing capability of the telescope is not confined.

Despite this flexibility, instrumental restrictions constrain the operational range to distances larger than 30 m. At this distance, the minimum achievable laser spot diameter is ca. 1.5 mm, thereby attaining a maximum available irradiance of just over 8 GW cm^{-2}.

Finally, after producing the distant plasma plumes, the emitted light is collected first from the primary mirror. From there, light is reflected on the secondary mirror, which directs it towards the *In/Out compartment*. After passing through the dichroic mirror, the image of the plasma light is exactly focused at the tip of the optical fiber (see *Fig. 4*, lower diagram).

Detection system

The complete system for optical emissions detection is composed by an optical fiber and a spectrometer. For the investigations involving the works within this Doctoral Thesis, two different detection systems have been used.

Whatever the LIBS application, the **optical fiber** cable acts as an interface to guide the plasma light imaged by the telescope towards the entrance slit of the spectrometer. Depending upon the instrumental requirements, the two fibers used can be detailed as follows: first, a solarization-resistant fiber assembly (UV/SR-VIS High OH content) to prevent transmission degradation in the UV, with a 600 µm in

diameter silica core and an efficient wavelength range from 200 nm to 1100 nm; second, a 600 µm optical fiber (four-furcated cable, 4 × 600 µm fibers, all legs SMA terminated, total 2 m long, splitting point in the middle).

In the same vein, for the different applications developed, two *Czerny-Turner* **spectrometers** have been used.

✓ The first spectrometer (*Fig. 6A*) is integrated by the Shamrock 303i spectrograph (303 mm focal length, f/4, 100 µm slit) seamlessly integrated with an intensified charge coupled device –iCCD– (1024 × 1024 pixel, 26 mm^2 pixel, intensifier tube diameter 25 mm). The spectrograph is fitted with a triple turret of interchangeable diffraction gratings, thereby allowing to record variable-size wavelength ranges. Nonetheless, the dimension of such spectral windows is closely tied to the detail at which the component wavelengths are dispersed. Hence, the wider the spectral window the lower the spectral resolution, and vice versa.

✓ The second spectrometer (*Fig. 6B*) consists of a 4-channels miniature spectrograph (75 mm focal length), fitted each with a CCD. An effective spectral range spanning from 230 nm to 950 nm is set. However, as mentioned, the dichroic mirror (see *In/Out compartment section*) constrains this spectral range below 330 nm. The timing parameters used for optical signal acquisition are enabled by default at: 1.28 µs of delay time from the external trigger input (considered 0 time) supplied by the Q-switch output signal of the laser, and 1.1 ms of integration time (gate width).

A) B)

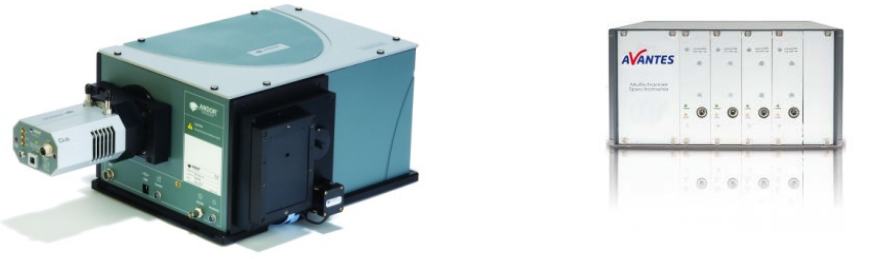

***Fig 6*.** Images of the two spectrometers used.

The LIBS sensor described above is the common instrumentation used for all the investigations involving the works within this Doctoral Thesis. For the convenience of the reader, the experimental particularities of each specific investigation will be disclosed in the related chapter.

Chapters

Publicaciones y
Divulgación Científica

UNIVERSIDAD
DE MÁLAGA

Section 1.

Standoff LIBS Fundamentals

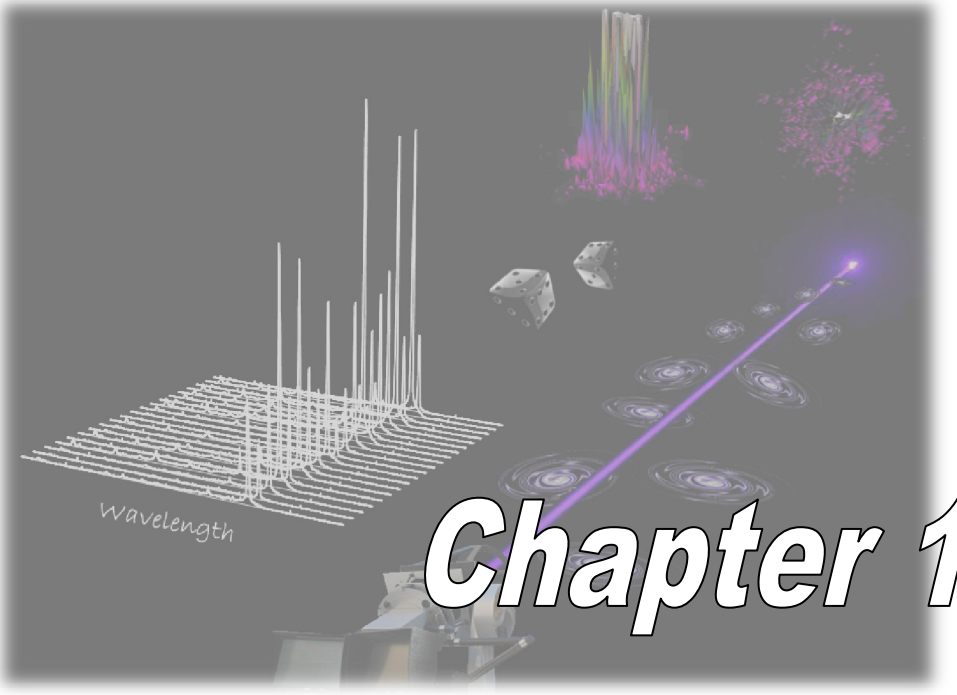

Chapter 1

Chapter 1. New Insights into the Potential Factors Affecting the Emission Spectra Variability in *Standoff* LIBS

Abstract

Interest in the use of laser-based sensors operating in *standoff* mode is increasing due to the wide range of options offered in the evaluation of distant targets. However, despite this high potential, the performance aspects of any sensor for analysis at a distance are curtailed as compared with its use *in situ*. The present work addresses a sensitive topic in *standoff* laser-induced breakdown spectroscopy (*ST-LIBS*) which is the larger variability observed within the emission signals registered from faraway targets. A *field-deployable* LIBS sensor has been used to ascertain how atmospheric propagation affects the laser pulses delivered to a distant target and the emitted light from the plasma plume created. In this way, the extent of the contribution of the alterations of each optical pathway to the signal uncertainty in *ST-LIBS* has been isolated. As has been experimentally verified, the amount of laser energy reaching the target remains constant, whatever the distance. In contrast, the laser beam cross section is distorted during its travel towards the target; an alteration that becomes ever larger as the distance to the target increases. This circumstance leads to further and random deterioration of the irradiance, thus resulting in plasma events notably differing in their intensity, which, in turn, have proven to be in direct correlation with the intensities and variability of the spectral responses collected by the system. The positional displacement of the laser-induced plasmas has no impact on the sensitivity and uncertainty of the *standoff* LIBS signals.

1 Introduction

Over the last few years optical sensors based on lasers have found their place in a wide range of applications because they provide a unique set of capabilities that are well-suited to difficult measurement tasks. The potential for these sensors to operate without contact, quickly and with appropriate sensitivity for the design of *field-deployable*, compact, robust and versatile diagnostic systems, have made them highly appealing tools for analytical work. These spectroscopic sensors are able to qualify and quantify the concerned targets through different physical mechanisms, including absorption, emission, or scattering of electromagnetic radiation by atoms or molecules in a sample [1]. These distinct mechanisms, which are chosen depending on the intended application, offer the chance to characterize different kinds of materials, either in a condensed phase or as a gas, by revealing specific analytical information.

Particularly, atomic emission spectroscopy assisted by laser breakdown (that is, LIBS), for instance, provides a multi-elemental spectral signature of the chemical composition of the sample based on the light emission from the ionized matter [2, 3]. Such analytical information has proved useful in a wide range of research, especially as a result of the facility to use portable, remote, and *standoff* instruments for field measurements [4, 5]. Among all these various operational configurations, the most functional approach for field analysis of distant objects is, at the same time, the most demanding application. The ability to analyze samples located in harsh environments, or the analysis of targets located in difficult to access areas, are the main advantages of the *standoff* LIBS configuration. These features have led to use of the technique in explosive detection [6, 7], care and maintenance of cultural heritage [8, 9], space exploration [10, 11], industrial processes [12-14] and environmental chemistry [15] to name a few examples.

The underlying principle of operation in *standoff* LIBS involves a double optical path: first, the delivery of tightly focused laser pulses towards the distant target through the atmosphere, and second the subsequent atmospheric transmission of the light emitted by the induced plasma plume back to the spectrometer. Apart from optical absorption by the components of the air, a large source of perturbation in both paths is related to turbulence, constantly present in the atmosphere to a greater or lesser extent. The disturbance resulting from this turbulence is responsible for random microscopic fluctuations in the transmitted light as a result of changes in the refractive index of air with changing temperature. All these turbulent motions persistently exert influences on the behavior of the light when propagating along its optical path. To cite just a few examples, these random variations affect the directionality and the position (*wandering*) of the transmitted beam as well as the energy distribution (*scintillation*) of the propagating optical wave [15-17]. In addition, the presence of particulate matter and aerosols has been proven to alter the propagating waves as a result of different atmospheric phenomena including scattering and absorption [18-21].

These effects have an impact on the final outcome of any *standoff* LIBS analysis as compared to when the technique operates in close-contact mode [18]. While the measurement significantly affected by these phenomena is the emission intensity, one of the major issues in the *standoff* operation of LIBS is related to the remarkable fluctuations in the *shot-to-shot* signals; a circumstance that degrades the qualitative and quantitative information provided by the technique. The negative effect of this large uncertainty observed in *standoff* LIBS information has urged the LIBS community to devise a variety of methods for mitigating its potential impact, based on algorithms [22, 23] or thresholds [24] designed to remove what some consider to be "anomalous spectra" [25]. However, spectral rejection, as well as being a data improvement routine, may be considered to be a misinterpretation of real events.

That is why, instead of arbitrary data reduction, it is preferable to elucidate the origin of these *shot-to-shot* emission signal fluctuations, what their causes are, and thus, improve the efficiency of these sensors. Although in the past some efforts have been devoted to this issue [22-25] the cause-effect relationship for the large variability of the spectral signals have been not thoroughly addressed so far.

In the present research, alterations suffered by 1064 nm ns laser pulses focused towards distant targets and by the corresponding emissions collected from aluminum plasmas have been evaluated. The study attempts to isolate the sources of variability contributing to the observed uncertainty within the *standoff* LIBS signals. Changes in the properties of the laser pulses reaching the distant target and the variations in the features of the produced plasmas, when propagating through the atmosphere, have been examined.

2 Experimental section

The *ST-LIBS* sensor used to perform these investigations has been described in detail in the "Experimental" chapter of this Doctoral Thesis. Plasma light was spectrally resolved using a gated *Czerny–Turner* spectrometer (303 mm focal length, f/4) fitted with an intensified coupled-charged device detector. A time delay of 600 ns and an integration time of 9 µs were established as timing parameters for data acquisition.

Together with the *ST-LIBS* sensor, some additional instruments were required for experimentation. Thorough diagnosis of the laser beam was performed using a camera-based beam profiling system which featured a 2/300 format CMOS (complementary metal oxide semiconductor) 1280 × 1024 array with 6.7 µm square pixels; for a total beam imaging area of 8.6 mm × 6.9 mm. For the specific monitoring of the plasma, values reported by such device –originally expressed in energy units– were converted to power units using the camera exposure time (30

ms) and the radiant flux. In turn, a laser power and energy meter (short pulse, fitted with a heat sink, 50 mm aperture, with multiband coating) was used for pulse parameter measurements.

Homogeneous aluminum foils (4 × 4 × 0.2 cm^3) were used as samples to induce the plasma plumes. To avoid any contribution whatsoever to the uncertainty within the emission signals, all the measurements were performed on static targets with a fixed position for lasing (without telescope movement). Sensor operations were evaluated in both laboratory (inside a partially closed corridor) and open-field (the instrument was kept indoors in a warehouse, while the samples or devices were placed outside in the open environment during measurements) domains. The experimental corridor was equipped with two gaps, at the ground and the roof level, each 5 cm wide, along the entire length of one of the lateral sides. This design enabled air to flow from the inlet to the outlet induced by natural convection, thereby creating slight air streams. The indoor atmospheric conditions were at an average temperature of 20 °C and an average relative humidity of 50%. In contrast, the average temperature outdoors was 10 °C and the average relative humidity was 70%. Furthermore, outdoors there was a light wind with occasional gusts no stronger than 7 $km \cdot h^{-1}$.

3 Results & discussion

In order to assess the influence of the *shot-to-shot* signal variability within *standoff* LIBS spectra, a thorough investigation of the feasible distortions that may affect the laser light when delivered to a distant target and the gathered light returning to the sensor has been made. Operations were performed in two domains, indoors, where the sensor was placed inside the lab facilities and the targets were located inside a partially closed corridor, and outdoors, where the

sensor was kept inside a warehouse and the targets were located outside in an open field.

3.1 Indoors evaluation

3.1.1 Laser pulse delivery. On a microscopic scale the motion of the atmosphere, *via* small turbulent eddies with life spans from seconds to minutes, leads to small temperature gradients that result in micro fluctuations in the atmosphere's refractive index. This is why a series of phenomena such as *beam wandering*, *beam spreading*, and *scintillation* affect the delivered laser pulse when it propagates through the atmosphere. *Beam wandering* refers to random variations in the position of the beam centroid of the laser pulses, whereas *beam spreading* is the distortion of the wave front in the laser pulse. However, while *wandering* is generally caused by larger turbulent eddies, *spreading* is produced by micro eddies in the beam path of the laser pulse. In contrast, *scintillation*, that is intensity fluctuation, has no significant effect on laser ranging [26-28].

Fig. 1 shows the beam cross section at the exit of the cavity (*Fig. 1a)* and when focused 30 m from the sensor. In this last instance, the effects of *beam spreading* and *beam wandering* relative to the axis of propagation are clearly observed in *Fig. 1b* and *c*, respectively. The center of the circle indicates the point where the beam was focused and is used as a reference for measuring the displacement of the beam. Furthermore, the circle itself was set as a reference for the size of the laser beam wavefront. *Fig. 1b* shows that the spatial distribution of the beam propagated through the atmosphere is distorted when compared with the beam cross section at the exit of the laser head. In addition to the cited distortion, *Fig. 1c* shows displacement of the beam centroid with respect to the intended center of the beam. These faltering alterations that randomly affect the transmission of the laser pulse may arise simultaneously but are not necessarily

related. Indeed, *spreading* and *wandering* seem to be high frequency and low frequency effects, respectively.

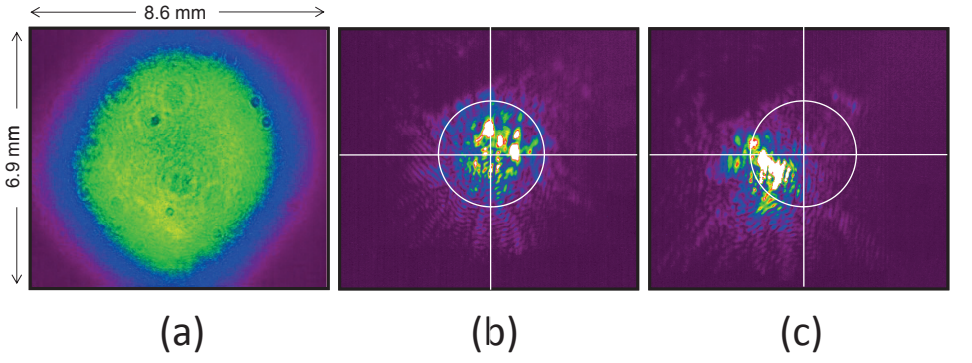

Fig. 1. Representative images of the effects of (b) *beam spreading* and (c) *beam wandering*, on a focused laser pulse travelling towards a distant target (30 m inside a partially enclosed corridor) as compared to the collimated pulse (a) at the exit of the laser head. Identical dimensions for the total imaging area (8.6 mm × 6.9 mm) of the laser beam profiling, system are displayed for all three images.

A thorough analysis of these phenomena within a series of successive laser pulses was performed using their laser beam profiles captured by CCD camera. A sequence of 500 laser shots delivered to a distance of 30 m at a repetition rate of 5 Hz was studied. *Fig. 2* depicts the variation in the position of the beam centroid in the vertical and horizontal axes with respect to the centroid position of the first pulse. As shown, the laser pulses exhibited continuous and random displacement in both directions over the surface impacted. This effect—known as *beam wander*—is due to the random unsteady motion of eddies, which are thermal in origin, that ultimately lead to unsystematic fluctuations in the atmosphere refraction index. These atmospheric flows at the micrometric scale persistently exert influences on the behavior of the light propagating along its optical path. Although the small scale turbulent motions are statistically isotropic (*i.e.* no preferential spatial direction can be discerned), it is observed that the perturbations over the horizontal axis are larger than those occurring in the vertical direction. The relative standard deviations (*RSD*) of the beam position with respect the centroid position of the first

pulse are 12% and 5%, respectively. This behavior is due to the geometry of the experiment, in which the beam is transmitted parallel to the ground surface, and thereby experiences displacement in the horizontal direction to a larger extent, due to the preferred direction of the convection currents inside the corridor.

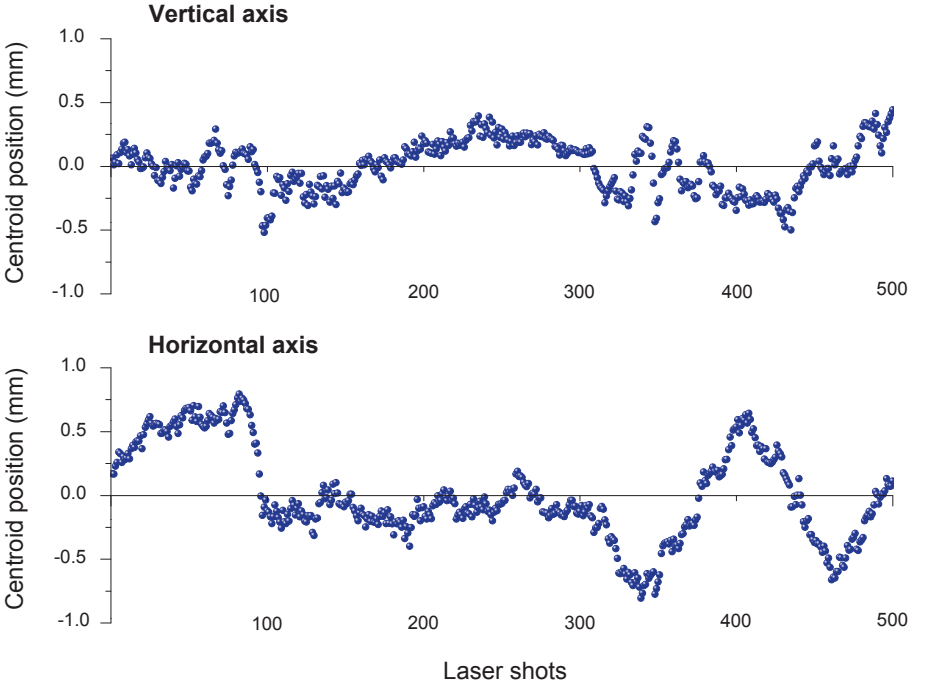

Fig. 2. Monitoring of the location of 500 successive laser shots throughout two dimensions—height and width—that define the surface of a distant target (30 m).

In turn, it is also observed that the *wandering* exhibits two distinct components. First, a high frequency fluctuation of the instantaneous center of the laser beam, also known as *beam jitter* (observed clearly between shots 200 and 300), is evidenced. Second, a low frequency, larger amplitude deviation beyond the bounded position, known as beam dancing is detected [15]. As shown, this low frequency deviation of the beam position in the horizontal axis can be as large as *ca.* 0.8 mm. A direct consequence of these effects is that, during a point focused laser based inspection of a target, the laser beam may randomly examine distinct

positions across the surface. As a result, the data may refer to different entities, thus leading to conflicting information.

The *beam spreading* observed in *Fig. 1b* may also have significant effects on the irradiance at the target. To evaluate how this phenomenon affects the laser beam, the size and intensity properties of a sequence of laser pulses delivered at a 30 m distance with a repetition rate of 5 Hz were monitored. *Fig. 3* shows the behavior of the diameter and the beam energy for a series of 500 successive laser shots. Values were computed according to the $1/e^2$ width criterion that excludes those points for which the intensity falls below 0.135 times the maximum [29-31].

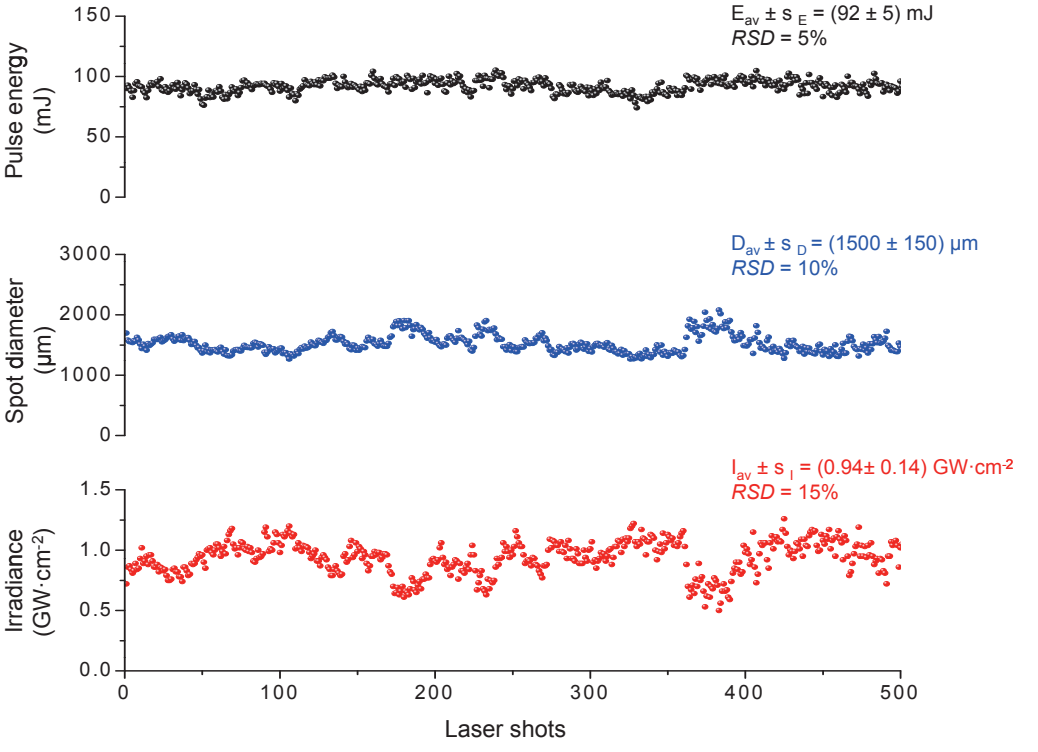

Fig. 3. Evolution of the behavior some properties—from top to bottom: pulse energy, spot diameter, and irradiance level—that characterize 500 successive focused laser pulses when they reach a hypothetical target located at a 30 m distance.

Fig. 3 also shows the pattern of the resulting irradiance computed from the combined actuation of these two parameters. As shown, the *shot-to-shot* variability

of the pulse energy (4x attenuated) remains practically within a 5% *RSD*. However, the variation of the corresponding spot diameter is twice as high. These significant changes in the effective diameter of the laser shots are closely related to the *beam spreading* phenomenon.

As a result, the irradiance reaching the target mainly follows a behavior opposite to that of the spot size, although featuring a global uncertainty deriving from both sources of variability. As shown, the larger the alteration of the laser pulse—reflected by an increase in its diameter—the larger the instability in the irradiance at the target. Hence, *beam spreading* is a relevant source of uncertainty in the formation of plasmas on distant targets. This variability is expected to be systematically transferred to the LIBS signals.

3.1.2 Plasma signal collection. A similar investigation to assess the alterations experienced by the returning light from the plasma and their repercussions for the acquired LIBS signals was performed. The precision in focusing the plasma images on the tip of the optical fiber as well as some properties of these images were carefully checked.

Fig. 4 plots the position of successive images from 500 aluminum plasmas. In this experiment, the beam analyzer was placed on the focal plane of the telescope and was centered with respect to the fiber tip that collects the plasma image and transfers the light to the spectrometer. The almost circular shape of the captured images and the Gaussian energy distribution of the profile should be noted. As shown, the diameter of the image is *ca.* 550 mm whereas the diameter of the fiber is 600 mm, thus, there should be no loss of light at the fiber tip. The figure shows that the plasma image formed by the telescope was also subject to small displacements in both directions over the image plane. However, it should be noted that, although the path of the returning light is identical to that for the beam travelling to the target, the range of the image deviation is only *ca.* 25 µm in both

the vertical and the horizontal axes. Furthermore, unlike the shifts that occured during the delivery of the laser pulses to the target through the atmosphere, in this case there were no preferential directions, revealed by the uniform *RSD* values observed in both axes (0.2%). This fact results from the special properties of the parabolic and hyperbolic reflectors in the *Cassegrain* telescope used here [32]. These reflectors were positioned so that both shared one focus and, at the same time, the second focus of the hyperbolic mirror was at the point at which the plasma image was collected, that is, exactly at the tip of the optical fiber. Thus, the positioning disturbances observed when the laser pulses are delivered—that under the present conditions amount to as much as 0.8 mm in the target plane—result in a negligible displacement (barely 25 µm) of the plasma image in the telescope focal plane.

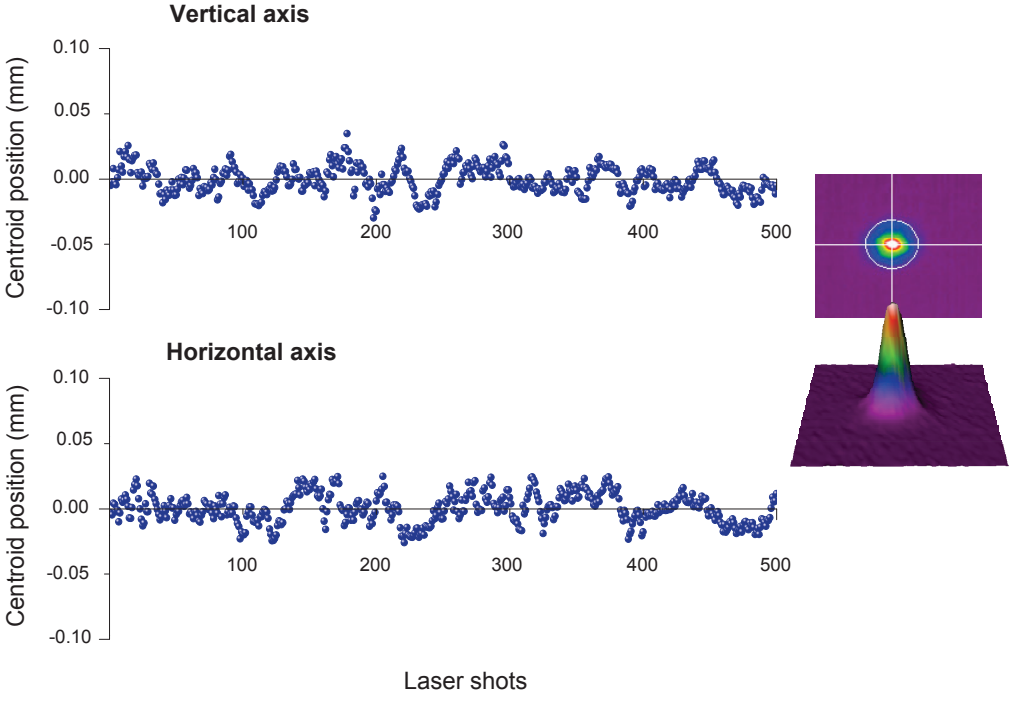

Fig. 4. Monitoring of the location of 500 successive aluminum plasma images in the two dimensions—height and width—that define the telescope image plane.

In addition, the radiometric and dimensional quantities of the plasma images were simultaneously monitored. *Fig.5* shows the behavior of the radiant flux (mW) and the image diameter for the sequence of plasmas studied. These parameters were computed using the same criteria as used to measure the features of the delivered laser shots. As an indicator of the plasma light emission, the trend for the resulting irradiance ($mW \cdot mm^{-2}$) is also plotted.

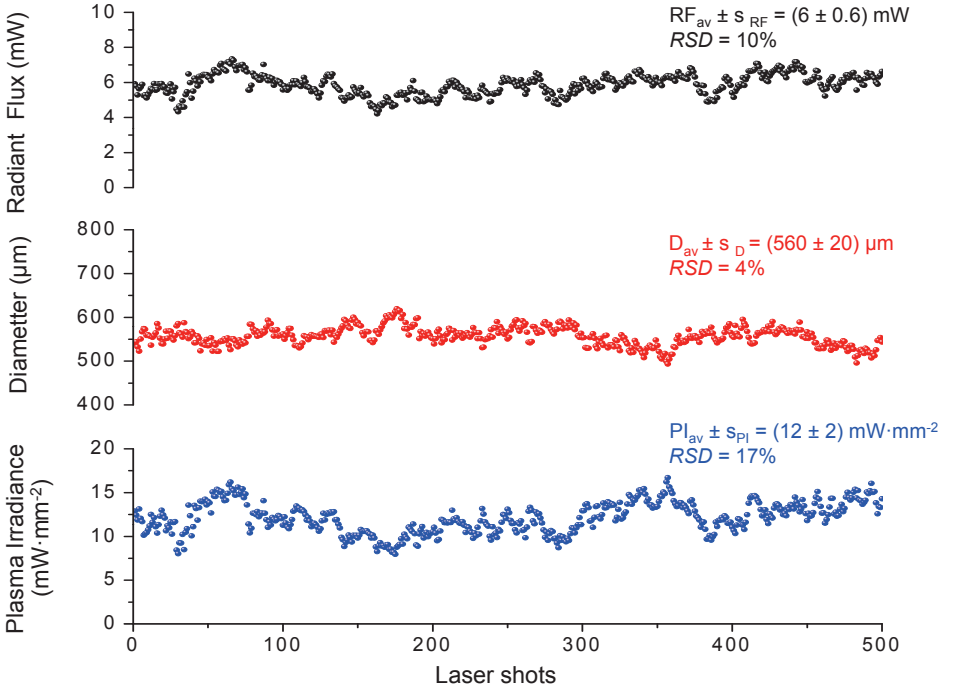

Fig. 5. Evolution of the behavior of some properties —from top to bottom: radiant flux, image diameter, and radiant flux— that characterize the 500 successive plasma images induced at a 30 m distance when they were collected by the detection device.

As shown, significant and random fluctuations (*RSD* = 10%) in the radiant flux of the plasma images were observed. These variations derive from the fluctuating character of the plasmas formed, as described above. In contrast, variations in the size of the plasma images at the telescope pupil were notably smaller (*RSD* = 4%).

Both sources of uncertainty are propagated in the plasma irradiance, which amounts to 17% *RSD*. Far from the influence of atmospheric factors on the plasma light collection, such oscillations in the plasma irradiance seem to be directly connected with fluctuations in the irradiance at the target as noted before.

In order to corroborate or rule out any influence from atmospheric factors on the returning light signal, synchronized measurement of the optical emission from the aluminum targets and the plasma image intensity gathered by the sensor was performed. In this experiment, the optical emission signal was acquired using a collimating lens securely attached to the tip of an optical fiber located at a distance of 5 cm from the produced plasma. Simultaneously, the intensity of images from produced plasmas was acquired with a beam analyzer located at the telescope focal plane 30 m from the sample. In this way, while alterations observed at close-contact should be attributed exclusively to distortions of the laser pulses during their transmission through the atmosphere, the variations in the observed plasma images would be derived from a global contribution from the atmospheric effects in both the delivery and the return paths. *Fig.6* plots the behavior of the atomic emission at 396 nm and of the measured irradiance from aluminum plasmas produced by a series of 500 laser shots. As observed, there is a close correspondence between both signals throughout the whole sequence. For instance, in the proximity of shot number 300, both the emission intensity and the plasma irradiance exhibit a peak, and the downwards drift of the intensity in the first 40 shots is paralleled by a similar trend in the plasma irradiance. Despite this connection between the patterns, it is convenient to clarify why the magnitude of the fluctuation in the close-contact emission intensity is significantly larger than that of the plasma signal observed in the *standoff* mode of operation. While the signal variability is 77% *RSD* in the first case, a mere 12% *RSD* is measured in the second instance. In the close-contact measurements, the global uncertainty is due to the combined effect of *wandering* and *spreading* of the laser pulses. The large

shot-to-shot emission fluctuations reflect the displacement at the point where the plasma is being produced, meaning that the successive laser pulses are hitting different positions on the surface. Consequently, the plasma emission is moving, either partially or totally, in and out of the field of view of the collimating lens (5 mm in diameter). In fact, even when the plasma irradiance is detected at a distance, the optical emission detected in close-contact is null. This fact is observed in *Fig. 6* in the proximity of shot 40. Additional fluctuations from the changing plasma events due to the unstable irradiance on the target as a consequence of the *beam spreading* also contribute. All these alterations are directly reflected in the varying intensities of the optical emissions measured.

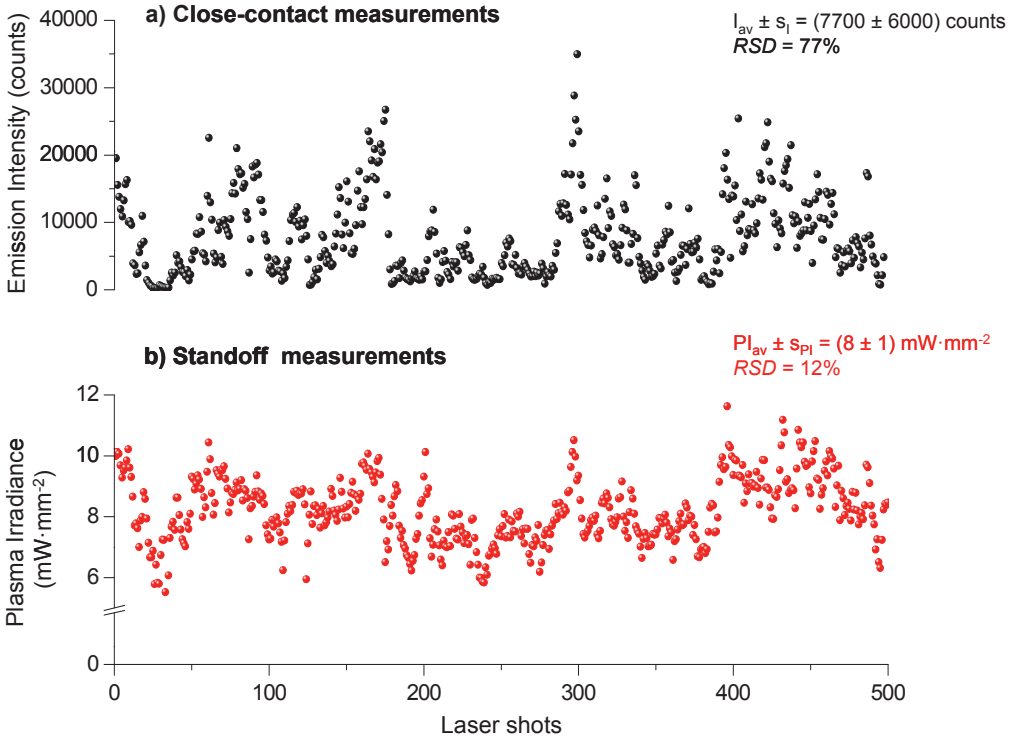

Fig. 6. Monitoring of the paired correspondence between the spectral emission intensity (semi-*standoff* mode) and the irradiance (*standoff* mode) from 500 successive aluminum plasma plumes (30 m distance). More details in the body of the text.

In contrast, in the *standoff* measurements, the imaging capabilities of the telescope tend to alleviate the fluctuating plasma positions discussed above. As a result, the uncertainty in the *standoff* signals is markedly reduced as compared to that for the close-contact measurements. Hence, it is proved that the observed signals in *standoff* LIBS follow the fluctuating plasma intensities derived from differences in the properties of the beam at the target, namely the variations in the spatial distribution of the energy along the beam cross section. This fact is also reinforced by the close connection between the magnitudes of uncertainty of the two irradiances, the availability of the laser pulses to induce the plasmas (15%, *Fig. 3*) and the corresponding intensity released by the plasmas (12%, *Fig. 6*). Findings demonstrate that the variability in *standoff* LIBS measurements is mainly derived from distortions suffered by the laser beam along the path towards the target. Once the plasma is produced, additional sources of uncertainty are of minor significance.

3.2 Outdoors evaluation

So far, the sources of variability in plasma production and the ensuing LIBS signals in a partially controlled environment and at a fixed range have been discussed. In this section, laser beam distortions in real scenarios and at increasing distances from the target are assessed.

3.2.1 Delivery of laser pulses. *Fig. 7* depicts the energy of the converging beam at various distances (30 m to 90 m) from the instrument, measured with a pyroelectric energy meter. A series of 250 successive laser pulses at a repetition rate of 5 Hz were measured. To avoid damaging the sensing head, the energy meter was placed slightly out of focus. As shown, the average pulse energies measured remain virtually constant with changing distance ($RSD_{\text{inter-ranges}}$ = 2%), which means that atmospheric attenuation of the outgoing laser energy was negligible. These

results, obtained with a 1064 nm focused laser beam, confirm the observation previously reported [33] with collimated beams and are in agreement with the theoretical prediction for focused beams [18]. Furthermore, the pulse-to-pulse fluctuation of the beam energy remains more or less static ($RSD_{\text{intra-range}}$ = 0.5%) regardless of the measurement distance.

The conditions under which the laser energy is reaching the distant target were also evaluated. The laser beam was focused at the prescribed distances in order to concentrate it into the smallest spot possible, resulting in plasma ignition.

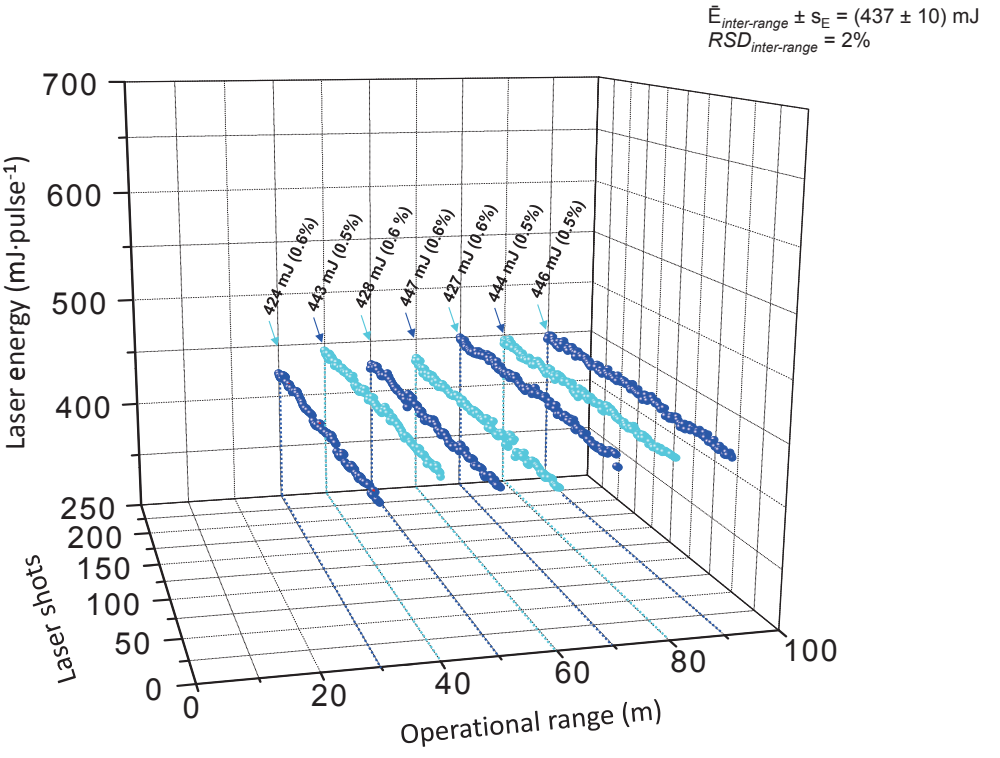

Fig. 7. Profiles of the laser energy levels reaching a distant target as a function of its location. The specific labels display the average intra-range laser energy (250 laser shots) together with the corresponding variability expressed as relative standard deviation (*RSD* (%)).

Fig. 8 plots the variation in the laser spot diameter as a function of the distance to the target. At each distance, the prints on heat-sensitive paper from 10

laser pulses were accurately quantified using *Visilog 6* software (for image processing applications). The spot diameters were measured from the burnt pattern which reflected the entire damaged area. Some specific representative images of these prints are displayed.

The minimum achievable spot diameter *(d)* at which a Gaussian laser beam can be focused is given by [25]:

$$d = \frac{4\lambda M^2 r}{\pi D} \qquad \text{(Equation 1)}$$

where λ is the wavelength of the laser light; M^2 is the beam quality parameter; *r* is the distance to the target and *D* is the diameter of the section of the primary mirror illuminated by the laser beam. In the *Cassegrain* telescope used here, the focus at variable distances is achieved by changing the position of the secondary mirror with respect to the primary mirror. This in turn affects the size of the expanded beam, *D*. Consequently, the diameter of the focused spot changes with both *r* and *D* and the exact dependence of the spot size on the range is a complex function of both variables. In our system, it has been experimentally verified that the change in *D* over the operational range assayed (from 30 to 90 m) is negligible, thus making d a linear function of *r*. As shown, the data in *Fig. 8* fit to a linear function up to approximately 70 m from the target in accordance with equation (1). The experimental behavior departs from linearity at the longest distance tested (90 m). This circumstance derives from the degrading quality of the laser beam with the distance. Also, this deviation departure may result from the insufficient sensitivity of the thermal-sensitive paper to print the beam profile at large distances and thus to accurately estimate the beam size. In summary, in the absence of any significant attenuation of the delivered laser energy at increasing distances, this increasing spread is the most noticeable factor afflicting the

irradiance achieved at the target by the system. Hence, the intensities (and reproducibility) of the plasma plumes will be directly affected by this less-uniform irradiance experienced by the distant targets. Furthermore, such events will directly affect the level and the uncertainty of the emission signals as discussed below.

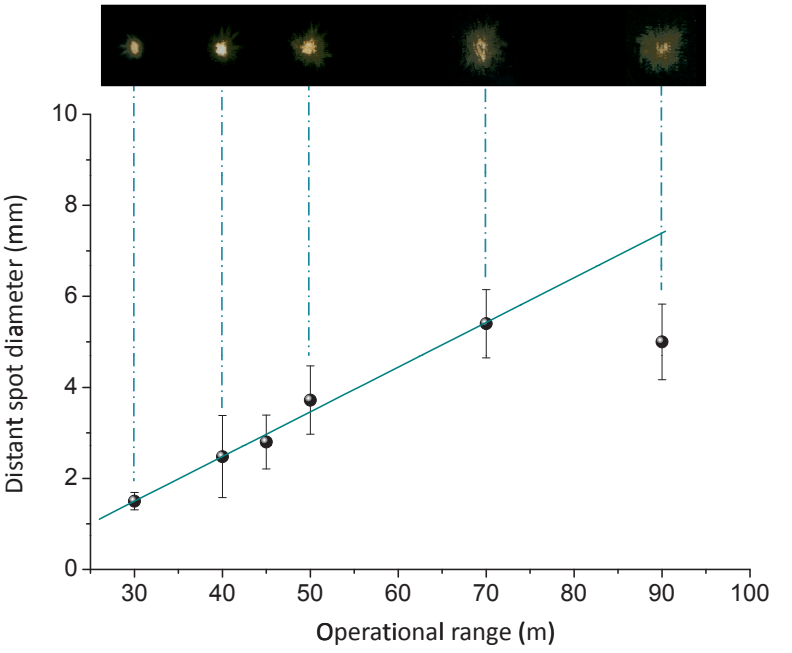

Fig. 8. Variation in the experimental diameters of focused laser pulses as a function of the distant location of the target. Inset shows in detail some representative images of prints from laser pulses on heat-sensitive paper at specific distances. The solid line traces the trend theoretically expected for the spot size. More details in the body of the text.

3.2.2 Plasma signal collection. In order to evaluate the impact of the increasing atmospheric propagation of the laser beam on the analytical response, emissions from plumes created at different distances were gathered. *Fig. 9* shows the experimental intensities registered for the most sensitive signal (396 nm) from aluminum plasmas as a function of the distance to target. In addition, the $1/r^4$ theoretical dependence of the signal is shown as a dotted line. The variation in the signal relative standard deviation is also plotted. As shown, the *standoff* LIBS signal drops markedly with increasing operational range. This circumstance is attributed

to the overall contribution of distortions that the light (either monochromatic or white) suffers throughout the entire optical path. At all events, the effects will be individually examined in light of the ongoing considerations, first, the plasma formation, then, the light gathering. The intensity of the plasma plume is directly proportional to the laser fluence concentrated on an area of the distant target [34]:

$$I = \frac{F}{\pi\left(\frac{d}{2}\right)^2} \qquad \text{(Equation 2)}$$

where the irradiance *I* depends on the fluence *F* and the minimum achievable spot area of the laser beam at the target. Substituting equation (1) for *d*, equation (2) can be rewritten as:

$$I = \frac{F\pi D^2}{4\lambda^2 M^4 r^2} \qquad \text{(Equation 3)}$$

Hence, equation (3) reveals an inverse square attenuation of the irradiance with increasing operational range during the laser beam travel from the sensor towards the target.

In addition, the light gathered by the telescope from a target located at range *r* decreases with the inverse of the range squared [35]. The contribution of these two phenomena accounts for the r^4 dependence on the range of the decrease in the *standoff* LIBS signal. As observed in *Fig. 9* the average experimental emission intensities correspond with this theoretical model based on the inverse fourth power decay with operational range. In parallel, the variability within the emission signals enlarges progressively at increasing distances. This increment of variability in the successive emissions is due to the joint effect of the decrease in the irradiance together with its stochastic alterations at the increasingly distant target.

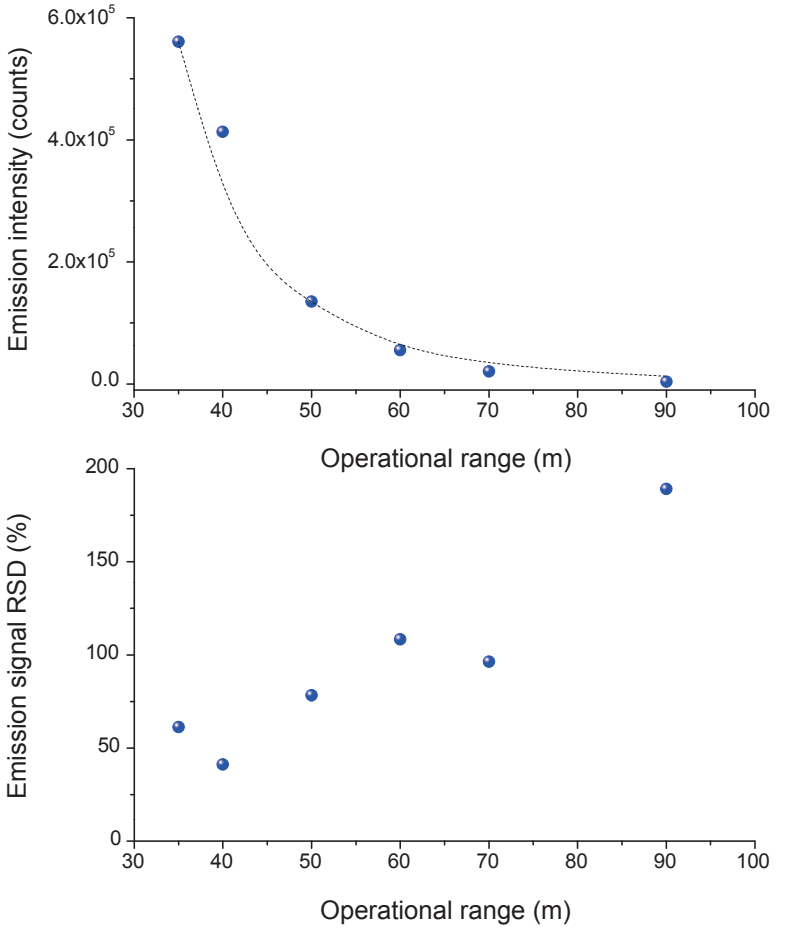

Fig. 9. The evolution of the emission intensity (upper plot) for the most sensitive emission line of aluminum (396 nm) as a function of the location of the target, together with the trend in its associated uncertainty (lower plot).

Despite the decreasing irradiance, in the absence of such changing alterations, the uncertainty of the plasma events would be in clear correspondence with their intensities. Thus, these random alterations resulting from *spreading* of the laser pulses cause fluctuations in the irradiance that impact on the changing characteristics of the induced plasmas. This is why a higher, but random, deterioration of the laser beam is expected for ever growing distances from the target. As the optical path increases, the plasma production becomes much less

reproducible, and a much more significant variability in the emissions collected from faraway distances is evidenced.

4 Conclusions

In the present manuscript the main sources of uncertainty in emission signals in *standoff* LIBS measurements have been elucidated. Distortions suffered by laser pulses during their delivery to a distant target as well as alterations afflicting the plasma images when acquired, have been evaluated. Operations have been carried out on an *ad hoc* basis in order to reveal how variability is propagated into the final emission signal. As demonstrated, no matter what the distance to the target, laser pulse energy fluctuations are negligible, so their direct influence on the ensuing LIBS intensity variability is irrelevant. In contrast, while virtually all the energy flux reaches the target, the loss of beam quality during its transmission through the atmosphere leads to a noticeable uncertainty in its distribution. This circumstance leads to a detrimental impact on the laser irradiance. As a result, the plasmas produced significantly differ in their properties. These varying plasma events are easily detected through significant changes in their irradiance, which in turn have been proven to be in direct correlation with the unstable spectral emission collected by the optical system. In addition, the larger the range the greater the deterioration in laser irradiance. These effects increase the *shot-to-shot* uncertainty within the emission signals. Additionally, regardless of the operating range, the process of plasma light propagation was found to have no significant influence on the overall variability, at least, in the absence of severe weather events. The random variation in the location of the laser beam centroid on the target (*beam wander* effect) does not directly affect the position of the plasma image at the telescope focal plane where the tip of the optical fiber used for light collection is located. Hence, in essence, it is no longer a question of how much or where, but of

how the laser beam is spread on the target. Indeed, these random distributions are suggested to be "the spark that lights the fuse of variability" due to their direct influence on the laser–material coupling, sample ablation, laser pulse–plasma interactions, and so on, contributing to the entire variability being encountered within successive emission spectra that are collected from multiple consecutive laser shots. Now that the most significant cause of uncertainty for distant LIBS signals has been identified, new studies on the particular effects caused by those factors involving the surroundings, like temperature, humidity, wind, rain, fog and the presence of particulate matter are under development.

5 References

[1] W. Demtröder, Laser Spectroscopy: Basic Principles, Vol. 1, 4th edition, *Springer*, Berlin (2008).

[2] D.A. Cremers, L.J. Radziemski, Handbook of Laser Induced Breakdown Spectroscopy, *John Wiley & Sons*, Chichester (2006).

[3] F.J. Fortes, J. Moros, P. Lucena, L.M. Cabalín, J.J. Laserna, Laser-induced breakdown spectroscopy, *Anal. Chem.* 85 (2013) 640–669.

[4] F.J. Fortes, J.J. Laserna, The development of fiedable laser-induced breakdown spectrometer: No limits on the horizon, *Spectrochim. Acta Part B* 65 (2010) 975–990.

[5] D.W. Hahn, N. Omenetto, Laser-induced breakdown spectroscopy (LIBS), part II: review of instrumental and methodological approaches to material analysis and applications to different fields, *Appl. Spectrosc.* 66 (2012) 347–419.

[6] C. López-Moreno, S. Palanco, J.J. Laserna, F. De Lucia, Jr, A. Miziolek, J. Rose, R.A. Walters, A.I. Whitehouse, Test of a stand-off laser-induced-breakdown spectroscopy sensor for the detection of explosive residues on solid surfaces, *J. Anal. At. Spectrom.* 21 (2006) 55–60.

[7] J.L. Gottfried, F.C. De Lucia, Jr, C.A. Munson, A.W. Miziolek, Strategies for residue explosives detection using laser-induced breakdown spectroscopy, *J. Anal. At. Spectrom.* 23 (2008) 205–216.

[8] I. Gaona, P. Lucena, J. Moros, F.J. Fortes, S. Guirado, J. Serrano, J.J. Laserna, Evaluating the use of standoff LIBS in architectural heritage: surveying the Cathedral of Málaga, *J. Anal. At. Spectrom.* 28 (2013) 810–820.

[9] R.Grönlund, M. Lundqvist, S. Svanberg, Remote imaging laser-induced breakdown spectroscopy and remote cultural heritage ablative cleaning, *Opt. Lett.* 30 (2005) 2882–2884.

[10] D.A. Cremers, Remote analysis by LIBS: application to space exploration, Laser-Induced Breakdown Spectroscopy, *Elsevier Science*, Amsterdam (2007).

[11] B. Sallé, D.A. Cremers, S. Maurice, R.C. Wiens, Evaluation of a compact spectrograph for in-situ and stand-off Laser-Induced Breakdown Spectroscopy analyses of geological samples on Mars missions, *Spectrochim. Acta Part B* 60 (2005) 805–815.

[12] P. Werheit, C. Fricke-Begemann, M. Gesing, R. Noll, Fast single piece identification with a 3D scanning LIBS for aluminium cast and wrought alloys recycling, *J. Anal. At. Spectrom.* 26 (2011) 2166–2174.

[13] A. González, J. Ruiz, L.M. Cabalín, J.J. Laserna, On-line laser induced breakdown spectroscopy determination of Mg coating thickness on electrolytically galvanized steel in motion, *Appl. Spectrosc.* 64 (2010) 1342–1349.

[14] S. Palanco, S. Conesa, J.J. Laserna, Analytical control of liquid steel in an induction melting furnace using a remote laser induced plasma spectrometer, *J. Anal. At. Spectrom.* 19 (2004) 462–467.

[15] L.C. Andrews, R.L. Phillips, Laser beam propagation through random media, *SPIE Press*, Bellingham (2005).

[16] L.C. Andrews, R.L. Phillips, C.Y. Hopen, M.A. Al-Habash, Theory of optical scintillation, *J. Opt. Soc. Am. A* 16 (1999) 1417–1419.

[17] G.P. Berman, V.N. Gorshkov, S.V. Torous, Scintillation reduction for laser beams propagating through turbulent atmosphere, *J. Phys. At. Mol. Opt. Phys.* 44 (2011) 1–34.

[18] A. Ferrero, J.J. Laserna, A theoretical study of atmospheric propagation of laser and return light for stand-off laser induced breakdown spectroscopy purposes, *Spectrochim. Acta Part B* 63 (2008) 305–311.

[19] D.A. Zimnyakov, E.A. Isaeva, A.A. Isaeva, M.V. Pavlova, A.P. Sviridov, V.N. Bagratashvili, Attenuation and speckle modulation of laser light in dispersive dye-doped media: Competition of absorption and scattering processes *Opt. Commun.* 285 (2012) 2377–2381.

[20] H. Weichel, Laser beam propagation in the atmosphere, *SPIE Press*, Bellingham (1990).

[21] A. Ishimaru, Wave propagation and scattering in random media, *Academic Press*, New York (1978).

[22] I. Schechter, Direct aerosol analysis by time resolved laser plasma spectroscopy – improvement by single shot measurements, *Anal. Sci. Technol.* 8 (1995) 779–786.

[23] J.E. Carranza, D.W. Hahn, Sampling statistics and considerations for single-shot analysis using laser-induced breakdown spectroscopy, *Spectrochim. Acta Part B* 57 (2002) 779–790.

[24] V. Lazic, F. Colao, R. Fantoni, V. Spizzicchino, Laser-induced breakdown spectroscopy in water: Improvement of the detection threshold by signal processing, *Spectrochim. Acta Part B* 60 (2005) 1002–1013.

[25] B. Sallé, P. Mauchien, S. Maurice, Laser-Induced Breakdown Spectroscopy in open-path configuration for the analysis of distant objects, *Spectrochim. Acta Part B* 62 (2007) 739–768.

[26] A.A. Zemlyanov, Y.E. Geints, Effect of Diffraction on Stimulated Raman Scattering of Laser Radiation in the Middle Atmosphere, *Opt. Spectrosc.* 99 (2005) 620–629.

[27] P.T. Mannion, J. Magee, E. Coyne, G.M. O'Connor , T.J. Glynn, The effect of damage accumulation behaviour on ablation thresholds and damage morphology in ultrafast laser micro-machining of common metals in air, *Appl. Surf. Sci.* 233 (2004) 275–287.

[28] J. Recolons, L.C. Andrews, R.L. Phillips, Analysis of beam wander effects for a horizontal-path propagating Gaussian-beam wave: Focused beam case, *Opt. Eng.* 46 (2007) 086002-1–086002-11.

[29] J. Alda, Laser and Gaussian beam propagation and transformation, in Encyclopedia of Optical Engineering, R.G. Driggers and C. Hoffman (Eds.), *Marcel Dekker*, New York (2003) 999–1013.

[30] ISO 11146–1:2005(E), Lasers and laser-related equipment-test methods for laser beam widths, divergence angles and beam propagation ratios.

[31] M.T. Tavis, H.T. Yura, Short-term average irradiance profile of an optical beam in a turbulent medium, *Appl. Opt.* 15 (1976) 2922–2931.

[32] J.W. Hardy, Adaptive optics for astronomical telescopes, *Oxford University Press*, New York (1998).

[33] W. Yu, M.Y. Yu, J. Zhang, L.J. Qian, X. Yuan, P.X. Lu, R.X. Li, Z.M. Sheng, J.R. Liu, Z.Z. Xu, Long-distance propagation of intense short laser pulse in air, Phys. Plasmas 11 (2004) 5360–5362.

[34] R.M. Measures, Laser remote chemical analysis, *John Wiley & Sons*, New York (1988).

[35] J. Moros, J.A. Lorenzo, K. Novotny, J.J. Laserna, Fundamentals of stand-off Raman scattering spectroscopy for explosive fingerprinting, *J. Raman Spectrosc.* 44 (2013) 121–130.

Section 2.
Standoff LIBS Applications

Chapter 2. Evaluating the Use of *Standoff* LIBS in Architectural Heritage: Surveying the Cathedral of Málaga

Abstract

Laser-induced breakdown spectroscopy (LIBS) is a cutting-edge technology which offers appealing features for its application in the field of the cultural heritage. It is a proven technology for the fast and simultaneous detection of major and trace elements with minimal destructiveness, using easily compactable instrumentation into movable platforms for the *in situ* and *standoff* chemical analysis of objects in real time. In the present work, a *standoff* LIBS sensor has been used for surveying the Cathedral of Málaga. The spectroscopic measurements were gathered *in situ* although from an averaged distance of 35 m. A comprehensive characterization of the materials composing the main façade as well as identification of the noticeable pollutants at their surfaces has been performed. The *standoff* LIBS results have fitted neatly with the mineralogical analysis of all the stones assayed. The large emissions of Si, Al, Ca and Mg have confirmed that the structure was almost entirely built using sandstone. In turn, the sensitivity to carbonate chemistry has demonstrated the capability of *standoff* LIBS for coherently classifying different marbles, thus allowing the identification of their origins. *Standoff* LIBS has also allowed the detection of pollutants such as Si, Ca, Mg, Fe, Al, Ba and Sr, originating from natural sources such as the transport of re-suspended dust and atmospheric particulate matter related to marine aerosols. In addition, trace elements such as Ti, Pb and Mn from exhausts of gasoline and diesel engines are also involved in the pollution triggering of materials. To obtain all these findings, scaffolding or other intrusive facilities have not been required.

1 Introduction

Cultural heritage is a valuable resource inherited from the history and a unique legacy that broadens our understanding of the diversity of society and its constant evolution. Whether they are objects or archaeological sites, or ancient and historic monuments of the world, all of them inform and help connect us to our cultural origins. Therefore it is a real and irreplaceable treasure of outstanding value, considered worthy of preservation. Unfortunately, the rapid and on-going evolution of society has brought about a large deterioration of these vast sources of culture. Effects not only from anthropogenic sources but also from natural causes can result in unlimited and irreversible damage in cultural heritage. All this has meant that the conservation of cultural heritage and its protection against possible damage due to pollution has received growing scientific interest. In order to find the best possible measures for proceeding with protection of cultural heritage material, provision of analytical information for its characterization is a vital requirement. Further, research efforts to better assess and understand the pollution sources and mechanisms damaging the cultural heritage material cannot be set aside. Strong evidence of the growing importance of these physical and chemical diagnostics is the wide aim of analytical techniques used for this end [1, 2]. Scientific assessment of the materials for cultural heritage poses specific, and often, difficult analytical challenges. The primary requirement is that no significant modification or alteration of the artifact occurs, so as not to compromise the historical, cultural and/or archaeological value when extracting as much information as possible [3]. Also, the capability of working *in situ* and in real time, either during the research campaigns [4, 5] or after the consequent conservation tasks [6], is often necessary due to the impossibility of moving historical artifacts to laboratory facilities. The use of compact, robust, and versatile analytical systems is highly desirable [7]. Finally, the limited or complex accessibility to the assets is

often incompatible with conventional methods of analysis. This circumstance requires the use of instruments to operate in a contactless way, but rapidly and with appropriate sensitivity [8].

Although few analytical techniques pool all these demands, laser-induced breakdown spectroscopy (LIBS) is an appealing tool for analysis that combines the above requirements [9, 10]. LIBS is an established technology having several advantages over conventional elemental analysis methods. Its capacity for rapidly and simultaneously detecting almost all elements after the ablation of barely a few nanograms of a target analyzed from several tens of meters from the portable platform is now a reality [11]. The potential of LIBS in the analysis of works of art and objects of archaeological importance has been demonstrated by several research papers that have appeared in the last few years [12]. They describe its use in the major and trace element analysis of paintings [13], frescoes [14], pottery [15, 16], marbles [17], alloys [18] and ancient stones [19], among others, for dating and characterizing provenance [20]. Furthermore, LIBS has also been used to diagnose contamination [21, 22] of heritage assets and as a tool either to deal with cleaning tasks or for their diagnosis [23, 24]. The versatility of connecting LIBS with other laser analytical techniques, such as laser-induced fluorescence (LIF) spectroscopy [25], Raman microscopy [26–28], X-ray fluorescence (XRF) [29], as well as its capability of operating underwater [30] makes LIBS a cutting-edge technique to be used.

Up to date, only fluorescence LIDAR (Light Detection And Ranging) has been able to address the remote, non-invasive diagnostics of cultural heritage stone in the outdoor environment [31]. Early experiments on monuments date back to the mid 1990s, when fluorescence LIDAR point measurements were conducted on the Cathedral and Baptistery of Parma, Italy [32]. Experiments dealing with the remote monitoring of biodeteriogens on stone surfaces [33] (important cause of the weathering of a monument) and the characterization of different types of stones of

the building materials [34] were performed. Subsequently, the technique has taken further advantage of the introduction of imaging capabilities in LIDAR instrumentation, thereby allowing the acquisition of hyperspectral fluorescence maps from an extended area at distances as large as 65 m, as for example for the documentation of past conservation interventions on the Coliseum, Rome [35]. However, despite this technique's ability to supply valuable analytical information, its main disadvantage arises from its "one wavelength–one transition" selectivity which prevents it from getting the entire atomic information that LIBS gathers.

In this work, the potential of LIBS technology to obtain multielemental information about materials and their contamination from the analysis *in situ* but from away (35 meters) has been demonstrated for the first time from a case study on one of the most important Renaissance architectural jewels in Andalusia, the Cathedral of Málaga. A thorough characterization of the sandstones, marbles and metals making up the most highlighted section of the main façade of this historical building has been performed. In turn, the identification of the most relevant pollutants that are damaging its appearance has also been accomplished.

2 Experimental section

The *ST-LIBS* sensor used to perform these investigations has been described in detail in the "Experimental" chapter of this Doctoral Thesis. Plasma light was spectrally resolved using a gated *Czerny–Turner* spectrometer (303 mm focal length, f/4) fitted with an intensified coupled-charged device detector. A 1200 grooves·mm^{-1}, 300 nm blazed grating, providing a spectral window that ranges from 370 nm to 440 nm. The timing parameters used for spectral acquisition are: 2 µs as the delay time from the input of an external trigger (considered as zero time) to the opening of the intensifier tube of the detector device, and 5 µs as the integration time.

Scenario description

The Cathedral of Málaga is a noteworthy piece of Renaissance architecture in Spain. This historical monument was constructed between 1528 and 1782. The façade is divided into three well-defined areas, separated by *Corinthian* columns. In the present work, the central wing of the lower level was studied. The analysis of the medallion therein located, and those ornamental elements that flank it, was the focus of our investigations. *Fig. 1* shows a model of the Cathedral locating the working scenario. The sensor emplacement and a detailed image of the tested area are also highlighted. A thorough *in situ standoff* LIBS survey to characterize the composition of the materials and to detect potential pollutants spoiling the appearance of the most significant ornate stoneworks within this area was performed. The most adequate sampling strategy that best reflected what was while early laser events were considered for the detection of pollutants, the characterization of materials was made from the latter laser events.

3 Results & discussion

3.1 Multielemental profiling

With the aim of identifying the chemical composition of the materials forming part of the architectural objects within the investigated section of the Cathedral's main façade, a broad deployment of surface laser interrogations was carried out. The following results show both the spectral data gathered by scanning defined surface areas and the elemental composition of remarkable objects obtained by point analysis.

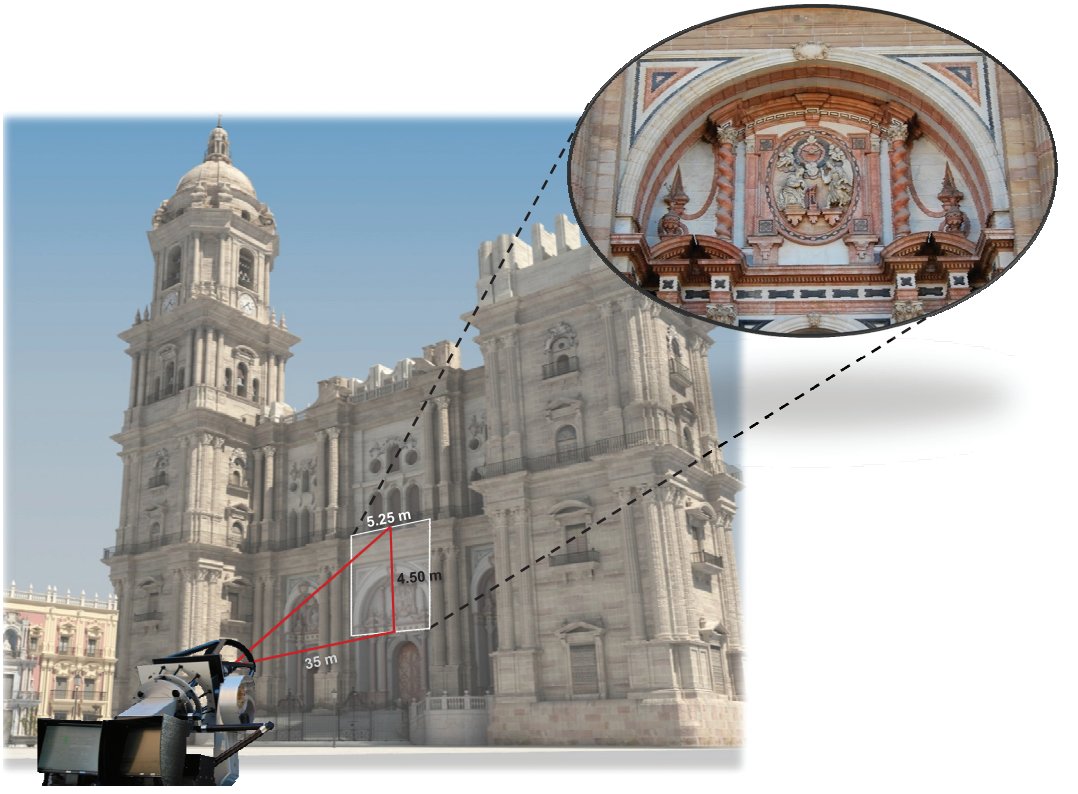

Fig. 1. Descriptive scheme on the working scenario. The emplacement of the LIBS platform, and section investigated, are highlighted.

3.1.1 ***Chemical composition of sandstone***. On the basis of existing documentation on the construction of Málaga Cathedral [36] and previous mineralogical and petrographical studies as well as the chemical analysis of major, minor and trace elements [37], sandstone in the main façade (constructed between 1721 and 1782) has been labeled as an intermediate sandstone consisting of *protoquartzites* and *subarkoses*, which are composed of quartz (70–90% SiO_2), feldspars [$M(Al_xSi_yO_8)$] and dolomite (5–25% [$CaMg(CO_3)_2$]). Fe and Mn are also associated with dolomite in its mineralogical formation.

Fig. 2 depicts a representative *single-shot* spectrum (the most reproducible one within the spectral series) of the sandstone, a common sedimentary rock that constitutes virtually the entire structure of the Cathedral, as well as a series of chemical maps associated to a 40 cm × 40 cm cornice section. These maps were acquired by scanning the surface with a lateral resolution of 2 cm. The area inspected is located at *ca.* 35 m from the sensor. As observed, *standoff* LIBS analysis fits neatly with the mineralogical analysis. Intense atomic emissions of Si at 390.6 nm, Al at 396.1 nm, Ca at 396.9 nm, and Mg at 383.8 nm are readily assigned along with faint emissions of Mn at 403.1 nm, Sr at 407.8 nm and Fe at 404.6 nm. Also, information from the maps related to the element distribution profiles of the sandstone surface reinforces the results from the chemical analysis. As seen, along the normal direction to the tested surface, the spatial distribution is virtually identical for the elements found. Nevertheless, although highly correlated, some variability in the intensities is observed. This circumstance derives from the porous nature of the sandstone which exhibits bottleneck shaped voids of size <4 μm [38].

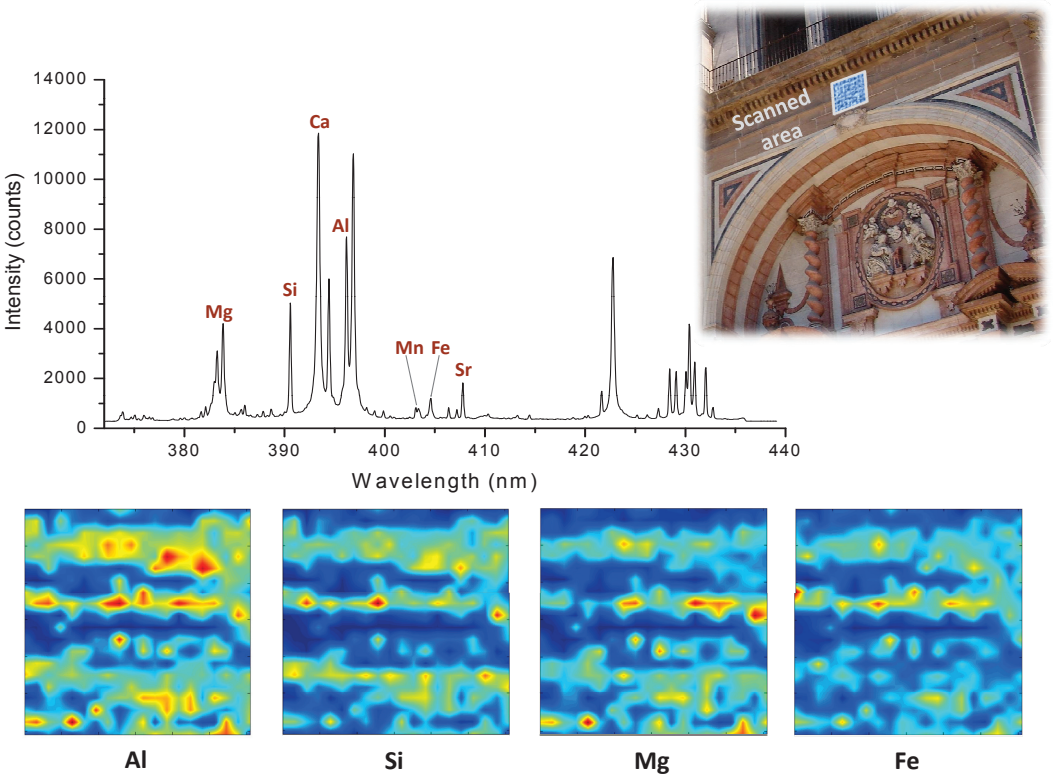

Fig. 2. Representative *single-shot standoff* LIBS spectrum of sandstone from the cornice upper to the central medallion together with chemical maps related to aluminum, silicon, magnesium, and iron distribution profiles. The intensity in each map has been normalized. More details in the body of the text.

3.1.2 Chemical composition of marbles. The composition of significant marble sections of the distinctive medallion located in the front façade was also characterized. *Fig. 3* shows a picture of the area inspected. The materials are distinguishable to the naked eye by their different colors (white, black and rose). Marbles are metamorphic rocks whose main minerals are calcite ($CaCO_3$) or dolomite, according to the geological setting of their provenance. *Fig. 3* also depicts characteristic LIBS spectra from each marble. As shown, the spectra of the three marbles are dominated by atomic and ionic emissions of Ca, *self-reversal* in some lines being observed. Small contributions of Al and Ti are also noticed. However, while the spectrum of the rose marble (the background of the dove) displays mainly

Ca lines with very slight contributions of Mg(I) and Sr(II), the spectra of the black and white marbles reveal larger spectral features for these elements. Black marble (*prie-dieu*) exhibits emissions of Sr and Mg of comparable intensity, whereas in the white marble (*statue of the Virgin Mary*) the abundance of Mg is significantly larger than that of Sr.

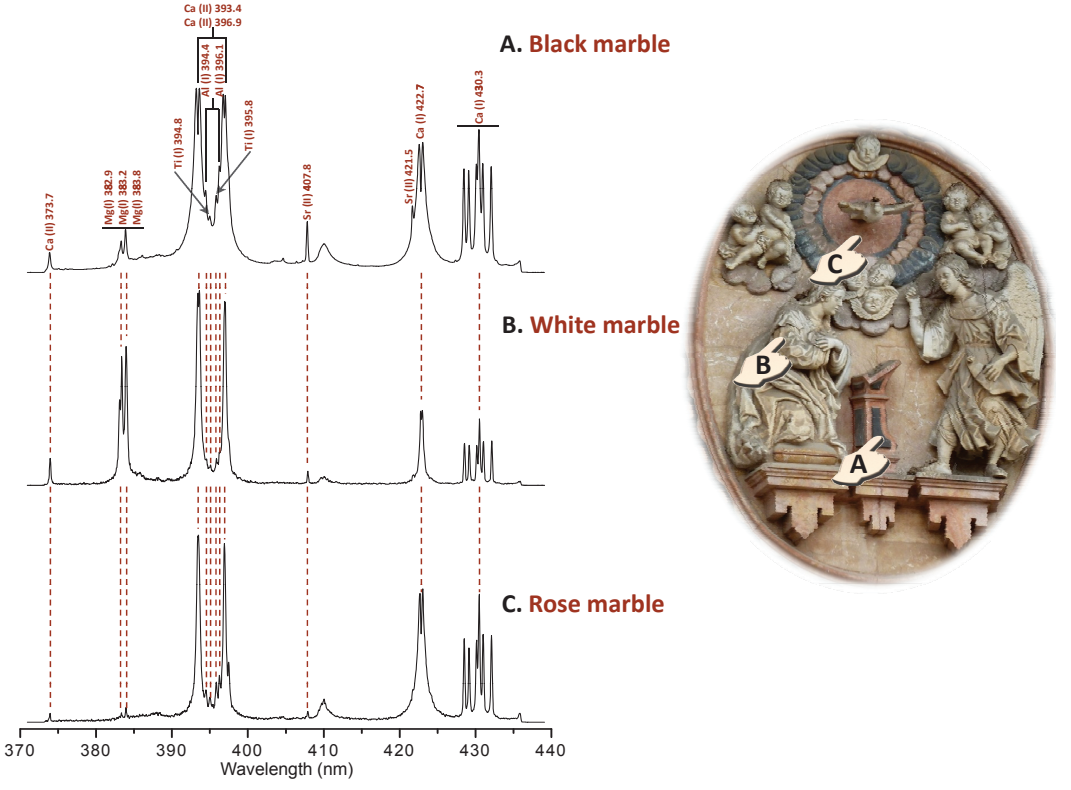

Fig. 3. Characteristic LIBS spectra from the different types of marbles within the main medallion; from top to bottom: black, white and rose.

To check for the consistency of LIBS to discriminate the marble materials, a large set of data acquired on specific positions on the medallion was processed. For this purpose, ratios of intensity for different elements, Sr(I) at 407.8 nm and Mg(I) at 383.8 nm) to the Ca(I) emission (431.9 nm), were examined. *Fig. 4* displays a *3D* scatter plot projected onto the subspace of the Sr/Ca and Mg/Ca intensity ratios.

Each series of 500 LIBS spectra was gathered from five refreshed sampling points (100 spectra each) within each type of marble.

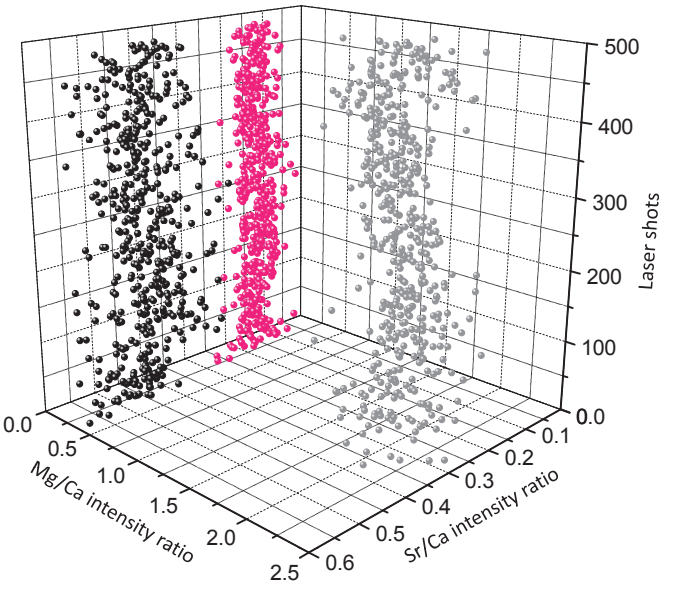

Fig. 4. *3D* scatter plot projected onto the subspace of the Sr/Ca and Mg/Ca emission intensity ratios for series of 500 *single-shot* LIBS spectra gathered each from three types of marbles composing the most distinctive medallion and distinguishable by different colorations (white, black and rose).

As reflected, the three datasets are grouped in three well-defined clouds. White marble shows Mg/Ca intensity ratios centered near 1.6, whereas the corresponding values for black and rose marbles are close to 0.3. In turn, black and rose marbles differed clearly in their Sr/Ca intensity ratios, ≈0.45 and ≈0.17, respectively. This sensitivity to carbonate chemistry just discussed demonstrates the capability of *standoff* LIBS for consistently sorting materials of the same kind. Indeed, the spectral characteristics of the marbles may be used as identity cards for these materials. It is expected that the quantitative intensities of optical emissions in the marbles of the Málaga district are distinctive enough for identifying the provenance of these different carbonate materials.

Hence, based on the spectroscopic information and according to the geology of the quarries of Málaga [38] it is possible to suggest that the white marble comes from any nearby dolomitic quarries (Monda, Coín, Mijas or Alhaurín de la Torre) whereas black and rose marbles both may originate from Alhaurín el Grande, which is the closer quarry solely supplying calcitic materials [39].

Standoff LIBS was also used to analyze marbles from different sections of the façade in order to identify their provenance. Three sets of materials, constituted by marble samples of the same color, were examined. *Table 1* summarizes the data.

Table 1. Ratios of Mg/Ca and Sr/Ca emission intensities corresponding to the different marbles employed in the front façade of Malaga's cathedral.

Marbles description		**Emission intensity ratios**			
Color	**Location**	**Mg/Ca**		**Sr/Ca**	
		Mean ± s	***RSD (%)***	***Mean ± s***	***RSD (%)***
Black	A (*Decorative border upper the front door*)	0.42 ± 0.07	16	0.41 ± 0.08	19
	B (*Elliptical frame of the medallion*)	0.56 ± 0.10	19	0.43 ± 0.09	21
	C (*Prie-dieu)*	0.35 ± 0.05	13	0.46 ± 0.07	16
White	A (*Decorative border upper the front door*)	1.63 ± 0.33	20	0.13 ± 0.07	56
	B (*Carved capital from the Solomonic column*)	1.60 ± 0.23	15	0.16 ± 0.04	24
	C (*Statue of the Virgin Mary*)	1.86 ± 0.70	40	0.12 ± 0.04	33
Rose	A (*Background of the Dove*)	0.25 ± 0.07	26	0.12 ± 0.04	34
	B (*Solomonic column*)	0.25 ± 0.09	37	0.14 ± 0.03	19
	C (*Squared frame of the medallion*)	0.22 ± 0.04	14	0.17 ± 0.03	16

As observed, in the same vein, meaningful information again maximized the inter-class differences, that is, between marbles of different colors. In contrast, no statistically significant *intra-class* differences were noticed. To recap, the data suggest that the same colored marbles had the same provenance.

3.1.3 Chemical composition of ornamental metallic objects. To close this section, a number of decorative metallic objects located in the façade were analyzed. *Fig. 5* depicts the representative *standoff* LIBS spectra from two metallic ornamental details, namely, the flowers in the vases alongside the medallion and the seals in the corners of the squared frame.

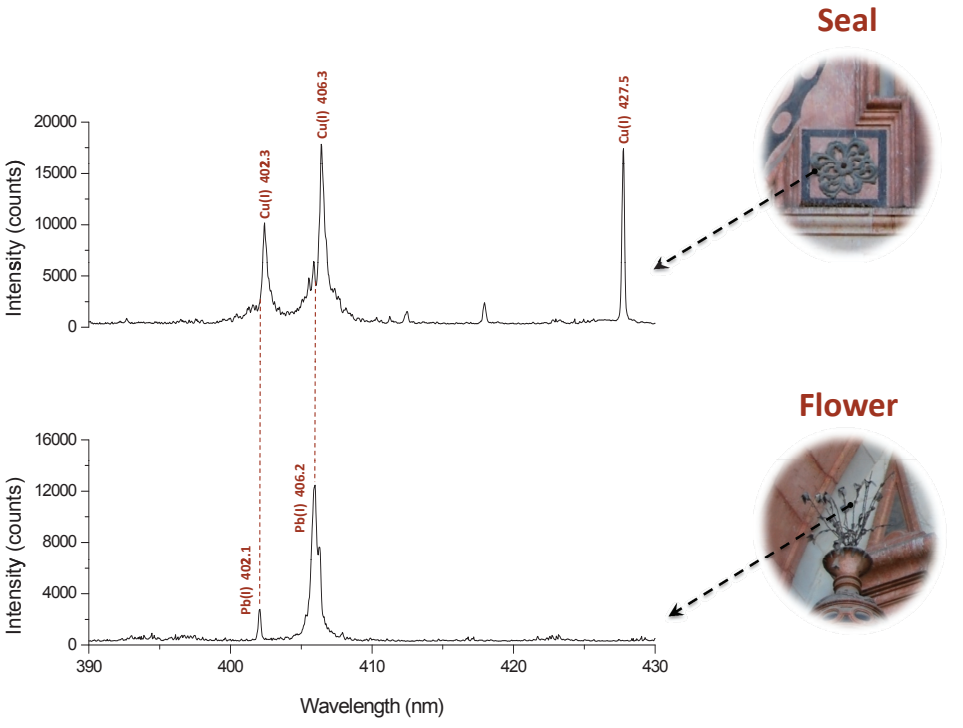

Fig. 5. Representative *standoff* LIBS spectra of two metallic ornamental elements.

As observed, flowers are exclusively constituted by Pb, identified through its characteristic emissions at 405.8 nm. In contrast, the seals were featured by atomic and ionic Cu emissions with small contributions of Pb at 405.8 nm. No significant spectral features apart from mere impurities were eventually identified. These results suggest that the seals are made from the Cu–Pb alloy commonly called *molybdochalkos* (95% Cu/5% Pb) or old Greek metal, a leaded copper bronze often

used during the Renaissance [40]. Justification for this seems to lie in the requirements of each ornament. Thus, while a malleable material such as pure Pb was suitable for the elaboration of the flowers, a more rigid material was needed for making the seals.

3.2 Detection of pollutants

Due to its actuation over the course of several hundred years, air pollution severely contaminates and damages the building materials of ancient artifacts. Estimation of both the nature and the amount of pollutants is of crucial importance before advancing in future conservation programs. Phenomena that cause building decay are complex due to the numerous intervening factors. In urban environments, worrisome air pollutants include SO_2, SO_4^{2-}, NO_x, NO^{3-}, Cl^-, CO_2, O_3, particulate matter (especially soot from diesel vehicle emissions), and acid rain. On the other hand, the most sensitive materials to pollutants are metals and calcareous stones [41]. With the aim of obtaining quick, *in situ* information on the profiling of contamination, LIBS analysis of the soiling on these materials was also pursued.

3.2.1 ***Inconspicuous contamination***. *Fig. 6* compares LIBS spectra acquired for the lead flowers in the vases. The top spectrum corresponds to the first shot on the surface, whereas the bottom spectrum was obtained after 300 shots on a single position. Apart from Pb, the first spectrum reveals the presence of pollutant elements, namely Mg, Fe, Si, Ca, Al, Ti, Mn and Sr. This finding suggests that in addition to the ubiquitous elements mainly due to wind blowing from the nearby coast (Mg, Si, Ca, Al, and Sr), anthropogenic sources (characteristically road traffic in urban areas) are also involved in the contamination (Fe, Ti, and Mn).

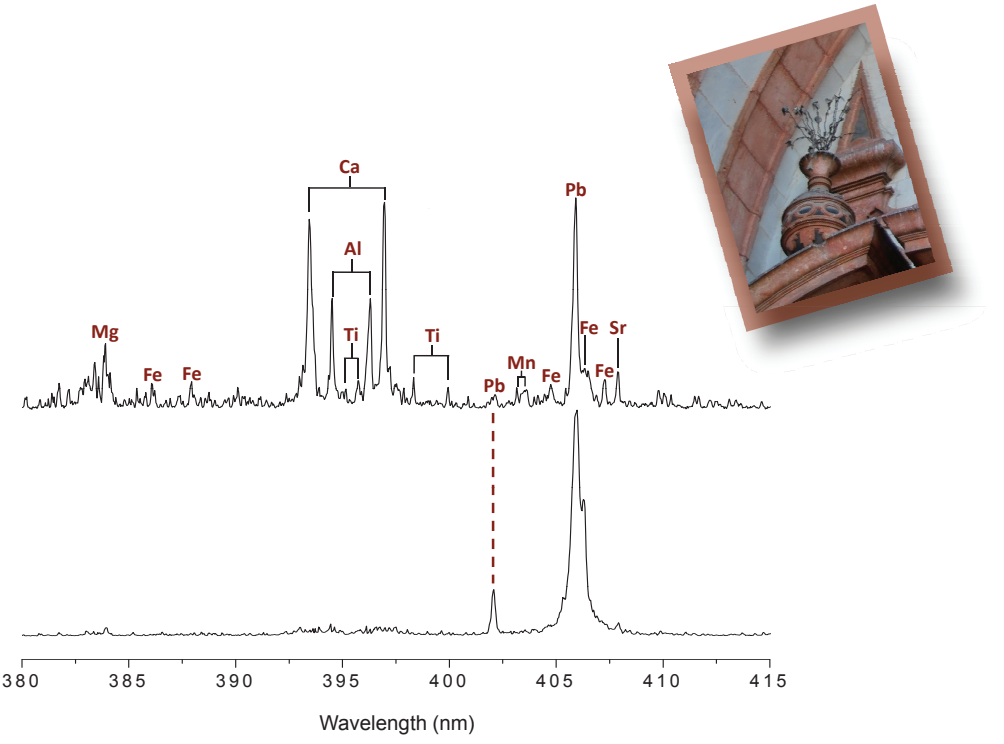

Fig. 6. Comparison between LIBS spectra from polluted and clean cases for the lead flowers in the vases.

Fig. 7 depicts the depth profile of Cu (406.3 nm) normalized to Ca (431.9 nm) from 500 laser pulses delivered to the metallic seal. As can be seen, while the ratio values remain virtually constant along the first 300 laser shots, a progressive increase in the values is observed for deeper pulses. This increase is the result of surface cleaning when the pollutant content relative to Cu decreases. Additionally, the large number of laser pulses to reach the base material gives an approximate idea of the thickness of the contamination layer. The sudden decrease of the Cu/Ca ratio value is due to the hopping of the laser beam to a fresh position within the contaminated seal (see the discussion below on *beam wander* effects).

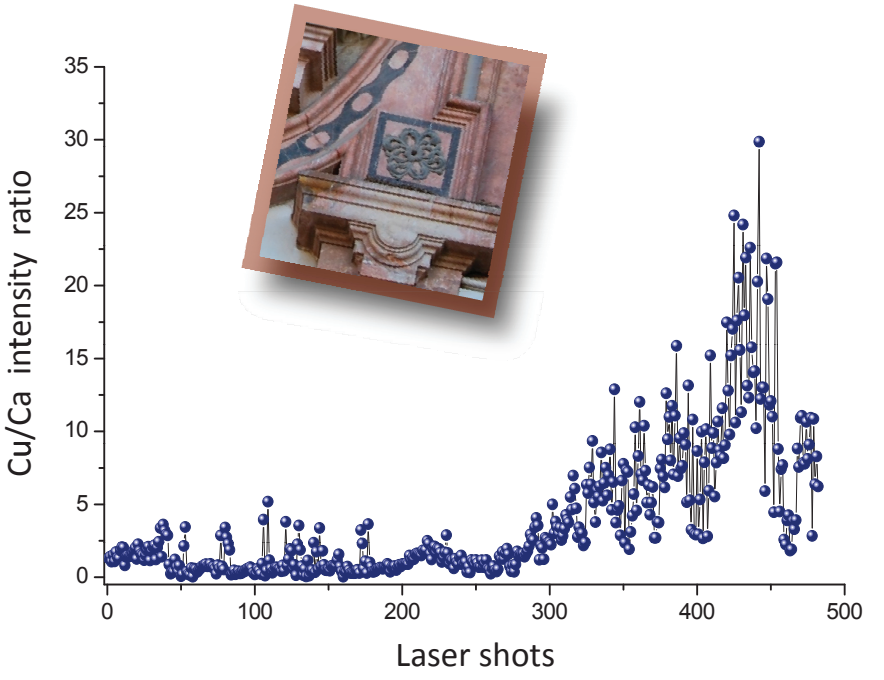

Fig. 7. Evolution profile of the Cu (406.3 nm)/Ca (431.9 nm) intensity ratio from 500 laser pulses in depth on the seal.

3.2.2 Gross contamination. While pollution can go unnoticed by observations at long distances, deposits are more than evident in some areas of the façade. Indeed, dust deposits tend to accumulate in decorative details with pronounced embossments and complex geometry. That fact is evidenced in *Fig. 8* which shows a picture from a Solomonic column made of rose marble. As seen in the twisted column, despite its equivalent temporal exposure to weather, two clearly disparate areas due to the orientation of its sections are distinguished: the downward parts that are seemingly clean, and the upward parts showing dirt crusts. *Fig. 8* also shows representative LIBS spectra of each section. As shown, the spectrum corresponding to the "*clean*" surface of the column is characterized by Ca, Al and Ti emissions with small contributions from Mg and Sr, in agreement with the composition of the rose marble studied in the medallion (see *Fig. 3*).

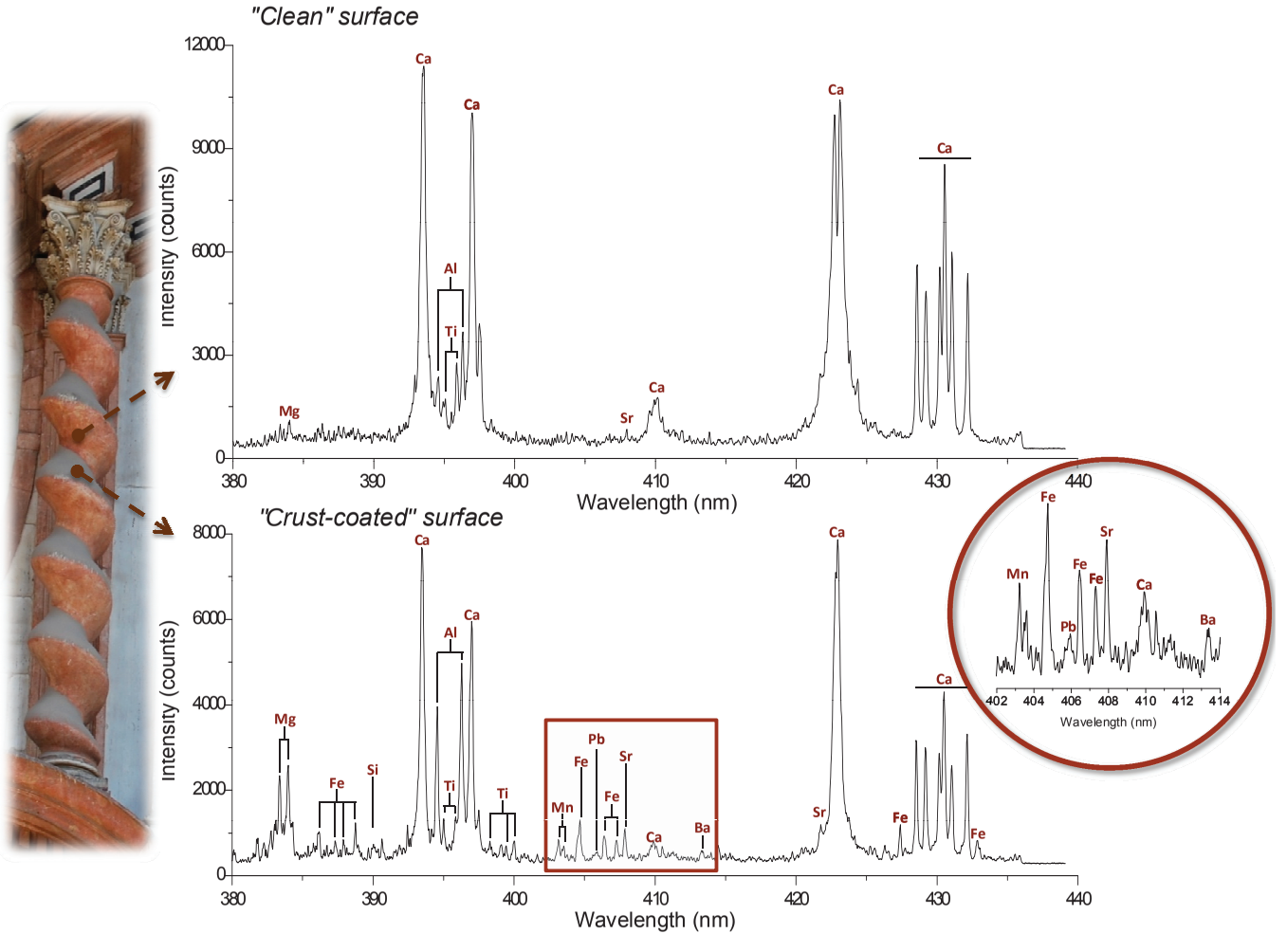

Fig. 8. Spectral comparison between "*clean*" and "*crust-coated*" sections within the Solomonic column.

In the spectrum of the "*crust-coated*" surface, apart from Ca, Al and Ti, the intensities of Mg and Sr are much larger than in the clean surface. New lines corresponding to Fe, Si, Mn, Pb and Ba are observed. *Table 2* lists the emission wavelengths corresponding to these elements assigned in the *standoff* LIBS spectrum. Also, the concentrations obtained by inductively coupled plasma optical emission spectrometry (*ICP-OES*) are quoted. After the crust was carefully removed from the surface, the powdered crust was dissolved through the use of a mixture of HNO_3/HCl/H_2O_2/HF/H_3BO_3. Finally, after microwave-assisted acid digestion of the silicate matrix, the total element composition was by *ICP-OES* under the follow operating conditions: radiofrequency power of 1500 W, nebulizer gas flow of 0.70 L· min^{-1}, plasma gas flow of 15 L·min^{-1} and auxiliary gas flow of 0.2 L·min^{-1}.

Table 2. Emission lines featured in the *standoff* LIBS spectrum acquired from the soiling that covers the Solomonic column together with the quantitative amount of the detected elements estimated by *ICP-OES*.

		ICP-OES	
Element	**Wavelength (nm)***	***Concentration (mg·g^{-1})***	***RSD (%)***
Si	390.6	142.0	2.0
Ca	393.4$^{(II)}$, 396.9$^{(II)}$, 422.7, 428.3, 428.9$^{(II)}$, 429.9, 430.3, 430.8, 431.9	135.0	2.0
Mg	382.9, 383.2, 383.8	50.0	3.0
Fe	386.0, 387.9, 388.9, 390.0, 404.6, 406.4, 407.2, 427.2, 432.6	46.0	2.0
Al	394.4, 396.1	33.0	2.0
Ti	394.8, 395.8, 398.2, 399.0, 399.9	2.5	1.0
Pb	402.1, 406.2	0.8	0.5
Ba	413.1	0.8	1.0
Mn	403.1, 403.3, 403.4	0.4	1.0
Sr	407.8$^{(II)}$, 421.5$^{(II)}$	0.2	2.0

*ionic lines have been highlighted with $^{(II)}$

As observed, high levels of elements such as Si and Ca, as well as intermediate concentrations of Mg, Fe and Al were detected. These findings may be justified basically with the transport of re-suspended dust or of atmospheric particulate matter from the sea coast located nearby. In the same vein, sources for trace elements such as Ba and Sr may be related to marine aerosols and/or to dust from the Sahara desert, a few hundred kilometers distant from Málaga [42]. Further, trace elements such as Ti, Pb and Mn were detected by *standoff* LIBS. Hence, anthropogenic factors are not discarded. Soot and metallic particles bearing Pb (major element) as well as Ti and Mn (trace elements) from exhaust emissions of gasoline and diesel engines, respectively, are also considered to trigger the pollution of materials.

In order to better assess the long-term adverse effects of contamination, its in-depth profile behavior on marble was examined. This study did not intend to be exhaustive in describing the environmental characteristics of the deposits. Instead, the capabilities of *standoff* LIBS for describing the behavioral patterns of the pollutants were investigated.

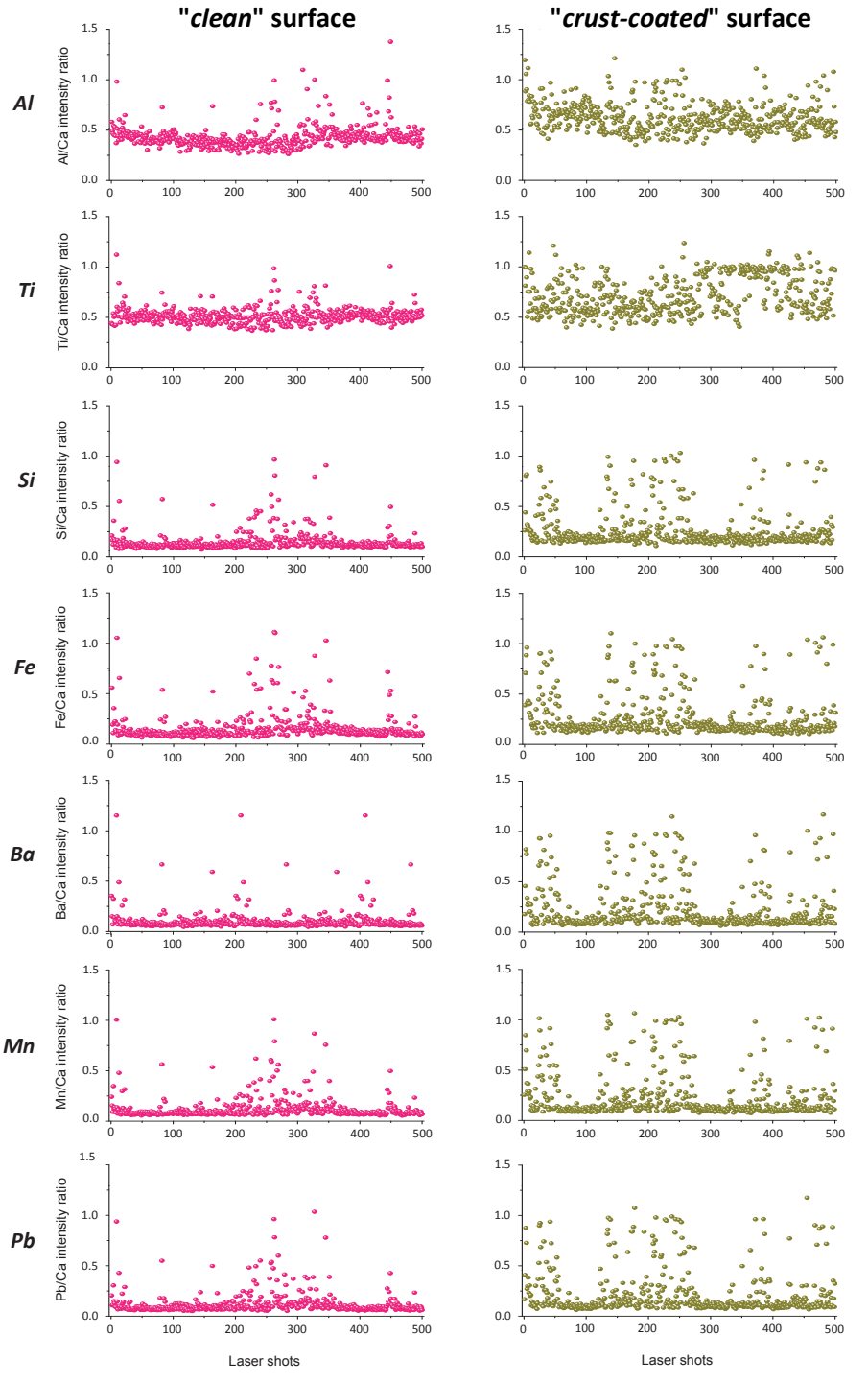

Fig. 9. Evolution profile of intensity of distinct detected elements (from top to bottom: Al, Ti, Si, Fe, Ba, Mn, Pb) to the Ca signal, from 500 laser pulses in depth on "*clean*" and "*crust-coated*" sections within the Solomonic column.

Intensity ratios of several detected elements to the Ca signal (431.9 nm) –the most abundant element in the samples– were considered. *Fig. 9* plots the progression profiles of the ratios for series of 500 *standoff* LIBS spectra gathered from the two surfaces of the Solomonic column. As observed, all datasets are fitted to well-defined profiles for the "*clean*" surface. However, while the Al/Ca and Ti/Ca ratios revealed values around 0.5, the remaining ratios showed values close to 0 due to the absence in the parent material of the elements involved. It should be noticed that increased ratio values are recorded in the first few shots of all profiles. These initial large ratio values derive from the inconspicuous pollutants present even on the "*clean*" surface. The excess ratios are also randomly distributed along the profiles and are due to the sampling of fresh positions. Such an observation is a consequence of the *wandering* of the beam on the surface caused by wind gusts [43].

In the "*crust-coated*" surface, the depth profiles follow a similar trend, also exhibiting the effects of wind gusts, especially noticeable in the profiles of Si, Fe, Ba, Mn and Pb. However, unlike the discrete variations observed in the clean section of the column, the Al/Ca and Ti/Ca values undergo substantial changes. Aluminum is present in both the mother rock and in the soiled column. This is clearly noticed since the average value of the Al/Ca ratio along the profile (0.63) is almost 70% larger than that observed in the "*clean*" surface (0.43). Similar holds true in the case of Ti, passing from 0.52 to 0.72.

Three colored marbles from one of the corners framing the main arc were also assessed. *Fig. 10* exhibits a *3D* scatter plot projected onto the subspace of the Al/Ca and Ti/Ca emission intensity ratios for series of 500 LIBS spectra gathered from each marble section. As reflected, the three datasets line up in three well-defined clouds.

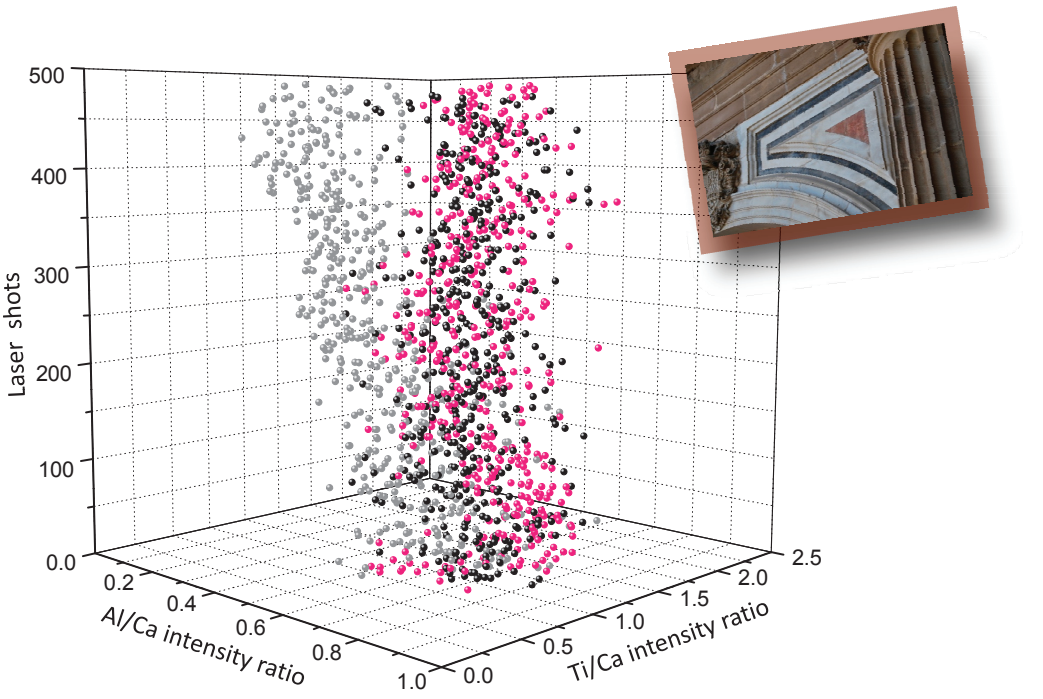

Fig. 10. *3D* scatter plot projected onto the subspace of the Al/Ca and Ti/Ca emission intensity ratios for series of 500 LIBS spectra gathered from each of the three types of marbles within the corners framing the main arc and distinguishable by different colorations (white, black and rose).

However, although there is similarity between these colored marbles, the values for ratios differ from those obtained in the case of the Solomonic column, thus reflecting that pollution is changing from one area to another. In addition, in the case of the white marble a substantial fall in the values of both ratios is detected after ca. 200 laser shots, *i.e.* when the laser drills deeper into the sample. This circumstance is due to the Al and Ti content relative to Ca content being significantly less, suggesting that those two elements may be relevant pollutants embedded in the surface of the marbles. Furthermore, this disparity between the trends indicates that the stability of the scabs on the surfaces of the black and rose marbles is higher than on the surface of the white marble. Circumstances fit perfectly with the more serious effect of sulphation process on calcitic marbles than on dolomitic ones [44].

4 Conclusions

This work presents, for the first time, the use of LIBS for an *in situ standoff* characterization of the materials forming an historical building and the nature of their cumulative soiling over time. These studies were conducted in the frame of a project aimed at verifying the feasibility of *standoff* LIBS analysis of unmovable and tangible architectural heritage material. Marbles, sandstone and metals of the ornamental assets in the architectural scenes of the front façade of the Cathedral of Málaga have been described. Further, the LIBS technique has been demonstrated to display high sensitivity to detect the presence of inconspicuous soiling and gross crusts on the surfaces of different ornamental elements. Nevertheless, the possibility to faithfully attribute pollution to either anthropogenic sources or to be influenced by the vicinity of a marine and coastal environment is still an issue. Procurement of all this site-specific information is of primary importance prior to planning restoration programs or taking decisions about whether a close-contact access plan is needed or not. Further studies are underway to confirm these results and uncover the sources and mechanisms of such a contamination. Several improvements on the sensing platform are under development. A long-range, high-definition imaging subsystem is being installed with the aim of contributing to monitoring the appearance of the treated surface in real-time, the degree of cleaning or any unwanted effect induced by laser irradiation. Results demonstrate that scaffolding of huge dimensions is not necessary for inspection surveys of architectural heritage in so far as there is a line of sight towards the target.

5 References

[1] O. Hahn, Analytical techniques in art, archaeology and conservation science, *Anal. Bioanal. Chem.* 402 (2012) 1411.

[2] B.H. Stuart, Analytical Techniques in Art Conservation, *John Wiley & Sons*, Chichester (2007).

[3] Non-destructive microanalysis of cultural heritage materials, K. Janssens and R. Van Grieken (Eds.), *Elsevier*, The Netherlands (2004).

[4] G. Vittiglio, S. Bichlmeier, P. Klinger, J. Heckel, W. Fuzhong, L. Vincze, K. Janssens, P. Engstromo, A. Rindby, K. Dietrich, D. Jembrih-Simburger, M. Schreiner, D. Denis, A. Lakdar, A. Lamotte, A compact μ-XRF spectrometer for (in situ) analyses of cultural heritage and forensic materials, *Nucl. Instrum. Methods Phys. Res. Sect. B* 213 (2004) 693–698.

[5] F.J. Fortes, J. Cuñat, L.M. Cabalín, J.J. Laserna, In situ analytical assessment and chemical imaging of historical buildings using a man-portable laser system, *Appl. Spectrosc.* 61 (2007) 558–564.

[6] I. Cacciari, D. Ciofini, M. Mascalchi, A. Mencaglia, S. Siano, Novel approach to the microscopic inspection during laser cleaning treatments of artworks, *Anal. Bioanal. Chem.* 402 (2012) 1585–1591.

[7] J.Cuñat, F.J. Fortes, L.M. Cabalín, F. Carrasco, M.D. Simón, J.J. Laserna, Man-portable laser-induced breakdown spectroscopy system for in situ characterization of karstic formations, *Appl. Spectrosc.* 62 (2008) 1250–1255.

[8] B. Sallé, P. Mauchien, S. Maurice, Laser-Induced Breakdown Spectroscopy in open-path configuration for the analysis of distant objects, *Spectrochim. Acta Part B* 62 (2007) 739–768.

[9] R. Gaudiuso, M. Dell'Aglio, O. De Pascale, G.S. Senesi, A. De Giacomo, Laser induced breakdown spectroscopy for elemental analysis in environmental, cultural heritage and space applications: A review of methods and results, *Sensors* 10 (2010) 7434–7468.

[10] C. Fotakis, D. Anglos, V. Zafiropulos, S. Georgiouand, V. Tornai, Lasers in the Preservation of Cultural Heritage. Principles and Applications, *Taylor and Francis*, Boca Raton (2007).

[11] F.J. Fortes, J.J. Laserna, The development of fieldable laser-induced breakdown spectrometer: No limits on the horizon, *Spectrochim. Acta Part B* 65 (2010) 975–990.

[12] A. Giakoumaki, K. Melessanaki, D. Anglos, Laser-induced breakdown spectroscopy (LIBS) in archaeological science-applications and prospects, *Anal. Bioanal. Chem.* 387 (2007) 749–760.

[13] S. Duchêne, V. Detalle, R. Bruder, J. B. Sirven, Chemometrics and laser induced breakdown spectroscopy (LIBS) analyses for identification of wall paintings pigments, *Curr. Anal Chem.* 6 (2010) 60–65.

[14] L. Caneve, A. Diamanti, F. Grimaldi, G. Palleschi, V. Spizzichino, F. Valentini, Analysis of fresco by laser induced breakdown spectroscopy, *Spectrochim. Acta Part B* 65 (2010) 702–706.

[15] E. Xenogiannopoulou, C. Andreouli, C. Stournaras, Application of LIBS technique for the compositional analysis of an attic black pottery, *J. Nano Res.* 8 (2009) 61–70.

[16] L. Angeli, C. Arias, G. Cristoforetti, C. Fabbri, S. Legnaioli V. Palleschi, G. Radi, A. Salvetti, E. Tognoni, Spectroscopic techniques applied to the study of Italian painted neolithic potteries, *Lasers Chem.* 2006 (2006) 1–8.

[17] P. Maravelaki-Kalaitzaki, Black crusts and patinas on Pentelic marble from the Parthenon and Erechtheum (Acropolis, Athens): Characterization and origin, *Anal. Chim. Acta* 532 (2005) 187–198.

[18] F.J. Fortes, M. Cortés, M.D. Simón, L.M. Cabalín, J.J. Laserna, Chronocultural sorting of archaeological bronze objects using laser-induced breakdown spectrometry, *Anal. Chim. Acta* 554 (2005) 136–143.

[19] M. Brai, G. Gennaro, T. Schillaci, L. Tranchina, Double pulse laser induced breakdown spectroscopy applied to natural and artificial materials from cultural heritages. A comparison with micro-X-ray fluorescence analysis, *Spectrochim. Acta Part B* 64 (2009) 1119–1127.

[20] F. Colao, R. Fantoni, P. Ortiz, M.A. Vazquez, J.M. Martín, R. Ortiz, N. Idris, Quarry identification of historical building materials by means of laser induced breakdown spectroscopy, X-ray fluorescence and chemometric analysis, *Spectrochim. Acta Part B* 65 (2010) 688–694.

[21] P. Maravelaki-Kalaitzaki, D. Anglos, V. Kilikoglou, V. Zafiropulos, Compositional characterization of encrustation on marble with laser induced breakdown spectroscopy, *Spectrochim. Acta Part B* 56 (2001) 887–903.

[22] M.P. Mateo, T. Ctvrtnckova, E. Fernández, J.A. Ramos, A. Yáñez, G. Nicolas, Laser cleaning of varnishes and contaminants on brass, *Appl. Surf. Sci.* 255 (2009) 5579–5583.

[23] F. Colao, R. Fantoni, V. Lazic, A. Morone, A. Santagata, A. Giardini, LIBS used as a diagnostic tool during the laser cleaning of ancient marble from Mediterranean areas, *Appl. Phys. A: Solids Surf.* 79 (2004) 213–219.

[24] F. Colao, R. Fantoni, V. Lazic, L. Caneve, A. Giardini, V. Spizzichino, LIBS as a diagnostic tool during the laser cleaning of copper based alloys: Experimental results, *J. Anal. At. Spectrom.* 19 (2004) 502–504.

[25] R. Grönlund, M. Lundqvist, S. Svanberg, Remote imaging laser-induced breakdown spectroscopy and laser-induced fluorescence spectroscopy using nanosecond pulses from a mobile lidar system, *Appl. Spectrosc.* 60 (2006) 853–859.

[26] A. Giakoumaki, I. Osticioli, D. Anglos, Spectroscopic analysis using a hybrid LIBS-Raman system, *Appl. Phys. A: Mater. Sci. Process.* 83 (2006) 537–541.

[27] R. Bruder, V. Detalle, C. Coupry, An example of the complementarity of laser-induced breakdown spectroscopy and Raman microscopy for wall painting pigments analysis, *J. Raman Spectrosc.* 38 (2007) 909–915.

[28] M. Hoehse, A. Paul, I. Gornushkin, U. Panne, Multivariate classification of pigments and inks using combined Raman spectroscopy and LIBS, *Anal. Bioanal. Chem.* 402 (2012) 1443–1450.

[29] M.F. Alberghina, R. Barraco, M. Brai, T. Schillaci, L. Tranchina, Double laser LIBS and micro-XRF spectroscopy applied to characterize materials coming from the Greek-Roman theater of Taormina, in Proc. of SPIE O3A: Optics for arts, architecture, and archaeology II, L. Pezzati and R. Salimbeni (Eds.), 7391 (2009) 739107.

[30] S. Guirado, F.J. Fortes, V. Lazic, J.J. Laserna, Chemical analysis of archeological materials in submarine environments using laser-induced breakdown spectroscopy. On-site trials in the Mediterranean Sea, *Spectrochim. Acta Part B* 74–75 (2012) 137–143.

[31] V. Raimondi, G. Cecchi, D. Lognoli, L. Palombi, R. Grönlund, A. Johansson, S. Svanberg, K. Barup, J. Hällström, The fluorescence LIDAR technique for the remote sensing of photoautotrophic biodeteriogens in the outdoor cultural heritage: A decade of in situ experiments, *Int. Biodeterior. Biodegrad.* 63 (2009) 823–835.

[32] P. Weibring, D. Lognoli, R. Chiari, G. Cecchi, H. Edner, T. Johansson, L. Pantani, S. Svanberg, D. Tirelli, M. Trambusti, Lidar remote sensing of the parma cathedral and baptistery, in Proc. of SPIE Laser techniques and systems in art conservation, R. Salimbeni (Ed.) 4402 (2001) 114–120.

[33] D. Lognoli, G. Lamenti, L. Pantani, D. Tirelli, P. Tiano, L. Tomaselli, Detection and characterization of biodeteriogens on stone cultural heritage by fluorescence LIDAR, *Appl. Opt.* 41 (2002) 1780–1787.

[34] G. Cecchi, L. Pantani, V. Raimondi, L. Tomaselli, G. Lamenti, P. Tiano, R. Chiari, Fluorescence LIDAR technique for the remote sensing of stone monuments, *J. Cult. Herit.* 1 (2000) 29–36.

[35] L. Palombi, D. Lognoli, V. Raimondi, G. Cecchi, J. Hällström, K. Barup, C. Conti, R. Grönlund, A. Johansson, S. Svanberg, Hyperspectral fluorescence lidar imaging at the Colosseum, Rome: Elucidating past conservation interventions, *Opt. Express* 16 (2008) 6794–6808.

[36] A. Llordén, Historia de la construcción de la catedral de Málaga, *Universidades y Academias*, España (1999).

[37] E. Galán, M.I. Carretero, E. Mayoral, A methodology for locating the original quarries used for constructing historical buildings: Application to Malaga Cathedral, Spain, *Eng. Geol.* 54 (1999) 287–298.

[38] M.P. Lapuente, B. Turi, P. Blanc, Marbles from Roman Hispania: Stable isotope and cathode luminescence characterization, *Appl. Geochem.* 15 (2000) 1469–1493.

[39] F. Origlia, E. Gliozzo, M. Meccheri, J.E. Spangenberg, I. Turbanti Memmi, E. Papi, Mineralogical, petrographic and geochemical characterisation of white and coloured Iberian marbles in the context of the provenancing of some artifacts from Thamusida (Kenitra, Morocco), *Eur. J. Mineral.* 23 (2011) 857–869.

[40] B.M. Weisman, C.L. Reedy (2002). Technical Studies on Renaissance Bronzes. Mater. *Res. Soc. Symp. Proc.* 712, II10.1 doi:10.1557/PROC-712-II10.1.

[41] J. Watt, J. Tidblad, V. Kucera, R. Hamilton, The effects of air pollution on cultural heritage, *Springer*, Berlin (2009).

[42] C. Guieu, M.D. Loyë-Pilot, C. Ridame, C. Thomas, Chemical characterization of the Saharan dust end-member: some biogeochemical implications for the western Mediterranean Sea, *J. Geophys. Res.* 107 (2002) 4258–4268.

[43] J.J. Laserna, R. Fernández Reyes, R. González, L. Tobaria, P. Lucena, Study on the effect of beam propagation through atmospheric turbulence on standoff nanosecond laser induced breakdown spectroscopy measurements, *Opt. Express* 17 (2009) 10265–10276.

[44] K. Malaga-Starzec, I. Panas, O. Lindqvist, Model study of initial adsorption of SO_2 on calcite and dolomite, *Appl. Surf. Sci.* 222 (2004) 82–88.

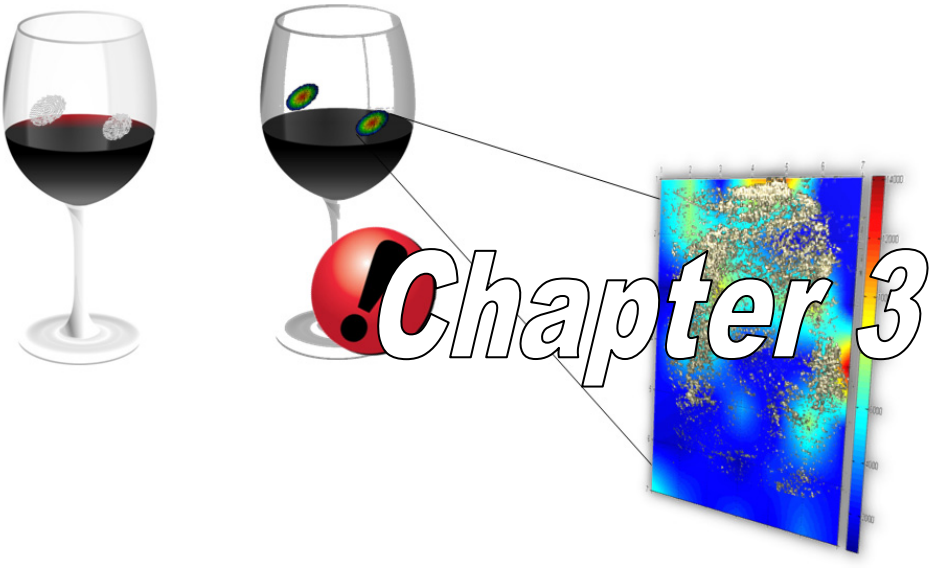

Chapter 3. Location and Detection of Explosive-Contaminated Human Fingerprints on Distant Targets Using *Standoff* Laser-Induced Breakdown Spectroscopy

Abstract

Detection of explosive-contaminated human fingerprints constitutes an analytical challenge of high significance in security issues and in forensic sciences. The use of a laser-induced breakdown spectroscopy (LIBS) sensor working at 31 m distance to the target, fitted with *2D* scanning capabilities and designed for capturing spectral information from laser-induced plasmas of fingerprints is presented. Distribution chemical maps based on Na and CN emissions are used to locate and detect chloratite, *DNT*, *TNT*, *RDX* and *PETN* residues that have been deposited on the surface of aluminum and glass substrates. An efectiveness of 100% on fingerprints detection, regardless the substrate scanned, is reached. Through LIBS responses, the detection capabilities of fingerprints on the basis of their prevalence over time, without participation of weather phenomena like rain or wind, are also discussed.

1 Introduction

The increased activity in the manufacture of improvised explosive devices (*IEDs*) places the scientific community's priority attention to the detection of explosives. The fact that most *IEDs* contain hidden explosives complicates its detection. However, the transfer of explosive particulate matter through fingerprints makes it possible to detect concealed explosives through surface sampling [1]. In fact, fingerprints are considered one of the main mechanisms of transferring explosive residues during handling and preparation of *IEDs*.

The process of transferring material to a surface via fingerprint is highly variable. Verkouteren sized *RDX* and *PETN* particles from *C4* and *Semtex-1A* and demonstrated that the mass may be concentrated in relatively few particles that may not be homogeneously distributed over the fingerprint area [2]. The same author characterized *C4* fingerprints and showed that the number of particles varies significantly from print to print and within a print [3]. When attempting to characterize explosive residues at low to trace levels, the most critical step in the analysis is to locate the material in the surface inspected. Once collected at the scene, the sample must be packaged so that its evidentiary value is not lost, whereas contamination during sample handling should be avoided. A survey of techniques used for sampling and concentration, and for detection/identification of explosive residues in laboratory or in field has been presented [4].

Detection/identification techniques were classified according to their application to: organic explosives using chromatographic techniques, Raman spectroscopy, ion mobility spectrometry and mass spectrometry; inorganic explosives using ion chromatography and capillary electrophoresis. For operational and safety reasons, detection methods capable for *standoff* (*ST*) operation are extremely valuable. *ST* detection techniques are divided into two broad categories, namely bulk detection techniques (X-rays, infrared, terahertz, microwaves, neutrons, gamma rays, magnetic resonance and magnetic fields) and trace

detection techniques (optical absorption, fluorescence, laser imaging detection and ranging (LIDAR), differential absorption LIDAR and differential reflectance LIDAR, array biosensors using captured antibodies, biomimetic sensors)[5].

The sensor providing at the same time the sensitivity, analysis speed and selectivity requirements for explosive detection is still to be developed. Most attempts are conditioned by the physical limits or the circumstances of a particular scenario. Canine-based detection is known to be the most reliable method for explosive detection. The complex training, their subjective response and the limited operational time of the animals are significant drawbacks of this approach. Singh published a review focused on the sensors developed in the last 5 years, ranging from electrochemical methods to immunosensors [6].

Recent advancements have been directed at improving the capabilities of detecting explosives in packages and baggage by X-ray diffraction [7] and using photons and neutrons as incident particles [8-10]. The presence of nitrogen bearing substances has been investigated by methods based on nuclear quadrupole resonance [11], ion mobility spectrometry [12], electrochemical sensors [13] and fluorescence [14, 15]. Special efforts have been made to explosive detection in the development of portable sensors [16] and *standoff* instruments [17, 18].

In 2005, the first test of a *standoff* LIBS (laser induced breakdown spectroscopy) sensor for detection of explosive residues at a distance of 30 m from the target was completed [19]. A fingerprint (10–100 ng) deposited on a car body was considered as a satisfactory indication of the detection power for *standoff* LIBS. Later, De Lucia *et al*. used double pulse LIBS to reduce the air entrained in the analytical plasma in an attempt to improve the discrimination between explosives and potential interferents [20]. Explosive residue detection is possible behind a barrier (polymethylmethacrylate and glass) placed between the target and the *standoff* LIBS sensor [21]. The estimated concentration of explosive on the

substrate was about 500 ng·mm^{-2}. Gottfried *et al.* reviewed the application of LIBS for detection of trace explosives [22].

To the best of our knowledge, the demonstration of the scanning capabilities and performance of a practical system for locating and recognizing explosives at fingerprint level has not been reported before. Analysis of explosive residues in human fingerprints using a laboratory scale instrument has been described using *optical catapulting*-LIBS (*OC-LIBS*) [23]. The main advantage of *OC-LIBS* over conventional LIBS is the absence of spectral contribution from the substrate, although the analysis is constrained by the need of optical access to the back of the sample.

In this work, LIBS is used to locate and detect the presence of explosive traces in human fingerprints deposited on targets placed at 31 m of the sensor. Fingerprint features and detection statistics are also reported. Two other important aspects of this application are addressed. Since the LIBS sensor interrogates only discrete areas across the surface, the analysis speed may become an issue when inspecting large objects. The detection capability is thus studied versus the spatial resolution and the number of data points acquired during the scan. Environmental factors that affect the persistence of the fingerprint response are also discussed.

2 Experimental section

The *ST-LIBS* sensor used to perform these investigations has been described in detail in the "Experimental" chapter of this Doctoral Thesis. Plasma light was spectrally resolved using a gated *Czerny–Turner* spectrometer (303 mm focal length, f/4) fitted with an intensified coupled-charged device detector. A 150 grooves·mm^{-1}, 500 nm blazed grating, providing a spectral window that ranges from 250 nm to 800 nm. The timing parameters used for spectral acquisition are: 600 ns as the delay time from the input of an external trigger (considered as zero time) to

the opening of the intensifier tube of the detector device, and 9 µs as the integration time.

Targets assayed

Samples analyzed in this work include the home-made explosive chloratite and the organic explosives 2,6-dinitrotoluene (*DNT*), 2,4,6-trinitrotolune (*TNT*), 1,3,5-trinitro-1,3,5,-triazine (*RDX*) and pentaerythritoltetranitrate (*PETN*), all of them used in powder form. The fingerprint area from the thumb of an individual impregnated with ink was 397 mm^2 as calculated using image analysis software by averaging 35 measurements. An optical microscope was used to estimate the thickness of fingerprints.

3 Results & discussion

3.1 Features of fingerprints containing explosive

A fingerprint is the visible, invisible or molded printing that is produced by the contact between of the ridges of the fingers on a surface. After handling, a substance may appear as a residue attached to the grooves of the fingers and therefore its presence will be reflected in the print. The impression of the fingerprint will depend on the history of the individual and the substrate where it is deposited. Therefore, characteristics such as size, thickness and mass vary in broad margins from sample to sample.

For guidance purposes, *Fig. 1* shows the impression of a thumb fingerprint on glass that has been previously impregnated with *DNT*. A micrograph (4× magnification) of a particular area of the fingerprint is also shown. The fingerprint is 15 mm wide and 24 mm in length. It should be noticed the large dispersion degree of the particles that constitute the residue.

To obtain an estimation of the superficial concentration of explosive from a fingerprint, several energetic materials including chloratite, *DNT*, *TNT* and *PETN*

have been studied. *Table 1* lists some relevant features of explosive fingerprints calculated from thirty replicates. As observed, regardless of the explosives assayed and subsequently their physical properties, all men fingerprints weights were found to be less than 1 mg. Hence, from these amounts, superficial concentrations of explosive fingerprints were calculated to be in the range from 130 to 240 $\mu g \cdot cm^{-2}$. Additionally, mean thickness of those fingerprints were measured to span from 20 to 60 µm. Large variabilities in both weight (*RSD* values over 35%) and thickness (*RSD* values up to 50%) clearly reflect heterogeneity of fingerprints. This circumstance may complicate LIBS analysis since a laser event may lack of spectral information about the fingerprint even having hit it.

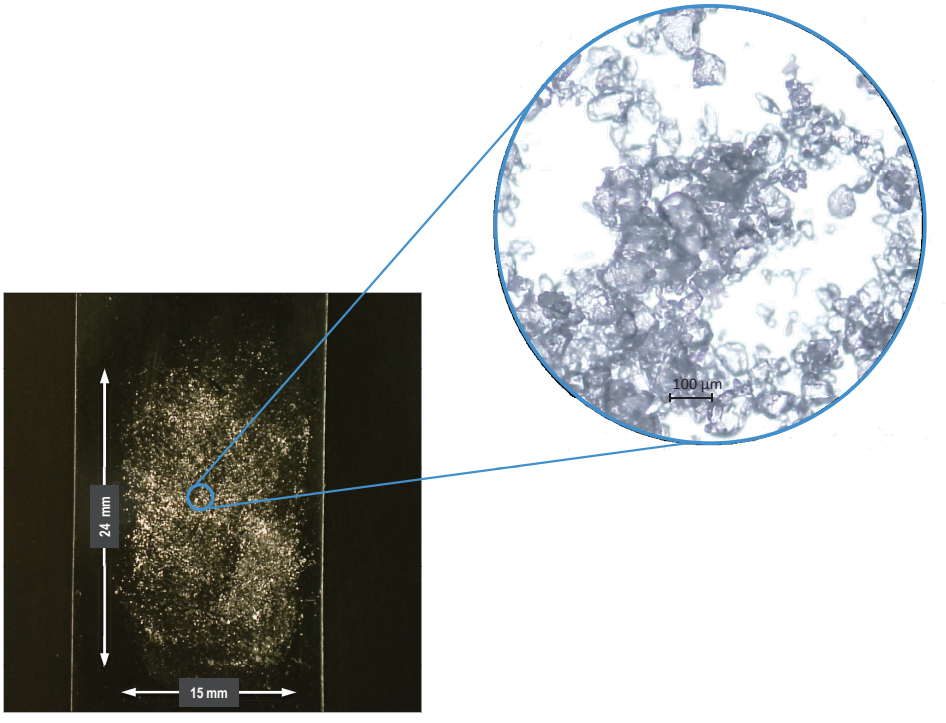

Fig. 1. Photograph of a *DNT* fingerprint left on the surface of a glass slide. Inset shows, in detail, an optical micrograph (4× magnification) of a discrete part within the fingerprint.

Table 1. Features of explosive fingerprints when deposited on a glass slide.

	Weight (µg)				*Thickness (µm)*		
Explosive	***Mean***	***± s***	***RSD (%)***	***Concentration (µg·cm^{-2})***	***Mean***	***± s***	***RSD (%)***
Chloratite	670	± 250	40	170	40	± 9	20
DNT	950	± 570	60	240	60	± 30	50
TNT	510	± 210	40	130	20	± 7	30
PETN	710	± 420	60	180	25	± 8	30

3.2 Spectral emission from fingerprints

An analysis of the relevant literature shows that few LIBS spectra of explosive fingerprints acquired in *standoff* mode of operation have been published so far [19, 22, 24, 25]. In order to advance in this topic, in a first step, spectral differences between three Al surfaces were studied: a clean surface, a surface previously handled and aged but free from explosive and a surface contaminated with a *DNT* fingerprint. *Fig. 2* shows *single-shot* LIBS spectra obtained at 31 m from those samples. As shown, the spectrum in *Fig. 2A* exhibits aluminum lines from the substrate as well as aluminum oxide bands. The spectrum obtained from the raw fingerprint shows lines of calcium and sodium in addition to aluminum lines (see *Fig. 2B*). Both calcium and sodium are typical components found in surfaces that have been manipulated by naked fingers. The spectrum from the *DNT* fingerprint shows CN bands and C_2 bands among other spectral features. The molecular bands provide evidence of the presence of an organic compound. The hydrogen line appears slightly increased in the spectrum with trace explosive when compared with the other two spectra. These data reveal the unique capabilities of LIBS. No other analytical technique has demonstrated so far this potential.

For all explosives studied, the limits of detection (*LOD*) for *standoff* LIBS analysis at 31 m were estimated from a fingerprint with a known concentration of explosive using the Equation (1):

$$LOD = 2\sqrt{2}(0.01)\frac{(RSDB)C}{S/B} \qquad \text{(Equation 1)}$$

where *RSDB* is the relative standard deviation of background, C is the explosive concentration in mass per unit area and *S/B* is the signal-to-background ratio.

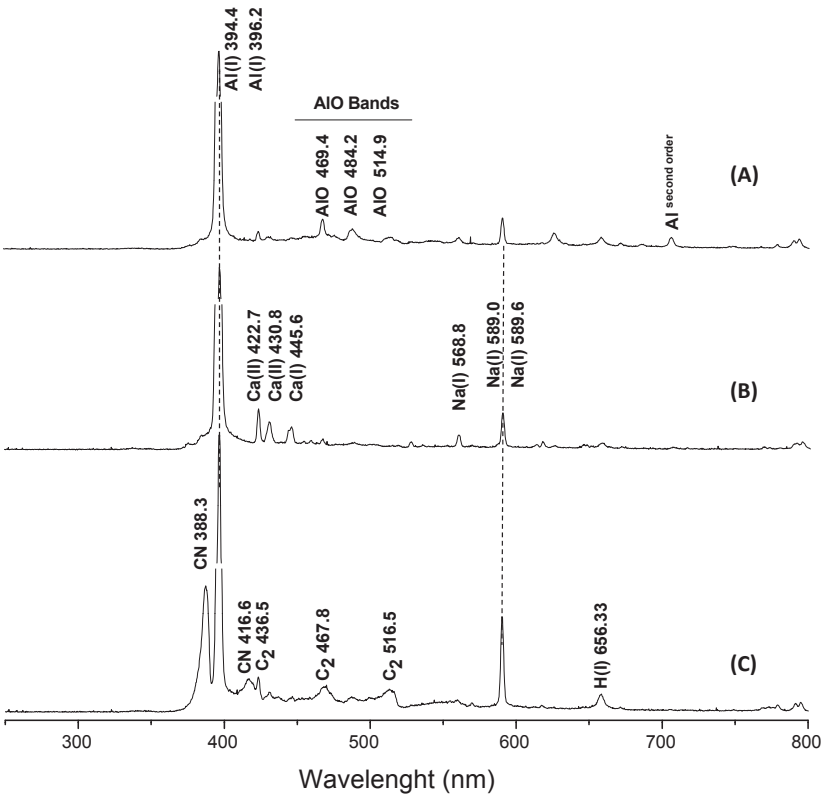

Fig. 2. *Standoff single-shot* LIBS spectra collected from the surface of clean aluminum substrate (A), contaminated with a raw fingerprint (B), and after the deposition of a *DNT* fingerprint (C). Operational conditions are detailed across the text.

The signal of CN at 388.3 nm was used to estimate the *LOD* of organic explosives. Thus, *LODs* on glass were 20 μg·cm^{-2} for *DNT*, 28 μg·cm^{-2} for *TNT* and 10 μg·cm^{-2} for *PETN*. The *LOD* for chloratite is not quoted since this material is a mixture of sodium chlorate, potassium chlorate, sulfur and sugar and the relative concentration of each component is not known in the particular formulation used here.

3.3 Fingerprint LIBS imaging

Fingerprint detection in an area suspected of containing an explosive involves the analysis of the sensor response when the laser beam scans across the surface inspected. *Fig. 3* shows the photograph of an aluminum plate (4 × 4 cm^2) containing the fingerprint of an individual that handled chloratite. This sample has been analyzed by the sensor using 4 laser shots, two of which are targeted on the fingerprint. LIBS spectra related to each laser event are also displayed. The increase in sodium intensity for shots hitting within the fingerprint is evident. Also, differences in sodium intensities due to variable surface concentration of explosive across the fingerprint are apparent. It is clear that the *shot-to-shot* variability observed in the figure also reflect the measurement uncertainty of LIBS for this type of measurements. We did not attempt to isolate the individual contribution of each source of uncertainty in these data. Additionally, at the bottom of the figure, the ratio of sodium-to-aluminum intensities reflects the differences between sampling points, indicating the absence of fingerprint (shots 1 and 4) as well as the varying concentration of sodium within the fingerprint (shots 2 and 3). Low sodium emissions detected in laser events hitting outside the fingerprint are due to mere environmental pollution.

As shown, the probability of missing a fingerprint increases as the scan resolution decreases (distance between shots of 20 mm or larger). The position and contour of the fingerprint is better defined as the number of shots in the scan

increases. However, an excess resolution may result in a decreased spectral intensity due to the unnecessary proximity between laser events. Therefore, the success in the detection of fingerprint residues is the right choice of resolution setting, which should be balanced with the total acquisition time as a function of the actual scene investigated. For the detection of chloratite on aluminum, a lateral resolution between 15 and 7.5 mm seems appropriate, and higher resolution reports no additional information.

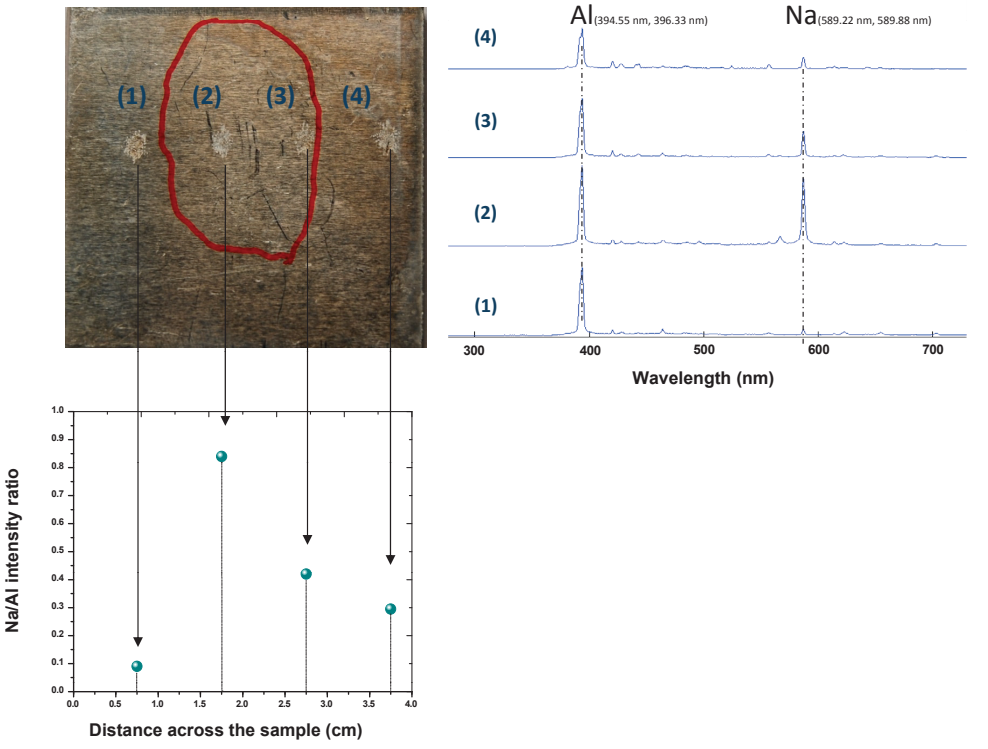

Fig. 3. Linear *standoff* scanning of a chloratite fingerprint left on the surface of an aluminum substrate. For easily inspection, the fingerprint emplacement has been highlighted in red. LIBS spectra linked to each one of the shots are displayed on the right. At the bottom, Na/Al intensity ratio calculated from those spectra are depicted.

To assess the response of the sensor when an organic explosive is interrogated, nitro aromatics, *RDX* and *PETN* in several substrates have been tested.

Similar chemical images were obtained from LIBS scanning for the fingerprint location of *DNT* and *TNT* deposited on aluminum and *TNT*, *RDX* and *PETN* deposited on glass. The scan features are: area 81 cm^2 for aluminum substrates with nine fingerprints and 30 cm^2 for glass substrates with four fingerprints. The lateral resolution was 7.5 mm. The CN signal at 388.3 nm is plotted as a function of the spatial coordinates. The results are discussed in the next section.

3.4 Fingerprint detection statistics

In order to evaluate the capabilities of the sensor to detect explosive fingerprints, the testing protocol described above was performed in the working scenario of our laboratory with the ultimate goal of deciding whether explosives are present or not in a particular sample.

Table 2 presents the statistics of detection. The test was blind for the sensor. Nine fingerprints contaminated with explosives were deposited on aluminum plates and three on glass substrates. For each scan with a specific lateral resolution, the table lists the number of shots per scan; the number of shots hitting within the boundaries of any fingerprint and the percent of fingerprints hit. Shots hitting within the boundaries of any fingerprint were confirmed by visual inspection. The table also reports the total number of true positive responses across the scanned surface. These true responses are derived from all fingerprints present in the inspected surface, although some fingerprints may be missed by the sensor.

A true positive response is established when the sensor provides an emission signal characteristic of an explosive larger than 3 times the background standard deviation. Sodium signals are used to locate chloratite, whereas CN emissions are used for *DNT*, *TNT*, *RDX* and *PETN*. The column named *PRR* stands for positive response rate, *i.e.*, the percent of positive responses of all shots that hit within a fingerprint. Finally, the percent of total fingerprints detected is also quoted.

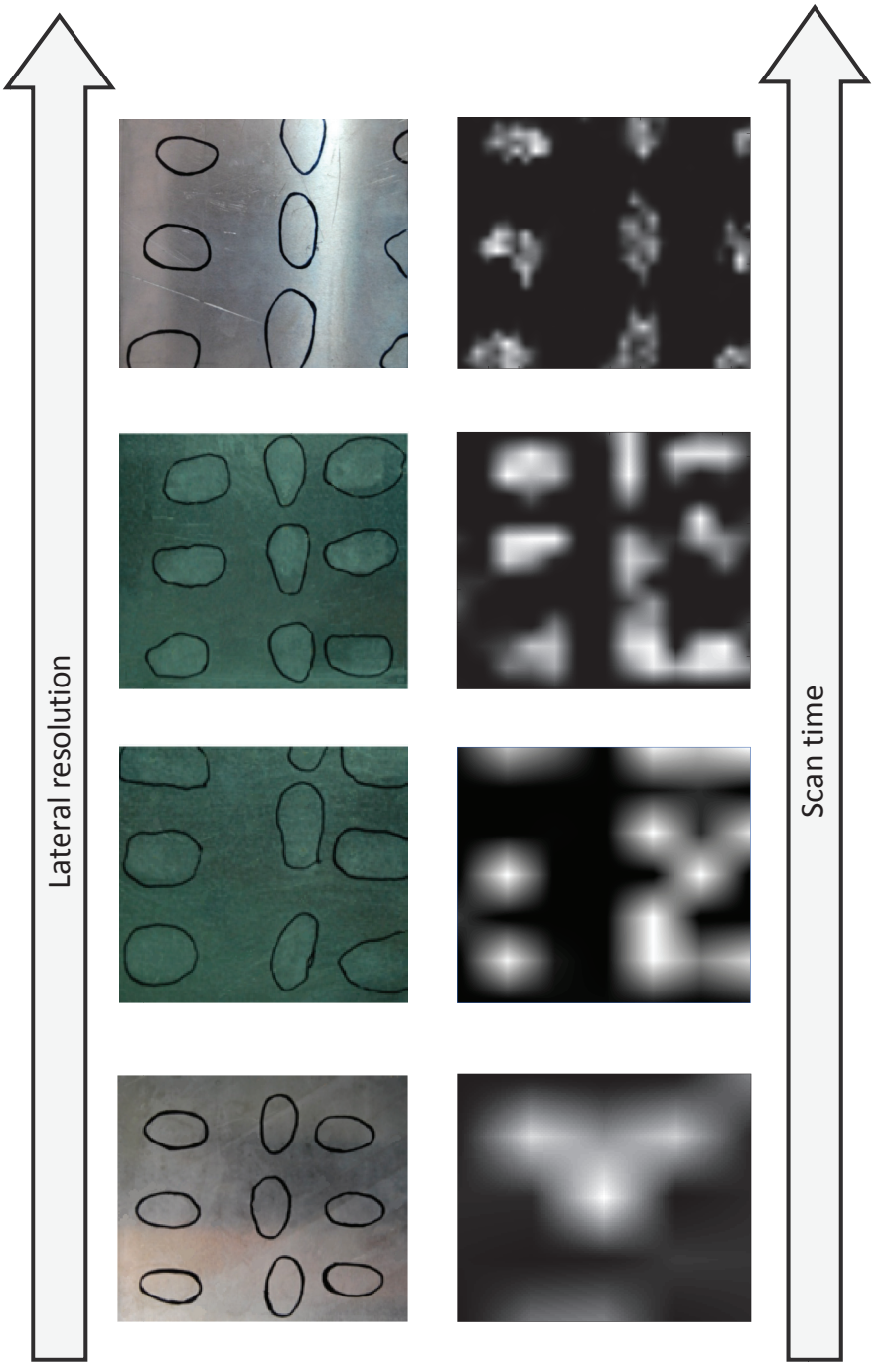

Fig. 4. Chemical maps constructed on the basis of the Na line at 589.2 nm for the distribution of chloratite fingerprints located on aluminum supports, when increasing both the lateral resolution and the scan time.

In the table, the first 6 rows refer to the detection of chloratite on aluminum. As expected, the number of shots hitting within fingerprint boundaries increases with the spatial resolution. However, a resolution of 15 mm is large enough to hit all fingerprints present in the plate. The true positive rate, which is related to the detection sensitivity, increases with the scan resolution, whereas the PRR values are better than 85% in all cases. This means that more than 85% of all shots hitting within fingerprints analyzed were positive hits. This large percent rate demonstrates the outstanding performance of the sensor for trace explosive detection at 31 m. Indeed, using the right lateral resolution, 100% of the chloratite fingerprints present in the plate were detected as quoted in the far right column of the *Table 2*.

The remaining rows involve the detection of organic explosives. As compared to chloratite, the *PRR* values are significantly smaller and decline as the number of true positives decrease. The inferior *PRR* performance for organics derives mainly from their poor detection limits. Indeed, the lower intensity of the CN emission band of *DNT*, *TNT*, *RDX* and *PETN* when compared to the Na emission line in chloratite contributes decisively to complicate the detection. The last column was included to account for the possibility that some fingerprint could not be detected in the scanning. As shown, except in three cases, the possibility of interrogating each fingerprint by several laser shots permits that 100% of the explosive fingerprints are detected. The ultimate performance of the sensor will depend on the particular combination of explosive/substrate as defined by the particle density at the surface deposited by the fingerprint. The density depends on the forces acting on the adhesion of the organic particles to the substrate considered.

Table 2. Statistics on *standoff* detection of human fingerprints located on surfaces of aluminum and glass substrates.

Explosive-Substrate	*Lateral resolution* [a]	*Number of scan shots*	*Shots Hitting within fingerprints*	*Fingerprint hit rate (%)*	*True positives* [b]	*PRR* [c] *(%)*	*Total explosive fingerprints detected (%)*
Chloratite-aluminum	20.0	25	3	33	3	100	33
	15.0	49	14	100	12	86	100
	10.0	100	20	100	19	95	100
	7.5	169	50	100	46	92	100
	5.0	361	73	100	73	100	100
	3.0	961	187	100	185	99	100
DNT-aluminum	10.0	100	27	100	14	52	100
DNT-aluminum	7.5	169	49	100	25	51	78
TNT-aluminum	7.5	169	50	100	34	68	89
TNT-Glass	7.5	63	20	100	12	60	100
RDX-glass	7.5	63	23	100	16	70	100
PETN-Glass	7.5	63	23	100	8	35	100

[a] Distance between consecutive shots in mm.
[b] Laser events providing an intensity level for the emission signal characteristic of an explosive larger than 3 times the background standard deviation. Dimensionless.
[c] Percent of positive responses from all those shots that have hit within a fingerprint.

3.5 Ageing of fingerprints

Two important factors to evaluate in the detection of explosive residues are the persistence of the LIBS response when fingerprints are aged on a surface and the effect that environmental contamination may have on the sensitivity of the detection. For this purpose, a series of aluminum plates (4 × 4 cm^2) were prepared on which we deposited one chloratite fingerprint per plate. Targets were stored into a partially closed facility for a maximum of 30 days, easy to access for environmental contamination, but without being exposed to the action of neither wind nor rain. During these days, temperature fluctuates between 20 and 26 degrees Celsius, whereas relative humidity ranged between 45% and 60%.

Then, for distinct number of exposition days, a blind detection test was performed on the concerned target. The test consisted of scanning the sample using 36 single laser shots, thereby covering the full plate, while measuring the LIBS signal of Na due to chloratite. Since the experiment was performed in an area near the sea coast, where a significant amount of NaCl and other salts can be deposited on the plates from sea water aerosols, a contribution to the Na response from atmospheric particles is also expected when measuring aged chloratite fingerprints. *Fig. 5* shows the LIBS response of the plates aged for 5, 12 and 27 days together with the response of a fresh plate (day 1). To understand the LIBS response of a fingerprint deposited on an aluminum plate exposed to contamination, the sodium-to-aluminum and the sodium-to-calcium intensity ratios were studied. The sodium-to-aluminum ratio corresponds to the respective responses of the residue particles (chloratite fingerprint and/or environmental dust) and the substrate. The sodium-to-calcium ratio is related solely to residue particles. While chloratite shows only Na signals, environmental dust exhibits both Na and Ca signals. To assist in the interpretation, the data in this figure have been sorted from the lowest to the highest value observed in the 36 shots data set acquired for each plate and plotted as a function of the number of laser shots.

In order to distinguish the source of Na detected in the plate, *i.e.*, the maximum contribution of environmental Na to the observed readings, a parallel experiment was performed. Thus, two replicate clean aluminum plates –exempted of explosive fingerprint and any environmental contamination– were allowed to age in the same environment for 90 days and used as control targets. Then, these controls were analyzed using the same protocol described for the samples containing the explosive residue and the results were added to *Fig. 5*. Ratio values exhibited by the control plates limit the ratio values where the source of sodium is due to environmental dust. Ratio values above this threshold level must be necessarily due to the explosive fingerprint.

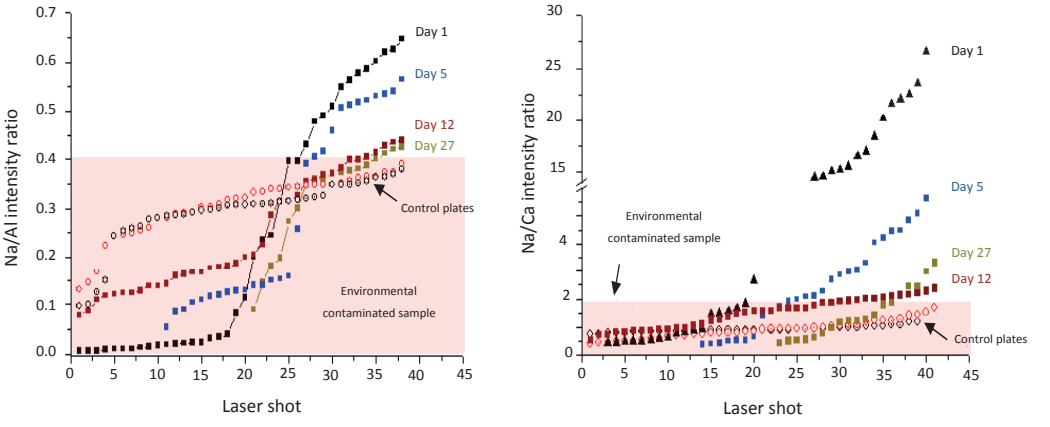

Fig. 5. Na/Al and Na/Ca intensity ratios from the interrogation of chloratite fingerprints left on the surface of aluminum supports and analyzed at successive days after their deposition. The ratios have been voluntarily sorted in increasing order of values for comparison purposes. Intensity ratios from two aluminum foils (control plates) exposed during 90 days to the mere environment are also shown.

In the fresh sample, large values of the Na/Al ratio indicate shots that hit within the chloratite fingerprint, whereas shots providing ratio readings close to zero correspond to the plate section that is free from the explosive residue. Aged samples provide distinct responses both in the low and in the high range of

intensity ratios. The lower values are increased as compared to the fresh sample as a result of the plate contamination with environmental Na. Contrarily to what one would expect the measurements in the high ratio readings are smaller than in the fresh sample. The contribution of the substrate to the observed emission decreases as the thickness of the residue increases since most of the laser energy is consumed in the excitation of the deposit. Under these circumstances, excitation of residue particles cannot be assisted by the ionization of the substrate as when the residue is a thin layer of deposited particles [26]. The general intensity observed now is decreased, thus resulting in a distortion of the ratio values with readings approaching the environmental contamination levels. Similar results were obtained when only lines from the residues were measured, *i.e.* Na/Ca ratios. In this case, as the samples are aged the Na/Ca intensity ratios decrease to reach the readings corresponding to the control plates. *Fig. 6* shows the fingerprint images obtained from the previous experiment. The images depict the distribution of sodium and have been plotted using the same scale of intensities.

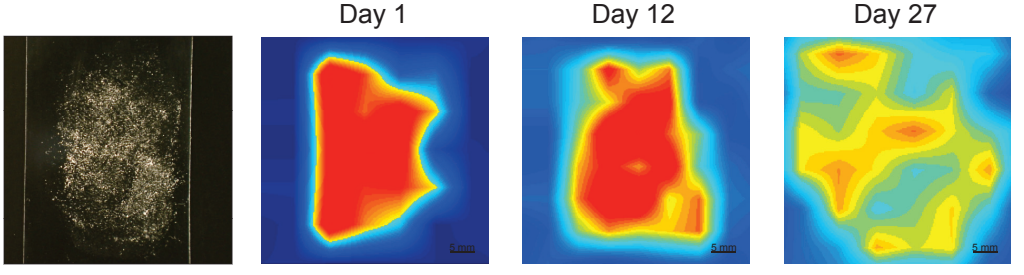

Fig. 6. Chemical images constructed on the basis of the Na line at 589.2 nm from the scanning, at different dates after the deposition, of aluminum surfaces containing chloratite fingerprints.

As shown, the image contrast is progressively lost as the samples are exposed to environmental dust. Moreover, the intensity of Na decreases with aging despite the fact that the Na content on the sample surface increases as dust is deposited on the plate. These results demonstrate that there is a limited persistence of the LIBS

response in weathered plates and suggest that analysis should be performed within a certain time period after the imprint of the fingerprints, irrespective of the explosive mass present on the surface inspected.

4 Conclusions

The possibility of scanning a surface by *standoff* LIBS provides a promising alternative in terms of trace explosive detection. Residues from human fingerprints of several explosives have been successfully detected at 31 m from the sensor. Parameters involved in establishing the sensor performance include the lateral resolution and the data acquisition time, which in turn depends on the laser pulse repetition rate. The sensor works better for the home-made explosive chloratite since the detection power of LIBS for inorganic compounds, in particular for the sodium line of chloratite, is superior to that for organic materials irrespective of the spectral line used. Nevertheless, for residue surface concentrations of hundreds of micrograms per cm^2, the scanning mode LIBS reaches 100% sensitivity in fingerprint recognition. This high success rate derives from the capability of the sensor to interrogate the same fingerprint by several laser events. This work also evaluated the effect that environmental pollution may have on the sensitivity detection of chloratite fingerprints deposited on aluminum plates. The deposition over time of particulate matter from surrounding may reduce the LIBS capability to detect a fingerprint that was left on a surface long ago. In our particular case, in absence of phenomena that may cause the remove of fingerprint (wind and rain) but close to a marine environment, a two-week time period was established for a positive detection of chloratite with a reasonable confidence level.

5 References

[1] D.J. Phares, J.K. Holt, G.T. Smedley, R.C. Flagan, Method for characterization of adhesion properties of trace explosives in fingerprints and fingerprint simulations, *J. Forensic Sci.* 45 (2000) 774–784.

[2] J.R. Verkouteren, Particle characteristics of trace high explosives: RDX and PETN, *J. Forensic Sci.* 52 (2007) 335–340.

[3] J.R. Verkouteren, J.L. Coleman, I. Cho, Automated mapping of explosives particles in composition C-4 fingerprints, *J. Forensic Sci.* 55 (2010) 334–340.

[4] E.B. Byal, Explosives Report, Detection and Characterization of Explosives and Explosive Residue: A Review, 1998–2001. 13th INTERPOL Forensic Science Symposium, Lyon, France, 16–19 October (2001).

[5] Committee on the review of existing and potential standoff explosive detection techniques National Research Council, Existing and Potential Standoff Explosives Detection Techniques, *The National Academic Press*, Washington D.C., U.S. (2004).

[6] S. Singh, Sensors—an effective approach for the detection of explosives, *J. Hazard. Mater.* 144 (2007) 15–28.

[7] C. Crespy, P. Duvauchelle, V. Kaftandjian, F. Soulez, P. Ponard, Energy dispersive X-ray diffraction to identify explosive substances: spectral analysis procedure optimization, *Nucl. Instrum. Methods Phys. Res. A* 623 (2010) 1050–1060.

[8] R.C. Runkle, T.A. White, E.A. Miller, J.A. Caggiano, B.A. Collins, Photon and neutron interrogation techniques for chemical explosives detection in air cargo: a critical review, *Nucl. Instrum. Methods Phys. Res.* A 623 (603) (2009) 510–528.

[9] S.K. Sharma, S. Jakhar, R. Shukla, A. Shyam, C.V.S. Rao, Explosive detection system using pulsed 14MeV neutron source, *Fusion Eng. Des.* 85 (2010) 1562–1564.

[10] A.L. Lehnert, K.J. Kearfott, Preliminary identification of flags for a novel algorithm-based approach for explosives detection using neutron interrogation for a simulated idealized cargo container scenario, *Nucl. Instrum. Methods Phys. Res. A* 638 (2011) 201–205.

[11] A. Gregorovic, Tomaz Apih, 2,4,6-TNT detection with 14N NQR: multipulse sequences and matched filter, *J. Magn. Reson. B* 198 (2009) 215–221.

[12] M. Tabrizchi, V. ILbeigi, Detection of explosives by positive corona discharge ion mobility spectrometry, *J. Hazard. Mater.* 176 (2010) 692–696.

[13] P.K. Sekhar, E.L. Brosha, R. Mukundan, K.L. Linker, C. Brusseau, F.H. Garzon, Trace detection and discrimination of explosives using electrochemical potentiometric gas sensors, *J. Hazard. Mater.* 190 (2011) 125–132.

[14] M.S. Meaney, V.L. McGuffin, Investigation of common fluorophores for the detection of nitrated explosives by fluorescence quenching, *Anal. Chim. Acta* 610 (2008) 57–67.

[15] T. Caron, M. Guillemot, P. Montméat, F. Veignal, F. Perraut, P. Prené, F. Serein-Spirau, Ultra trace detection of explosives in air: development of a portable fluorescent detector, *Talanta* 81 (2010) 543–548.

[16] L. Yu, Y. Huang, X. Jin, A.J. Mason, X. Zeng, Ionic liquid thin layer EQCM explosives sensor, *Sensor. Actuat. B-Chem.* 140 (2009) 363–370.

[17] K.W. Loschke, W.L. Dunn, Detection of chemical explosives using multiple photon signatures, *Appl. Radiat. Isot.* 68 (2010) 884–887.

[18] J. Moros, J.A. Lorenzo, P. Lucena, L.M. Tobaria, J.J. Laserna, Simultaneous Raman spectroscopy-laser-induced breakdown spectroscopy for instant standoff analysis of explosives using a mobile integrated sensor platform, *Anal. Chem.* 82 (2010) 1389–1400.

[19] C. López-Moreno, S. Palanco, J.J. Laserna, F. De Lucia Jr., A.W. Miziolek, J. Rose, R.A. Walters, A.I. Whitehouse, Test of a stand-off laser-induced breakdown spectroscopy sensor for the detection of explosive residues on solid surfaces, *J. Anal. At. Spectrom.* 21 (2006) 55–60.

[20] F.C. De Lucia, Jr., J.L. Gottfried, C.A. Munson, A.W. Miziolek, Double pulse laser-induced breakdown spectroscopy of explosives: initial study towards improved discrimination, *Spectrochim. Acta Part B* 62 (2007) 1399–1404.

[21] R. González, P. Lucena, L.M. Tobaria, J.J. Laserna, Standoff LIBS detection of explosive residues behind a barrier, *J. Anal. At. Spectrom.* 24 (2009) 1123–1126.

[22] J.L. Gottfried, F.C. De Lucia Jr., C.A. Munson, A.W. Miziolek, Laser-induced breakdown spectroscopy for detection of explosives residues: a review of recent advances challenges, and future prospects, *Anal. Bioanal. Chem.* 395 (2009) 283–300.

[23] M. Abdelhamid, F.J. Fortes, M.A. Harith, J.J. Laserna, Analysis of explosive residues in human fingerprints using optical catapulting-laser-induced breakdown spectroscopy, *J. Anal. At. Spectrom.* 26 (2011) 1445–1450.

[24] F.C. De Lucia Jr., J.L. Gottfried, C.A. Munson, A.W. Miziolek, Multivariate analysis of standoff laser-induced breakdown spectroscopy spectra for classification of explosive-containing residues, *Appl. Opt.* 47 (2008) G112–G121.

[25] J.L. Gottfried, F.C. De Lucia Jr., C.A. Munson, A.W. Miziolek, Strategies for residue explosives detection using laser-induced breakdown spectroscopy, *J. Anal. At. Spectrom.* 23 (2008) 205–216.

[26] A. Fernández-Bravo, P. Lucena, J.J. Laserna, Selective sampling and LIBS analysis of organic explosive residues on polymer surfaces, *Appl. Spectrosc.* 66 (2012) 1197–1203.

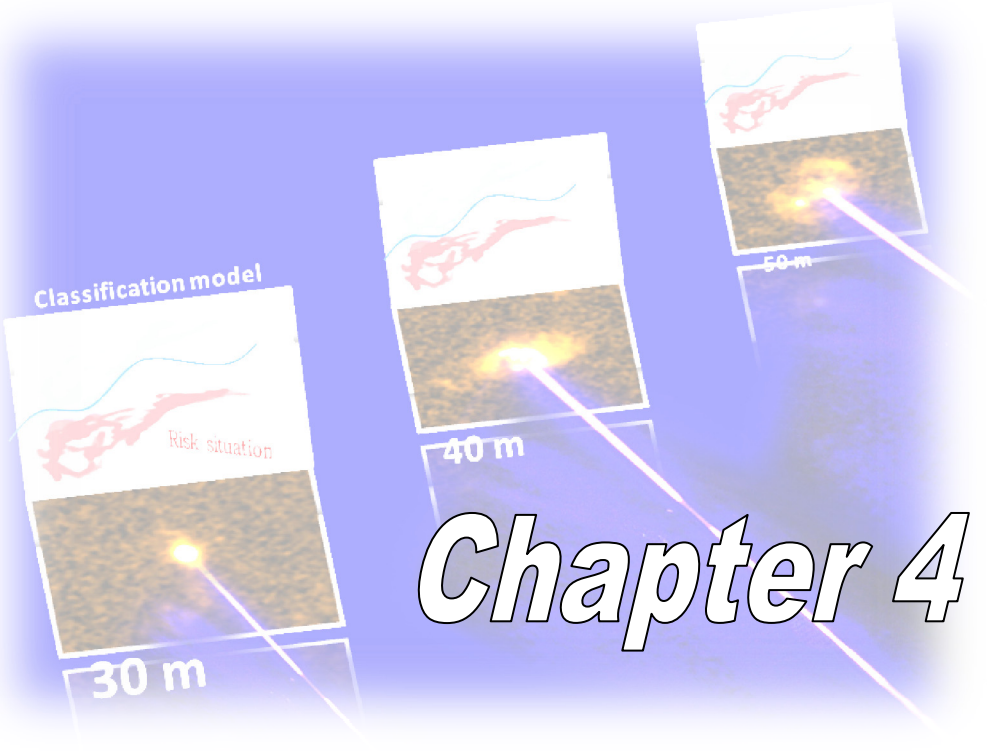

Chapter 4

Chapter 4. Range-Adaptive *Standoff* Recognition of Explosive Fingerprints on Solid Surfaces Using a Supervised Learning Method and Laser-Induced Breakdown Spectroscopy

Abstract

The distance between the sensor and the target is a particularly critical factor for an issue as crucial as explosive residues recognition when a laser-assisted spectroscopic technique operates in a *standoff* configuration. Particularly for laser ablation, variations in operational range influence the induced plasmas as well as the sensitivity of their ensuing optical emissions, thereby confining the attributes used in sorting methods. Though efficient classification models based on optical emissions gathered under specific conditions have been developed, their successful performance on any variable information is limited. Hence, to test new information by a designed model, data must be acquired under operational conditions totally matching those used during modeling. Otherwise, the new expected scenario needs to be previously modeled. To facing both this restriction and this time-consuming mission, a novel strategy is proposed in this work. On the basis of machine learning methods, the strategy stems from a decision boundary function designed for a defined set of experimental conditions. Next, particular semi-supervised models to the envisaged conditions are obtained adaptively on the basis of changes in laser fluence and light emission with variation of the sensor-to-target distance. Hence, the strategy requires only a little prior information, therefore ruling out the tedious and time consuming process of modeling all the expected distant scenes. Residues of ordinary materials (olive oil, fuel oil, motor oils, gasoline, car wax and hand cream) hardly cause confusion in alerting the presence of an explosive (*DNT*, *TNT*, *RDX* or *PETN*) when tested within a range from 30 m to 50 m with varying laser irradiance between 8.2 $GW \cdot cm^{-2}$ and 1.3 $GW \cdot cm^{-2}$. With error rates of around 5%, the experimental assessments confirm that this semi-supervised model suitably addresses the recognition of organic residues on aluminum surfaces under different operational conditions.

1 Introduction

Over the past few years there have been many efforts to identify trace explosives on the surface of distant objects using spectroscopic techniques [1]. Whether through emission spectroscopy [2] Raman spectroscopy [3], photoacoustic spectroscopy [4], photothermal deflection spectroscopy [5], or infrared photothermal imaging [6], the answer to that challenge is being addressed due to its immediate relevance in countering terrorist threats.

Nonetheless, to these extreme scenarios, although the operation at *standoff* detection regime offers safety advantages over close-contact scheme, complexity on the using of that design is more than evident. In *standoff* instruments, beyond the technical hurdles for a flexible working, the distance between the interrogated target and the sensing platform plays a large role in determining the signal and noise of the gathered information. In laser-induced breakdown spectroscopy (LIBS) based sensors, added to the decrease in emission signal with the range squared, the irradiance also declines with the square of the distance, thus resulting in a fourth-power dependence of the LIBS intensity with the range [7]. To put this in context, consider the exemplary scheme presented in *Fig. 1*. The multifactorial nature of the emission response in *standoff* regime is illustrated as a big cube. The particular response of a target is embodied by each one of the subcubes that are composing the complex network. Any variation, simultaneous or not, in the irradiance or in the distance of the interrogated target involves a series of changes in the emission signal. As the increase in the irradiance should result in a more sensitive response, whereas the parallel decrease of the analysis distance would lead to enhance this positive impact. In contrast, when the irradiance level is extremely low or distance is particularly large, useless spectral information can be anticipated. In addition, the transient environmental conditions can also affect the emission signal even when operational conditions have remained identical. In

conclusion, the emission response occurs from a specific substance governed by explicit conditions. Hence, as it is predictable, any change on the analysis conditions accounts a significant constraint for those classification techniques whose background focuses on a spectral features-based labeling.

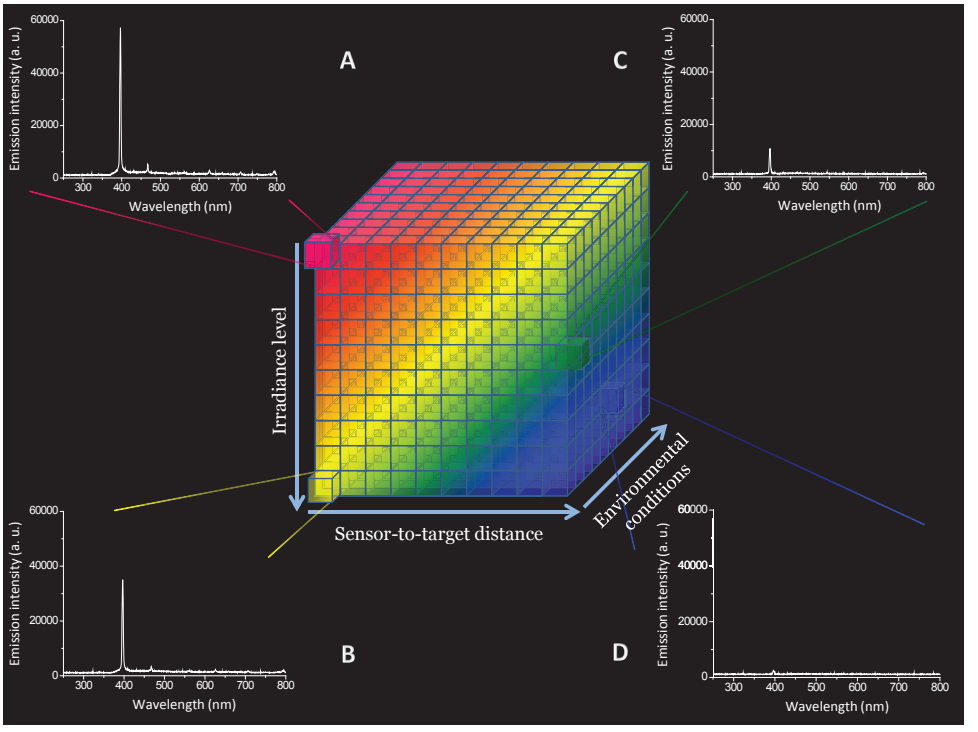

Fig. 1. Exemplary scheme of the multifactorial nature of the optical emission response for the laser-assisted ablation at *standoff* regime.

A number of chemometric methods including linear correlation [8], principal components analysis (*PCA*) [9,10], partial least squares discriminant analysis (*PLS-DA*) [11, 12], the method of the normalized coordinates (*MNC*) [13] and soft independent modeling of class analogy (*SIMCA*) [8] have proved to handle residues sorting at a *standoff* distance of tens of meters. Nonetheless, despite this widespread research, effectiveness of all these models in an unknown scenario lies

in conducting the recognition process under operational conditions totally matching those used during modeling. Otherwise, the new expected scenario needs to be previously modeled, since variations on conditions cause a departure of the emission intensities for the interrogated target beyond the upper and lower boundary levels of the modeled cases. Consequently, predictions almost certainly result in mislabeling of the unknown target. To tackle this constraint, a comprehensive strategy to recognize residues, whatever the situations, is required for ruggedizing the technology.

In this manuscript we present for the first time a residues recognition algorithm based on the transient response of a *standoff* LIBS sensor. Using supervised learning techniques [14-16] on spectral features from *standoff* emission responses, a general framework for sorting distant residues with an adaptive model to varying conditions is offered. Nonetheless, instead to entail a learning of all expected instances, only a moderate number of input variables are needed. Two frameworks are considered to tackle with the design, whose fundamentals are centered on the fourth power dependence on the range of the emission signal [7]. The first approach, called backpropagation-based, seeks to match emissions collected at the interrogation distance to a built and trained model at a fixed distance. The second scheme, named adaptive-based, consists on a scoring propagation to fit the model designed at a fixed distance to the sensing distance concerned.

The first approach simplifies the classification model but does not directly operate with real values of the spectral information. Also, since signals from increasingly distant targets experience greater random fluctuations, such uncertainties within the emissions are concurrently propagated towards the model. In contrast, in adaptive supervised fixed scoring, although complicates the model and requires its computation to harmonize with emissions levels, no additional distortions arise. Hence, to mitigate as much as possible the uncertainties on the

final decisions, this last design was decided for addressing the present investigations.

Operation for variation in distance from 30 m to 50 m –irradiance changing from 8.2 $GW \cdot cm^{-2}$ to 1.3 $GW \cdot cm^{-2}$– was modeled. The effects of the changing weather conditions were neglected due to its complex control in every dynamic environment. Thus, for the current outline, a comprehensive analysis of how results on residue classification vary with regards to the lasing conditions, but from LIBS data acquired under similar seasonal parameters, is provided.

2 Experimental section

The *ST-LIBS* sensor used to perform these investigations has been described in detail in the "Experimental" chapter of this Doctoral Thesis. Plasma light was spectrally resolved using a 4-channels miniature spectrograph (75 mm focal length), fitted each with a CCD image sensor. An effective spectral range spanning from 330 nm to 950 nm is set. The timing parameters used for optical signal acquisition are enabled by default at: 1.28 µs of delay time from the external trigger input (considered 0 time) supplied by the Q-switch output signal of the laser, and 1.1 ms of integration time (gate width).

Targets assayed

For the current investigation, a closed-list of organic materials was decided. Four energetic compounds, namely, 2,6-dinitrotoluene (*DNT*), 2,4,6-trinitrotoluene (*TNT*), cyclotrimethylenetrinitramine (*RDX*) and pentaerythritoltetranitrate (*PETN*) – these last three supplied by Laboratorio Químico Central de Armamento, Ministry of Defense, Madrid, Spain– were considered. In addition, a total of 7 widespread products whose traces are likely to be confused with explosives, were selected. The list comprised some goods as olive oil, fuel oil, motor oil from two brands, gasoline,

car wax, and hand cream, which can remain in the hands after an everyday action and to be transferred to a manipulated item. The similarity of the emission responses for all these products –explosives and confunsants– is remarkable, all of them feature the same particular optical signals –CN, C_2, N, H, and O– to some degree.

Experimental targets were prepared by successively leaving fingerprints of products on the surface of aluminum foils (4 × 4 × 0.2 cm^3), slightly, but intentionally, scratched to facilitate the adherence of solid residues. Despite the heterogeneity on the distribution of residues in the fingerprints, each LIBS analysis (*single-shot*) was performed on a refreshed area within the concerned target. Thereby, a precise quantification of the residues is not expected. Furthermore, the accurate identification of each residue has not been rigorously sought, but rather a general labeling of the case according to hazardousness of the residues.

Semi-supervised adaptive model for recognition of distant traces

For the development of the approach, *standoff* LIBS spectra (a total amount of 1100) were gathered from the eleven residues on aluminum at a fixed distance of 30 m. This information was split into two equal datasets –*training* and *testing*. Fifty spectra from each residue were used to design and train the original model, whereas the remaining fifty spectra were used to test the algorithm. By using these datasets, the conventional approach of machine learning [14-16] was applied in a stage of knowledge generalization. Thus, particular spectral features within the labeled data from the *training* set were considered to construct a subdimensional space where an original classification model of residues according to their hazardousness was designed. Then, the performance –*accuracy*, *sensitivity* and *error rates*– of such model at this fixed distance was judged by using information from the *testing* set.

Once constructed and fitted, this original algorithm is real-time adapted to any new condition. In order to introduce the framework of this approach, consider the graphical example presented in *Fig. 2*. The above cited subdimensional space corresponds to a *3D* scatter plot that is built from spectral features, either simple emission intensities or intensity ratios. At fixed conditions, an original boundary surface between residue classes is embodied in this space on the basis of the emitting behavior of explosive traces and innocuous residues. The parametric representation of this hypersurface is described by the following general expression:

$$f(x,y,z) = \left(x^a + y^b + z^c + D\right)_{r_0,\, I_0} \qquad \text{(Equation 1)}$$

Taking as starting point this original classifier (r_0 = 30 m, I_0 = 8.2·GW cm^{-2}), the identification of a target under the new conditions ($r_0+\Delta r$, $I_0-\Delta I$), is addressed with a particular semi-supervised auto-adapted boundary surface. The transferring of the classification model is centered on the adapting the original coefficients of the hyperplane to the novel situation using the following equation:

$$\left(x^a + y^b + z^c + D\right)_{(r_0+\Delta r,\, I_0-\Delta I)} = \frac{\left(x^a + y^b + z^c + D\right)_{r_0, I_0}}{\left(\frac{r_0 + \Delta r}{r_0}\right)^n} \qquad \text{(Equation 2)}$$

Thus, as shown in *Fig. 2*, the adaptation of the boundary surface runs in parallel with the modification of the circumstances. At each increased distance, whether or not involving a change on the irradiating fluence, a decrease in the LIBS signal occurs. However, there is a limit to handle all the situations and the transferring of the adaptive algorithm stops when one of the dimensions of the subspace is missed. In short, a global correction of the original hypersurface's representation on the basis of the attenuation of the irradiance with increasing

operational range and the ensuing decreasing of light emission with the inverse of the distance [6]. Accordingly, the range of values that *n* may adopt covers from 2 to 4. An *n* value of 2 implies that the laser fluence is preserved and so is the achievable spot area of the laser beam at the distant target. Thus, only the attenuation of the light emission influences to the correction. On the contrary, an *n* value of 4 denotes the contribution of the two phenomena to the modification of the coefficients. In the present experiments, the total distance range evaluated changed from 30 m to 50 m. The spot diameter of the laser beam varies from 1.5 mm up to 3.8 mm along this range. Under these circumstances an inverse square attenuation of the irradiance with increasing operational range during the laser beam travel from the sensor towards the target occurs. Consequently, *n* adopts the value of 4.

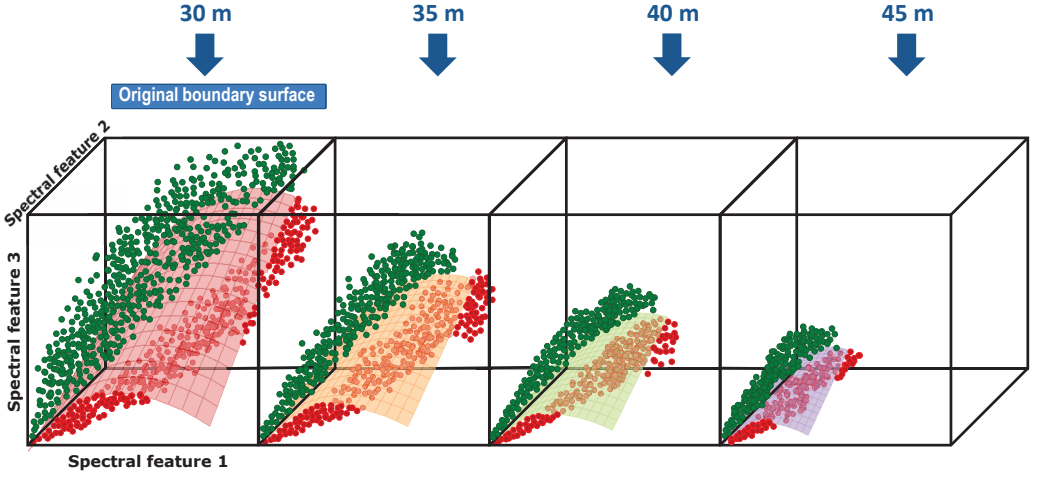

Fig. 2. Schematic illustration of the adaptation process for a boundary surface intended to identify objects on the basis of changing conditions to the LIBS analysis.

Despite that a large variety of classifiers were tested for comparing their classification capabilities, only the most significant results are presented in this manuscript. Classifiers parameter tuning and classification processes were conducted by *PRtools4* –a Matlab (The Mathworks Inc., South Natick, MA) toolbox for pattern recognition– [17]. Since the aim of the present work is to prove the

classifiers ability to adapt and remain effective when the operational range changes, readers are encouraged to explore additional references for deeper details of basis on learning classifiers [18, 19].

3 Results & discussion

3.1 LIBS Spectra of distant targets

Fig. 3 illustrates *standoff* LIBS spectra at 30 m corresponding to unquantified residues of *RDX* and fuel oil when encountered on the surface of an aluminum foil. The emission spectrum from the "*clean*" surface, that is, free from any willful residue, is also shown. As observed, intense emissions of aluminum –394 nm and 396 nm, and the corresponding second orders of these lines– are featured within the signal due to the participation of the substrate when the laser pulse dislodges the residue particles from the surface. Small spectral features due to the organic compounds are also revealed. This circumstance highlights the proportionality between residue and substrate composing the experimental target, that is, an extremely thin layer of organic particles over a vast metallic surface.

As far as the spectra from organic traces refer, the emission band related to the CN fragment (coming from the recombination of C and N inside the plasma plume) is evidenced at 388 nm. Unlike the CN signal, C_2 emission bands –observed at 471 nm, 516 nm and 563 nm and due to doubly bonded carbon dimers directly released from the parent organic- are broadly masked by dominant signals associated to aluminum oxide (AlO). Emission atomic lines of hydrogen at 656 nm, N (triplet at 742 nm, 744 nm and 746 nm), and O (unresolved triplet at 777) are also easily recognized. Nonetheless, these emissions are nor distinctive nor exclusive to the presence of organic traces. Their emergence within the spectrum from the "*clean*" substrate evidences the effect of the surrounding atmosphere, namely air and ambient humidity. As these spectral features are also exhibited by most organic

residues, the difficulties for detection and classification of the finding grow considerably.

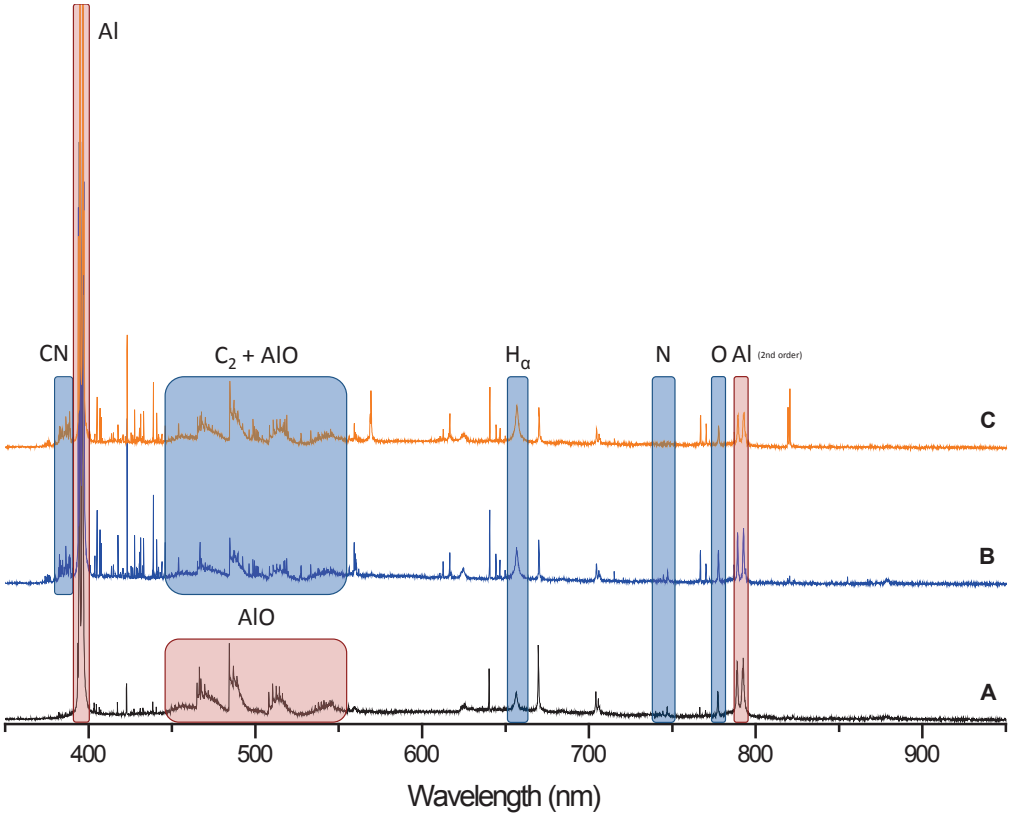

Fig. 3. *Standoff single-shot* LIBS spectrum of an aluminum clean support (***A***) compared with the spectra from the analysis of residues not further quantified of *RDX* (***B***) as well as fuel oil (***C***) when located on the surface of such support.

3.2 Emission patterns for residue classes

In order to elucidate the most functional spectral features to identify organic residue classes, emissions of CN, H, N, and O were considered. Carbon was not used as the C(I) 247 nm line falls out of the effective spectral window (350–950 nm) of our sensor, whereas emissions of C_2 fragments are interfered by the overlapping emissions from AlO [20].

Subsequently, usable intensities were graphed in multidimensional scatter plots, thus seeking the representation that maximizes differences between residue classes while minimizing differences between traces of identical nature. Although using close-contact emission data, this strategy has been described in detail in a previous work [14], so only the key basics are mentioned here.

Table 1 lists the values of the *RDR* (residual discriminatory region) estimator, which quantifies the differentiation power to distant residues (30 m) within *n*-dimensional scatter plots. Whether calculated on the basis of overlapping areas (*2D* graphs) or volumes (*3D* graph), the parameter keeps the same meaning: the lowest the *RDR* value, the highest the usefulness of the scatter plot. To consolidate these results, *Fig. 4* shows some of these scatter plots. As observed, mislabeling of residues is anticipated in the bidimensional graphs combining both molecular and atomic information where the two datasets are fully intermingled. In contrast a proper differentiation between classes is drawn in the *2D* plots that combine H_α intensity with that of atomic lines of N or O (graphs *#4* & *#5* in *Table 1*). Nonetheless, as shown, connection between emissions deriving exclusively from a common origin source, such as N and O from air, are useless for classification purposes. This circumstance highlights the critical role played by the interaction of the generated plasma with components of the surrounding atmosphere including the ambient humidity.

From those useful *2D* scatter plots, a general trend on the emissions patterns can be drawn: explosive residues show larger N and O intensities than harmless traces for the same level of H_α signal. This specific trend does not result from a simple cause. Indeed, it is the result of the sum of different contributions, namely, the molecular composition of the residues and the particular impact of the ensuing plasma plume with the surrounding atmosphere.

As for *RDR* values from *3D* plots listed in *Table 1*, only an efficient performance to classification has been reflected when CN, H_α, and O emissions are

jointly plotted (plot *#8*). When these three variables are put together into play, *RDR* value (0.19) is almost halved as compared to that reported by the *2D* plot (*#5*) that exclusively involves the concerned atomic signals (*RDR* = 0.30). This improvement to differentiate between residues is argued by a more complete description of the investigated target. When CN signal is added, information on the fragmentation pattern of the residues is included.

Table 1. Values for the *RDR* parameter computed from scattering of emission intensities extracted from LIBS spectra of tested residues within the different subspaces projected by the involved spectral features.

Scatter plot #	***Scatter plot features (wavelength, nm)***	***Residual Discriminatory Region (RDR)***
1	CN (388) *vs* H_α (656)	1.65
2	CN (388) *vs* N (746)	1.72
3	CN (388) *vs* O (777)	1.65
4	H_α (656) *vs* N (746)	1.19
5	H_α (656) *vs* O (777)	0.30
6	N (746) *vs* O (777)	1.44
7	CN (388) *vs* H_α (656) *vs* N (746)	0.77
8	CN (388) *vs* H_α (656) *vs* O (777)	0.19
9	CN (388) *vs* N (746) *vs* O (777)	0.87

These results evidence the complete correspondence between *RDR* values and both size and shape of data clouds. In addition, the complete agreement between these findings and those obtained for close-contact LIBS [14] confers a greater robustness to the considered approach.

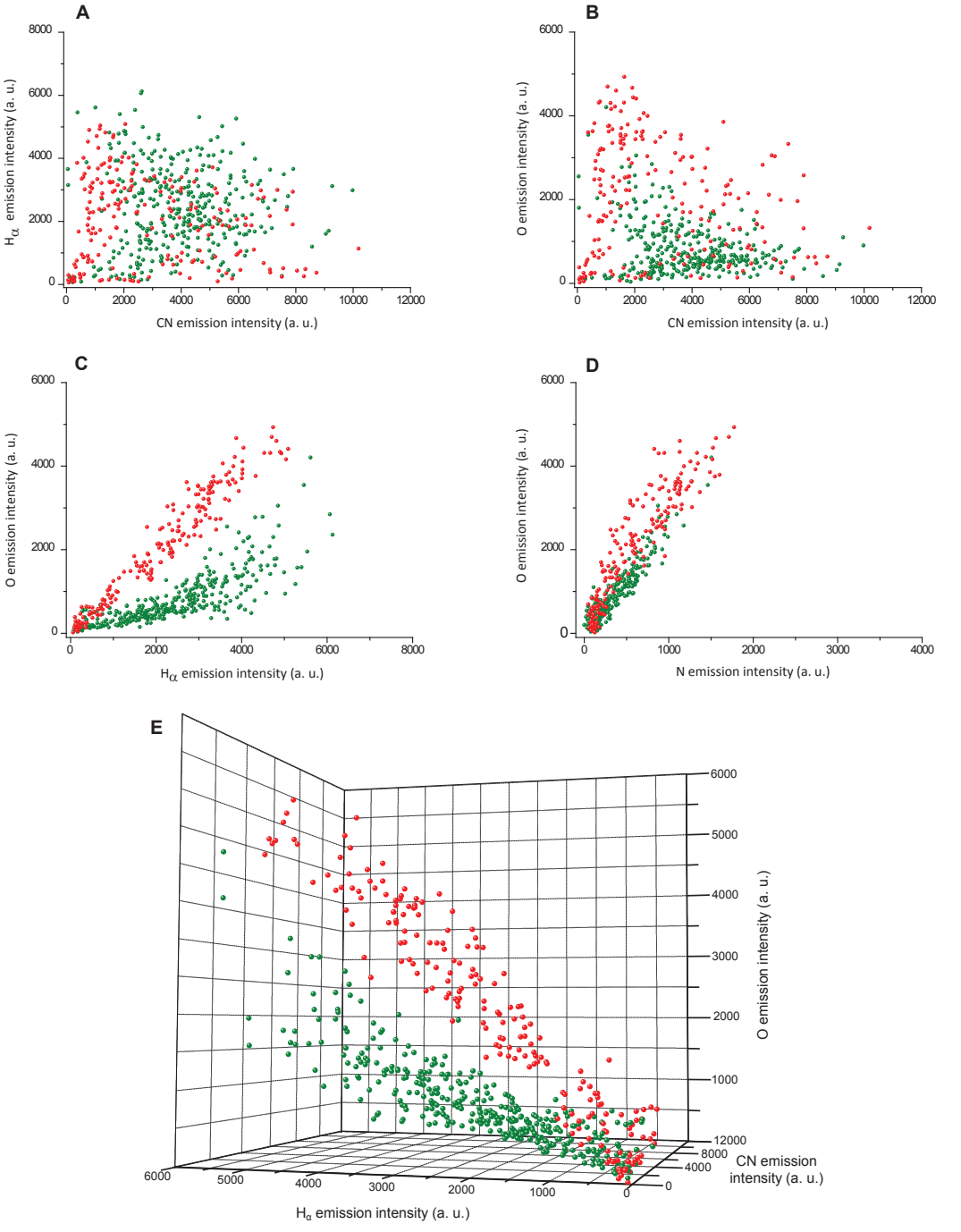

Fig.4. Scatter plots projected onto the n-dimensional subspaces built from spectral features: (***A***) CN (388 nm) and H_α (656 nm); (***B***) CN (388 nm) and O (777 nm); (***C***) H_α (656 nm) and O (777 nm); (***D***) N (746 nm) and O (777 nm); and (***E***) CN (388 nm) and H_α (656 nm) and O (777 nm). Therein each point correspond to the intensities of spectral signals involved from the plasma of whether an explosive residue (in red) or a harmless trace (in green), when located on an aluminum surface at a distance of 30 m.

3.3 Designing the Classification Model

Once identified the most useful scatter plot, several classifiers were designed and trained. *Table 2* reports the performance parameters of all designed classifiers to the *testing* of residues for the conditions established at the *training* stage. These performance parameters reveal the proportion of correct and incorrect predictions made by the classification model compared to the true outcomes. All models were trained using original intensity from line peaks; neither pre-processing functions (baseline correction, normalization ...) nor mathematical enhancements (mean centering, variance scaling ...) were applied.

As shown, accuracy of all the designed classifiers was satisfactory, with a proportion of the total number of correct predictions close to 90%. Precision of the models, established from the proportion of positive cases that were correctly identified, was near 80%. The classifiers also present high sensitivity and specificity. Indeed, most models correctly identified actual harmless traces as negative cases (in ca. 90% of the cases), thus indicating that only a few harmless residues are identified as a risk. Almost all real positive cases were labeled as explosives. These data also demonstrate that the ability of the models to identify explosives does not largely differ depending on the classifier used. Nonetheless, from a commitment to the total of residues mislabeled, the Gaussian mixture model classifier (*mogc*) was considered the best to fulfill well on the identification of the nature of the traces. This argument is plainly identified from its low values for both false positive and false negative rates.

Table 2. Performance parameters (expressed in %) of different classifiers on the distant identification (30 m) of organic residues on aluminum supports.

			Performance parameters (%)				
Scatter plot features	***Classifier***	***Accuracy***	***Precision***	***Sensitivity***	***Specificity***	***False positive rate***	***False negative rate***
CN vs H_α vs O	***ldc***	89	77	100	83	17	0
	qdc	91	80	100	86	14	0
	parzenc	90	80	97	86	14	3
	dtc	88	77	97	83	17	3
	mogc	94	87	97	92	8	3
	lmnc	92	85	97	90	10	3
	svmc	92	84	99	89	11	1

Note: *ldc* and *qdc* are Bayes linear and quadratic classifiers, respectively; *parzenc* is a *Parzen*-window classifier; *dtc* indicates a decision-tree classifier, *lmnc* denotes a neural network classifier trained by the Levenberg–Marquardt rule, *mogc* is a mixture of Gaussians classifier, and *svmc* is a support vector machine classifier.

3.4 Adaptation and performance of the semi-supervised classification model to shifting conditions

On the basis of Equation 2, original coefficients representing the hyperplane displayed by the *mog* classifier were adapted to distinct scenarios. The new set of computed coefficients leads to semi-supervised classification models to be used on emission data associated to the envisaged new operational conditions. Hence, once adapted, the classification models were tested for identification of concerned residues. For this purpose, two datasets were evaluated. Such data sets were obtained from optical responses of some particular targets at increasing operational distances. These datasets consisted of spectral information associated to traces of the same substances considered for modeling, but located at a further distance (40 m and 50 m, respectively), and consequently interrogated under the inherent lower irradiances (2.7 GW·cm^{-2} and 1.3·GW cm^{-2}, respectively). Residues from other substances were discarded. *Fig. 5* depicts the distribution of the residues data within the *3D* subdimensional space considered. As shown, under more adverse conditions, that is, at larger distances and lower irradiances, data clouds concentrate in a much smaller volume. Nonetheless, the distribution of residues keeps the original trend.

Table 3 lists performance parameters of the adapted classifiers and those provided by the original model when used to identify organic traces under the new circumstances. As shown, when the original classifier is used to label readings obtained under different conditions, the model performance degrades. This inappropriate handling of the original classifier has a deleterious effect on both the accuracy and precision of the results obtained, that as shown are progressively worst as the distance grows.

On the contrary, when the classifier is conveniently adapted, the effectiveness on residues categorization is preserved. Performance parameters

reflect how well the original hyperplane for highly scattered data adapts to the new denser representations. The accuracy of the adapted classifiers was large, with a proportion of the total number of correct predictions close to 95%, whereas the precision was near 90%. In the same vein, the new classifiers also exhibited improved sensitivity and specificity values. No significant drop of false positive and false negative rates is evidenced. Despite the lower intensity observed as the distance grows, the adapted model keeps reliable identification performance –close to 95%–. These findings demonstrate that the new algorithm resolves the identification of organic residues on aluminum surfaces located at variable distance from the instrument without modeling the new experimental conditions.

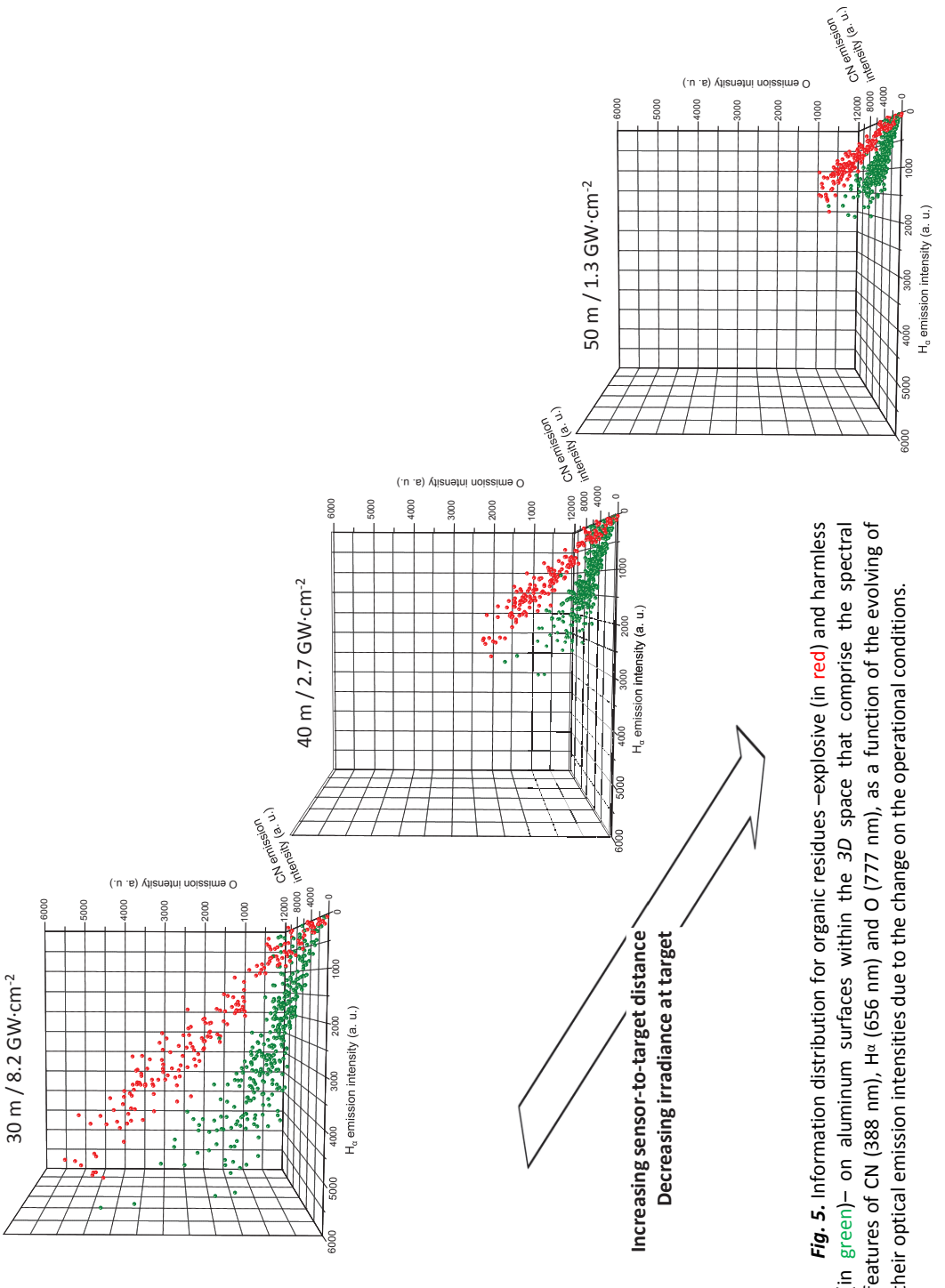

Fig. 5. Information distribution for organic residues –explosive (in red) and harmless (in green)– on aluminum surfaces within the *3D* space that comprise the spectral features of CN (388 nm), H^{α} (656 nm) and O (777 nm), as a function of the evolving of their optical emission intensities due to the change on the operational conditions.

Table 3. Performance parameters (expressed in %) of the supervised *mog* classifier to the identification of organic residues on aluminum supports at different conditions.

Operating conditions			***Performance parameters (%)***					
Distance (m)	***Laser irradiance (GW cm^{-2})***	***Model***	***Accuracy***	***Precision***	***Sensitivity***	***Specificity***	***False positive rate***	***False negative rate***
30	***8.2***	***Original***	94	87	97	92	8	3
40	***2.7***	***Original***	84	75	85	83	17	15
		Adaptive	94	88	97	93	8	3
50	***1.3***	***Original***	66	52	93	50	50	7
		Adaptive	94	90	93	94	6	7

4 Conclusions

In the current manuscript, a novel algorithm based on the adaptation of a supervised classification model to changing experimental situations has been designed. The supervised learning not only has been implemented here for the first time on data from a *standoff* configuration but also has reinforced robustness through the huge concordance between its operating effectiveness and that previously achieved using a close-contact scheme.

As demonstrated, the machine learning method properly handles the inherently multifactorial nature of the *standoff* LIBS analytical response. Based on LIBS tests on 11 organic residue/aluminum targets located at ranges from 30 m to 50 m –irradiance changing from 8.2 $GW \cdot cm^{-2}$ to 1.3 $GW \cdot cm^{-2}$–, findings herein demonstrate a high accuracy and reliability of the scheme used to label the character of organic traces.

As shown, correctly assignment of readings from known targets lets to a judgment on the hazardousness of an unknown finding. Hence, the adequate choice of spectral features and the design of the accurate model on the classes' distribution are key stages on the performance of the global strategy. No doubt that a universal strategy coping all possible changes is extremely difficult to accomplish. Due to the light propagation through the atmosphere, weather conditions may also alter the strength of the remote spectral emissions displayed. Since any fluctuation on spectral signals can lead to a classification model termed "inconsistent", some additional trials are in development right now. Currently, assessment of the ruggedness and robustness of the model to cope with identification of mixtures of explosives with potential interfering substances is in progress. Furthermore, evaluating the consistency of the strategy to significant changes on environmental conditions is our next task.

5 References

[1] H. Schubert, A. Rimski-Korsakov, Stand-Off Detection of Suicide Bombers and Mobile Subjects. NATO Security through Science Series, *Springer*, Berlin (2006).

[2] C. López-Moreno, S. Palanco, J.J. Laserna, F. DeLucia Jr, A. Miziolek, J. Rose, R.A. Walters, A.I. Whitehouse, Test of a stand-off laser-induced-breakdown spectroscopy sensor for the detection of explosive residues on solid surfaces, *J. Anal. At. Spectrom.* 21 (2006) 55–60.

[3] B. Zachhuber, G. Ramer, A. Hobro, E.T. Chrysostom, B. Lendl, Stand-off Raman spectroscopy: a powerful technique for qualitative and quantitative analysis of inorganic and organic compounds including explosives, *Anal. Bioanal. Chem.* 400 (2011) 2439–2447.

[4] C.W. Van Neste, L.R. Senesac, T. Thundat, Standoff photoacoustic spectroscopy, *Appl. Phys. Lett.* 92 (2008) 234102-1–234102-3.

[5] C.W. Van Neste, L.R. Senesac, D. Yi, T. Thundat, Standoff detection of explosive residues using photothermal microcantilevers, *Appl. Phys. Lett.* 92 (2008) 134102-1–134102-3.

[6] R. Furstenberg, C.A. Kendziora, J. Stepnowski, S.V. Stepnowski, M. Rake, M.R. Papantonakis, V. Nguyen, G.K. Hubler, R.A. McGill, Stand-off detection of trace explosives via resonant infrared photothermal imaging, *Appl. Phys. Lett.* 93 (2008) 224103-1–224103-3.

[7] I. Gaona, J. Moros, J.J. Laserna, New insights into the potential factors affecting the emission spectra variability in standoff LIBS, *J. Anal. At. Spectrom.* 28 (2013) 1750–1759.

[8] J.L. Gottfried, F.C. De Lucia, Jr., C.A. Munson, A.W. Miziolek, Strategies for residue explosives detection using laser-induced breakdown spectroscopy, *J. Anal. At. Spectrom.* 23 (2008) 205–216.

[9] F.C. De Lucia, Jr., J.L Gottfried, C.A. Munson, A.W. Miziolek, Multivariate analysis of standoff laser-induced breakdown spectroscopy spectra for classification of explosive-containing residues, *Appl. Optics* 47 (2008) G112–G121.

[10] J.L Gottfried, F.C. De Lucia, Jr., C.A. Munson, A.W. Miziolek, Double-Pulse Standoff Laser-Induced Breakdown Spectroscopy for Versatile Hazardous Materials Detection, *Spectrochim. Acta Part B* 62 (2007) 1405–1411.

[11] J.L. Gottfried, F.C. De Lucia, Jr., A.W. Miziolek, Discrimination of explosive residues on organic and inorganic substrates using laser-induced breakdown spectroscopy, *J. Anal. At. Spectrom.* 24 (2009) 288–296.

[12] F.C. De Lucia, Jr., J.L Gottfried, Influence of variable selection on partial least squares discriminant analysis models for explosive residue classification, *Spectrochim. Acta Part B* 66 (2011) 122–128.

[13] R. González, P. Lucena, L.M. Tobaria, J.J. Laserna, Standoff LIBS detection of explosive residues behind a barrier, *J. Anal. At. Spectrom.* 24 (2009) 1123–1126.

[14] J. Moros, J. Serrano, C. Sánchez, J. Macías, J.J. Laserna, New chemometrics in laser-induced breakdown spectroscopy for recognizing explosive residues, *J. Anal. At. Spectrom.* 27 (2012) 2111–2122.

[15] J. Moros, J. Serrano, F.J. Gallego, J. Macías, J.J. Laserna, Recognition of explosives fingerprints on objects for courier services using machine learning methods and laser-induced breakdown spectroscopy, *Talanta* 110 (2013) 108–117.

[16] J. Serrano, J. Moros, C. Sánchez, J. Macías, J.J. Laserna, Advanced recognition of explosives in traces on polymer surfaces using LIBS and supervised learning classifiers, *Anal. Chim. Acta* 806 (2013) 107–116.

[17] R.P.W Duin, P. Juszczak, P. Paclik, E. Pekalska, D. de Ridder, D.M.J. Tax, S. Verzakov, PRTools4.1, A Matlab Toolbox for Pattern Recognition, Delft University of Technology, (2007).

[18] F. Van der Heijden, R.P.W. Duinde, D. Ridder, D.M.J Tax, Classification, Parameter Estimation and State Estimation: An Engineering Approach Using MATLAB, *John Wiley & Sons*, Chichester (2004).

[19] J. Drugowitsch, Design and Analysis of Learning Classifier Systems: A Probabilistic Approach, *Springer-Verlag*, Berlin (2008).

[20] C.G. Parigger, J.O. Hornkohl, Computation of AlO $B_2\Sigma^+ \rightarrow X_2\Sigma^+$ emission spectra, *Spectrochim. Acta Part A* 81 (2011) 404–411.

Chapter 5

Chapter 5. Evaluation of LIBS Analysis Potential for Addressing Radiological Threats from a Distance

Abstract

Although radioactive materials are nowadays valuable tools in nearly all fields of modern science and technology, the dangers stemming from the uncontrolled use of ionizing radiation are more than evident. Since preparedness is a key issue to face the risks of a radiation dispersal event, development of rapid and efficient monitoring technologies to control the contamination caused by radioactive materials is of crucial interest. Laser-induced breakdown spectroscopy (LIBS) exhibits appealing features for this application. This research focuses on the assessment of LIBS potential for the *in situ* fingerprinting and identification of radioactive material surrogates from a safe distance. LIBS selectivity and sensitivity to detect a variety of radioactive surrogates, namely ^{59}Co, ^{88}Sr, ^{130}Ba, ^{133}Cs, ^{193}Ir and ^{238}U, on the surface of common urban materials at a distance of 30 m have been evaluated. The performance of the technique for nuclear forensics has been also studied on different model scenarios. Findings have revealed the difficulties to detect and to identify the analytes depending on the surface being interrogated. However, as demonstrated, LIBS shows potential enough for prompt and accurate gathering of essential evidence at a number of sites after the release, either accidental or intentional, of radioactive material. The capability of *standoff* analysis confers to LIBS unique advantages in terms of fast and safe inspection of forensic scenarios. The identity of the radioactive surrogates is easily assigned from a distance and the sensitivity to their detection is in the range of a few hundreds of ng per square centimeter.

1 Introduction

Radioactivity refers to the emission of ionizing (high-energy) radiation, namely alpha (α), beta (β), X or gamma (γ), from the spontaneous and random transformation (radioactive decay) of an unstable atomic nucleus, resulting in new elements or a lower energy state of the atoms [1]. Most of the ionizing radiation we are exposed to (about 82 percent of the total) consists of natural background radiation from radon gas and other natural terrestrial sources (radioactive elements in rocks, soil, water, and plants), whereas the remaining 18 percent is from man-made sources. Since the discovery of X-rays in 1895, man-made radiation has been becoming a very common tool that lets us do many things that would be impossible without it [2]. Thousands of new practical and beneficial uses of ionizing radiation have been devised till its complex structure within the present-day life [3]. Ionizing radiation is ubiquitous and indispensable for medical techniques and practices of diagnosing and treating –e. g. for identifying broken bones and healing of tumors [4]– as well as on nuclear power plants for sustaining exothermic processes to generate heat and electricity [5], to mention the most common. Its use also extends to metabolic studies, genetic engineering and environmental protection studies. The ionizing radiation from radioisotopes is also used in agriculture to breed new seed varieties and to preserve different varieties of food [6]. Similarly, it is applied in industry, manufacturing and engineering for improving the quality of manufactured goods [7].

Although the benefits of radiation are more than apparent, living and working with it is not only hazardous but also may entail risks that cannot be overlooked. With a view to putting in perspective the menaces from ionizing radiation, all them can cause to any form of life, whether it be human, plants, or animals many adverse consequences not just at a cellular level but on a genetic level as well. The amount of damage caused by ionizing radiation depends on its half-life and on both the dose and the period of exposition.

Radiological dispersal events from nuclear and radioactive sources may arise from an unfortunate natural disaster. Just to cite the most recent example, the incidents at Fukushima nuclear reactors because of the earthquake and the subsequent tsunami of March, 2011, demonstrate the extreme dangers associated to these events. Furthermore, malicious actions by those who seek to unleash a radiological mayhem are today more than a real threat [8]. In these cases, the most commonly used civilian radiation sources are malevolently exploited to prepare a radiological dispersive device (*RDD*), also known as "*dirty bomb*", using conventional explosives to pulverize and disperse the radioactive material.

Preparedness to establish the release or presence of an injurious agent in a given location is a fundamental interest for any successful response policy against these threats. Sensing technologies are needed at the three stages of the dispersal incident: I) before, allowing a continuous monitoring either to prevent the incident (*detect-to-protect*) or for early warning in the case that the incident occurs (*detect-to-treat*); II) during, allowing first responders to identify the precise nature (*detect-to-identify*) and the extent (*detect-to-quantify*) of the release and to organize the response accordingly; and III) after, allowing confirmation either on the persistence of the threat or on a complete area decontamination (*detect-to-confirm*). Analytical detection thus contributes to at least four of the core objectives of civil protection, *i.e.* prevention, protection, response and recovery.

A variety of *field-deployable* and hand-held portable instruments are available for detecting and measuring radioactive materials [9]. Hand-held survey meters are able to search, locate, and detect alpha (α), beta (β), gamma (γ), and neutron radiations. However, releasing the radionuclide identity is available only for some particular emitting sources. For instance, while radiation from ^{90}Sr -a pure beta emitter- can be easily detected and measured with a *Geiger-Mueller* survey meter connected to a pancake probe, it will not be detected by a sodium iodide instrument or other types of gamma identification devices. In addition, some

instruments saturate and provide low or no readings in a very high radiation field [10].

Thus, since one of the most critical steps in first responding to a radiological disaster is the identification of the emitter present, it is in this direction that laser-induced breakdown spectroscopy (LIBS) may provide a fruitful and meaningful contribution. Technology based on LIBS has appealing features for radiological analysis including the capacity for fast and simultaneous detection of almost all elements, *in situ* operation using *field-deployable* designs, and contactless inspection with nanograms sensitivity. From these properties, LIBS-based sensors may be able to make a quick determination of the element responsible of the radiation, and the distribution profile of the element in the contaminated zone. It is not a coincidence that LIBS tracking instruments have become the most complete sensing systems to apply to chemical, biological, radiological, and nuclear (*CBRN*) threats.

The potential of LIBS to detect and discriminate chemical and biological warfare surrogate agents on a variety of substrates and in the presence of interferents has been explored [11, 12]. Detection of aerosolized CBW agents has been also studied [13]. A number of studies have evidenced the extensive experience of LIBS on recognition of explosives residues [14-17]. The use of LIBS for the design of a potential rapid *in situ* field portable unit for nuclear safeguard inspection, environmental surveillance and detecting weapons of mass destruction [18], as well as in-field forensic applications [19] is currently being explored. Interests have been mostly focused on open air detection of uranium in solids [20-22], as a residue on aluminum, plastic and ceramic surfaces [18], and as a surrogate of highly radioactive glass waste [23]. Detection of other surrogates for nuclear sensitive materials such as strontium [24, 25] and cesium [25] has been also discussed.

The present investigation focuses on the assessment of the LIBS potential in benefit of designing a *field-deployable* sensor to tackle the radiological sensing from a distance. The measurement range in these experiments has been established in 30 m (the minimum operating distance for our sensor). A number of tasks including identification of surrogate radiological residues and establishing their detectable amounts have been faced. Selectivity and sensitivity of LIBS to confirm different elements, namely ^{59}Co, ^{88}Sr, ^{130}Ba, ^{133}Cs, ^{193}Ir and ^{238}U, over surfaces linked to common urban materials have been verified. Solid supports have been used to emulate the sensing procedure at suspected locations as most of the airborne radioactive dust has settled to the ground in about 10 minutes. The LIBS power for forensic analysis has been also tested.

2 Experimental section

The *ST-LIBS* sensor used to perform these investigations has been described in detail in the "Experimental" chapter of this Doctoral Thesis. Together with the *ST-LIBS* sensor, for performance comparison, a laboratory set-up similar has been also tested. The excitation source is a Q-switched 1064 nm Nd:YAG laser (20 Hz, 54 mJ·pulse^{-1}, 8 ns pulse width). The laser beam is delivered to the target through an optical train involving a 1064 nm plane mirror and a 75-mm focal length plane-convex quartz lens. Light from the created plasma is collected using a collimating lens securely attached to the tip of the optical fiber. Plasma image was spectrally resolved using the 4-channels miniature spectrograph (75 mm focal length), fitted each with a CCD image sensor. An effective spectral range spanning from 330 nm to 950 nm is set. The timing parameters used for optical signal acquisition are enabled by default at: 1.28 µs of delay time from the external trigger input (considered 0 time) supplied by the Q-switch output signal of the laser, and 1.1 ms of integration time (gate width). Whatever the approach, *standoff* or close-contact, laser spot size

and laser energy at the target have been matched to get identical irradiance at the sample (3 $GW \cdot cm^{-2}$) for plasma plume production.

Targets assayed

In this attempt to elemental detection and quantification of potential radioactive sources, surrogate, non-radioactive materials have been operated. Hydrated salts including $Co(NO_3)_2 \cdot 6H_2O$, $SrCl_2 \cdot 6H_2O$, $UO_2(CH_3COO)_2 \cdot 2H_2O$, and $IrBr_3 \cdot xH_2O$, have been used as Co, Sr, U and Ir suppliers, respectively. Other inorganic compounds including $BaSO_4$ and Cs_2CO_3 have been utilized as convenient sources of Ba and Cs, correspondingly.

Starting from the idea that a LIBS sensor is aimed to assess an area contaminated with radioactive material, several common items easily found in urban areas have been examined: aluminum from traffic signs, glass from bus shelters, building bricks, concrete and pavement (sidewalk). These objects have been used as supports for locating the residues. For identification and characterization of the surrogates of interest, the compounds have been spread onto the raw surface (without any physical treatment such as a buffing to smooth) of each support in milligram quantities. In parallel, surface concentrations of elements at few (0.5-2.0) mg per square centimeter level have been disposed to ascertain the LIBS detection capability at a distance.

3 Results & discussion

Implicit in risk assessment during the inspection of a contaminated zone is the identification and quantification of the radiation source according to the presence or absence in the operational scenario of a particular analyte. In the successive sections, a discussion on the capabilities of LIBS for *standoff* detection and quantification of radioactive surrogates over distinct surfaces is presented. The ability for a parallel detection of the radioactivity source and the corresponding

explosive propellant after the possible detonation of a "*dirty bomb*" has been also appraised.

3.1 Detection specificity

First, identifiable spectral features of radioactive surrogates on the surface of tested objects were established. The identification capability of a residue may be affected by the substrate composition, since part of the support is usually ablated together with the material of interest. Accordingly, elements composing the substrate contribute to the plasma plume and, therefore, are also involved in the emission observed thus reducing the probabilities of a positive finding. *Fig. 1* shows the *standoff* emission spectra of the tested supports.

As observed, the LIBS spectrum of aluminum is quite simple. Sensitive atomic lines at 394.40 nm and 396.15 nm together with the emission sequence of gaseous aluminum oxide (AlO) are easily identifiable [26]. In contrast, the spectrum of glass exhibits virtually no spectral features. This fact is due to the low optical absorption of glass at 1064 nm that hampers the heating and subsequent vaporization of the surface to result in plasma formation. The spectrum of glass scarcely shows emission signals from its main constituents (SiO_2, Na_2O, CaO, MgO and K_2O) [27]. On this substrate, emissions from the analytes are free from spectral interferences and a broad selection of lines can be used for identification purposes. An entirely opposed situation occurs with the spectral profiles of mortar and clay. As shown in *Fig. 1*, the spectra of these materials are full of spectral features as a result of their multielemental composition –$Al_2O_3 \cdot 2SiO_2 \cdot H_2O$ and varying amounts of oxides from Ca, K, Mg and Na. Strong molecular emissions of CaO and CaOH in the spectral region (540 nm–660 nm) are also observed [28].

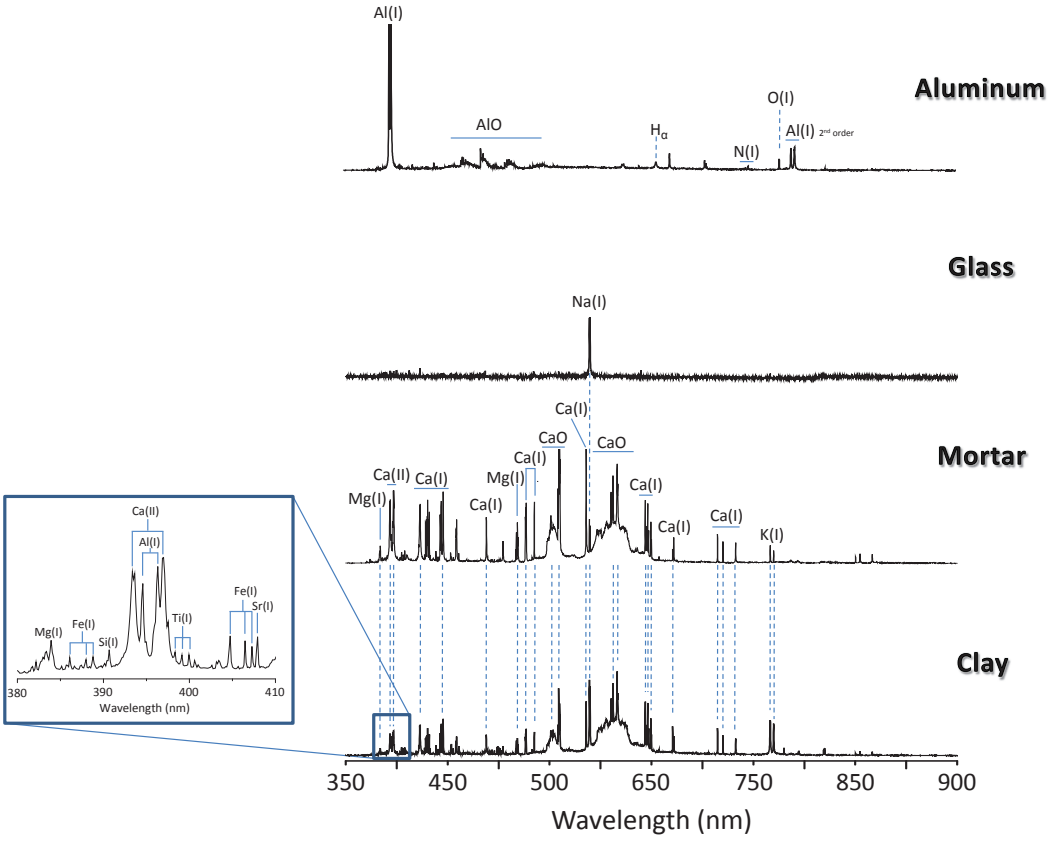

Fig. 1. *Standoff* LIBS spectra of the tested blank supports.

Beyond the greater or lesser richness of emission features within the support signal, effectiveness in identifying the presence of an analyte depends on the potential masking between spectral features of both, residue and substrate [29]. In this connection, *Table 1* lists the most prominent atomic and ionic emission lines that identify each element. As noted, the analytical use of these lines depends on the spectral characteristics of the substrate where the residue is located. While over glass, all the LIBS features are interference-free, in the rest of supports, only specific lines are suitable to prove the presence of the species in the target.

Table 1. Level of selectivity for the most relevant emission signals from the radioactive.

Surrogate radionuclide	*Emission wavelength (nm)*	*Supports*			
		Aluminum	*Glass*	*Mortar*	*Clay*
^{59}Co	350.23 (I)	✓	✓	✓	✓
	352.98 (I)	✓	✓	✓	✓
	356.93 (I)	✓	✓	✓	✓
	389.41 (I)	✓	✓	✓	✓
	399.53 (I)	✓	✓	✓	✓
	411.88 (I)	✓	✓	✓	✓
	412.13 (I)	✓	✓	✓	✓
^{88}Sr	407.77 (II)	✓	✓	✓	✓
	421.55 (II)	✓	✓	✗	✗
	460.73 (I)	✓	✓	✓	✓
	679.10 (I)	✓	✓	✓	✓
	687.83 (I)	✓	✓	✓	✓
	707.01 (I)	✓	✓	✓	✓
	868.89 (II)	✓	✓	✓	✓
^{130}Ba	455.40 (II)	✗	✓	✓	✓
	493.41 (II)	✗	✓	✓	✓
	553.55 (I)	✓	✓	✗	✗
	614.17 (II)	✓	✓	✗	✗
	649.69 (II)	✓	✓	✓	✓
	728.03 (I)	✓	✓	✓	✓
^{133}Cs	455.53 (I)	✗	✓	✓	✓
	459.32 (I)	✗	✓	✓	✓
	672.44 (II)	✓	✓	✓	✓
	697.33 (I)	✓	✓	✓	✓
	852.11 (I)	✓	✓	✓	✓
	894.35 (I)	✓	✓	✓	✓
^{193}Ir	357.37 (I)	✓	✓	✓	✓
	362.87 (I)	✓	✓	✓	✓
	380.01 (I)	✓	✓	✓	✓
	397.63 (I)	✓	✓	✓	✓
	439.95 (I)	✓	✓	✓	✓
^{238}U	385.96 (II)	✓	✓	✓	✓
	393.20 (II)	✓	✓	✗	✗
	409.01 (II)	✓	✓	✓	✓
	502.74 (I)	✓	✓	✓	✓
	591.54 (I)	✓	✓	✓	✓
	682.69 (I)	✓	✓	✓	✓

As an example of the LIBS detection capability, *Fig. 2* depicts the emission spectra of plasmas from the different radioactive surrogates when located on aluminum.

As shown, regardless the signal intensity, at least one spectral feature within the spectrum is free from interference, thus allowing identification of each surrogate element. In the spectra, a number of oxide bands are evidenced. In the case of Sr, emission bands from strontium dioxide radicals appear in the spectral region covering from 590 nm to 690 nm [24], whereas the lines of AlO are absent. Similarly, AlO is absent in the spectrum of Ba, which exhibits lines of barium oxide, a weak emitter in the yellow and green regions of the spectrum (495 nm – 590 nm) [30]. The absence of AlO in these materials is due to the thermodynamically favored reaction of dissociated atmospheric oxygen with Sr and Ba atoms evaporated from the sample as compared to the reaction of oxygen with aluminum. By contrast, cobalt and iridium do not exhibit emissions from their corresponding oxides [31, 32]. Although these elements have also the capability to form oxygen clusters, emissions from these compounds are not observed in the spectrum.

As a result of their similar affinity for oxygen, Cs and U oxide bands are accompanied by emissions of AlO. Emissions of Cs_nO_m clusters appear in the blue-green region of the spectrum near 550 nm, close to those of AlO. However, emissions from UO_2, UO_3, and U_3O_8 [33] occur in the same region than those from AlO –spanning from 475 nm to 600 nm–, thereby causing a superposition of both spectral systems. The dominance of AlO in the spectrum is due to the minute amount of uranyl residue deposited on the aluminum support.

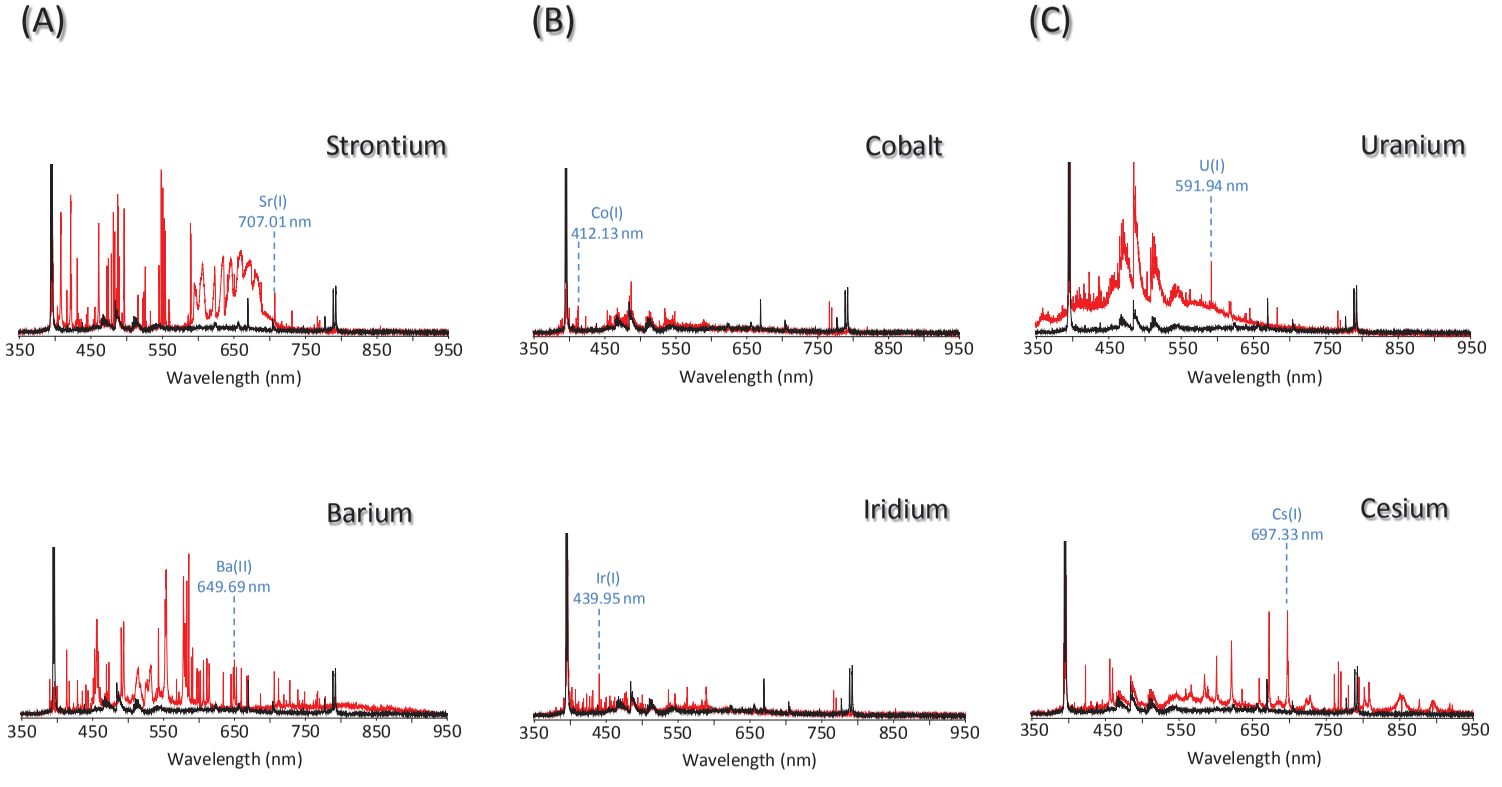

Fig. 2. *Standoff* LIBS spectra for different residues of radioactive surrogates on aluminum. From left to right: (A) Sr and Ba, (B) Co and Ir, and (C) U and Cs. The spectrum of the blank support is also displayed for comparative purposes.

Despite the many factors contributing to the spectral behavior of the concerned elements, it can be argued that their oxygen affinity is well matched with their electronegativity (χ = using the Pauling scale) as well as with their electronic structures. For instance, while Ba (χ = 0.89) and Sr (χ = 0.95) are alkaline earth metal elements, a relationship exists between Co (χ = 1.88) and Ir (χ = 2.20), which are Group 9 elements. The alkaline-earth metals have electronic configurations with a filled s subshell but easily lose electrons to become positive ions (cations). As a result, these elements having a lower electronegativity as compared to that of Al (χ = 1.61) exert a stronger attractive force over the oxygen. Due to the high plasma temperature and the excess oxygen, Ba and Sr are able to form oxides (O^{2-}), as well as peroxides (O_2^{2-}). Contrarily, the transition metals are characterized by a partially-filled d subshell in their free elements and cations. Consequently, their relatively high electronegativity implies a lower or no flexibility in forming oxides in the case that the Al or other elements having less electronegativity are present. In any case, although the formation of all these oxides leads to a general alteration, mainly a decreasing on intensity, of the atomic and ionic spectral signals of the elements due to the depletion of such species within the plasma plume, their occurrence within the emission spectrum –clearly confirmed in *Fig. 2(A)*–, may also act as an exclusive marker indicating the presence of a particular element.

3.2 Potential for Detection

The sensitivity of a sensor is indicated by the minimum amount of a particular analyte that must be present in the analysis scenario in order to warn with guarantees about its presence. In order to check the detection potential of the *standoff* LIBS method, the limit of detection (*LOD*) of the considered elements on different surfaces has been studied. For this purpose, microvolumes of aqueous solutions from concerned salts –at thousand ppm level– were homogeneously

dispersed over each support. Once the water was evaporated, ten single laser shots were directed on refreshed locations within the area. From the average of these ten emission responses, *LODs* have been computed by using the following equation:

$$LOD = \frac{0.01 \cdot 3 \cdot RSD_{bckgrnd} \cdot C}{\frac{S_{net}}{S_{bckgrnd}}} \qquad \text{(Equation 1)}$$

where $RSD_{bckgrnd}$ is the relative standard deviation (expressed in percent) of the spectral background, S_{net} is the net emission intensity of the line considered, $S_{bckgrnd}$ is the intensity of the background signal, and C (expressed in mass per unit area) is the calculated surface amount of analyte exposed to the laser shot (depending on the laser spot size that ablates the targeted material) [34]. Except in self-reversed or interfered lines, *LODs* have been calculated from the most sensitive emission line for each particular analyte. *Table 2* lists the *standoff* detection limits for the radionuclide surrogates in terms of mass of the element per unit area. For comparison purposes, the corresponding detection limits achieved in close-contact LIBS are also reported.

Standoff LODs vary from a few up to several hundred micrograms per square centimeter. Apart from the inherent spectral properties of the elements, some differences in the *LODs* on a same support may arise in connection with the capability for oxide formation. The *LOD* of an element may change since oxide formation alters the population of its atomic and ionic states. Clear examples are the cases of Sr and Ba on aluminum. Despite the low *LODs* reported for these elements, the capability for their detection is underestimated. Their tendency to form emitting oxides (as shown in *Fig. 2(A)*) leads to less intense lines from atoms and ions. That is why *standoff LODs* substantially lower (better) than 17 µg·cm^{-2} and 2 µg·cm^{-2} should be expected for Sr and Ba, respectively.

Table 2. LIBS LODs of radioactive surrogates when encountered on surfaces of different common urban materials

		LOD (μg·cm^{-2})							
		Aluminum		***Glass***		***Mortar***		*Clay*	
Surrogate isotope	***Emission line (nm)***	***Close-contact***	***Standoff***	***Close-contact***	***Standoff***	***Close-contact***	***Standoff***	***Close-contact***	***Standoff***
^{59}***Co***	*412.13 (I)*	*25*	*25*	*105*	*133*	155	127	300	230
^{88}***Sr***	*707.01 (I)*	*13*	*17*	*75*	*86*	125	153	140	193
^{130}***Ba***	*649.69 (II)*	*2*	*2*	*25*	*12*	23	27	8	9
^{133}***Cs***	*697.33 (I)*	*15*	*7*	*190*	*48*	1050	307	750	440
^{193}***Ir***	*439.95 (I)*	*20*	*11*	*50*	*20*	280†	107†	225†	120†
^{238}***U***	*591.54 (I)*	*30*	*21*	*80*	*69*	150	167	320	250

† Limits of detection have been calculated from depositions of iridium salt in solid form due to the matrix induced effects when the aqueous solutions were used.

Differences in the *LOD* of a particular analyte in different surfaces result also from the chemical and physical properties of the complete matrix [35]. Although the dependence of the *LODs* with the substrate is not tied to any fixed pattern, it is possible to extract some detailed influences. Despite the low ablation rate induced in pure glass, efficient detection of elements is ensured at this support. This circumstance is due to the presence of the compound itself, which leads to a larger optical absorption. Furthermore, the scarce contribution of the support to the final emission signal leads to a larger signal-to-noise ratio.

On the other side, although intense plasma plumes are produced in aluminum, mortar and clay surfaces, significant differences in detection sensitivity are evidenced. The variations in the *LOD* for a same element on these different matrices is elucidated through the properties of the plasmas formed. In order to verify this extreme, the electron temperature (T_e) and electron number density (N_e) of the plasmas of barium residues on these supports have been calculated. Electron temperatures were calculated using the following equation:

$$\ln\left(\frac{\lambda_{mn} I_{mn}}{A_{mn} g_m}\right) = -\frac{E_m}{K T_e} + \ln(hcN) \qquad \text{(Equation 2)}$$

where λ_{mn} is the wavelength of the transition lines, I_{mn} is the integrated line intensity of the transition involving an excited level (m) and a lower level (n), A_{mn} (s^{-1}) is the transition probability, g_m (s^{-1}) is the statistical weight of the excited level (m), E_m (eV) is the energy of the excited level, K ($eV \cdot K^{-1}$) is the Boltzmann's constant, h (J·s) is the Plank's constant, c ($m \cdot s^{-1}$) is the speed of light and $N(T)$ (m^{-3}) is the total number density. By plotting the left hand side term *vs.* E_m, the plasma temperature is obtained from the slope of the straight line [36].

Electron number densities were computed from the line profiles of the isolated barium line (Ba II) at 649.69 nm [37]. Although N_e is associated with a global contribution of different broadening mechanisms, it was computed from the

measured *full-width-at-half-maximum* (*FWHM*) of the *Stark* broadened line profile. The instrumental broadening contribution was subtracted. The following relation was used:

$$\Delta\lambda_{\frac{1}{2}} = 2\omega\left(\frac{N_e}{10^{16}}\right) \qquad \text{(Equation 3)}$$

where ω is the electron impact width parameter.

Fig. 3A shows the Boltzmann plots obtained in the three supports considered. The slope of the curves yields T_e values of 14000 K, 6500 K and 3700 K in aluminum, clay and mortar, respectively. In the same vein, *Fig. 3B* plots the correspondence between the conditions for Ba residues plasmas and the associated *LOD* at each support (*Table 2*). As observed, large values of temperature and density of the plasma plume lead to the best detection. Consequently, the *LOD* calculated in the aluminum surface is better than that in mortar and clay.

Regarding the sensitivity of *standoff* LIBS when compared to the close-contact counterpart, no significant differences in the *LODs* of Co, Sr, Ba and U are observed. Contrarily, the *standoff LODs* of Cs and Ir are even better than those calculated in close-contact. Such results are unforeseen, to some extent, since, if all operating conditions were identical (in terms of laser energy and spot size), the *standoff* LIBS signal should be smaller than the proximity measurement due to the inverse square law drop of the signal with the range [38]. Hence, *LODs* should be predictably larger for *standoff* mode as compared to close-contact framework. However, in the *standoff* measurements the area sampled by the laser beam is by far larger than that excited in the close-contact approach. Consequently, the *standoff* spot size of 1500 µm in diameter is much more crucial for sampling than that of 450 µm for close-contact approach; a circumstance that also mitigates the lack of uniformity on the distributions of the residues. Nonetheless, differences in

LODs between approaches are much more pronounced when absolute amount is computed. For instance, the 280 µg·cm^{-2} and the 107 µg·cm^{-2} of Ir, that are detected in mortar, turn into quantities of ca. 0.5 µg and 2.0 µg, for close-contact and *standoff* configurations, respectively. In any case, whatever the approach, the technique exhibits a large sensitivity for the considered elements.

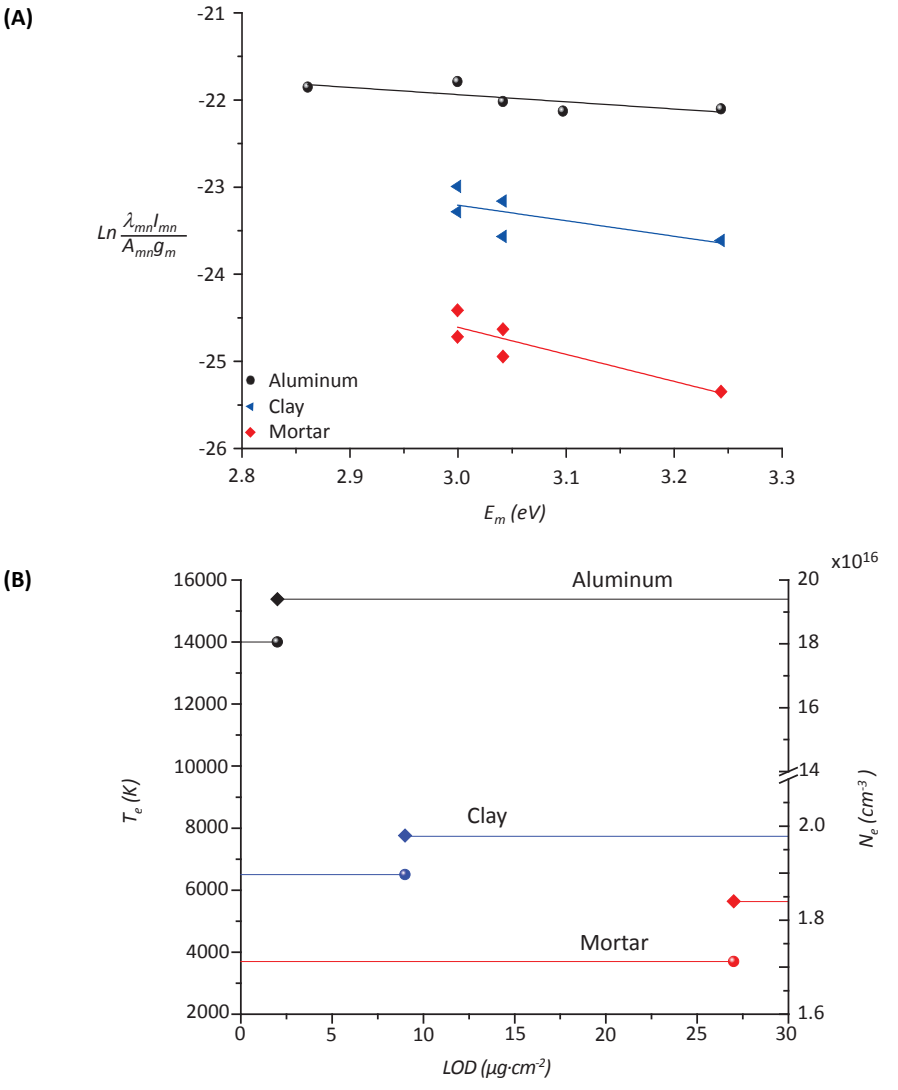

Fig. 3. (A) Saha-Boltzmann plots obtained from the spectral emissivity of selected lines of Ba for plasma temperatures calculation on aluminum (black), clay (blue) and mortar (red) supports and (B) Dual correspondence between the electron temperature (●) and the electron density (♦) characterizing the plasmas of Ba residues on the concerned supports and the associated sensitivity.

3.3 Identification of forensic evidences [39]

In the present section, the suitability of the LIBS portable device for fingerprinting radioactive surrogates in potential scenarios of nuclear forensics has been investigated. Two modeled scenes on the post-detonation of a dirty bomb and the accidental release of radioactive material have been considered.

3.3.1 Premeditated radiological dispersion. The investigation of a "*dirty bomb*" scene mainly seeks identifiable chemical evidences at witness debris materials close to the "actual" target to determine any type of intention. Nonetheless, these compelling evidences are very limited. As the afterburning products resulting from the detonation of an organic explosive are mainly water vapor and gases like CO, H_2 and N_2, the expected post-blast residues are limited to solid carbon and traces of the non-reacted explosive accompanied by several interfering impurities, in amounts that are orders of magnitude higher [40]. In this context, two LIBS sensing tests over supposed debris resulting from detonations by trinitrotoluene (*TNT*) of Cs- and Co-based "*dirty bombs*" have been performed. Aluminum plates (15 × 15 cm^2) have been used as debris, emulating fragments of the sealed metal containers that store the radioactive source. Particles from *TNT*-surrogate solid mixtures at variable proportions (from 0%-100% w/w up to 100%-0% w/w) have been dispersed between well-defined areas (2 × 10 cm^2 each) over the aluminum surfaces. The CN molecular signal and the intense atomic emissions of Cs at 697.33 nm and Co at 412.13 nm have been used as markers of the explosive material and the radioactive surrogates, respectively.

Fig. 4 depicts the spatial mappings on the composition and distribution of the dispersed evidences. As shown, in the case of *TNT*:Cs mixtures (left panels), the chemical screening for both the explosive and the radioactive surrogate is accurately described regardless the concentration ratio studied.

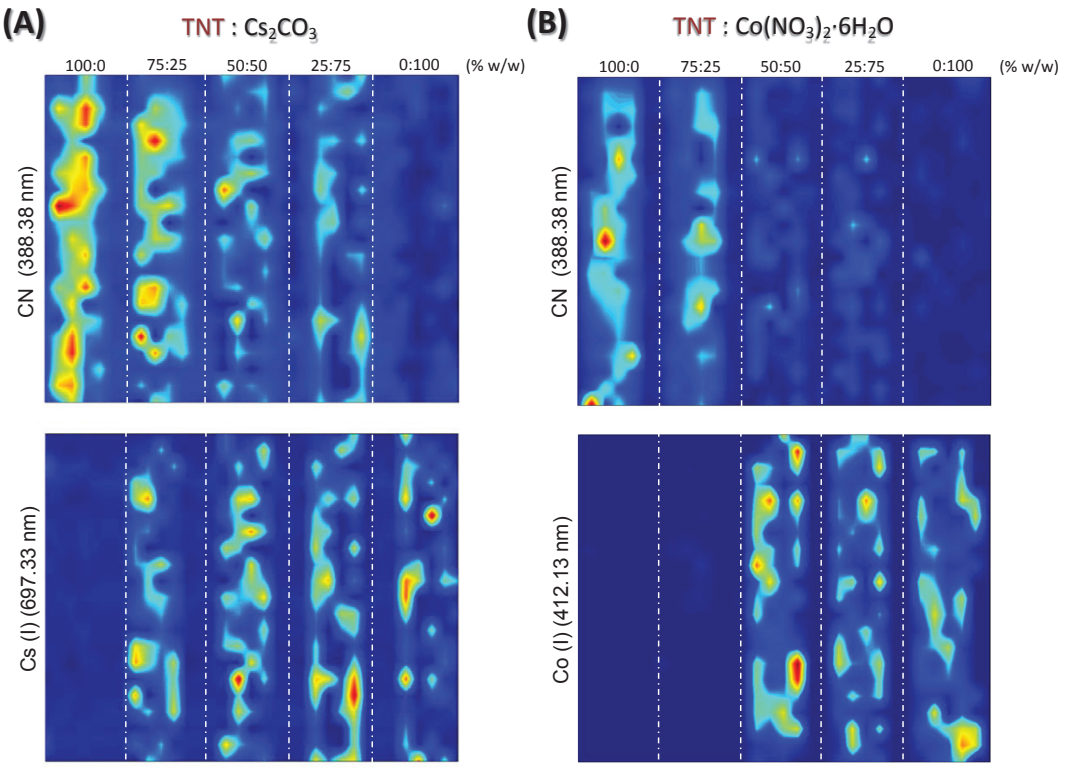

Fig. 4. Mapping of chemical distribution of evidence for hypothetical aluminum debris corresponding to simulated post-detonations of two "*dirty bombs*": Cs-TNT (left panels) and Co-TNT (right panels). Intensity maps, by laser-assisted *standoff* emission spectroscopy, of evidences mixtures at five variable levels –vertical stripes– for the explosive (CN band at 388.83 nm) as well as the radioactive surrogates, Cs (697.33 nm) and Co (412.13 nm), respectively.

For the *TNT*:Co mixtures (right panels), some evidences pass unnoticed. As seen, *TNT* is virtually not detected unless it is at a ratio of 75% to the radioactive surrogate (upper map). Likewise, cobalt (map below) is not detected even when it accounts for a one quarter of the mixture. In contrast, in the hypothetical case of a Cs-based dirty bomb, both the element and the explosive are detected whatever the concentration in the mixture is. Thus, from the point of view of a positive finding, the interrogation of this scenario reveals evidence of a detonation. The simultaneous detection of *TNT* and Cs at a proportion of 25:75 fits with a minute

amount of explosive, which has survived the blast, within a relatively large amount of radioactive material.

3.3.2 Accidental radiological release. For the study of the accidental release of radioactive material to the environment, a well-delimited area (24 × 24 cm^2) within the surface of a rustic terracotta flooring tile has been contaminated with residues of Ir, Sr, Co, and Cs. Identification tests have been organized across the surface which was divided into four quadrants (12 × 12 cm^2 each), one for each element. The inspected target has been located at 30 m from the sensor and scanned with a lateral resolution of 1 cm. *Fig. 5* shows the photograph of the prepared scenario together with the resulting chemical maps associated to the overall 24 cm × 24 cm section when the particular emission of each analyte is monitored.

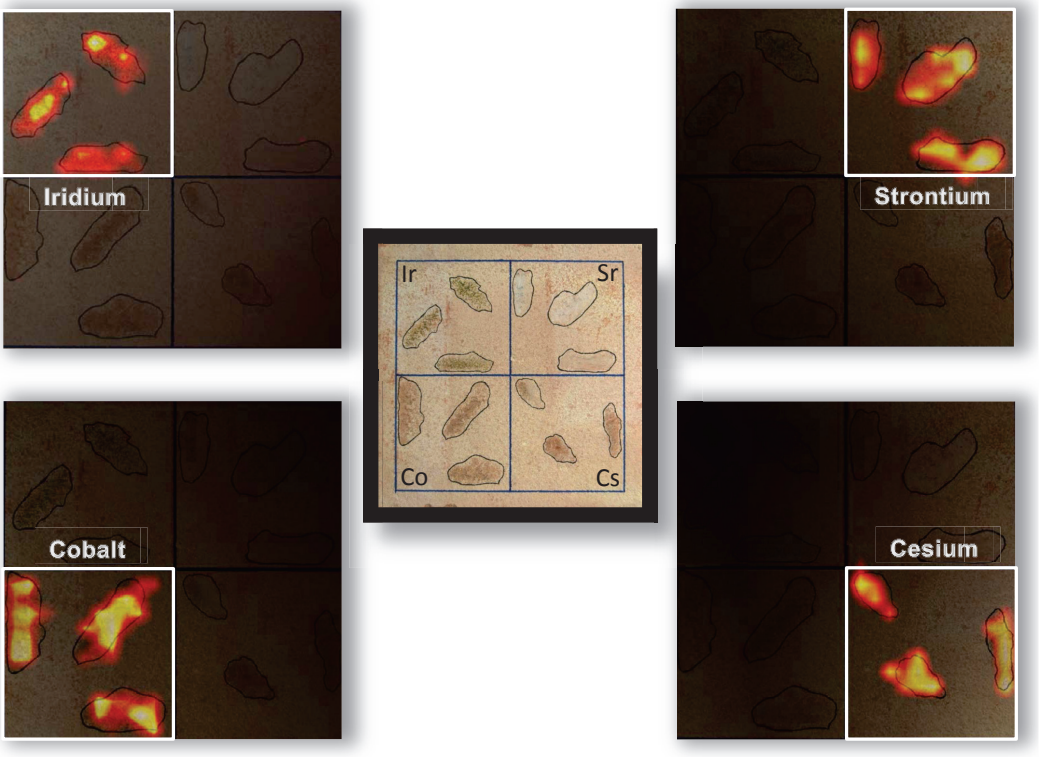

Fig. 5. Mapping of residuals of different radioactive surrogates over a terracotta flooring tile. Intensity maps, by laser-assisted *standoff* emission spectroscopy of evidence for Ir (439.95 nm), Sr (707.01 nm), Co (412.13 nm), and Cs (697.33 nm), respectively.

The emission lines used were 439.95 nm for Ir, 707.01 nm for Sr, 412.13 nm for Co and 697.33 nm for Cs. As observed, *standoff* LIBS analysis along the normal direction to the interrogated surface fits neatly with the spatial distribution profiles of the original depositions for the concerned elements. The particular identity of each surrogate is accurately monitored without interferences from other more outstanding emissions within the spectral signal.

4 Conclusions

The present work deals with assessing the potential of LIBS as a field sensor for monitoring of radiological threats from a safe distance. From the measurement of a variety of radioactive surrogates -Co, Sr, Ba, Cs, Ir and U-, LIBS has displayed a high selectivity to detect the presence of all these elements on the surface of different common urban materials. This study also confirms that the sensitivity of LIBS is satisfactory for the distant detection of these materials. *Standoff* LIBS is an effective option to complete the suite of available radiation detection technologies on gathering chemical evidence at a disaster area.

5 References

[1] E. Rutherford, J. Chadwick, C. Drummond Ellis, Radiations from Radioactive Substances, digital ed., *Cambridge University Press*, New York (2010).

[2] J. Magill, J. Galy, Radioactivity Radionuclides Radiation, *Springer-Verlag*, Berlin (2005).

[3] G. Lowenthal, P. Airey, Practical Applications of Radioactivity and Nuclear Radiations, *Cambridge University Press*, New York (2001).

[4] T.K. Gupta, Radiation, Ionization, and Detection in Nuclear Medicine, *Springer-Verlag*, Berlin (2013).

[5] C.D. Ferguson, Nuclear Energy: What Everyone Needs to Know, *Oxford University Press*, New York (2011).

[6] C.H. Sommers, X. Fan, Food Irradiation Research and Technology, *Blackwell Publishing & IFT Press*, Oxford (2006).

[7] K. Makuuchi, S. Cheng, Radiation Processing of Polymer Materials and its Industrial Applications, *John Wiley & Sons*, New Jersey (2012).

[8] S. Allison, Nuclear Terrorism. The Ultimate Preventable Catastrophe, *Henry Holt and Company*, New York (2004).

[9] G.F. Knoll, Radiation Detection and Measurement, fourth edition, *John Wiley & Sons*, New Jersey (2010).

[10] Handbook for Responding to a Radiological Dispersal Device. First Responder's Guide–he First 12 Hours, Conference of Radiation Control Program Directors Inc. Frankfort (2006).

[11] J.L. Gottfried, F.C. DeLucia Jr., C.A. Munson, A.W. Miziolek, Standoff detection of chemical and biological threats using laser-induced breakdown spectroscopy, *Appl. Spectrosc.* 62 (2008) 353–363.

[12] J.L. Gottfried, Discrimination of biological and chemical threat simulants in residue mixtures on multiple substrates, *Anal. Bioanal. Chem.* 400 (2011) 3289–3301.

[13] T. Tjärnhage, P. Gradmark, A. Larsson, A. Mohammed, L. Landström, E. Sagerfors, P. Jonsson, F. Kullander, M. Andersson, Development of a laser-induced breakdown spectroscopy instrument for detection and classification of single-particle aerosols in real-time, *Opt. Commun.* 296 (2013) 106–108.

[14] C. López-Moreno, S. Palanco, J.J. Laserna, F. De Lucia Jr., A.W. Miziolek, J. Rose, R.A. Walters, A.I. Whitehouse, Test of a stand-off laser-induced breakdown spectroscopy sensor for the detection of explosive residues on solid surfaces, *J. Anal. At. Spectrom.* 21 (2006) 55–60.

[15] J. Moros, J. Serrano, C. Sánchez, J. Macías, J.J. Laserna, New chemometrics in laser-induced breakdown spectroscopy for recognizing explosive residues, *J. Anal. At. Spectrom.* 27 (2012) 2111–2122.

[16] P. Lucena, I. Gaona, J. Moros, J.J. Laserna, Location and detection of explosive-contaminated human fingerprints on distant targets using standoff laser-induced breakdown spectroscopy, *Spectrochim. Acta Part B* 85 (2013) 71–77.

[17] J. Moros, J. Serrano, F.J. Gallego, J. Macías, J.J. Laserna, Recognition of explosives fingerprints on objects for courier services using machine learning methods and laser-induced breakdown spectroscopy, *Talanta* 110 (2013) 108–117.

[18] R.C. Chinni, D.A. Cremers, L.J. Radziemski, M. Bostian, C. Navarro-Northrup, Detection of uranium using laser-induced breakdown spectroscopy, *Appl. Spectrosc.* 63 (2009) 1238–1250.

[19] F.R. Doucet, G. Lithgow, R. Kosierb, P. Bouchard, M. Sabsabi, Determination of isotope ratios using laser-induced breakdown spectroscopy in ambient air at atmospheric pressure for nuclear forensics, *J. Anal. At. Spectrom.* 26 (2011) 536–541.

[20] X.K. Shen, Y.F. Lu, Detection of uranium in solids by using laser-induced breakdown spectroscopy combined with laser-induced fluorescence, *Appl. Optics* 47 (2008) 1810–1815.

[21] Y.S. Kim, B.Y. Han, H.S. Shin, H.D. Kim, E.C. Jung, J.H. Jung, S.H. Na, Determination of uranium concentration in an ore sample using laser-induced breakdown spectroscopy, *Spectrochim. Acta Part B* 74–75 (2012) 190–193.

[22] E.J. Judge, J.E. Barefield, J.M. Berg, S.M. Clegg, G.J. Havrilla, V.M. Montoya, L.A. Le, L.N. Lopez, Laser-induced breakdown spectroscopy measurements of uranium and thorium powders and uranium ore, *Spectrochim. Acta Part B* 83–84 (2013) 28–36.

[23] E.C. Jung, D.H. Lee, J.I. Yun, J.G. Kim, J.W. Yeon, K. Song, Quantitative determination of uranium and europium in glass matrix by laser-induced breakdown spectroscopy, *Spectrochim. Acta Part B* 66 (2011) 761–764.

[24] X. Mao, A.A. Bol'shakov, I. Choi, C.P. McKay, D.L. Perry, O. Sorkhabi, R.E. Russo, Laser ablation molecular isotopic spectrometry: Strontium and its isotopes, *Spectrochim. Acta Part B* 66 (2011) 767–775.

[25] M.Z. Martin, S. Allman, D.J. Brice, R.C. Martin, N.O. Andre, Exploring laser-induced breakdown spectroscopy for nuclear materials analysis and in-situ applications, *Spectrochim. Acta Part B* 74–75 (2012) 177–183.

[26] C.G. Parigger, J.O. Hornkohl, Computa. on of AlO B2Σ+→X2 Σ+ emission spectra, *Spectrochim. Acta Part A* 81 (2011) 404–411.

[27] R. González, P. Lucena, L.M. Tobaria, J.J. Laserna, Standoff LIBS detection of explosive residues behind a barrier, *J. Anal. At. Spectrom.* 24 (2009) 1123–1126.

[28] K.L. Maxwell, M.K. Hudson, Spectral study of metallic molecular bands in hybrid rocket plumes, *J. Pyrotech.* 21 (2005) 59–69.

[29] D.W. Hahn, N. Omenetto, Laser-induced breakdown spectroscopy (LIBS), Part I: Review of basic diagnostics and plasma–particle interactions: Still-challenging issues within the analytical plasma community, *Appl. Spectrosc.* 64 (2010) 335A–366A.

[30] R.W.B. Pearse, A.G. Gaydon. The Identification of Molecular Spectra. 2nd Edition, *John Wiley & Sons*, New York (1950).

[31] S. Yin, W. Xue, X.L. Ding, W.G. Wang, S.G. He, M.F. Ge, Formation, distribution, and structures of oxygen-rich iron and cobalt oxide clusters, *Int. J. Mass Spectrom.* 281 (2009) 72–78.

[32] X. Zhou, J. Yang, C. Li, Theoretical study of structure, stability, and the hydrolysis reactions of small iridium oxide nanoclusters, *J. Phys. Chem. A* 116 (2012) 9985–9995.

[33] G. Wang, Y. Su, D.L. Monts, Parametric investigation of laser-induced fluorescence of solid-state uranyl compounds, *J. Phys. Chem. A* 112 (2008) 10502–10508.

[34] J. Moros, J.A. Lorenzo, J.J. Laserna, Standoff detection of explosives: critical comparison for ensuing options on Raman spectroscopy–LIBS sensor fusion, *Anal. Bioanal. Chem.* 400 (2011) 3353–3365.

[35] C. Chaleard, P. Mauchien, N. Andre, J. Uebbing, J.L. Lacour, C. Geersten, Correction of matrix effects in quantitative elemental analysis with laser ablation optical emission spectrometry, *J. Anal. At. Spectrom.* 12 (1997) 183–188.

[36] J.J. Curry, Compilation of Wavelengths, Energy Levels, and Transition Probabilities for Ba I and Ba II, J. Phys. Chem. Ref. Data 33 (2004) 725–746.

[37] B. Duan, M.A. Bari, Z.Q. Wu, J. Yan, Y.M. Li, Electron-impact broadening parameters for Be II, Sr II, and Ba II spectral lines, A&A 555 (2013) A144.

[38] I. Gaona, J. Moros, J.J. Laserna, New insights into the potential factors affecting the emission spectra variability in standoff LIBS, *J. Anal. At. Spectrom.* 28 (2013) 1750–1759.

[39] K.J. Moody, P.M. Grant, I.D. Hutcheon, Nuclear Forensic Analysis, *CRC Press*, Boca Raton (2005).

[40] F. Volk, F. Schedlbauer, Analysis of post detonation products of different explosive charges, *Propell. Explos. Pyrot.* 24 (1999) 182–188.

Conclusions and Outlook

Beyond a mere collection of analytical applications, the works involved in the present Doctoral Thesis seek to disclose a series of real needs of today, in parallel with the strengths and weaknesses of the probably sole analytical tool able to perform these investigations at such scenarios.

From research findings achieved during the development of the present Doctoral Thesis, the following some general conclusions can be drawn.

- The LIBS capability on surveying, distantly but *in situ*, the elemental composition of the materials forming unmovable and tangible architectural heritage material has been developed.
- *ST-LIBS* has also demonstrated its feasibility to detect and characterize not only the gross cumulative crusts over different materials, but also inconspicuous soiling embedded as time goes on.
- The usefulness of *ST-LIBS* as a diagnostic tool to anticipate threats as well as to gather chemical evidences at a disaster area has been strengthened.
- The LIBS potential to locate, detect and identify from a distance, and under changing operational conditions, the nature of organic residues from human fingerprints when located on aluminum surfaces has been attested.
- Both, the selectivity and the specificity of *ST-LIBS* to gather chemical evidences from radiological surrogates on the surface of different objects from the urban furniture have been revealed.

Despite this larger versatility offered by *ST-LIBS* as compared to the close-contact operating mode, its performance entails additional complexities. Thus, it has been demonstrated that:

- While almost all the laser energy flux delivered towards the distant target reaches the sample surface, propagation through the atmosphere alters its distribution within the wave front.
- Although random, this distortion is closely tied to the distance of the optical path: the larger the range the higher the alteration.
- Consequently, the random loss of laser beam quality due to atmospheric propagation reverts to an unsystematic irradiance being available to produce the plasma plume.
- This circumstance leads to a deleterious impact in the reproducibility of the induced plasmas at a distance as well as in their accompanying properties.
- Whatever the operating range, in absence of severe weather effects, plasma light does not suffer significant distortions during its propagation, beyond its intensity decrease with the inverse of the range squared.
- The random variation in the positioning of the laser beam centroid onto the distant target (*beam wander* effect) does not affect the position of the plasma image at the tip of the optical fiber.
- Hence, as demonstrated, the large shot-to-shot unstability in the laser irradiance is the main direct cause responsible of the high variability in the emission intensity of the corresponding *standoff* LIBS signals.

Thus, from all these results and conclusions, two clear prospects for the future may be suggested:

- A thorough investigation on the influence of the changing weather conditions, not only on the basic processes governing the *standoff* approach, but also on the analytical information registered, in order to widening the technique for as many different situations as possible.
- The broadening of the closed-list of interrogated targets to transfer the implementability of *ST-LIBS* to as many scenarios as possible, mainly those referred to the anticipation of threats.
- A comprehensive examination in the performance of *ST-LIBS* for the envisaged applications when shorter laser wavelengths (Vis and UV) are used, from the influences exerted by surrounding atmosphere, up to the quality of the analytical information in terms of sensitivity and reproducibility.

Más allá de una mera colección de aplicaciones analíticas, el contenido de la presente Tesis Doctoral busca mostrar una serie de necesidades analíticas reales existentes hoy en día, junto con el potencial de la que es probablemente la única herramienta que dispone de los atributos necesarios para afrontar las investigaciones demandadas en ese tipo de escenarios.

De los resultados obtenidos durante el desarrollo de la presente investigación, pueden extraerse las siguientes conclusiones generales.

- Ha sido probada la capacidad de LIBS para realizar inspecciones, *in situ* pero desde la distancia, sobre la composición elemental de los materiales que integran el patrimonio arquitectónico inamovible.

- *Standoff* LIBS también ha demostrado su viabilidad para detectar y caracterizar, no sólo las deposiciones de contaminación acumulada sobre diferentes materiales, sino también la polución incrustada dentro del material con el paso del tiempo.

- Se ha reforzado la utilidad de *standoff* LIBS como herramienta de diagnóstico para anticipar potenciales amenazas, así como para reunir evidencias químicas después de cualquier trágica incidencia.

- Se ha probado el potencial de LIBS para localizar, detectar e identificar residuos orgánicos según su peligrosidad, desde la distancia y bajo condiciones operativas cambiantes, dejados por huellas dactilares sobre superficies de aluminio.

- Se ha mostrado la selectividad y especificidad de *standoff* LIBS para reunir evidencias químicas de sustitutos radiológicos sobre la superficie de distintos objetos relacionados con objetos del mobiliario urbano.

A pesar de la mayor versatilidad de LIBS en su configuración *standoff* al ser comparada con el modo operacional en contacto directo, su rendimiento implica complejidades adicionales. Por tanto, se ha demostrado que:

- Si bien casi todo el flujo de energía del láser emitido alcanza cualquier objetivo ubicado a cierta distancia, su distribución en el frente de onda se ve alterada como consecuencia de su propagación a través de la atmósfera.

- Esta distorsión, aunque aleatoria, está estrechamente vinculada a la trayectoria óptica, ya que al aumentar dicho trayecto esta distorsión se ve incrementada.
- Como consecuencia, se produce una pérdida aleatoria de la calidad del haz láser, debido a la propagación atmosférica, que trasciende en fluctuaciones no sistemáticas del nivel de *irradiancia* disponible para producir los plasmas.
- Esta circunstancia supone un agravio para la reproducibilidad de los plasmas inducidos con la distancia, así como en sus propiedades implícitas.
- Cualquiera que sea el rango de operación, en ausencia de efectos climatológicos severos, la luz del plasma no sufre distorsiones significativas al ser colectada por el dispositivo detector, más allá de su descenso de intensidad con el inverso del cuadrado de la distancia.
- Aunque acontezca cualquier desviación al azar en el posicionamiento del centroide del haz láser sobre el objetivo distante (efecto *beam wander*) la posición de la imagen del plasma en el plano receptor de la fibra óptica no se ve apenas alterada.

Así, a partir de todos estos resultados y conclusiones, se sugieren algunas perspectivas de trabajos futuros:

- Una investigación a fondo sobre la influencia de las condiciones climatológicas cambiantes, no sólo en los posibles procesos que puedan influir en el enfoque *standoff*, sino también en la información analítica

registrada, con el fin de ampliar la funcionalidad de la técnica en tantas situaciones como sea posible.

- La ampliación de la lista de muestras analizadas para transferir la aplicabilidad de *standoff* LIBS a tantos escenarios como sea posible, sobre todo a aquellos relacionados con la anticipación de amenazas.
- Un examen exhaustivo en el rendimiento de *ST-LIBS* para las aplicaciones previstas cuando se utilizan longitudes de onda laser más cortas (visible y ultravioleta), desde las influencias ejercidas por la atmósfera circundante, hasta la calidad de la información analítica en términos de sensibilidad y reproducibilidad.

Appendix 1

JAAS

RSC Publishing

PAPER

View Article Online
View Journal | View Issue

New insights into the potential factors affecting the emission spectra variability in standoff LIBS

Cite this: *J. Anal. At. Spectrom.*, 2013, **28**, 1750

I. Gaona, J. Moros and J. J. Laserna*

Interest in the use of laser-based sensors operating in standoff mode is increasing due to the wide range of options offered in the evaluation of distant targets. However, despite this high potential, the performance aspects of any sensor for analysis at a distance are curtailed as compared with its use *in situ*. The present work addresses a sensitive topic in standoff laser-induced breakdown spectroscopy (ST-LIBS) which is the larger variability observed within the emission signals registered from faraway targets. A field deployable LIBS sensor has been used to ascertain how atmospheric propagation affects the laser pulses delivered to a distant target and the emitted light from the plasma plume created. In this way, the extent of the contribution of the alterations of each optical pathway to the signal uncertainty in ST-LIBS have been isolated. As has been experimentally verified, the amount of laser energy reaching the target remains constant, whatever the distance. In contrast, the laser beam cross section is distorted during its travel towards the target; an alteration that becomes ever larger as the distance to the target increases. This circumstance leads to further and random deterioration of the irradiance, thus resulting in plasma events notably differing in their intensity, which, in turn, have proven to be in direct correlation with the intensities and variability of the spectral responses collected by the system. The positional displacement of the laser-induced plasmas has no impact on the sensitivity and uncertainty of the standoff LIBS signals.

Received 24th May 2013
Accepted 13th August 2013

DOI: 10.1039/c3ja50181g

www.rsc.org/jaas

1 Introduction

Over the last few years optical sensors based on lasers have found their place in a wide range of applications because they provide a unique set of capabilities that are well-suited to difficult measurement tasks. The potential for these sensors to operate without contact, quickly and with appropriate sensitivity for the design of field-deployable, compact, robust and versatile diagnostic systems, have made them highly appealing tools for analytical work. These spectroscopic sensors are able to qualify and quantify the concerned targets through different physical mechanisms, including absorption, emission, or scattering of electromagnetic radiation by atoms or molecules in a sample.[1] These distinct mechanisms, which are chosen depending on the intended application, offer the chance to characterize different kinds of materials, either in a condensed phase or as a gas, by revealing specific analytical information.

Particularly, atomic emission spectroscopy assisted by laser breakdown (that is, LIBS), for instance, provides a multi-elemental spectral signature of the chemical composition of the sample based on the light emission from the ionized matter.[2,3] Such analytical information has proved useful in a wide range of research, especially as a result of the facility to use portable, remote, and standoff instruments for field measurements.[4,5] Among all these various operational configurations, the most functional approach for field analysis of distant objects, is at the same time, the most demanding application. The ability to analyze samples located in harsh environments, or the analysis of targets located in difficult to access areas, are the main advantages of the standoff LIBS configuration. These features have led to use of the technique in explosive detection,[6,7] care and maintenance of cultural heritage,[8,9] space exploration,[10,11] industrial processes[12–14] and environmental chemistry,[15] to name a few examples.

The underlying principle of operation in standoff LIBS involves a double optical path: first, the delivery of tightly focused laser pulses towards the distant target through the atmosphere, and second the subsequent atmospheric transmission of the light emitted by the induced plasma plume back to the spectrometer. Apart from optical absorption by the components of the air, a large source of perturbation in both paths is related to turbulence, constantly present in the atmosphere to a greater or lesser extent. The disturbance resulting from this turbulence is responsible for random microscopic fluctuations in the transmitted light as a result of changes in the refractive index of air with changing temperature. All these turbulent motions persistently exert influences on the behavior of the light when propagating along its optical path. To cite just a few examples, these random variations affect the directionality and the position (wandering) of the transmitted beam as well as the energy distribution (scintillation) of the propagating

Department of Analytical Chemistry, University of Malaga, E-29071 Málaga, Spain. E-mail: laserna@uma.es; Fax: +34 952 13 2000; Tel: +34 952 13 1881

Appendix 2

JAAS

Journal of Analytical Atomic Spectrometry

www.rsc.org/jaas

Volume 28 | Number 6 | June 2013 | Pages 771–960

ISSN 0267-9477

RSC Publishing

PAPER

J. J. Laserna *et al.*

Evaluating the use of standoff LIBS in architectural heritage: surveying the Cathedral of Málaga

0267-9477(2013)28:6;1-0

JAAS

RSC Publishing

PAPER

Evaluating the use of standoff LIBS in architectural heritage: surveying the Cathedral of Málaga

Cite this: *J. Anal. At. Spectrom.*, 2013, **28**, 810

I. Gaona, P. Lucena, J. Moros, F. J. Fortes, S. Guirado, J. Serrano and J. J. Laserna*

Laser-induced breakdown spectroscopy (LIBS) is a cutting-edge technology which offers appealing features for its application in the field of the cultural heritage. It is a proven technology for the fast and simultaneous detection of major and trace elements with minimal destructiveness, using easily compactable instrumentation into movable platforms for the *in situ* and standoff chemical analysis of objects in real time. In the present work, a standoff LIBS sensor has been used for surveying the Cathedral of Málaga. The spectroscopic measurements were gathered *in situ* although from an averaged distance of 35 m. A comprehensive characterization of the materials composing the main façade as well as identification of the noticeable pollutants at their surfaces has been performed. The standoff LIBS results have fitted neatly with the mineralogical analysis of all the stones assayed. The large emissions of Si, Al, Ca and Mg have confirmed that the structure was almost entirely built using sandstone. In turn, the sensitivity to carbonate chemistry has demonstrated the capability of standoff LIBS for coherently classifying different marbles, thus allowing the identification of their origins. Standoff LIBS has also allowed the detection of pollutants such as Si, Ca, Mg, Fe, Al, Ba and Sr, originating from natural sources such as the transport of re-suspended dust and atmospheric particulate matter related to marine aerosols. In addition, trace elements such as Ti, Pb and Mn from exhausts of gasoline and diesel engines are also involved in the pollution triggering of materials. To obtain all these findings, scaffolding or other intrusive facilities have not been required.

Received 1st March 2013
Accepted 18th April 2013

DOI: 10.1039/c3ja50069a

www.rsc.org/jaas

1 Introduction

Cultural heritage is a valuable resource inherited from the history and a unique legacy that broadens our understanding of the diversity of society and its constant evolution. Whether they are objects or archaeological sites, or ancient and historic monuments of the world, all of them inform and help connect us to our cultural origins. Therefore it is a real and irreplaceable treasure of outstanding value, considered worthy of preservation. Unfortunately, the rapid and on-going evolution of society has brought about a large deterioration of these vast sources of culture. Effects not only from anthropogenic sources but also from natural causes can result in unlimited and irreversible damage in cultural heritage. All this has meant that the conservation of cultural heritage and its protection against possible damage due to pollution has received growing scientific interest. In order to find the best possible measures for proceeding with protection of cultural heritage material, provision of analytical information for its characterization is a vital requirement. Further, research efforts to better assess and understand the pollution sources and mechanisms damaging the cultural heritage material cannot be set aside. Strong evidence of the growing importance of these physical and chemical diagnostics is the wide aim of analytical techniques used for this end.[1,2]

Scientific assessment of the materials for cultural heritage poses specific, and often, difficult analytical challenges. The primary requirement is that no significant modification or alteration of the artifact occurs, so as not to compromise the historical, cultural and/or archaeological value when extracting as much information as possible.[3] Also, the capability of working *in situ* and in real time, either during the research campaigns[4,5] or after the consequent conservation tasks,[6] is often necessary due to the impossibility of moving historical artifacts to laboratory facilities. The use of compact, robust, and versatile analytical systems is highly desirable.[7] Finally, the limited or complex accessibility to the assets is often incompatible with conventional methods of analysis. This circumstance requires the use of instruments to operate in a contactless way, but rapidly and with appropriate sensitivity.[8]

Although few analytical techniques pool all these demands, laser-induced breakdown spectroscopy (LIBS) is an appealing tool for analysis that combines the above requirements.[9,10] LIBS is a established technology having several advantages over conventional elemental analysis methods. Its capacity for rapidly and simultaneously detecting almost all elements after the ablation of barely a few nanograms of a target analyzed from

Department of Analytical Chemistry, Faculty of Sciences, University of Málaga, E29071 Málaga, Spain. E-mail: laserna@uma.es; Fax: +34 95 213 2000; Tel: +34 95 213 1881

Appendix 3

Spectrochimica Acta Part B 85 (2013) 71–77

Contents lists available at SciVerse ScienceDirect

Spectrochimica Acta Part B

journal homepage: www.elsevier.com/locate/sab

Location and detection of explosive-contaminated human fingerprints on distant targets using standoff laser-induced breakdown spectroscopy

P. Lucena, I. Gaona, J. Moros, J.J. Laserna *

Department of Analytical Chemistry, Faculty of Sciences, University of Málaga, E29071 Málaga, Spain

ARTICLE INFO

Article history:
Received 9 July 2012
Accepted 8 April 2013
Available online 20 April 2013

Keywords:
LIBS
Standoff
Explosive
Fingerprint
Imaging

ABSTRACT

Detection of explosive-contaminated human fingerprints constitutes an analytical challenge of high significance in security issues and in forensic sciences. The use of a laser-induced breakdown spectroscopy (LIBS) sensor working at 31 m distance to the target, fitted with 2D scanning capabilities and designed for capturing spectral information from laser-induced plasmas of fingerprints is presented. Distribution chemical maps based on Na and CN emissions are used to locate and detect chloratite, DNT, TNT, RDX and PETN residues that have been deposited on the surface of aluminum and glass substrates. An effectiveness of 100% on fingerprints detection, regardless the substrate scanned, is reached. Environmental factors that affect the prevalence of the fingerprint LIBS response are discussed.

1. Introduction

The increased activity in the manufacture of improvised explosive devices (IEDs) places the scientific community's priority attention to the detection of explosives. The fact that most IEDs contain hidden explosives complicates its detection. However, the transfer of explosive particulate matter through fingerprints makes it possible to detect concealed explosives through surface sampling [1]. In fact, fingerprints are considered one of the main mechanisms of transferring explosive residues during handling and preparation of IEDs.

The process of transferring material to a surface via fingerprint is highly variable. Verkouteren sized RDX and PETN particles from C-4 and Semtex-1A and demonstrated that the mass may be concentrated in relatively few particles that may not be homogeneously distributed over the fingerprint area [2]. The same author characterized C-4 fingerprints and showed that the number of particles varies significantly from print to print and within a print [3].

When attempting to characterize explosive residues at low to trace levels, the most critical step in the analysis is to locate the material in the surface inspected. Once collected at the scene, the sample must be packaged so that its evidentiary value is not lost, whereas contamination during sample handling should be avoided. A survey of techniques used for sampling and concentration, and for detection/identification of explosive residues in laboratory or in field has been presented [4]. Detection/identification techniques were classified according to their application to: organic explosives using chromatographic techniques, Raman spectroscopy, ion mobility spectrometry and mass spectrometry; inorganic explosives using ion chromatography and capillary electrophoresis. For operational and safety reasons, detection methods capable for standoff (ST) operation are extremely valuable. ST detection techniques are divided into two broad categories, namely bulk detection techniques (X-rays, infrared, terahertz, microwaves, neutrons, gamma rays, magnetic resonance and magnetic fields) and trace detection techniques (optical absorption, fluorescence, laser imaging detection and ranging (LIDAR), differential absorption LIDAR and differential reflectance LIDAR, array biosensors using captured antibodies, biomimetic sensors)[5].

The sensor providing at the same time the sensitivity, analysis speed and selectivity requirements for explosive detection is still to be developed. Most attempts are conditioned by the physical limits or the circumstances of a particular scenario. Canine-based detection is known to be the most reliable method for explosive detection. The complex training, their subjective response and the limited operational time of the animals are significant drawbacks of this approach. Singh published a review focused on the sensors developed in the last 5 years, ranging from electrochemical methods to immunosensors [6].

Recent advancements have been directed at improving the capabilities of detecting explosives in packages and baggage by X-ray diffraction [7] and using photons and neutrons as incident particles [8–10]. The presence of nitrogen bearing substances has been investigated by methods based on nuclear quadrupole resonance [11], ion mobility spectrometry [12], electrochemical sensors [13] and fluorescence [14,15]. Special efforts have been made to explosive detection in the development of portable sensors [16] and standoff instruments [17,18].

In 2005, the first test of a standoff LIBS (laser induced breakdown spectroscopy) sensor for detection of explosive residues at a distance

* Corresponding author. Tel.: +34 95 213 1881; Fax: +34 95 213 2000.
E-mail address: laserna@uma.es (J.J. Laserna).

0584-8547/$ – see front matter © 2013 Elsevier B.V. All rights reserved.
http://dx.doi.org/10.1016/j.sab.2013.04.003

Appendix 4

analytical chemistry

Article

pubs.acs.org/ac

Range-Adaptive Standoff Recognition of Explosive Fingerprints on Solid Surfaces using a Supervised Learning Method and Laser-Induced Breakdown Spectroscopy

Inmaculada Gaona, Jorge Serrano, Javier Moros, and J. Javier Laserna*

Departamento de Química Analítica, Universidad de Málaga, E-29071 Málaga, España

ABSTRACT: The distance between the sensor and the target is a particularly critical factor for an issue as crucial as explosive residues recognition when a laser-assisted spectroscopic technique operates in a standoff configuration. Particularly for laser ablation, variations in operational range influence the induced plasmas as well as the sensitivity of their ensuing optical emissions, thereby confining the attributes used in sorting methods. Though efficient classification models based on optical emissions gathered under specific conditions have been developed, their successful performance on any variable information is limited. Hence, to test new information by a designed model, data must be acquired under operational conditions totally matching those used during modeling. Otherwise, the new expected scenario needs to be previously modeled. To facing both this restriction and this time-consuming mission, a novel strategy is proposed in this work. On the basis of machine learning methods, the strategy stems from a decision boundary function designed for a defined set of experimental conditions. Next, particular semisupervised models to the envisaged conditions are obtained adaptively on the basis of changes in laser fluence and light emission with variation of the sensor-to-target distance. Hence, the strategy requires only a little prior information, therefore ruling out the tedious and time-consuming process of modeling all the expected distant scenes. Residues of ordinary materials (olive oil, fuel oil, motor oils, gasoline, car wax and hand cream) hardly cause confusion in alerting the presence of an explosive (DNT, TNT, RDX, or PETN) when tested within a range from 30 to 50 m with varying laser irradiance between 8.2 and 1.3 GW cm^{-2}. With error rates of around 5%, the experimental assessments confirm that this semisupervised model suitably addresses the recognition of organic residues on aluminum surfaces under different operational conditions.

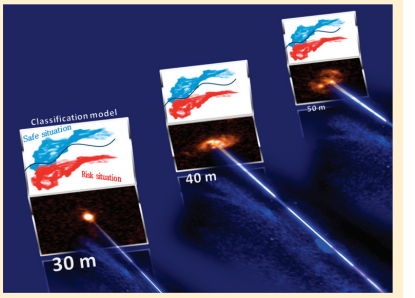

Over the past few years there have been many efforts to identify trace explosives on the surface of distant objects using spectroscopic techniques.[1] Whether through emission spectroscopy,[2] Raman spectroscopy,[3] photoacoustic spectroscopy,[4] photothermal deflection spectroscopy,[5] or infrared photothermal imaging,[6] the answer to that challenge is being addressed due to its immediate relevance in countering terrorist threats.

Nonetheless, to these extreme scenarios, although the operation at standoff detection regime offers safety advantages over close-contact scheme, complexity on the using of that design is more than evident. In standoff instruments, beyond the technical hurdles for a flexible working, the distance between the interrogated target and the sensing platform plays a large role in determining the signal and noise of the gathered information. In laser-induced breakdown spectroscopy (LIBS) based sensors, added to the decrease in emission signal with the range squared, the irradiance also declines with the square of the distance, thus resulting in a fourth-power dependence of the LIBS intensity with the range.[7] To put this in context, consider the exemplary scheme presented in Figure 1. The multifactorial nature of the emission response in standoff regime is illustrated as a big cube. The particular response of a target is embodied by each one of the subcubes that are composing the complex network. Any variation, simultaneous or not, in the irradiance or in the distance of the interrogated target involves a series of changes in the emission signal. As the increase in the irradiance should result in a more sensitive response, whereas the parallel decrease of the analysis distance would lead to enhance this positive impact. In contrast, when the irradiance level is extremely low or distance is particularly large, useless spectral information can be anticipated. In addition, the transient environmental conditions can also affect the emission signal even when operational conditions have remained identical. In conclusion, the emission response occurs from a specific substance governed by explicit conditions. Hence, as it is predictable, any change on the analysis conditions accounts a significant constraint for those classification techniques whose background focuses on a spectral features-based labeling.

A number of chemometric methods including linear correlation,[8] principal components analysis (PCA),[9,10] partial least-squares discriminant analysis (PLS-DA),[11,12] the method

Received: February 20, 2014
Accepted: April 28, 2014
Published: April 28, 2014

dx.doi.org/10.1021/ac500694j | *Anal. Chem.* 2014, 86, 5045−5052

Appendix 5

Spectrochimica Acta Part B 96 (2014) 12–20

Contents lists available at ScienceDirect

Spectrochimica Acta Part B

journal homepage: www.elsevier.com/locate/sab

Evaluation of laser-induced breakdown spectroscopy analysis potential for addressing radiological threats from a distance☆

I. Gaona, J. Serrano, J. Moros, J.J. Laserna *

Universidad de Málaga, Departamento de Química Analítica, E-29071 Málaga, Spain

ARTICLE INFO

Article history:
Received 22 November 2013
Accepted 7 April 2014
Available online 16 April 2014

Keywords:
LIBS
Radiological threat
Dirty bomb
Standoff sensing

ABSTRACT

Although radioactive materials are nowadays valuable tools in nearly all fields of modern science and technology, the dangers stemming from the uncontrolled use of ionizing radiation are more than evident. Since preparedness is a key issue to face the risks of a radiation dispersal event, development of rapid and efficient monitoring technologies to control the contamination caused by radioactive materials is of crucial interest. Laser-induced breakdown spectroscopy (LIBS) exhibits appealing features for this application. This research focuses on the assessment of LIBS potential for the in-situ fingerprinting and identification of radioactive material surrogates from a safe distance. LIBS selectivity and sensitivity to detect a variety of radioactive surrogates, namely ^{59}Co, ^{88}Sr, ^{130}Ba, ^{133}Cs, ^{193}Ir and ^{238}U, on the surface of common urban materials at a distance of 30 m have been evaluated. The performance of the technique for nuclear forensics has been also studied on different model scenarios. Findings have revealed the difficulties to detect and to identify the analytes depending on the surface being interrogated. However, as demonstrated, LIBS shows potential enough for prompt and accurate gathering of essential evidence at a number of sites after the release, either accidental or intentional, of radioactive material. The capability of standoff analysis confers to LIBS unique advantages in terms of fast and safe inspection of forensic scenarios. The identity of the radioactive surrogates is easily assigned from a distance and the sensitivity to their detection is in the range of a few hundreds of ng per square centimeter.

1. Introduction

Radioactivity refers to the emission of ionizing (high-energy) radiation, namely alpha (α), beta (β), X or gamma (γ), from the spontaneous and random transformation (radioactive decay) of an unstable atomic nucleus, resulting in new elements or a lower energy state of the atoms [1]. Most of the ionizing radiation we are exposed to (about 82% of the total) consists of natural background radiation from radon gas and other natural terrestrial sources (radioactive elements in rocks, soil, water, and plants), whereas the remaining 18% is from man-made sources. Since the discovery of X-rays in 1895, man-made radiation has been becoming a very common tool that lets us do many things that would be impossible without it [2]. Thousands of new practical and beneficial uses of ionizing radiation have been devised till its complex structure within the present-day life [3]. Ionizing radiation is ubiquitous and indispensable for medical techniques and practices of diagnosing and treating – e. g. for identifying broken bones and healing of tumors [4] – as well as on nuclear power plants for sustaining exothermic processes to generate heat and electricity [5], to mention the most common. Its use also extends to metabolic studies, genetic engineering and environmental protection studies. The ionizing radiation from radioisotopes is also used in agriculture to breed new seed varieties and to preserve different varieties of food [6]. Similarly, it is applied in industry, manufacturing and engineering for improving the quality of manufactured goods [7].

Although the benefits of radiation are more than apparent, living and working with it is not only hazardous but also may entail risks that cannot be overlooked. With a view to putting in perspective the menaces from ionizing radiation, all of them can cause to any form of life, whether it be human, plants, or animals many adverse consequences not just at a cellular level but on a genetic level as well. The amount of damage caused by ionizing radiation depends on its half-life and on both the dose and the period of exposition.

Radiological dispersal events from nuclear and radioactive sources may arise from an unfortunate natural disaster. Just to cite the most recent example, the incidents at Fukushima nuclear reactors because of the earthquake and the subsequent tsunami of March, 2011, demonstrate the extreme dangers associated to these events. Furthermore, malicious actions by those who seek to unleash a radiological mayhem are today more than a real threat [8]. In these cases, the most commonly used civilian radiation sources are malevolently exploited to prepare a radiological dispersive device (*RDD*), also known as "*dirty bomb*",

☆ Selected paper from the 7th Euro-Mediterranean Symposium on Laser Induced Breakdown Spectroscopy (EMSLIBS 2013), Bari, Italy, 16–20 September 2013.

* Corresponding author. Tel.: +34 952 13 1881; fax: +34 952 13 2000.
E-mail address: laserna@uma.es (J.J. Laserna).

http://dx.doi.org/10.1016/j.sab.2014.04.003
0584-8547/